Northumbria University
NEWCASTLE

SEASONAL SNOW AND WINTERTIME CARBON EMISSIONS IN ARCTIC SHRUB TUNDRA

VICTORIA R. DUTCH

PhD

2023

SEASONAL SNOW AND WINTERTIME CARBON EMISSIONS IN ARCTIC SHRUB TUNDRA

VICTORIA R. DUTCH

A thesis submitted in partial fulfilment of the requirements of the University of Northumbria at Newcastle for the degree of Doctor of Philosophy

Faculty of Environment & Engineering

May 2023

Abstract

The Arctic is at the forefront of global climate change, warming at a rate 4 times faster than the global average. Changes are particularly apparent during winter, which lasts for around 8 months of year. CO_2 emissions at this time of year make a considerable contribution to the annual Arctic carbon budget, with enhanced soil CO_2 losses due to winter warming exceeding growing season carbon uptake under future climatic conditions. However, high uncertainty surrounds estimates of winter CO_2 fluxes across the Arctic region, which vary by a factor of three and a half, with considerable variation between measured and simulated fluxes.

Simulations of the Community Land Model (CLM5.0) were examined to address uncertainties impacting simulations of Arctic carbon fluxes; firstly of snow insulation and soil temperatures, and secondly rates of net ecosystem exchange of CO_2. Improving simulated snow properties and the corresponding heat flux is important, as wintertime soil temperatures are an important control on subnivean soil respiration and hence impact Arctic winter carbon fluxes. The default model configuration was found to be inappropriate, with a change to the parameterisation of snow thermal conductivity required in order to correct for a cold soil temperature bias and better represent the insulation provided to the soil by the basal depth hoar not physically represented in CLM5.0.

Simulated CO_2 emissions were then examined through sensitivity testing of the parameterisation of relationships between soil temperature, moisture and respiration as well as snow thermal conductivity. The default value of the minimum soil moisture threshold for decomposition prevented soil respiration for the majority of the winter, with no CO_2 emission simulated between November and mid-May, in contrast to observations showing steady CO_2 emission throughout the winter. Failure to simulate CO_2 emissions for over half of the year has a considerable impact on the simulation of the annual Arctic carbon budget. Changes to the model parameterisation, most crucially a decrease in the minimum moisture required for soil decomposition, allowed emissions to occur throughout the winter.

Maintaining continuous wintertime eddy covariance measurements, typically used for model evaluation, in remote Arctic locations is very challenging. Consequently, as other measurement techniques would be advantageous, preliminary investigations with new low-cost CO_2 sensors are presented and evaluated. Low-cost sensor measurements are used to examine spatial and temporal

patterns in CO_2 flux, and how these vary with changes in snow properties across the footprint of the eddy covariance tower. Measurements of CO_2 flux using both new and established methods show similar magnitudes of CO_2 release during March and April 2022, and a similar relationship between CO_2 and subnivean temperatures as previously shown across the Pan-Arctic. Future development of low-cost sensors should allow uncertainties to be reduced and an improvement in our understanding of the processes governing carbon fluxes from Arctic environments throughout the snow-covered season.

Contents

List of Figures

List of Tables

Acknowledgements

First, I would like to thank my primary supervisor Dr. Nick Rutter, and my wider supervision team Drs. Leanne Wake, Mel Sandells, Chris Derksen and Richard Kelly. Thank you for your support and guidance throughout the course of this project, this thesis would not have existed without your help and support.

This work was supported by an RDF Studentship from Northumbria University and the Northern Water Futures project. Additional funding from the NERC-UK seedcorn project Carbon Emissions under Arctic Snow supported this thesis. Funding for travel to Montréal was provided by the Canada-UK Foundation. This thesis would not have been possible without collaboration, including data, discussion and advice on the interpretation of Arctic environmental systems, with Oliver Sonnentag, Gabriel Hould Gosselin, Paul Mann, Alex Marvoric and Alex Roy. I also thank Drs. Sevi Modestou and Stuart Umbo for assistance with the isotopic analysis and interpretation.

Fieldwork for this project was undertaken in the Inuviuluit Settlement Region of Inuit Nunangat, the traditional, ancestral and unceded lands of the Inuit people. I would like to thank the entire team at Trail Valley Creek in March 2022; Brandon, Rosy, Gabriel, Alex, George, Paul, Nick, Richard, Chris, Emma, Trevor and Troy. Additional logistical support was provided by the Aurora Research Institute.

Last, but by no means least, I thank the friends who have supported me throughout this process - both within the department, across the UK Polar Network, and those outside of work. Particular thanks to Matheus, Bridget, and my sister Amy.

Declaration

I declare that the work contained in this thesis has not been submitted for any other award and that it is all my own work. I also confirm that this work fully acknowledges opinions, ideas and contributions from the work of others.

Any ethical clearance for the research presented in this thesis has been approved. Approval has been sought and granted by the *Faculty Ethics Committee* in *December 2019*.

I declare that the Word Count of this thesis is 34330 words.

Name: Victoria R. Dutch

Date: 17 May 2023

At the time of submission, the contents of one chapter in this thesis have been published. Chapter 4 is published as:

Dutch, V. R., Rutter, N., Wake, L., Sandells, M., Derksen, C., Walker, B., Hould Gosselin, G., Sonnentag, O., Essery, R., Kelly, R., Marsh, P., King, J. and Boike, J. (2022), 'Impact of measured and simulated tundra snowpack properties on heat transfer', *The Cryosphere* **16**(10), 4201–4222.

Additionally, Chapter 5 has been submitted for publication and is currently in review as:

Dutch, V. R., Rutter, N., Wake, L., Sonnentag, O., Hould Gosselin, G., Sandells, M., Derksen, C., Walker, B., Meyer, G., Essery, R., Kelly, R., Marsh, P., Boike, J. and Detto, M. (2023), 'Simulating net ecosystem exchange under seasonal snow cover at an Arctic tundra site', *EGUSphere*.

Chapter 1

Introduction

1.1 Rationale

Traditionally, the Arctic has been understudied compared to warmer, more southerly and temperate regions (Euskirchen et al., 2022). However, many environmental processes at play in the Arctic are important at global scales. Emissions of greenhouse gases from the Arctic raise global atmospheric greenhouse gas concentrations and contribute towards further climate change. Despite its isolation and remoteness, what happens in the Arctic does not stay in the Arctic (Dodds, 2017). Northern winters were once thought to be a period of dormancy, but are now understood to have the potential for considerable biological activity and CO_2 release (Campbell et al., 2005; Olsson et al., 2003). Understanding of Arctic processes (many of which are seen in Fig. 1), and how to include these in projections of future Arctic (and global) change is limited. Relationships and interactions between snow, soil, biota and atmosphere control rates of wintertime CO_2 release, but such relationships are understudied and poorly parameterised. A scarcity of carbon flux measurements has resulted in critical knowledge gaps (Bastviken et al., 2022), with a lack of consensus on the magnitude or sign of the Arctic carbon budget (Euskirchen et al., 2022).

Many different definitions of the Arctic are in currently in use (Depledge and Kennedy-Pipe, 2020), with no single agreed-upon definition of the Arctic . Environmental definitions of the Arctic, defined in terms of vegetation type (Walker et al., 2002; Raynolds et al., 2019), sea-ice cover, permafrost cover or climate , do not correspond to the geographical definition of the Arctic as the area north of the Arctic circle (66.5 °N) (Callaghan et al., 2005), or political (highly contextual)

definitions of the Arctic (University of Lapland). Herein, we think of the Arctic as a bioclimatic region, one with tundra vegetation which is covered by snow for at least 6 months of the year (approximately as defined by Meltofte et al., 2013), and thus not strictly only above the Arctic Circle. Environments matching this description that lie south of the Arctic circle are sometimes termed "Sub-Arctic" (e.g. Sub-Arctic Tundra; Hobbie et al., 2021).

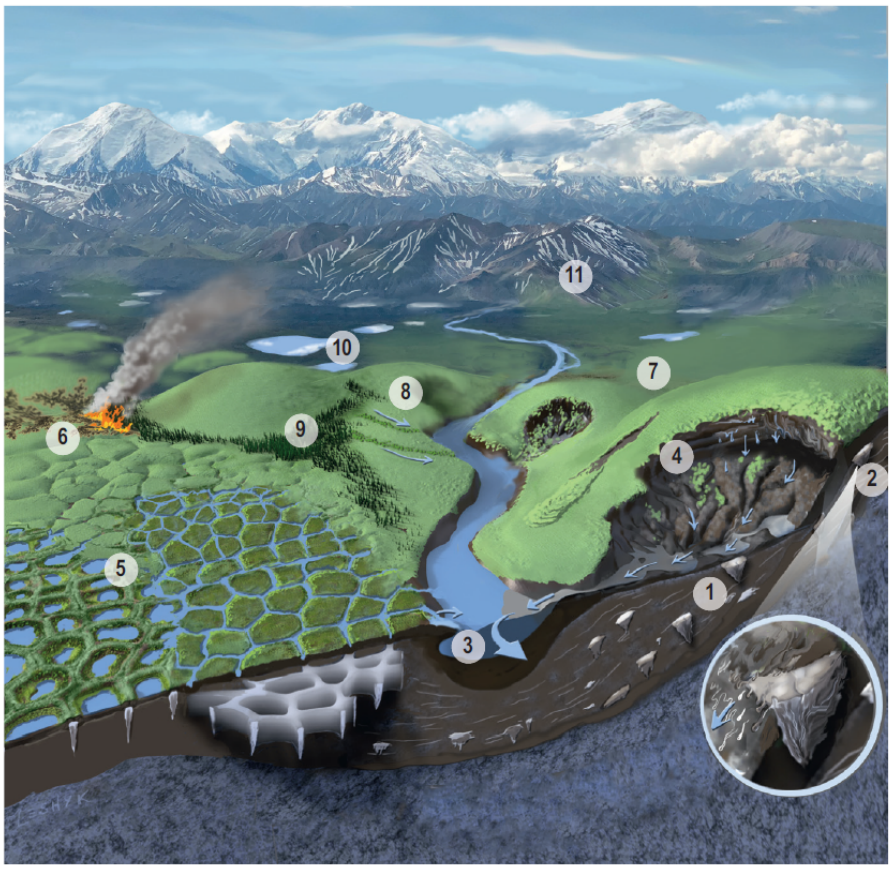

Figure 1: Land surface processes and elements involving the terrestrial Arctic cryosphere: 1) permafrost; 2) land ice; 3) river discharge; 4) abrupt thaw; 5) surface water; 6) fire ; 7) tundra ; 8) shrubs; 9) boreal forest ; 10) lake ice; 11) seasonal snow. All but 3), 6) and 10) are referenced in this thesis[2]. Figure from IPCC (2022).

The area of land north of the Arctic treeline covers almost 5% of the Earth's surface (Meltofte et al., 2013), with Arctic tundra covering an area of approximately 7.5 million km^2 (Bliss and Matveyeva, 1991). Tundra environments, defined in the Circumpolar Arctic Vegetation Map (Walker et al., 2005, p.268), are places with "low-growing vegetation beyond the cold limit of tree growth, both at high elevation (Alpine tundra) and at high latitude (Arctic tundra)". Shrub

[2]CO_2 can be released from aquatic environments within the terrestrial Arctic, likely during the winter and from under ice, but this is beyond the scope of this study.

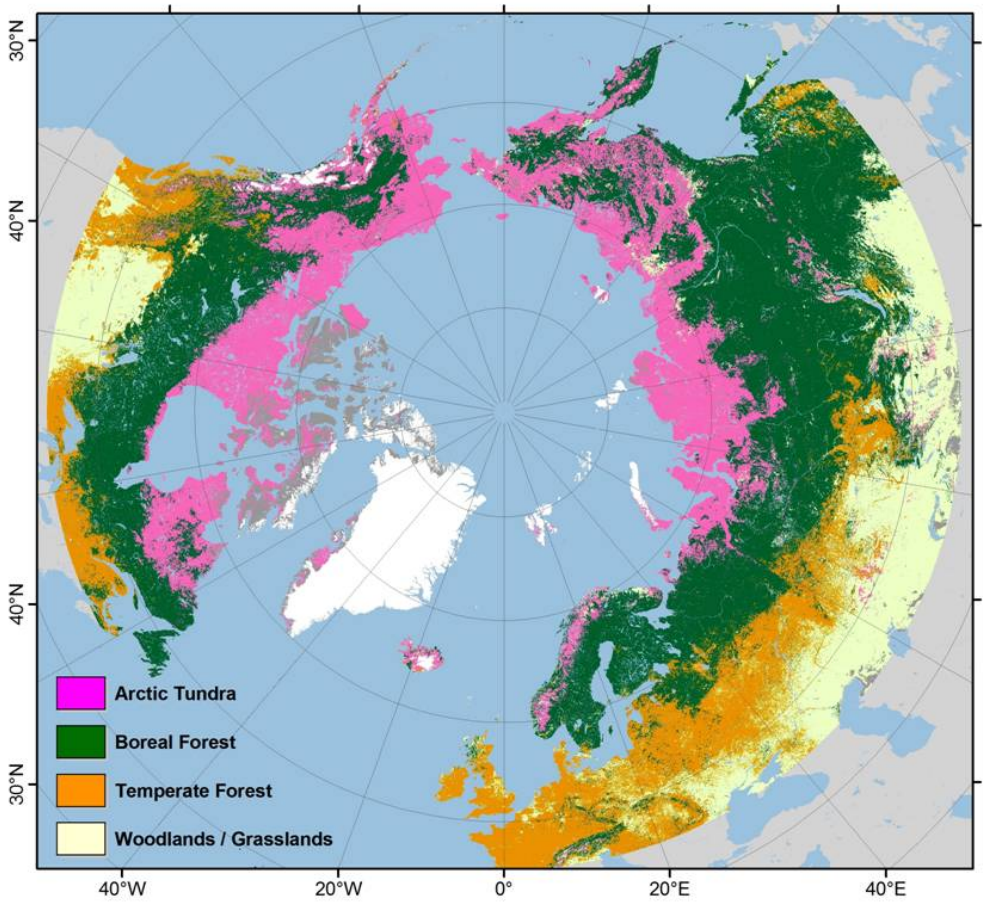

Figure 2: Biomes of the Northern Circumpolar area, with the extent of the Arctic tundra shown in pink. Sub-Arctic tundra, as defined by Hobbie et al. (2021) is also included within this definition of Arctic tundra. Figure from Bonanza Creek Long Term Ecological Research Station.

tundra environments make up a large proportion of the terrestrial Arctic. Broadly speaking, these environments are described as having 5 - 100% plant cover, with the density of plant cover decreasing from South to North (Nadelhoffer and Geiser, 2011); plant cover is dominated by shrub, dwarf shrub and cryptogram species (Walker et al., 2005). Arctic tundra environments have long cold winters, and short cool summers (Nadelhoffer and Geiser, 2011); mean summertime temperatures within Arctic shrub tundras vary from 6 - 12 °C, whilst in winter average temperatures may be as low as -34 °C . Annual precipitation is typically between 10 - 50 cm (Nadelhoffer and Geiser, 2011). Arctic tundra is typically underlain by continuous permafrost (Hobbie et al., 2021), frozen soils that store vast amounts of carbon.

Shrubless tundra environments are present in the high Arctic, but as $\sim$ 95% of Arctic tundra

falls into one of the 4 shrub-containing tundra sub-classes (Walker, 2002), this thesis focuses on shrub tundra. Additionally, non-shrub tundra is only present in the most northerly regions of the Arctic tundra, where conditions are less likely to be conducive to wintertime CO_2 emissions. Shrub tundra environments are changing under climate change, both in terms of their geographic extent (Kaplan and New, 2006), including northward expansion into historically shrubless areas (Tape et al., 2006), and changes in the community composition (Wookey, 2008) (see Section 2.2.3).

Arctic and sub-Arctic regions store more than half of Earth's soil carbon (Schuur et al., 2015), with the Arctic containing the world's largest store of terrestrial carbon (Euskirchen et al., 2022), which is stored within perennially frozen soils known as permafrost. Significant permafrost thaw is expected to result from and further contribute to current anthropogenic climate change (Section 2.2.3), so understanding the role of carbon in Arctic systems is important in helping us to understand, prepare for and potentially mitigate against of climate change.

Snow cover is a critically important feature of Arctic environments (Bokhorst et al., 2016) (Section 2.1), with the snow-covered season typically lasting for 7-10 months of the year (SWIPA, 2017). Biological processes continue throughout the snow season (Olsson et al., 2003), although logistical constraints have limited their study and hindered our understanding of carbon exchanges at this time. Changes to snow cover, in terms of snow depth, duration and extent are predicted with climate change (Section 2.2.3) and have already been observed in some parts of the Arctic. Such changes have an impact on permafrost, impacting ground temperatures and potentially affecting carbon release. An improved understanding of wintertime processes will help us to better quantify annual cycles and budgets of carbon, and aid in predicting how carbon cycling is likely to react under rapid Arctic climate change.

The Arctic includes the ancestral homelands of at least 40 different indigenous nations (Depledge and Kennedy-Pipe, 2020), with shrub tundra vegetation of key cultural significance for many of these groups (Kaplan and New, 2006). Climate change is likely to have major ecological and socioeconomic consequences in the Arctic (Kaplan and New, 2006), with observed (predominantly negative) impacts on human well-being and livelihoods, particularly for Indigenous people (IPCC, 2021). However, research on the societal implications of future climate change in these regions is limited (Ancin-Murguzur and Hausner, 2020). Improving our understanding and modelling capac-

ities of Arctic processes may enable people to make choices about how to adapt or mitigate against changes in these ecosystems, and to be able to maintain their cultures and livelihoods.

1.2 Aims, Objectives and Research Questions

This thesis aims to improve our understanding of wintertime CO_2 fluxes in shrub tundra environments, and the influence that the snowpack has on these fluxes. In order to do this, I look to answer two key research questions:

1. How do the properties of seasonal snow cover influence wintertime soil temperatures and carbon fluxes in Arctic environments?
2. Can uncertainty in Earth System Model (ESM) simulations of Arctic carbon fluxes be reduced through improving parameterisation of the snow cover and soil conditions?

Field measurements and simulations using the Community Land Model (CLM) of both snow properties (Fig 3; Blue) and carbon fluxes (Fig 3; Red) were combined in order to answer these questions. In addition, new field measurements are also used to begin to explore processes not currently represented in CLM.

The following objectives were developed in order to address these questions:

1. Evaluate the representation of seasonal snow cover in the Community Land Model 5.0 (CLM), and the influence this has on simulated soil temperatures
2. Improve parameterisation of winter carbon fluxes from Arctic environments in CLM, through testing the sensitivity of simulated fluxes to the representation of relationships between soil temperature, moisture and respiration, and snow thermal conductivity
3. Use field measurements of snowpack properties and gas fluxes to disentangle the influence of snowpack properties on CO_2 flux, and compare these measurements to those used to evaluate model simulations

1.3 Thesis Structure

The structure of this thesis is summarised in Fig. 3. All remaining chapters are outlined in further detail below:

Chapter 2: Theoretical Background

The role of seasonal snow in Arctic tundra environments is introduced. The importance of the winter season for terrestrial carbon cycle processes is discussed, and the impact of snowpack properties on both production and transport of subnivean CO_2 is explained.

Chapter 3: Methodology

Description of Trail Valley Creek, the Arctic shrub tundra location where this study takes is focused. Field measurement techniques used to measure CO_2 fluxes and snowpack properties at this site are introduced. Background is given on simulations of seasonal snow and CO_2 fluxes using the Community Land Model (CLM5.0).

Chapter 4: Impact of Measured and Simulated Tundra Snowpack Properties on Heat Transfer

Measured and simulated snow properties are compared. Adjustments to the snow thermal conductivity parameterisation in CLM5.0 are evaluated in order to improve the representation of the snow (and soil) properties likely to impact wintertime flux, as outlined in Research Aim 1.

Chapter 5: Simulating Net Ecosystem Exchange under Seasonal Snow cover at an Arctic tundra site

CLM5.0 Simulations of soil respiration and net ecosystem exchange are evaluated using eddy covarience observations. Poor performance of the default version of the model provides the motivation for a parameter sensitivity study, where the impact of the new snow thermal conductivity parameterisation identified in Chapter 4 is tested alongside changes to soil decomposition parameters.

Chapter 6: Measurements of CO_2 Flux within Snowpacks at an Arctic Tundra site

A multitude of field techniques to measure wintertime carbon flux are compared, in part to reduce limitations highlighted in Chapter 5 of solely using measurements of net ecosystem exchange

from eddy covarience systems. Timeseries measurements using new low-cost sensors are used to explore potential trends and mechanisms for wintertime CO_2 release emissions which are currently not represented in simulations using CLM5.0.

Chapter 7: Summary and Outlook

An overview of the findings of Chapters 2 - 6. Limitations of the investigation are discussed, questions of modelling and observational approaches are raised, and avenues for future work suggested.

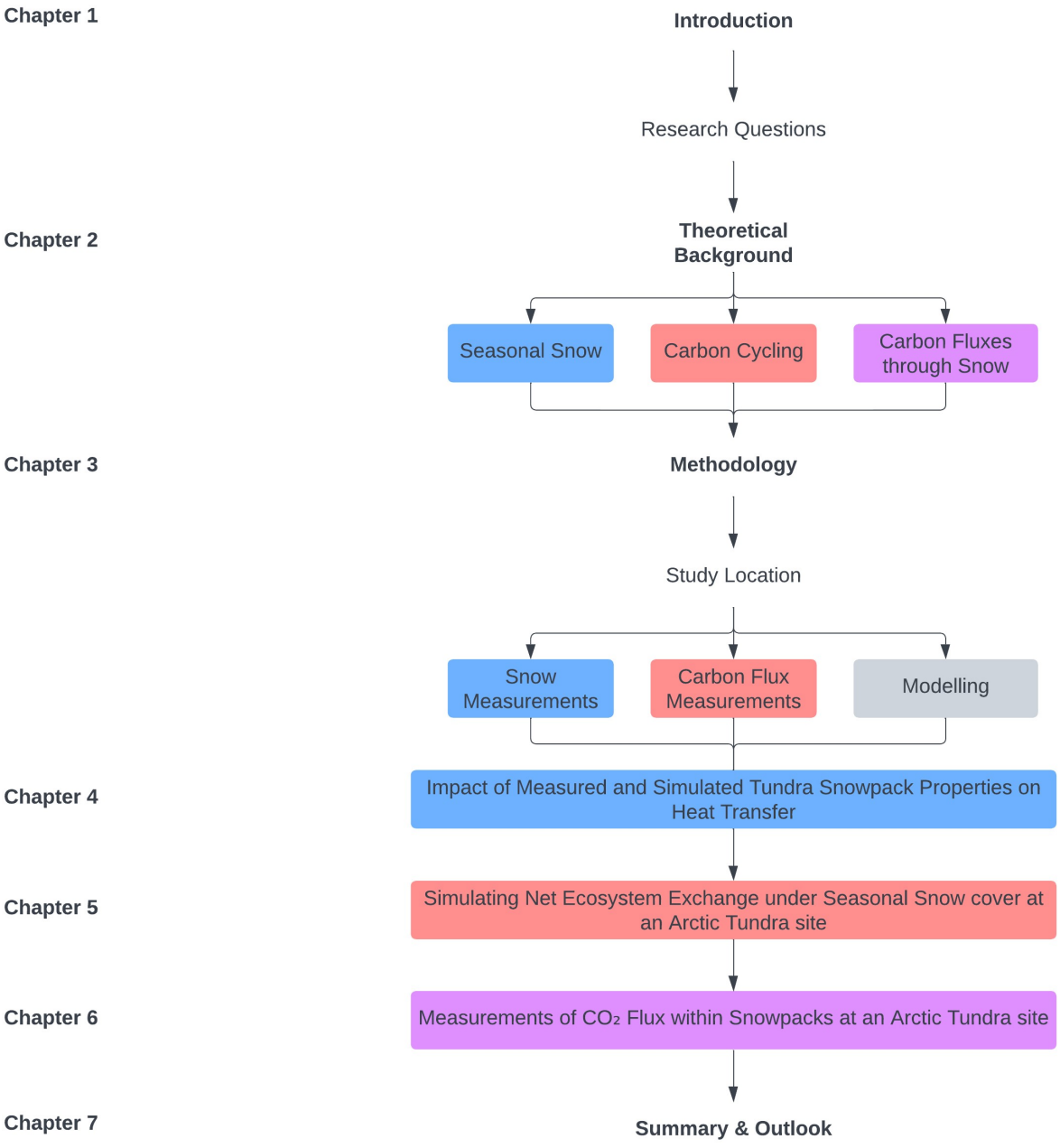

Figure 3: Summary of thesis structure. Sections in blue concern snowpack properties, sections in red look at carbon and those in purple examine the relationship between them.

Chapter 2

Theoretical Background

2.1 Overview of Seasonal Snow

2.1.1 Snow Stratigraphy

Snow is a layered medium, with new layers accumulating and evolving with each snowfall (and snow-melt) event (Pomeroy and Brun, 2001). Snowpacks in different environments vary, with different layers of different types and thicknesses (Sturm et al., 1995); herein we only discuss the properties of snowpacks in the Arctic tundra rather than reviewing the properties of all seasonal snowpacks. The environment in which snow falls has a strong control on the layering of the snowpack, and the physical properties such as density, thickness and grain morphology of the stratigraphic layers (Sturm et al., 1995). The precise sequence of the layers also has a profound effect on the physical properties of the snowpack (Colbeck, 1991). Snow is deeper in topographic depressions (Goncharova et al., 2019), such as those between hummocks. Thicknesses of different stratigraphic layers are controlled by the interplay between the subnivean environment (Rutter et al., 2019) and how snow is moved by wind over the topography (Derksen et al., 2014). Each snow layer has its own distinct microstructural characteristic (Leppänen et al., 2017) which may evolve over the course of the winter (Colbeck, 1991), such differences at our study site are expanded upon in Section 4.3.

Arctic tundra snowpacks are typically thought to be composed of three generalised layers; a thin surface snow layer (composed of recent snowfall), underlain by dense wind slab and a basal depth

hoar layer (Derksen et al., 2009). In general, insulation of the ground surface by the snow initiates a temperature gradient through the snowpack, causing a vapour pressure gradient and a "hand-to-hand" upward flux of water vapour (Yosida et al., 1955). This flux of water vapour from warm to cool leads to the creation of depth hoar (e.g. Adams and Brown, 1983; Baker, 2019; Colbeck, 1983; Fukuzawa and Akitaya, 1993; Sommerfeld and Lachapelle, 1970), as shown in Fig. 4. The formation of depth hoar is sometimes termed "constructive metamorphism" (Hall et al., 1986).

Simultaneously, strong arctic winds over the surface of the snowpack lead to the densification of the upper part of the snowpack, termed wind slab. These two archetypal layers, wind slab and depth hoar, have very different properties, and can be clearly visually distinguished as seen in Fig. 5. Wind slab layers consist of high density, compacted rounded crystals. Conversely, depth hoar layers are composed of large, weakly bonded faceted crystals with a low density. These two layers may be overlain by a thin layer of fresh or surface snow, made of up of recently deposited precipitation. This surface layer of loose dendritic crystals composes a low proportion of the snowpack ($< 20\%$; Rutter et al., 2019) and is easily blown away by strong arctic winds. The thickness of these individual layers (particularly the wind slab) controls the overall depth of the snowpack (Rutter et al., 2019).

2.1.2 Characterisation of Seasonal Snow

A snowpack can be characterised and quantified using many of its physical properties. These properties are outlined below, with their measurement described in Section 3.2. Most simply, snow can be described by its presence or absence, but a more thorough description of the properties of the snowpack is useful for considering the role of the snowcover on its surroundings. The depth of a snowpack is important in determining the mass of the snowpack (typically considered in terms of SWE; Snow Water Equivalent) and the insulation it provides to the underlying ground (see Chapter 4). Snow water equivalent is calculated as the depth of the snow multiplied by its density. After depth, density is the simplest snow property to measure, and thus is often used to characterise or derive other properties of snow (Carbone et al., 2010), such as thermal conductivity.

Both the size and shape of snow grains change over time (Baker, 2019), evolving as the season progresses through the metamorphic processes described in Fig. 4. The shape, size and arrangement

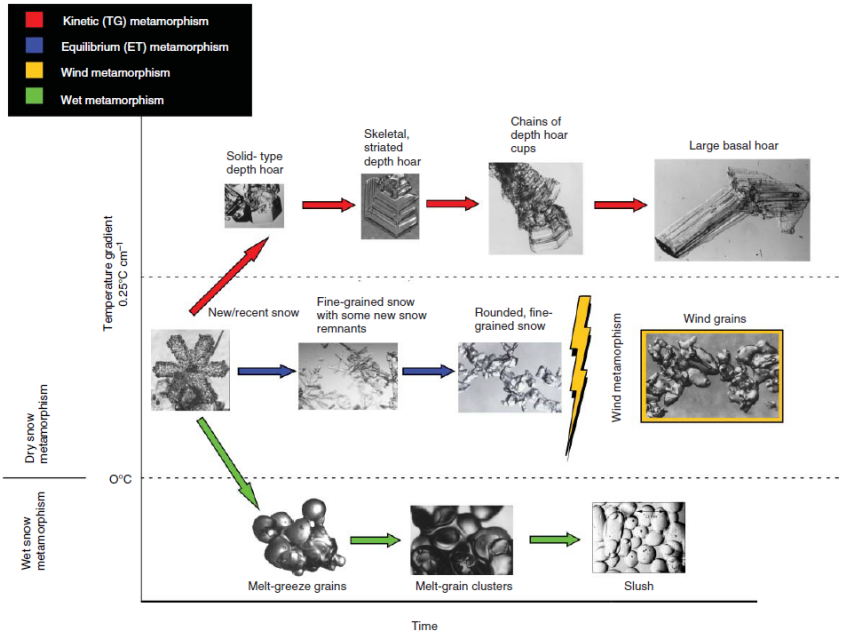

Figure 4: Different potential pathways for snow metamorphism. The formation of wind slab is denoted in yellow, and the formation of depth hoar in red. Taken from Sturm and Massom (2017).

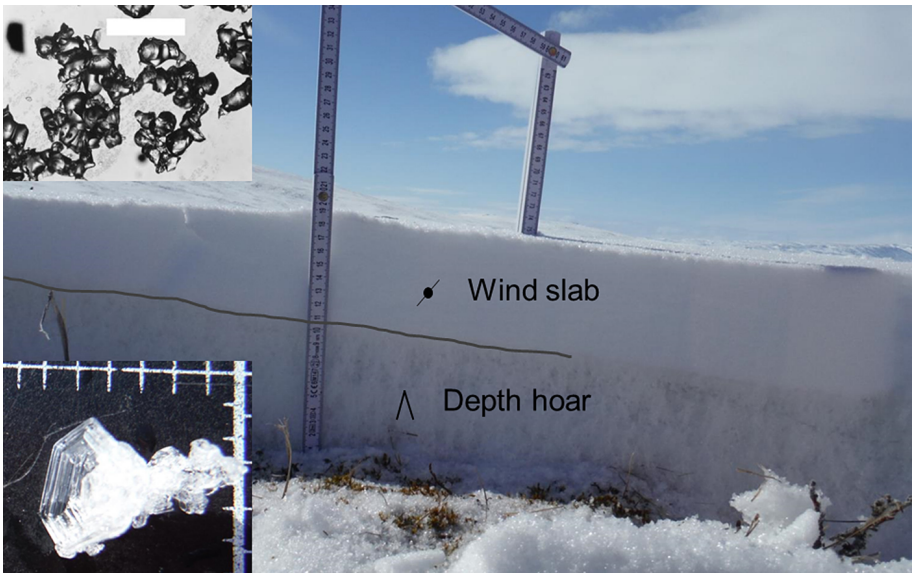

Figure 5: Photo of an Arctic Snowpack, taken from Domine et al. (2018). Symbols for each layer as per the International Classification of Seasonal Snow (Fierz et al., 2009). Insets show the size and shape of crystals in the wind slab (top left) and depth hoar (bottom left) layers.

of snow grains is termed the snow microstructure. The microstructure of snow determines many of its chemical and physical properties (Bartels-Rausch et al., 2012), including its density (Carbone et al., 2010). Relationships between density and other physical properties such as thermal conductivity exist because of complex relationships between microstructure and density (Sturm et al., 1997). Gas transport within a snowpack is also influenced by the arrangement of snow crystals (Section 2.3.1). For example, the tortuosity of a snowpack (the extent to which the space between snow grains is twisted; see Eq. 3.4) is controlled by metamorphism of snow grains, the presence of ice crusts or ice lenses, and the liquid water content of the snow (Jones et al., 1999).

The temperature of snow, both relative and absolute, and how it changes with depth throughout the snowpack, acts a control on metamorphic processes. Temperature can also influence gas transport, both directly (Section 3.3.2) and indirectly by causing changes to the snow microstructure. The conduction of heat through a snowpack is governed by its thermal conductivity. The snow thermal conductivity influences the temperature of the underlying ground, as well as temperature gradients through the snow and subsequent metamorphism. Although heat can be transferred in any direction, snow thermal conductivity typically refers to only the vertical component of this transfer, termed K_{eff} (Jafarov et al., 2014). This is discussed in more detail in Chapter 4.

Empirical relationships can be found between the thermal conductivity and density of a snowpack. Other factors, such as temperature and grain shape are also important in determining the thermal conductivity, but using density alone provides a useful first order approximation (Sturm et al., 2002). Many parameterisations have been derived to describe snow thermal conductivity as a function of density. Sturm et al. (1997) provides an overview of functions derived in the 20^{th} century, but multiple functions have been developed since as technological improvements have allowed us to examine and attempt to account for smaller scale physical processes. Most of these functions are simple quadratic formulae (as shown in Fig. 4 of Sturm et al., 1997).

For example, the parameterisation of Sturm et al. (1997) describes snow thermal conductivity as follows;

$$\begin{aligned} K_{eff} =& 3.233 \times 10^{-3}\rho^2 + 1.01 \times 10^{-3}\rho + 0.00138 \quad \text{if } 0.156 \geq \rho \geq 0.6 \\ & 0.234\rho + 0.023 \qquad\qquad\qquad\qquad\qquad\qquad\quad \text{if } \rho > 0.156 \end{aligned} \tag{2.1}$$

where ρ refers to the density of the snow in g cm^3. This relationship was derived from 488 needleprobe measurements taken in the Alaskan Arctic across a 7 year period. They find differences between the thermal conductivity of different snow types, with different equations more appropriate for snowpacks with a density above and below 0.156 kg cm^3.

Calonne et al. (2011) used μ-CT images of a wide variety of types of snow grains to derive their relationship between snow density and thermal conductivity:

$$K_{eff} = 2.5 \times 10^{-6}\rho^2 + 1.23 \times 10^{-4}\rho + 0.024 \tag{2.2}$$

Most recently, Fourteau et al. (2021a) suggest a new, temperature dependant relationship between snow density and thermal conductivity. Fourteau et al. (2021a) propose that previous assumptions about the microscale, hand-to-hand diffusion of water vapour lead to an underestimation of snow thermal conductivity by previous parameterisations. They also suggest that the parameterisation of snow thermal conductivity should vary with temperature (and provide equations for a selection of temperatures). For snow temperatures of -10 °C (approximately that experienced in Arctic snowpacks):

$$K_{eff} = 1.985\frac{\rho}{\rho_{ice}}^2 + 0.073\frac{\rho}{\rho_{ice}} + 0.0336 \tag{2.3}$$

where $\frac{\rho}{\rho_{ice}}$ is the volume fraction of ice in the snowpack. ρ_{ice} is given a constant value of 0.981 g cm^3.

As well as density, snow thermal conductivity may also be described using the thermal conductivities of ice and interstitial air, as in Jordan (1991):

$$K_{eff} = K_{air} + \left(\left(7.75 \times 10^{-5}\rho + 1.105 \times 10^{-6}\rho^2\right)\left(K_{ice} - K_{air}\right)\right) \tag{2.4}$$

where K$_{air}$ and K$_{ice}$ represent the thermal conductivities of ice and interstitial air respectively.

2.2 Overview of Carbon Cycling

2.2.1 The Global Carbon Cycle

Primary producers (chiefly plants, but also technically phytoplankton) photosynthesise, converting atmospheric CO_2 and sunlight to water and energy. This process, modelled as gross primary productivity (GPP; Green, Figure 6) removes CO_2 from the atmosphere, and is thus termed a "negative" carbon flux. Processes which increase the amount of CO_2 in the atmosphere are termed positive carbon flux (and represented using positive numbers). In the case of the terrestrial carbon cycle, this is predominately through the process of respiration. Living things convert energy (typically in the form of sugars) to carbon dioxide and water.

Respiration can be described and modelled on many scales, from individual plant components (eg. Root respiration), through the sub-environments, to the whole ecosystem (ER; Red in Fig. 6). Respiration may also be split into autotrophic[1] (AR; Yellow) and heterotrophic[2] (HR; Purple) components, with the balance of autotrophic respiration and GPP termed Net Primary Productivity (NPP; Blue). Net ecosystem carbon exchange (Net Ecosystem Exchange; NEE, Grey) is the balance of these processes of carbon uptake and release;

$$NEE = GPP - ER = GPP - (AR + HR) \tag{2.5}$$

and describes the overall change in the amount of carbon released into the atmosphere.

2.2.2 The Terrestrial Arctic Carbon Cycle

The Arctic terrestrial biosphere acts as an important global sink of carbon, contributing roughly 29% of the mean global land CO_2 sink (Liu et al., 2022). However, photosynthetic uptake of CO_2 is offset by respiration, and the magnitude of both photosynthetic and respiratory fluxes in the Arctic are somewhat contested, as described below. This complexity occurs in part due to limited consideration of the entire annual cycle of Arctic carbon fluxes. Growing season carbon fluxes in these environments have been more widely studied than those in the wintertime, largely due to reduced logistical complexities and larger daily magnitudes of flux.

[1] Autotroph: An organism that produces it's own energy through photosynthesis
[2] Heterotroph: An organism that needs to eat food to gain energy

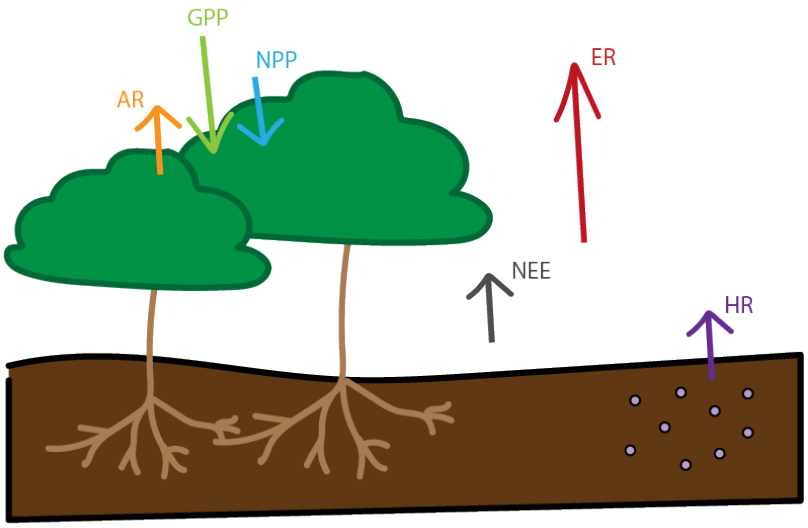

Figure 6: Abbreviations for the main component fluxes of the terrestrial carbon cycle. Acronyms are given in full below and in Section 2.2.1: AR = Autotrophic Respriration; HR = Heterotrophic Respriation; ER = Ecosystem Respriation (sum of AR and HR); GPP = Gross Primary Productivity, NPP = Net Primary Productivity (GPP - AR); NEE = Net Ecosystem Exchange (GPP - ER; Eq. 2.5).

Although carbon fluxes have been known to occur during the long, dark, cold Arctic winter since the late 1960s (Kelley et al., 1968), limited progress has been made since then in building our understanding of wintertime carbon flux. Soil respiration is the most poorly constrained global carbon flux (Knowles et al., 2016), even before accounting for limited observations and logistical challenges surrounding measurements and model validation in unique and challenging environments like the Arctic winter. Suggestions have been made that non-growing season emissions may account for up to 70% of annual CO_2 flux from tundra environments (Welker et al., 2000; Zhang et al., 2019). However, other studies suggest that photosynthetic uptake of CO_2 during the summertime may outweigh respiratory losses (Hayes et al., 2011); it is not yet known whether the circumpolar tundra acts as a source or sink of Carbon (Callaghan et al., 2005), with no scientific consensus about the sign or magnitude of the terrestrial arctic carbon budget (Euskirchen et al., 2022). Estimates of winter CO_2 release are highly uncertain and require further study, but are likely to make a significant contribution to annual carbon budgets in these environments (Natali et al., 2019).

Figure 7 shows a schematic of the annual carbon cycle in the tundra:taiga ecotone. In autumn, solar energy decreases, air temperatures get cooler, the soil starts to freeze and snow begins to

fall. As winter progresses and temperatures continue to fall the snowpack steadily builds. Strong temperature gradients within the snowpack enable the formation of distinctive wind slab and depth hoar layers (Section 2.1.1), which provide a high level of thermal insulation to the underlying soil. This is an additive process, with the insulation provided by the snowpack increasing for the rest of the season until thaw begins. Sequential soil freezing, from both the surface and the base of the active layer occurs over a number of months, with the full depth of the soil column not completely frozen until late December or January. Rates of soil respiration are thought to be at their highest in these early winter months prior to complete freeze-up (Olsson et al., 2003). In the coldest part of winter air temperatures may be as low as minus -40 °C, but soil temperatures rarely fall below about -15 °C. Such warmer conditions facilitate increased levels of soil respiration, as higher temperatures allow soil microbes to be more active. Though the daily magnitude of soil respiration may be low compared to the growing season, the 8-10 month duration of the Arctic winter means that relative contribution of this season makes up a large part of the annual carbon budget.

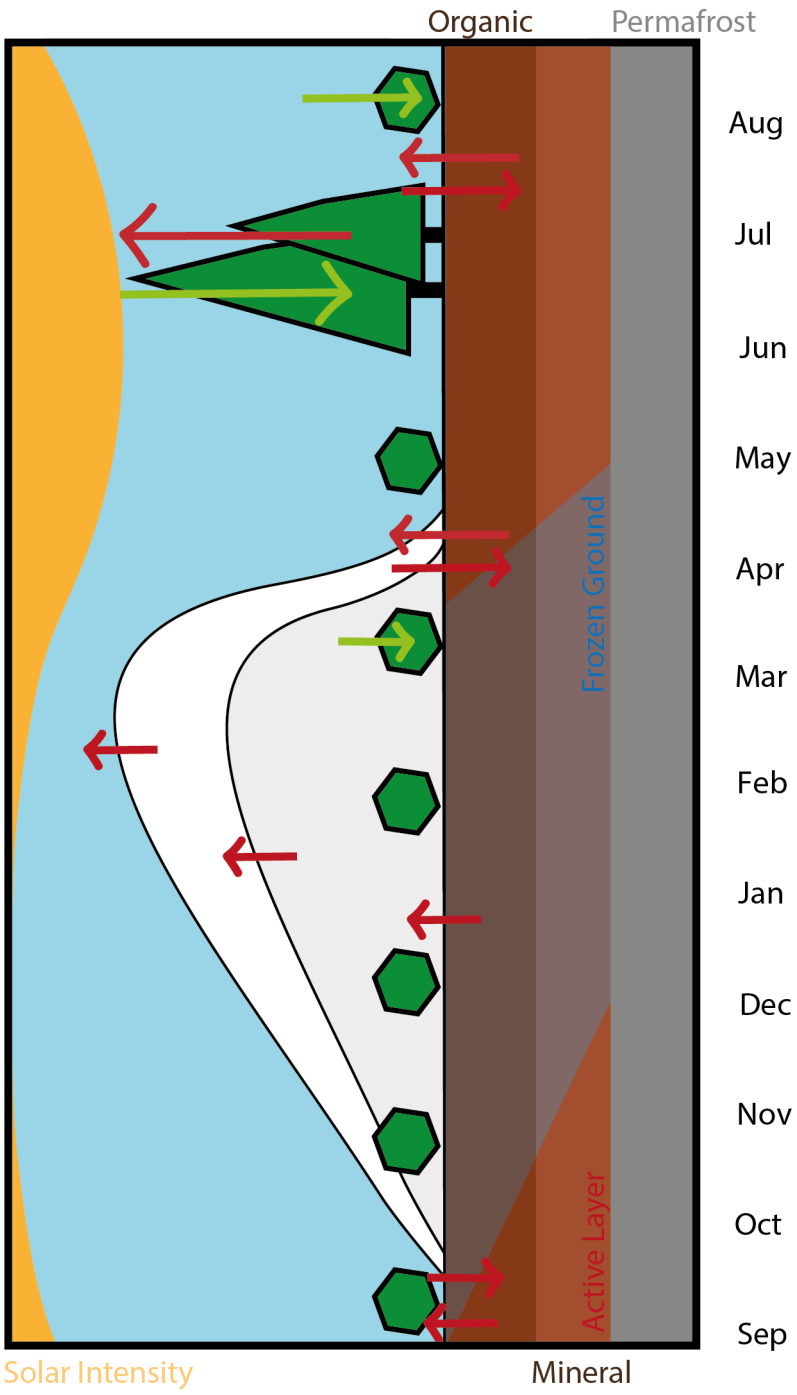

Figure 7: Schematic showing the release of CO_2 (red arrows) and CO_2 uptake through photosynthesis (green arrows) in the Arctic Tundra.

Additionally, there may be some potential for photosynthesis by lichens and evergreen plants at the end of winter and during the snowmelt period (Starr and Oberbauer, 2003; Campbell and Laudon, 2019). However, carbon flux is dominated by soil processes for the majority of the winter. After peak snow depth is reached in approximately April, the soil thaws and the snow melts far quicker than it accumulated, with the ground becoming snow-free by late May.

In order to discuss wintertime fluxes accurately, it is important to first define what is meant by the winter. Terms such as winter, the snow season and the non-growing season are often used interchangeably; different understandings of what is meant by winter have lead to considerable differences in the total season flux. Rafat et al. (2022) used 3 different parameters to define the non-growing season and found differences of approximately 25% in the average daily non-growing season CO_2 flux depending on the definition used for eddy covariance data from a Canadian peatland. For the results herein, winter is defined as the period where the ground is snow covered, unless explicitly stated otherwise. Using precipitation and the phase of water rather than a calendar definition, similar to Olsson et al. (2003), provides a clearer link to biological processes, including those controlling fluxes of carbon. Comparing studies with different definitions of winter, especially in the common case where what is meant by winter is not clearly defined, is likely to further contribute to uncertainties in wintertime carbon flux.

2.2.3 Arctic Amplification & Climate Change

Increases in atmospheric CO_2 concentrations have unambiguously been linked to rising global temperature (IPCC, 2013, 2021; Anderson et al., 2016). Atmospheric concentrations of CO_2 have risen, and are predicted to continue rising, as a result of human activities (IPCC, 2013, 2021; Friedlingstein and Solomon, 2005). The contribution of the Arctic in this, particularly in the wintertime is uncertain.

Significant warming has been observed in the Arctic over the last 30 years of the 20^{th} century (Serreze et al., 2000), and changes in many other elements of the arctic climate system have been clearly observable since the mid-1970s (Hinzman et al., 2005). Mean annual temperatures have risen by 1.5 °C relative to the period 1971-2000, with a projected further increase of 8 °C by 2100 under a business-as-usual scenario (IPCC, 2013; Overland et al., 2014). Temperature increases thus far have been particularly pronounced in winter, with winter temperatures rising by 3.7 °C

since 1971 (Box et al., 2019). Further increases in autumn and winter temperatures are expected, with 4 - 5 °C of warming above late 20th century temperatures projected before 2050 (SWIPA, 2017). The Arctic has warmed nearly four times faster than global average temperatures (Rantanen et al., 2022), and continued warming of the Arctic will exceed mean global surface temperature increases (IPCC, 2021) due to the process of Arctic amplification, regardless of future emission scenario (Post et al., 2019). A key driver of Arctic amplification is the snow albedo feedback (Thackeray et al., 2019). Decreasing snow (and sea ice) cover decreases the albedo, reducing the amount of radiation reflected back into the atmosphere; warming is faster as more radiation is absorbed (Thackeray et al., 2019). Differences in atmospheric temperature gradients at the poles and the tropics also contribute towards polar amplification, as does increased cloudiness and atmospheric humidity as a result of sea ice loss, among others (Previdi et al., 2021). A more detailed review of feedback processes contributing to Arctic Amplification is given in Previdi et al. (2021).

Arctic warming has a direct impact on the amount of precipitation falling as snow and on the timing and duration of snow cover (SWIPA, 2017). Warmer temperatures amplify the loss of seasonal snow cover (IPCC, 2021) leading to a decrease in the length of the snow season. The onset of snow cover across the Arctic is getting later by 2 days per decade (Thackeray et al., 2019), with annual snow cover durations projected to decrease by 10 – 20% across much of the Arctic (Callaghan et al., 2012). Decreases in Canadian snow covered area of up to 10% per decade are projected up to 2050 (Mudryk et al., 2018). However, in some parts of the Arctic, rising temperatures allow the air to hold more water, therefore leading to a greater amount of snowfall (Thackeray et al., 2019). Maximum snow water equivalent over much of the Arctic is projected to increase by 15% by 2050 (Callaghan et al., 2012). Such an increase in precipitation (leading to deeper snow cover) may offset a shorter snow covered season (Brown and Mote, 2009). Changes in snow properties and snow cover duration have also been observed by Indigenous communities and traditional knowledge holders at many locations across the Arctic (see Eerkes-Medrano and Huntington (2021) for a range of examples).

Arctic warming also has serious implications for the Arctic carbon cycle, due to the potential release of old carbon stores to the atmosphere as warming causes permafrost to thaw. Arctic soils hold approximately 50% of the world's soil carbon (SWIPA, 2017). Approximately 25%

of the land surface in the Northern Hemisphere (a total area of 17.8 x 10^6 km^2) is underlain by permafrost, storing 1300 PgC ± 200 PgC (Hugelius et al., 2014; Miner et al., 2022). Future permafrost loss is very dependent on future emissions but under a business as usual scenario, model intercomparisons suggest a decrease in permafrost area of between 6 and 16 million km^2, releasing a mean 340Pg of soil carbon to the atmosphere by 2300 (McGuire et al., 2018), with this feedback effect further exacerbating current climate change both in the Arctic and further afield (IPCC, 2022). Even under a more optimistic scenario (RCP4.5), a 20% decrease in permafrost area is projected by 2040 (Slater and Lawrence, 2013). The changing state of permafrost is very sensitive to the soil conditions, with only small increases in temperature needed to induce permafrost thaw in some areas. Changes to the temperature of permafrost can also result in soil moisture changes, in turn linked to changes in microbial activity and CO_2 emissions (Lawrence et al., 2015), with wetter conditions also linked to enhanced permafrost thaw (Jorgenson et al., 2010; Magnusson et al., 2022).

Changes in the climate are also reflected in a changing vegetation composition, with increasing "shrubification" of Arctic tundra (Mekonnen et al., 2021). This is likely to lead to an increase in growing season carbon sequestration (Box et al., 2019; Mekonnen et al., 2021), which may potentially offset increased CO_2 release from thawing permafrost (Schuur et al., 2009; Euskirchen et al., 2022). Changes in land cover can result in a lengthening of the growing season (Myers-Smith et al., 2020), which may also lead to increased uptake of CO_2. Tundra environments are becoming warmer (Hobbie et al., 2021), however, continued warming temperatures may lead to increased respiration as well as photosynthesis, so any such offset could be short-lived. Additionally, in other areas increased "browning" or vegetation die-back means this compensatory effect is less likely to be felt (Myers-Smith et al., 2020), and could even exacerbate carbon losses due to permafrost thaw (Euskirchen et al., 2022). Plant cover also plays a fundamental role in soil moisture and permafrost dynamics (Hinzman et al., 2005; Jorgenson et al., 2010), as well as influencing snow accumulation and spring snow melt (Thackeray et al., 2019). Changes in vegetation cover may also impact winter fluxes by inducing seasonal carryover effects (such as changes in the amount of plant matter available to be degraded in soil over winter), or by causing localised albedo and soil temperature or soil moisture changes (Bjorkman et al., 2018; Kaplan and New, 2006). With changes in winter climate conditions will come changes in winter carbon cycling.

Current levels of uncertainty and limited understanding of wintertime processes inhibits the accurate prediction of future carbon emissions, and how these are likely to evolve under climate change.

2.3 Carbon Fluxes through Snow

2.3.1 Structural Influences on Snow Gas Flux

"Significant" and "vigorous" fluxes of trace gases between snow and atmosphere occur throughout the winter (Bartels-Rausch et al., 2012; Helmig et al., 2009). Concentrations of CO_2 are typically higher within the snowpack than the overlying atmosphere (Fahnestock et al., 1998; Helmig et al., 2009). Under stable conditions it takes approximately one day to establish a stationary gas concentration profile in a porous snowpack (Pirk et al., 2016), but such conditions are rarely achieved in Arctic environments and other, non-steady state mechanisms of gas transport through snow should also be considered (Jones et al., 1999). Gas exchange between the air and the snowpack is influenced by both microscale and mesoscale meteorological processes (Clarke and Waddington, 1991; Colbeck, 1997) influencing snowpack gas concentrations through periodic release of snowpack CO_2 to the atmosphere (Seok et al., 2009).

The magnitude of this effect is unlikely to be uniform at the landscape scale (Seok et al., 2009) with the influence of wind speed on gas flux dependent on local topography. Sullivan et al. (2008) found tussock tundra was less sensitive to wind pumping than boreal forest environments when comparing two sites in the Alaskan Arctic. Although site specific factors influence the magnitude of wind pumping, its relative impact is sizable; with an additional $\sim$ 10 - 36% (Graham and Risk, 2018; Seok et al., 2009) of CO_2 released to the atmosphere over the duration of the winter season compared to diffusive CO_2 transport alone.

Wind pumping (and gas transport through the snow more generally) is influenced by the snowpack microstructure and stratigraphy. Rates of gas diffusion are dependent on snow density (Seok et al., 2009; see Section 3.3.2), thus snow microstructural features of varying densities provide different conditions for gas transport (Albert and Shultz, 2002; Proksch et al., 2016). For example, hoar layers are more prone to horizontal gas transport, particularly in windy conditions (Björkman et al., 2010b). Additionally, gases may be stored in pore spaces within the snow (Graham and

Risk, 2018; Helmig et al., 2009), with pooled CO_2 being rapidly released as snow thaws (Zhang et al., 2019). Features such as ice lenses may encourage horizontal CO_2 flux (Graham and Risk, 2018), with the permeability of ice lenses to gas fluxes dependent on how they are formed (van Bochove et al., 2001). Snowpacks with higher tortousity require gases to take a more circuitous route from soil to atmosphere, and thus impact rates of gas transport and carbon flux.

2.3.2 Subnivean Influences on Snow Gas Flux

The properties of the snow influence not only CO_2 transport but also CO_2 production through acting as a control on the soil environment. The relationship between snow thermal conductivity, snow depth and soil temperature is revisited in Chapter 4, chiefly in the context of the Community Land Model, but the theoretical basis for this and its subsequent impact on biological activity is described below.

Ecological controls on trace gas fluxes through snowpacks are not fully understood (Seok et al., 2009), though ecological processes are the main subnivean source of CO_2. Under laboratory conditions, production of CO_2 by soil microbes has been observed down to temperatures of below -40 °C (Panikov et al., 2006). Microbial respiration has been reported to occur in the subnivean environment down to temperatures of approximately -20 °C (Natali et al., 2019), with microbial biomass peaking during the winter season at some tundra locations (Williams et al., 2009). A variety of fauna are also biologically active at this time, including some species such as lemmings which overwinter within the snowpack (Domine et al., 2016b; Pruitt, 2005). Typically however, animals only play a minor role in the cycling of CO_2 (Olsen et al., 2015) and thus are herein assumed to have a negligible impact on wintertime emissions.

The presence of a snowpack acts to insulate the underlying soil. Soil temperatures at any given depth are expected to remain reasonably constant under an established snowpack (Musselman et al., 2005), as variations in air temperature are dampened by the snow. At a snow depth of approximately 20cm, soil and air temperatures become decoupled (Slater et al., 2017), though it is thought that the insulative effect provided by the snowpack may become saturated at greater snow depths (Lawrence and Slater, 2009; Zhang, 2005). The insulating effect of early-winter snow cover may keep the soil up to 50 °C warmer than the ambient air temperature (Kielland et al., 2006), although the pan-Arctic study of Zhang et al. (2018b) found an air:soil temperature

difference < 13 °C is more typical, with a mean temperature difference of 7.3 °C for sites with an air temperature of below -10 °C. Conversely, lower snow depths lead to colder soils, even at depth, with Jorgenson et al. (2010) finding a 2 °C reduction in 2 m soil temperatures with a 30% decrease in snow depth. The insulative capacity of snow is not controlled by depth alone; two snowpacks with the same depth can have different thermal conductivities (and thus a different effect on the underlying soil) depending on their stratigraphic properties.

Rates of soil respiration are strongly related to soil temperature with higher soil temperatures allowing for greater levels of soil respiration, leading to a higher production of CO_2. Elberling (2007) found approximately 90% of variation in soil respiration was due to a change in soil temperature. Alternately, when snowpacks are shallower and have a higher thermal conductivity, the temperature of the soil is reduced. A drop in soil temperature drop from -5 °C to -11 °C causes CO_2 production to decline by an order of magnitude (Zhang et al., 2018a). Additionally, although rates of soil respiration are lower than during the growing season under winter temperatures, the sensitivity of decomposition to changes in temperature (usually expressed in terms of Q10; the change in reaction rate for a 10°C change in temperature) is often higher for these lower temperatures experienced outside of the growing season (Azizi-Rad et al., 2022), i.e. smaller changes in temperature lead to a greater change in the amount of CO_2 produced when soils are cold.

Warmer soil temperatures due to snow insulation also have a secondary impact on unfrozen soil moisture, with warmer soils having more unfrozen water available for microbes to use in respiration (Azizi-Rad et al., 2022). CO_2 production in frozen soils is dependent on moisture availablity (Öquist et al., 2009). Liquid water remains available in films around soil particles as soils freeze as well as in small pore spaces (Hayashi, 2013). Soil microorganism activity within these films is sustained below subzero temperatures, particularly in soils insulated by persistent snow cover (Henry, 2007). Furthermore, increased snow depth provides more moisture to deeper soils, increasing annual respiration (Björkman et al., 2010b).

Microbial respiration in soils is more sensitive to the shift from frozen to thawed conditions than differences in the absolute temperature of frozen soils (Clien and Schimel, 1995), as different factors control respiration in frozen and unfrozen soils (Sullivan et al., 2008). Despite the harsh conditions they experience, bacterial populations in Arctic soils do not appear to be much lower than those of temperate soils and fungal biomass is higher than that of some temperate environ-

ments such as moorlands (Bliss et al., 1973). Microbial populations are highly variable throughout the winter season (Campbell, 2019), though most of the biomass under snow is dominated by fungi (Björk et al., 2008; Haei et al., 2011; Schadt et al., 2003). Factors such as nutrient availability and temperature influence microbial community compositions (Arndt et al., 2020), with "notable" differences in microbial communities between frozen and unfrozen soils (Buckeridge et al., 2013). Altered snowpack conditions can also affect the structure and dynamics of soil microbial communities (Aanderud et al., 2013; Zinger et al., 2009). A relationship likely exists between rates of biogeochemical cycling and the composition of microbial communities, with the findings of McMahon et al. (2009) showing greater carbon uptake by fungi than bacteria in late winter for Alaskan tundra soils. Additionally, changes in the rate of soil respiration with temperature (Q10) are likely due to changes in the microbial composition of the soil (Tong et al., 2021; Schmidt et al., 2008).

Changes in the depth and timing of snow cover can have significant implications on regional biogeochemistry (Lupascu et al., 2018). Deeper snows are more conductive to the growth of microbial communities, especially beyond a depth of $\sim$ 30 cm (Schmidt et al., 2008). Deep snows can alter soil nutrient availability (Zhang et al., 2019), stimulating microbial activity, and potentially leading to an increase in heterotrophic respiration (Aanderud et al., 2013). Zhang et al. (2019) found that measured CO_2 emissions increased in winters with thicker snow cover, with a threefold increase in respiration from flux tower observations seen in a year with anomalously high snow depths at their Disko Island site. Growing season conditions and vegetation patterns are influenced by snowpack conditions (Björkman et al., 2010a; Jones, 1999) which may lead to changes in carbon cycling beyond the length of the snow season (Björkman et al., 2010a; Blanc-Betes et al., 2016). Soils beneath deeper snow remain warmer even after the snow has melted (Semenchuk et al., 2015), increasing plant carbon fixation (Lupascu et al., 2018) and respiration (Lupascu et al., 2014) in the subsequent growing season.

Microbial respiration and subsequent CO_2 release is also influenced by the availability of labile (easily digestible) carbon. Areas where soils have a higher organic matter content release more CO_2 throughout the winter period (Schimel et al., 2004), as more material is readily available for respiration. Seasonal fluxes of CO_2 may be lower than initial rates as the carbon pool is depleted (Schimel et al., 2006). Microbes appear to change their substrate consumption as soils

freeze (Schimel et al., 2006), with older carbon stores more likely to be respired in winter (Lupascu et al., 2018). Additionally, nutrient cycling is dependent on the timing and amount of snow (Schimel et al., 2004), furthering the importance of snow cover properties on carbon cycling in Arctic environments. The field experiment of Rixen et al. (2008) found increased snow densities lead to warmer soil temperatures, leading to higher nitrogen mineralisation (where microbes shift their consumption from carbon rich to nitrogen rich substrates) and subsequently lower CO_2 production (Schimel et al., 2004).

Alongside biological controls on CO_2 fluxes, similar mechanical determinants of gas exchange are true of soils as described for snow in the previous section. CO_2 production and flux become decoupled in frozen soils (Sullivan et al., 2008) with either production or storage leading to an increase in the CO_2 concentration of subzero soils (Wilkman et al., 2021). Soils with a higher ice content have a lower diffusivity (Ohkubo et al., 2012; Knowles et al., 2016), trapping gas and releasing pulses of CO_2 when they crack (Schimel et al., 2006; Hayashi, 2013), which may happen either during freeze up or thaw. Estimating soil diffusivity is a major limitation for calculating carbon fluxes from seasonally frozen soils (Knowles et al., 2016).

Many questions persist surrounding the interaction between snow conditions and CO_2 flux in Arctic tundra environments. Many of the above-cited experiments take place under controlled laboratory conditions, with no temperature history to influence soil microbial activity. Model experiments allow us to examine the interaction between snow and soil temperatures (Chapter 4) and the importance of this temperature history on CO_2 fluxes (Chapter 5). Studies of the interaction between snow and soil respiration are limited to a small number of sites. In situ measurements of both snow properties and CO_2 concentrations are required to examine this relationship; new methods to both derive snow properties (Section 3.2) and measure CO_2 fluxes (Section 3.3.4) provide an ideal opportunity to attempt to advance our knowledge of CO_2 fluxes through snow.

Chapter 3

Methodology

3.1 Study Locations

3.1.1 Trail Valley Creek

Trail Valley Creek (TVC; 68°45'N, 133°30'W) is a 57 km^2 boreal-tundra transition research watershed located in the Inuvialuit Settlement Region, approximately 55 km northeast of Inuvik, NWT, Canada. TVC has an average elevation of approximately 100 m above sea level (Marsh et al., 2008) and a mean annual air temperature of -7.9 °C (for the period 1999 - 2018; Grünberg et al., 2020). Land cover at TVC predominately consists of graminoid tundra, with some lakes, small clusters of willow and alder shrubs and some isolated black spruce stands (Essery and Pomeroy, 2004; Grünberg et al., 2020; King et al., 2020b, & Figure 8). The terrain consists of mineral soil hummocks of up to a metre in diameter, and peaty inter-hummock hollows (Quinton and Marsh, 1998). The ground is underlain by continuous permafrost to a depth of 350 - 500 m (Wilcox et al., 2019), with a maximum active layer depth of up to 1 m at the end of the summer (Grünberg et al., 2020). Snow cover at TVC has a typical duration of 8 months (Pomeroy et al., 1993), with depths of 0.2 - 0.5 m, though drifts exceeding 1 - 2 m occur in areas with tall shrubs and in proximity to steep slopes (Marsh and Pomeroy, 1999). Data from 3 separate field campaigns at this site, alongside eddy covarience and meterlogical timerseries data described below, are used in this thesis. This data was collected and processed as outlined in Table 1, with the methods for data collection described in Sections 3.2 and 3.3.

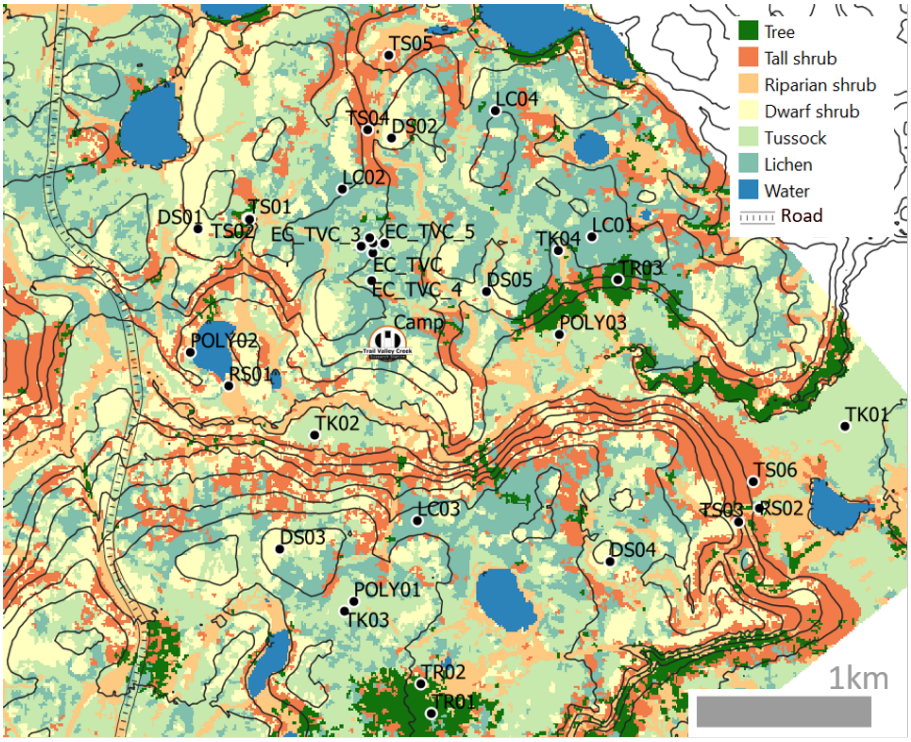

Figure 8: Land Cover at TVC, taken from Mavrovic et al., in prep. Land cover types from drone photography (Walker, 2019). Black dots give the locations of their study sites, some of which are also used as sampling locations in Chapter 6

Meteorological data measured at the TVC eddy covariance tower were used for all 3 studies herein. Half-hourly 2 m air temperatures were measured using a HMP35CF sensor (Campbell Scientific, Logan, Utah) and precipitation totals were measured using a weighted T-200B gauge (Geonor Inc., Branchville, New Jersey). Precipitation gauge under-catch is common in tundra environments such as TVC (Smith, 2008; Watson et al., 2008; Gray and Male, 1981), therefore precipitation was corrected as per Pan et al. (2016). Air temperature and relative humidity were measured at 2 m using a temperature/ humidity sensor (Vaisala HMP35CF, Vantaa, Finland). Shortwave and longwave radiation were measured at a height of 4.08 m using Kipp and Zonen CNR1 and CNR4 net radiometers. Wind speed and direction were measured at 6.1 m using an R.M. Young 05103-10 Wind Monitor. Automated snow depth measurements used were from the nearby Meteorological Service of Canada station and measured by a SR50a sensor (Campbell Scientific). Soil temperature profiles (Boike et al., 2020) were measured at 2, 5, 10 and 20 cm depths using 107B Thermistors (Campbell Scientific). Soil moisture content (Boike et al., 2020) was profiled at the same depths using CS615 soil water content reflectometers (Campbell Scientific).

Dataset	Dates of Data Collection	Collected by	Processed by
Snow Stratigraphy	Winter 2018	N. Rutter[1], C. Derksen[2], A. Roy[3], A. Royer[4], C. Vargel[4], A. Silis[2], P. Toose[2], R. Essery[5]& B. Walker[6]	V. Dutch[1]
	Winter 2019	N. Rutter, C. Derksen, A. Silis , P. Toose, J. King[2], R. Essery, B. Walker & A. Mavrovic[3]	V. Dutch
	Winter 2022	N. Rutter, C. Derksen, G. Woolley[1], R. Essery, G. Hould Gosselin[7], A. Mavrovic & V. Dutch	G. Wooley
Eddy Covarience	2013 - 2023	O. Sonnentag, G. Hould Gosselin, P Marsh[6]& M. Detto[8]	G. Hould Gosselin
Meteorology	2013 - 2023	P. Marsh, G. Hould Gosselin, B. Walker & J. Boike[9]	G. Hould Gosselin & B. Walker
CO_2 Profiles	Winter 2022	V. Dutch, A. Mavrovic & P. Mann[1]	V. Dutch
CO_2 Isotopes	Winter 2022	V. Dutch & P Mann	V. Dutch, S. Modestou[1]& P. Mann
Low Cost CO_2 Sensors	Winter 2022	V. Dutch, P. Mann & A Mavrovic	V. Dutch

1 Northumbria University, UK 2 Environment and Climate Change Canada, Canada 3 Université du Québec à Trois-Rivières, Canada 4 Université de Sherbrooke, Canada
5 University of Edinburgh, UK 6 Wilfred Laurier University, Canada 7 Université de Montréal, Canada 8 Princeton University, USA 9 Alfred Wegener Institute, Germany

Table 1: Summary of data from Trail Valley Creek used in this thesis. Institutional affiliations are given as footnotes.

3.2 Snow Measurements

3.2.1 Snowpits

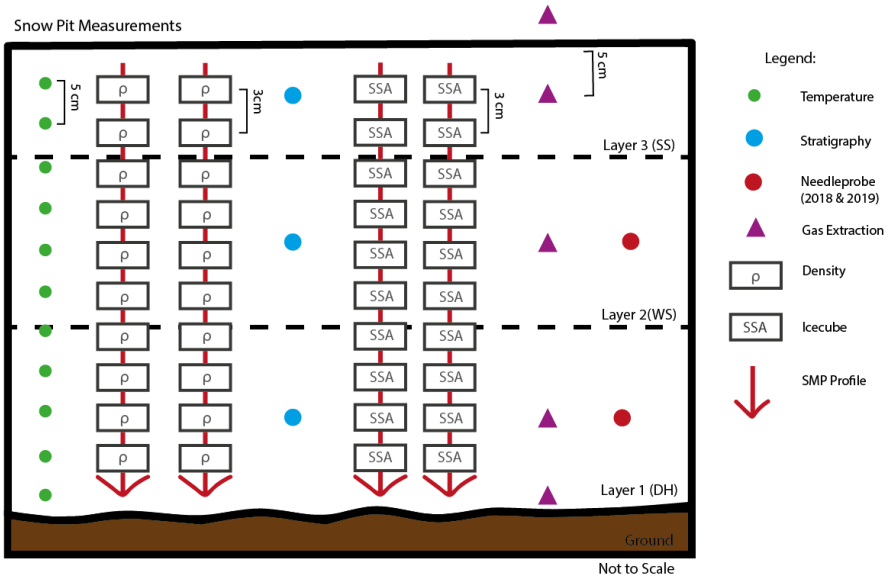

Figure 9: Snowpit sampling diagram, showing all types of measurement which may have been taken at any given snowpit. Not all techniques were used at all locations; no needleprobe data are available for winter 2022 due to instrument failure.

Characterisation of the snowpack was undertaken through traditional snow pits. Profiles of stratigraphy, density and temperature were made in each pit following Fierz et al. (2009), as shown schematically in Figure 9. Stratigraphic layers were visually determined and confirmed using hand hardness tests. Specific Surface Area (SSA) was also measured using an IceCube instrument (Gallet et al., 2009) alongside grain size observations in 2018 and 2019 and for some of the 2022 snowpits. Profiles of snow density were made in each snowpit at a 3 cm vertical resolution using a 100 cm^3 box cutter, after Conger and McClung (2009).

Pit locations in the footprint of each tower were chosen to cover the variability in the measured snow depth and land cover types (Fig. 8). Snow depth measurements were taken using a magnaprobe in spiral around the TVC tower in order to characterise the statistical distribution of snow depth in the study area. These were then used to decide on a small number of sites with snow conditions which captured small scale spatial variability for isotopic measurements. Snow depths were also measured at all gas sampling sites, with the depth of the wind slab:depth hoar interface

estimated using a two thirds: one third ratio as described at TVC by Rutter et al. (2019) at sites where snowpits were not dug.

Profiles of snow thermal conductivity were taken in the March 2018 and 2019 sampling campaigns using a TP02 needle probe (Hukseflux, Delft, Netherlands). This instrument consists of a long needle which undergoes heating and cooling cycles. The difference between the measured and expected temperature of the needle is then used to compute the conduction of heat away from the needle and through the measurement medium. More detail is given in Morin et al. (2010). However, underlying assumptions and practical limitations lead to uncertainty in the final measured value of K_{eff} (Section 4.2).

3.2.2 SMP

Spatially distributed Snow MicroPenetrometer (SMP; Schneebeli and Johnson, 1998) profiles were measured across the TVC sub-catchment. The SMP provides vertical profiles of penetration resistance at 40 µm resolution (Proksch et al., 2015). From these, profiles of other snow microstructural properties, chiefly density, can be derived at a much higher vertical resolution than is possible to measure using traditional snowpit methods. However, coefficients needed to provide an accurate density from microstructural metrics provided by the SMP are influenced by the type of snowpack (and the model of the SMP), and so new coefficients needed to be derived for tundra snowpacks for this study. Once recalibrated, SMP-derived densities can then be used to derive additional snowpack properties, such as thermal conductivity (Section 4), porosity and tortuosity (Section 3.3.2).

Bespoke coefficients to convert SMP force measurements to density were calculated for tundra snowpacks based on the methodology of King et al. (2020a) to derive high vertical resolution snow density profiles from the SMP force profiles from the March 2018 and 2019 field campaigns, with these coefficients were also applied to SMP force profiles from the Jan 2019 and March 2022 campaigns. This method is described in detail in Figure 10.

Co-incident SMP profiles and snowpit density measurements were available at 36 locations across the TVC catchment. A K-folds process is then used to derive new coefficients ($\boldsymbol{a} - \boldsymbol{d}$; Table 2) for Eq. 3.1 (Eq. 9 in Proksch et al., 2015):

$$\rho_{SMP} = \boldsymbol{a} + \boldsymbol{b} ln\tilde{F} + \boldsymbol{c} ln\tilde{F}L + \boldsymbol{d}L \tag{3.1}$$

where $\tilde{F}$ is the median force value over the vertical distance where density is calculated and L is the element size, the distance between points where force is exerted by the SMP - approximately the distance between snow grains (Löwe and van Herwijnen, 2012). Individual pairs of SMP derived and snowpit measured densities above the 95th percentile of absolute error were removed (Fig. 10 – Step 7), and the K-folds recalibration repeated (Step 8) to produce revised coefficients to recalibrate the entire SMP dataset (Step 9). This process was iterated until paired SMP-snowpit profiles with an R^2 of less than 0.7 were removed. Poor fitting between some paired SMP-snowpit profiles was due to the spatially heterogeneous nature of the snowpack (King et al., 2020a), as microtopographic variation in hummocky tundra can lead to considerable sub-metre snowpack variability. Coefficients (Table 2) were ultimately derived from 21 paired SMP-snowpit density profiles; 16 from the January 2019 campaign, and 5 from the March 2019 campaign (R^2 = 0.88, p < 0.001). These coefficients give a RMSE of 25.2 kg m^{-3}, compared to an RMSE of 125 kg m^{-3} for those of Proksch et al. (2015).

Prior to recalibration, negative force values were removed from the SMP profiles. These are erroneous values which can occur in the SMP output when ice gets caught in the cog wheel of the SMP or if part of the instrument is damaged (Lutz, 2009). Buried vegetation may also be present in the lower part of tundra snowpacks, and interaction between SMP and dense shrubs or branches may cause the SMP signal to overload and affect the quality of lower sections of the profile. A normalised percentage depth scale (with profiles rescaled to a resolution of 0.25% of total depth using linear interpolation) was used to compare SMP-derived profiles of density and K_{eff} from different snow depths (Steps 15 and 18). Any negative densities or resulting thermal conductivities were removed during the depth normalisation process.

Recalibrated density profiles from the SMP do not produce values below 200 kg m^3, despite obser-

	a	***b***	***c***	***d***
Proksch (2015)	420.47	102.47	-121.15	-169.96
King (2020b)	312.54	50.27	-50.26	-88.15
This Study	*307.36*	*43.51*	*-38.95*	*-79.36*

Table 2: Coefficients used to calculate density from SMP measurements.

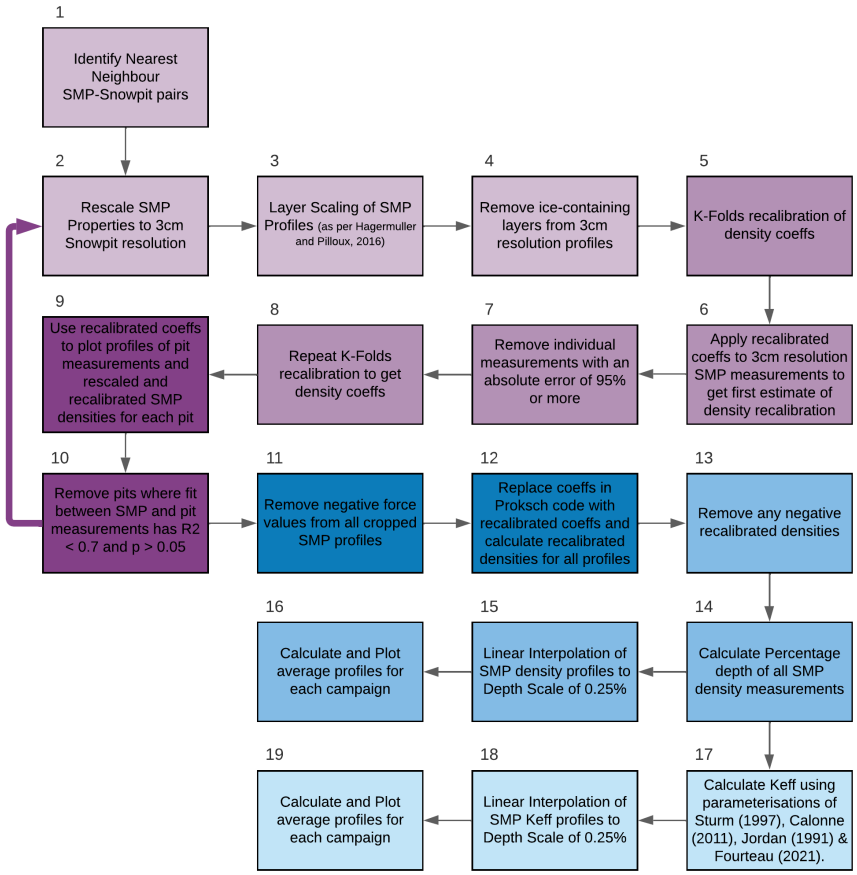

Figure 10: Recalibration process for SMP densities. Steps 2-9 (purple) mirror the process of King et al. (2020a), with Step 10 providing a quantitative threshold to assess whether the recalibration attempt is successful. Steps 11 to 19 (blue) apply the recalibration to the TVC dataset and derive thermal conductivity profiles from the recalibrated SMP densities.

vations of lower snow densities in Arctic depth hoar. Figure 11 shows a large spread in the value of L for the depth hoar samples, over a relatively small set of snowpit densities. Large element sizes, or distances between snow grain failures, are not unexpected in depth hoar but this results in a low signal to noise ratio (King et al., 2020a). Additionally, Fig. 11 shows the relationship between $\tilde{F}$ and L is not heteroscedastic as initially assumed, leading to an overestimation of the density (and density-derived K_{eff}) of this layer. Proksch et al. (2015) state that their model does not yet fully account for the anisotropic structure of some snow types, which is of particular relevance to depth hoar.

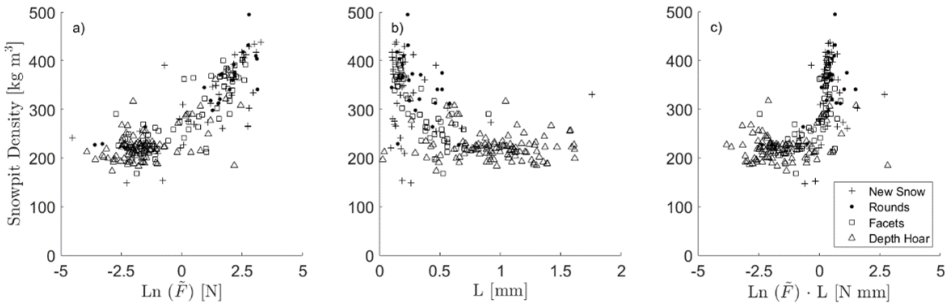

Figure 11: Relationships between the snowpit densities and SMP microstructural metrics from the paired profiles in the recalibration dataset, after Figure 5 of King et al. (2020a)

3.3 Carbon Flux Measurements

Although difficult, measurements of wintertime carbon flux are important in determining the annual carbon budget of the Arctic (Euskirchen et al., 2022). Different methods used to measure CO_2 efflux may result in calculated winter season fluxes that differ by of up to two orders of magnitude (Björkman et al., 2010b). Despite such variability, there is no clear "best technique" due to the different limitations of each method (Björkman et al., 2010a; Wilkman et al., 2021). In this section, the techniques used in this study to measure fluxes or concentrations of CO_2 at TVC (eddy covarience, profiles of diffusive flux and isotopic ratios, and low-cost CO_2 sensors) are described in turn, finishing with Table 3 to provide an overview of the merits and disadvantages of each. It is important to note that these methods do not all measure exactly the same thing; for example, eddy covariance measures the atmospheric boundary layer and the other three methods measure gases within the snowpack. Other methods may also be used to measure or quantify wintertime

carbon fluxes, such as the use of soda lime traps (Nobrega and Grogan, 2007), chamber studies (Virkkala et al., 2017), and snow fence experiments (e.g. Welker et al., 2000; Semenchuk et al., 2015; Morgner et al., 2016). However, these methods typically require a longer sampling period (soda lime, snow fences), a high level of supervision (chamber studies) or the destruction of the snowpack (most chamber studies, although some are occasionally placed on the snow surface) and were therefore unsuitable for this study.

3.3.1 Eddy Covariance

Eddy covariance (EC) measures the transport of gases between the land surface and the atmosphere. This micrometerological technique is based on the principle of atmospheric eddy transport, as represented in Figure 12. Each eddy moves an air parcel with different properties (e.g. gas concentration, humidity), and as the eddy passes the tower, the properties of the parcel of air it is transporting (either upwards or downwards) are measured using an Infra-Red Gas Analyser. Additionally, a sonic anenemometer on the tower measures the wind speed, in order to derive the speed of eddies, and whether the gas is moved upwards or downwards. Knowledge of the concentrations and speed and direction of the air parcels gives us the flux of the gas.

Measurements are taken at a very high frequency (typically 10 - 20 Hz) in order to be able to capture the movement of the smallest eddys. These measurements are averaged to a half-hourly frequency in order to account for the motion of larger eddys.

However, in order to calculate fluxes of gas concentration from eddy transport, a large number

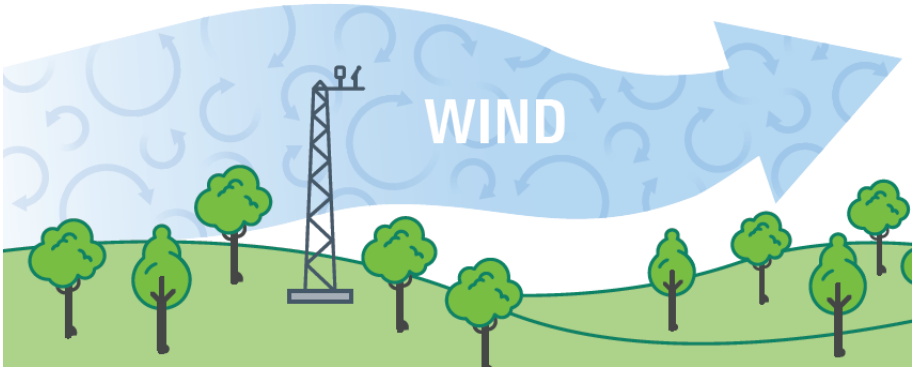

Figure 12: Atmospheric eddy transport past an eddy covarience tower. Eddys of different sizes rotate at different speeds, so fluxes are intergrated over window in order to account for the motion of all sizes of eddys. Taken from Burba (2022).

of assumptions need to be made. Firstly, the atmosphere is assumed to be turbulent, such that the motion of eddys is the dominant mode of transport. EC tower measurements taken under stable or stratified atmospheric conditions, such as commonly occur at nighttime or during the dark Arctic winter, are therefore subject to considerable uncertainties. Additionally, atmospheric density fluctuations are assumed to negligible, which again does not strictly hold under stratified or inverted atmospheric conditions caused by strong negative temperature gradients between ground surface and atmosphere. Atmospheric stability also leads to changes in the footprint of the EC tower (Burba and Anderson, 2005), increasing uncertainty about the area being measured and thus the magnitude per m^2 of the derived fluxes. Further assumptions include uniform, horizontal terrain and that the movement of air is not disrupted by the EC tower setup. Deviation from these assumptions, when known, can be accounted for through the use of various corrections, although this does add to the measurement uncertainty (See Appendix A.2).

Many limitations surround the collection and interpretation of wintertime EC data. Measurements in the deep winter (December - February; Olsson et al., 2003) are unlikely to be complete and may not be reliable. Data loss due to power issues is common; many difficulties are presented in maintaining a constant power supply at a remote Arctic fieldsite during periods of 24 hour darkness and extreme cold. Icing of the instrument, where the open-path (i.e. the path length of the instrument is exposed to the elements) sensor becomes blocked by rime or precipitation, temperatures below the specification of the instrument, and stable atmospheric conditions impact data quality and further contribute to data uncertainty at this time. Heat generated by open-path instruments may also induce convection and cause erroneous results (Lafleur and Humphreys, 2008) – however in our case this is likely to be lessened as instruments are not heated. Additionally, Pirk et al. (2017) suggest that fluxes derived from the eddy covariance method during snowmelt may be subject to sizable biases due to increased surface heterogeneity (i.e. patchy snow cover) and subsequent variable surface roughness lengths in the tower footprint.

3.3.2 Gas Profiles & Diffusive Flux

A graduated hollow stainless steel rod with holes at 5cm intervals, and two 3-way stopcocks at the end was used to extract gas samples from the snowpack (Fig. 13). A rubber bung was used to set the depth required for the sample before the rod was inserted into the snowpack. A 60ml butyl

rubber syringe was flushed three times with ambient air and then attached to the outer stopcock. The syringe was then purged, after which the gas sample was taken. The volume of the sample was noted, and then the process was repeated for all remaining sampling depths. Two profiles were taken at most sampling locations, one for the calculation of diffusive flux and one for isotopic analysis.

Concentrations of CO_2 from each snowpack gas sample used for the diffusive fluxes were measured using a LICOR LI-850 analyser (LI-COR Biosciences, Lincoln, Nebraska). The LICOR LI-850 is an infra-red gas analyser, which uses the amount of the emitted infra-red light source which is absorbed by the air sample to determine CO_2 and H_2O concentrations. To analyse the samples, a three-way stopcock was attached to the inlet valve on the LiCOR, and turned to close off the inlet valve. A sample syringe was then attached to the stopcock, the sample was slowly released, first to briefly flush the stopcock but the majority of the syringe (at least 40ml of gas) was injected into the LiCOR. Once the syringe was empty and the CO_2 concentration inside the LiCOR had stablised, this value was noted, and the syringe removed. The outlet valve was then opened to allow the sample to be expelled from the machine and the process repeated for each sample.

Diffusive fluxes (F_{CO2}) of CO_2 measured from these profiles were then calculated as per Seok et al. (2009):

$$F_{CO2} = \varphi t D_{CO2} \Delta CO_2 \tag{3.2}$$

where Δ_{CO2} equals the gradient of CO_2 concentration, D_{CO2} equals the diffusivity of CO_2 and φ and t represent the porosity and tortuosity of the snowpack respectively. The diffusivity of CO_2 (D_{CO2}) is calculated as a function of temperature:

$$D_{CO2} = (0.000001T^2 + 0.001T + 0.139)/10000 \tag{3.3}$$

where T is the mean temperature of the snowpit in °C. If snowpit temperature profiles were not available, a value of -12 °C was used. Snow tortuosity (t) is estimated from the porosity (φ) of the snowpack:

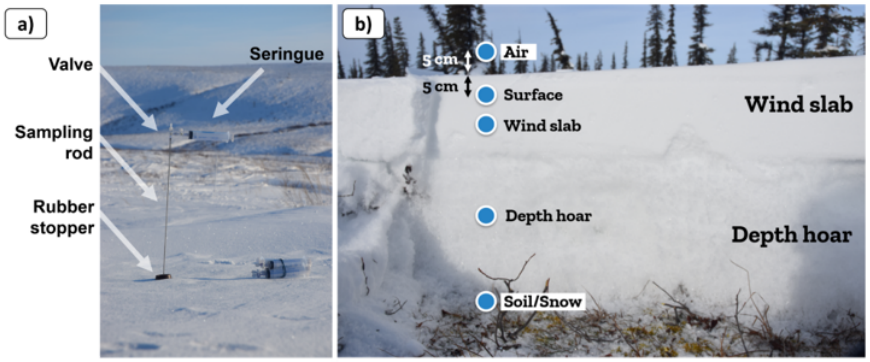

Figure 13: a) Equipment for snowpack gas profiles shown in-situ, b) Sampling protocol for snowpack gas profiles. Samples are taken from the top of the profile moving downwards towards the soil surface in order to reduce the opportunities for gas transport. Soil/Snow sample referred to as "Base" in Chapter 6 to reduce confusion with gas below the soil surface. Taken from Mavrovic et al., in prep.

$$t = 1 - (1 - \varphi)^{\frac{2}{3}} \tag{3.4}$$

which is in turn estimated from the snow density (ρ_{snow}) and the density of ice (ρ_{ice}; 0.981 kg m^{-3}):

$$\varphi = 1 - \frac{\rho_{snow}}{\rho_{ice}} \tag{3.5}$$

For profiles taken at snowpit locations, the mean value from the density cutter measurements was used for ρ_{snow}. Otherwise, mean snow densities were calculated from the nearest recalibrated SMP profiles. Snow depth heterogenities add an additional level of uncertainty to the use of the nearest neighbour SMPs in the calculation of diffusive flux (Section 6.3.7). The same approach was also taken to calculate diffusive fluxes from the (mostly co-located) IRMS CO_2 concentration measurements and for the low cost sensors described in the following subsections.

3.3.3 Isotope Ratios

For an atom of a given element, the number or protons must remain the same, but the number of neutrons may vary. Different versions of an atom can exist where the number of neutrons in one or more of the atoms differs from that typically expected of the parent atom. These are known as isotopes. Slight changes in the mass of a molecule due to differing numbers of neutrons may cause

slight differences in the physical properties of the molecule, resulting in isotopic fractionation (Sharp, 2017). Fractionation occurs where a process (e.g. respiration) discriminates between isotopologues (versions of a compound with different isotope ratios), leading to a change in the isotopic ratio of the substance.

Ratios of different stable carbon isotopes have been used to partition measurements of NEE into their components fluxes (photosynthesis and respiration). For example, ecosystem respiration can be separated into its different constituent fluxes using the isotopic composition of CO_2 to ascertain root respiration, microbial respiration etc. (Tu and Dawson, 2005). Soil CO_2 typically has an isotopic signature between that of soil respiration and atmospheric CO_2, as soil gas is impacted by both soil and gaseous processes (Tu and Dawson, 2005). We assume, that as an intermediary between soil and atmosphere, CO_2 gas in snow will have an isotopic signature between these two end members. As the provenance of the different CO_2 isotopologues varies between air and soil, measuring the ratios of these isotopes within the snowpack gas samples should give an idea of the relative influence of atmospheric and soil processes.

In order to assess the influence of changing meteorological conditions on the origin of the snowpack CO_2, a timeseries of daily measurements of the isotope ratio of sampled CO_2 was taken at the MainMet site ($\sim$ 50m north of the EC Tower; Fig 39) for the week of the first low-cost sensor deployment (Section 6.2). A profile of gas samples was taken through the snowpack, as detailed for the diffusive flux measurements (described in Section 3.3.2). Additionally, for this site, atmospheric samples were taken at three different heights above the snow surface. After collection, gas samples were injected in 12ml pre-evacuated exetainer vials (Labco Ltd, Lampeter, UK) with a double-walled septum. These vials maintain an air-tight seal for a minimum of 12 months, allowing ample time for sample transport and analysis. Vials were over-pressured to increase the sample volume for analysis and reduce the risk of sample loss, with approximately 25ml of sample injected into each vial. This also allowed a duplicate sample to be collected from each syringe, reducing the risk of sample loss during analysis.

The same sampling method was also used to collect snapshots of the isotopic composition at the majority of the diffusive flux profile locations and the locations of the low-cost sensors. Atmospheric samples for isotopic analysis were also collected outside of our field lab in order to aid in

detecting sample contamination. On return to Northumbria, samples were stored at room temperature for 5 - 6 months prior to analysis.

Isotope ratios were measured using Gasbench Isotope Ratio Mass Spectrometry (IRMS) at the NICEST (Northumbria Isotope and Clumped geothermometry for Environmental STudies) laboratory. Mass spectrometry is a long-established technique used to measure the isotope ratios of many different types of samples and substances (Sharp, 2017). Within a mass spectrometer, samples are ionised, accelerated and then focused into a beam. Beams are deflected into a array of cups by an electromagnet, with the degree of deflection a function of the atomic mass of the ion, so that each cup corresponds to ionic beams of a certain mass (Sharp, 2017). The amount of times each cup collects an ion therefore gives the relative intensities of the different isotopologues within a given sample.

For the isotopic analysis herein, We used a Gasbench II - Conflo IV - Delta V IRMS. With this instrumental set-up, samples are run through a gasbench to separate the different species within the sample prior to analysis, theoretically allowing the isotope ratios of multiple different gases to be analysed in the same sample. In practice, this (alongside helium dilution) was mostly for the purpose of reducing isobaric interference caused by nitrogen because some nitrogen and oxygen isotopologues have the same atomic mass as CO_2. Additional information required to conform with data standards for isotope geochemistry, as laid out by Skrzypek et al. (2022), are given in Appendix B.

The use of IRMS also facilitated the measurement of CO_2 concentrations in addition to the isotopic ratios. These concentrations were compared to samples measured in the field using the LiCOR and used to derive diffusive fluxes for comparison with both LiCOR and low-cost sensor data. However, gas concentrations from continuous flow IRMS, such as that used in this study, have limited accuracy. Propagated errors were calculated as outlined in Appendix B, and are discussed in more detail in Chapter 6.2, but solely relying on concentrations from this method to calculate CO_2 fluxes would be unwise (Pers. Comm., Modestou, 2023).

3.3.4 Low-Cost Sensors

All methods presented thus far have considerable limitations (see Table 3 for a more detailed comparison), with many caveats surrounding the interpretation of eddy covariance data and gas

profiles unable to be repeat sampled leading to a very low measurement resolution. Both of these methods also require considerable start-up costs. Additionally, flux gradient methods and eddy covariance can give considerably different estimates of the magnitude of wintertime carbon efflux (Rains et al., 2016). We therefore experimented with developing, testing and deploying low-cost CO_2 sensors (Chapter 6; Pictured in Fig. 14). Commercially available CO_2 sensors are not typically rated to the temperatures experienced in the Arctic winter, and those that are come at considerable cost[1]. Additionally, the one commercially available sensor with an appropriate temperature rating was undergoing development at the time of our campaign.

Sensors were designed after Bastviken et al. (2015). Sensors consisted of a Sensiron SCD30 CO_2 sensor (Sensirion AG, Stäfa, Switzerland), which measures CO_2 concentrations, temperatures and relative humidity, soldered to an Arduino Uno r3 shield (Arduino, Ivrea, Italy). An SD card reader was also connected to the circuit board in order to store the data, with the whole system powered by 6 D-Cell batteries.

The arduinos were each housed inside an off-white watertight plastic box, with dimensions 230 x 300 x 85 mm. Boxes were pale in colour in order to reduce the potential for radiative heating below the snow surface and subsequent measurement artifacts (Lundberg et al., 2016). Holes were drilled in the lid of each box, and a waterproof gas-permeable membrane (Polyflon Technology Limited, Stafford, UK) fixed behind using rubberised paint (Plasti-Dip UK, Hampshire, UK). Dessiccant packs were added to each box prior to deployment to reduce the risk of condensation biasing measured CO_2 concentrations or damaging the sensors (as noted by Bastviken et al., 2015), and any holes in the membrane (as a result of damage during transport or previous deployment) were sealed with tape.

Two different calibrations were derived for the majority of the sensors, detailed in Appendix C.1. The same calibration (derived from a linear fit between mean measured concentrations from the Los Gatos Analyser (LGA) and each individual low-cost sensor; Cal 2 in Appendix C.1) was used for both of the low-cost sensor deployments.

In order to measure diffusive fluxes, at least two boxes were buried in the snow at each site. The upper boxes were buried slightly above the wind slab:depth hoar interface with the membrane

[1]Quoted $3750 for an eosFD sensor in July 2021, a per unit cost over an order of magnitude greater than for the low-cost sensors detailed herein

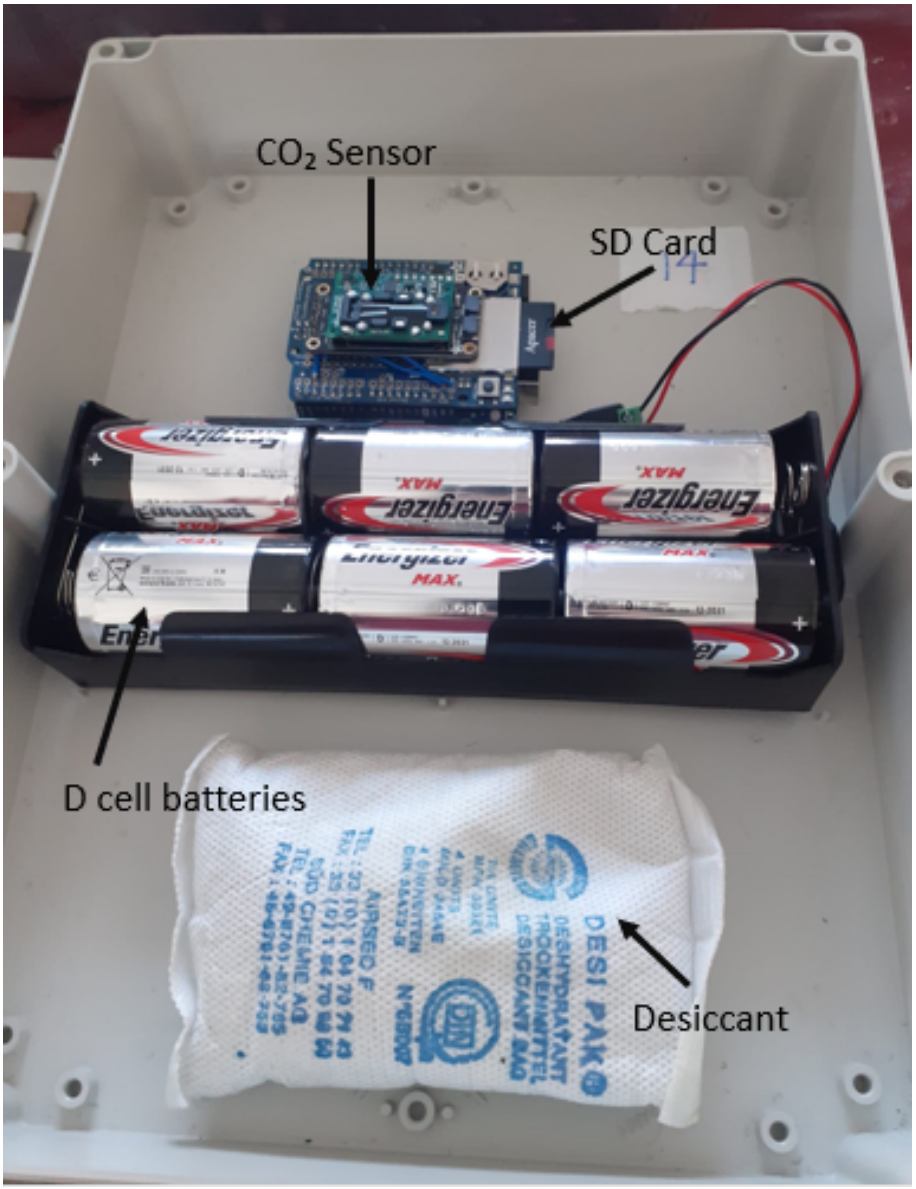

Figure 14: Photo of interior of low-cost CO_2 sensor

facing down. Although this meant that fluxes in the upper portion of the snowpack were not measured, this allowed the box to be somewhat insulated from cold and highly fluctuating surface temperatures, and thus preserved the battery life. The lower boxes were buried as close to the base of the snowpack as possible (vegetation occasionally prevented the box from being placed on the soil surface), with the membrane facing up. The flux between the two boxes (Fig 15) could then be calculated by subtracting the concentration measured at the lower box from the concentration in the upper box, and then substituting this value into Equation 3.2.

As a new, low-cost method still undergoing development, data from these sensors are subject to various uncertainties, both known and unknown. CO_2 sensors have a manufacturer specified accuracy of $\pm$ 30 ppm, which is lower than would be ideal, with differences between sensors commonly within this margin of error. Uncertainities surrounding the calibration of individual sensors (Appendix C.1) will be carried forward into measured concentrations and calculated fluxes. Bastviken et al. (2015) also note the potential for sensor drift over the course of longer deployments, although we did not notice this over the course of our experiment - likely because the longest measurement timeseries was only three weeks long. Also, the membrane was easily damaged, both during transport to the sites and during the deployments. Although holes in the membrane were patched between deployments, we cannot rule out changes in the area of the membrane (or free movement of gas through rips in the membrane) as an additional source of measurement uncertainty.

3.3.5 Intercomparison of CO_2 Methods

	Advantages	Disadvantages
Eddy Covariance	• Estabished method & protocols • No disturbance • Non-destructive measurement	• Expensive • Power intensive • Complex post-processing • High maintenance • Known data quality concerns • Inconsistent & heterogeneous footprint
Diffusive Flux Profiles	• High spatial coverage • Quickest setup • Variable vertical resolution	• Time consuming • Labour intensive • Low temporal resolution
Isotope Profiles	• Fingerprinting of CO_2 sources • High spatial coverage	• Expensive • Requires access to isotope analysis facility • Contamination of CO_2 signal by other atmospheric gases • Low temporal resolution • High uncertainities on CO_2 concentrations
Low Cost Sensors	• Cheap ($\sim$ £250) • Low power requirement • Citizen science potential • Easy to upscale • High temporal resolution • Low/no maintenance cost	• Limited precision • Sensor development is time intensive • High uncertainty and unknown unknowns • Digging snowpit disturbs original system

Table 3: Comparison of CO_2 measurement methods

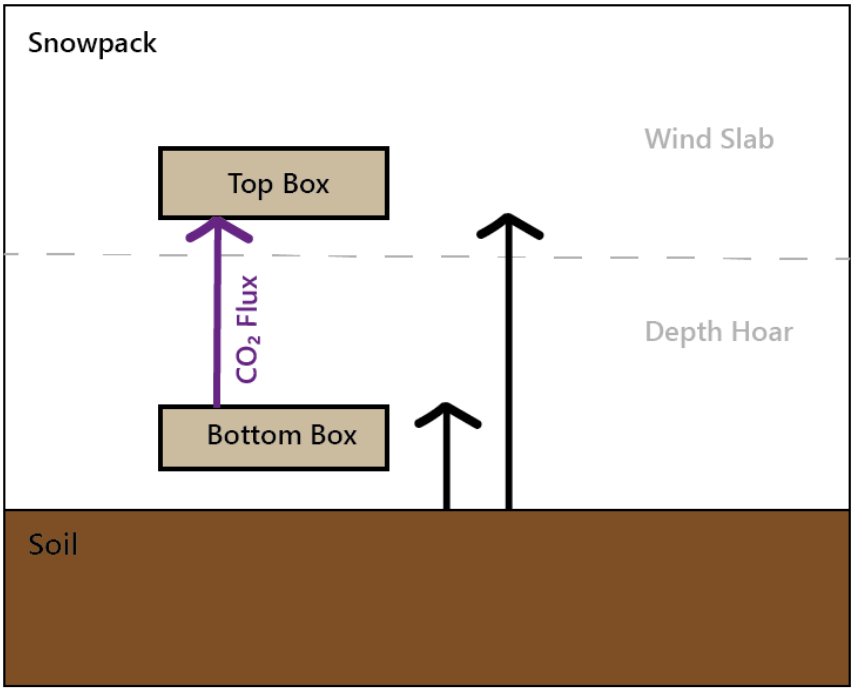

Figure 15: Schematic of Box Flux Calculation. Black arrows denote the heights of the upper and lower sensors, with the purple arrow showing the calculated CO_2 flux. Not to scale.

3.4 Modelling

3.4.1 Introduction to Earth System Modelling

Earth system models simulate the physical, chemical, and biological processes (and the relationships between these) which in turn govern global climate and potential futures under climate change (Bonan et al., 2019). Such processes are themselves represented mathematically, with equations to describe the exchanges of energy and mass between and within the different components of the earth system. Earth system models contain individual models for different components of the earth system, e.g. land, atmosphere, ocean and sea-ice (Bonan et al., 2019), and a ”coupler” to link these components.

The behaviour of Earth System Models (ESMs), and how representatively they can simulate key processes, is typically determined through comparison to other earth system models and benchmarking against observations. Different ESMs are typically made up of different combinations of component models, with differences in the parameterisation or description of some or other process. Trying to describe all these processes using a single mathematical representation is difficult (Fisher and Koven, 2020), and different modelling groups prioritise different things when building a model, leading to a large diversity between earth system models. Comparison of ESMs with observations allows the model representation and realism to be evaluated, but this is limited by the availability, frequency and quality of observational data - often a limiting factor in Arctic studies. As well as observational data, model intercomparison exercises (such as CMIP5 & CMIP6; Taylor et al., 2012; Eyring et al., 2016) can be used to understand and constrain estimates of future climate change. Additionally, such exercises allow us to evaluate the representation of individual processes and parameterisations in individual models. As all models are imperfect, model intercomparison exercises help us to constrain the uncertainty inherent in any given model prediction (Bonan and Doney, 2018).

Initially, land surface models were used as a bottom boundary condition for atmospheric models, and thus only represented basic fluxes of heat and momentum between the atmosphere and the land surface. However, the evolution of these models has allowed them to represent a large number of processes, such as shown for one such model (CLM5.0; the land surface model used in this study and described in Section 3.4.2) in Fig. 16. The range of processes simulated by any

given land surface model can range dramatically between different land surface models (Fisher and Koven, 2020), with some including human influences such as population growth and agricultural activity. Other, simpler, land surface models look solely at fluxes of water, energy and usually carbon. Crucially, most land surface models can simulate both ecological processes and biogeochemical cycling and their interplay with climatic changes. Predicting how climatic changes will influence the biosphere (and vice versa) is key for understanding how ecosystems may impact and be impacted by future change.

Models (including, but not exclusively referring to land surface models) which focus on terrestrial biosphere or ecosystem processes, such as the carbon uptake and nutrient cycling undertaken by plants, are sometimes referred to as Terrestrial Biosphere Models. As CLM pays a large amount of attention to such processes, but also examines the physics of the land surface, it may be thought of or referred to as either a Land Surface Model or a Terrestrial Biosphere Model. This distinction is elaborated on in Bonan et al. (2019). Both terms are used in this thesis, depending on the context in which CLM is discussed.

Earth system models (and their land surface components) are subject to considerable uncertainty in their representation of Arctic carbon cycling, both when considering the timing and magnitude of carbon fluxes. This is particularly true during wintertime (as discussed in Chapter 5), but different models also show variability (Euskirchen et al., 2022) or divergence from observations (Birch et al., 2021) in the timing of key events controlling growing season uptake. Many models assume zero biogeochemical activity when soils are frozen, leading to poor predictions of winter processes (Öquist et al., 2009). During the winter, model representations of snow are particularly key in determining how well climate and carbon are simulated. As snow cover modulates soil temperature, the representation of the snow and it's thermal properties is key to accurately represent the temperature of the soil (see Chapter 4) which in turn impacts simulated respiration (Chapter 5). However, no land surface models currently represent the density stratigraphy (i.e. wind slab & depth hoar layers) of Arctic snow (Marchand et al., 2018). Model parameterisations of snow properties, particularly snow thermal conductivity (K_{eff}), influence simulated carbon stocks (Wang et al., 2013), further impacting simulations of wintertime soil respiration and CO_2 flux.

3.4.2 The Community Land Model

The Community Land Model (CLM; Lawrence et al., 2019), the land surface component of the Community Earth System Model (CESM; Danabasoglu et al., 2020), is a commonly used land surface model and a major contributor to model inter-comparison experiments. CLM is one of the more complex land surface models, simulating a large suite of terrestrial processes (Fig. 16) such as hydrological cycles, biogeochemical cycling, and dynamic vegetation changes. CLM can be run on variety of spatial scales, from a 1D point to the entire earth surface, though for this study only point simulations of CLM5.0 were used, with a 0.1°x 0.1° grid cell centred on the TVC eddy covarience tower.

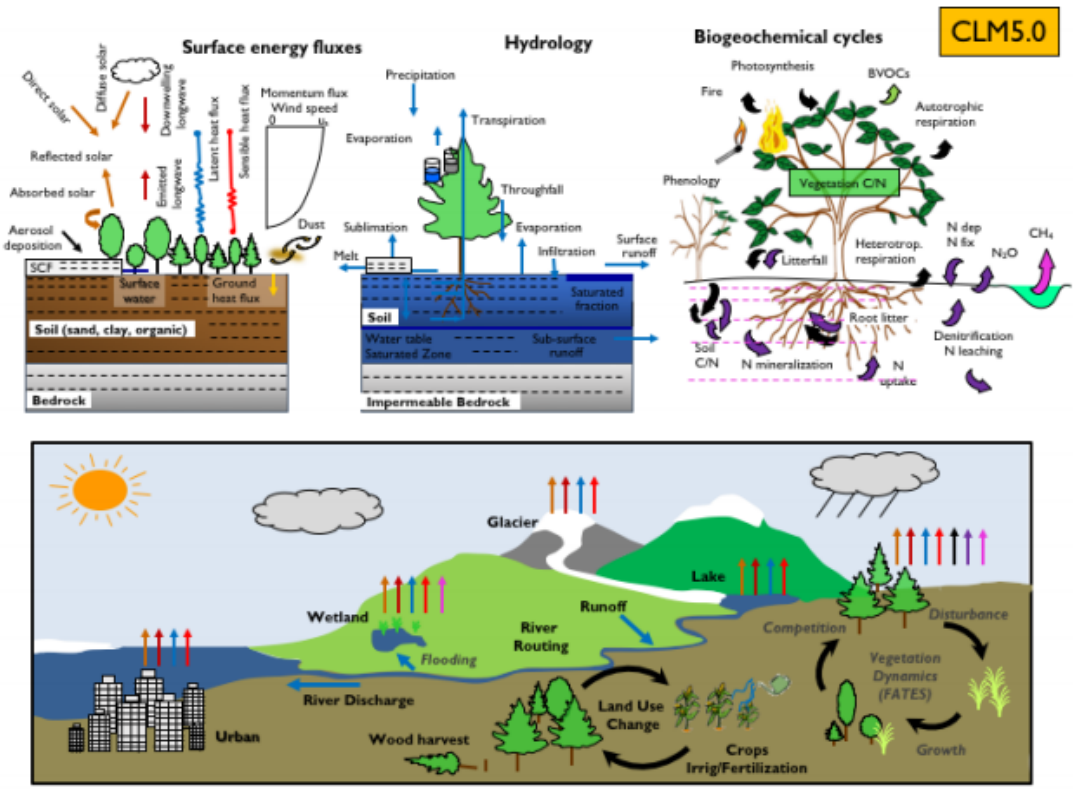

Figure 16: Processes Represented in CLM5.0. Figure taken from Lawrence et al. (2018)

Representation of Snow in CLM

Developments between CLM4.5 and CLM5.0, as outlined in van Kampenhout et al. (2017) improved the snow scheme in CLM. The newer version of the model used herein produces a computationally-layered snowpack, with the number of snow layers dependent on the snowpack depth, up to a theoretical maximum of 12 layers (as opposed to the 5 layer maximum in previous versions of

CLM). Once the total snow depth exceeds a given threshold, the initial snow layer is subdivided into two layers with equal properties. Snow layer formation continues in this manner as layer thicknesses surpass the prescribed ranges given in Jordan (1991). When a layer divides, the new layer is formed beneath it, rather than new layers being formed at the surface by new snowfall. As this process is not stratigraphically representative, layers are not described by snow type (i.e., as per Fierz et al., 2009), but instead numbered from the snow surface down (Fig. 17). Layer thicknesses are also influenced by snow compaction, parameterised following Anderson (1976). Unsaturated layers may compact due to overburden pressure, the breakdown of new snow crystals or melting, with the thickness of a snow layer a function of the snow thickness at the previous timestep and the rate of compaction. Snow depths below 1 cm are not discretely modelled and are instead combined into the surface soil layer.

Density, thickness and thermal conductivity are output as a daily mean for each layer. CLM calculates snow density as a function of the relative proportions of ice (mass of ice = m_i) and liquid water (mass of liquid water = m_{lw}), weighted by the snow cover fraction (F_{sno}) for each grid cell (Lawrence et al., 2018):

$$\rho = \frac{(m_i + m_{lw})}{F_{sno} \times h_{sl}} \tag{3.6}$$

In practice, due to the adjusted snow cover fraction (Section 3.4.3) and as liquid water in the snowpack is zero until the start of melt out, the computed snow layer density simplifies to the mass of ice (m_i) divided by the height of the snow layer (h_{sl}). Changes implemented in CLM5.0 also include a new snow densification scheme, whereby fresh snow density is parameterised as a function of temperature and windspeed. The density of fresh snow can increase through the process of wind-driven compaction if wind speeds exceed 0.1 m s^{-1} (van Kampenhout et al., 2017)[2]. Over time, the density of the snowpack evolves as a result of the compaction processes outlined above. CLM5.0 does not allow for temperature-gradient metamorphism, and thus does not represent the development of depth hoar layers (van Kampenhout et al., 2017).

The computed snow layer densities are then used to calculate snow layer effective thermal conductivities (K_{eff}), as per Jordan (1991) (Section 2.1.2; Eq 2.4), with the values for the thermal

[2]Units given in van Kampenhout et al. (2017) as m^-1

conductivities of ice and interstatial air as given in Lawrence et al. (2018). Snow (and soil) temperatures are defined for the midpoint of each layer at an hourly resolution, with the soil column consisting of 25 layers of increasing thickness (down to a depth of 49 m; as shown in Fig 17).

Description of Soil and Soil Respiration in CLM

CLM uses 25 soil layers, shown alongside the snow layers in Figure 17. Carbon (and nitrogen) cycling is modelled within the first 20 layers, constituting the top 8.6 m of the soil column. The remaining 5 layers (down to a depth of 49.6 m) are classed as bedrock layers, and only used to model transfers of heat and energy, not of matter. The midpoint of each layer is used to describe the layer depth. Soil sand, silt and clay fractions are taken from the mineral soil texture data set of Bonan et al. (2002), and soil organic matter fractions are from Hugelius et al. (2013).

CLM5.0 uses a vertically resolved Century-type (i.e. after the *fCentury* model; Parton et al., 1988) soil decomposition scheme as outlined in Koven et al. (2013). For each layer (i) of the 20 biogeochemically active soil layers (the upper 8.6 m of the soil column), carbon moves through 3 soil pools. These 3 pools each have a different residence time, with Soil 1 the most labile (i.e. short lived) and Soil 3 having the slowest turnover. Prior to entering the soil carbon reservoir, carbon moves through 3 litter pools and a coarse woody debris pool (Fig. 18). Carbon in the coarse woody debris pool cannot be respired, just cycled into one of the litter pools, from which it may move to another pool or be decomposed. The default turnover time (K_0, shown as τ in Fig. 18) of each of these pools is modified by the rate of decomposition (K):

$$K_i = K_{0,i} r_T r_W r_O r_Z \tag{3.7}$$

where r_T, r_W, r_O and r_Z are rate modifiers which scale the rate of decomposition depending on the soil layer temperature, moisture, oxygen content and depth respectively. The influence of temperature on decomposition is parameterised using a Q10 function:

$$r_T = Q_{10}^{(\frac{T_{soil_i} - T_{ref}}{10})} \tag{3.8}$$

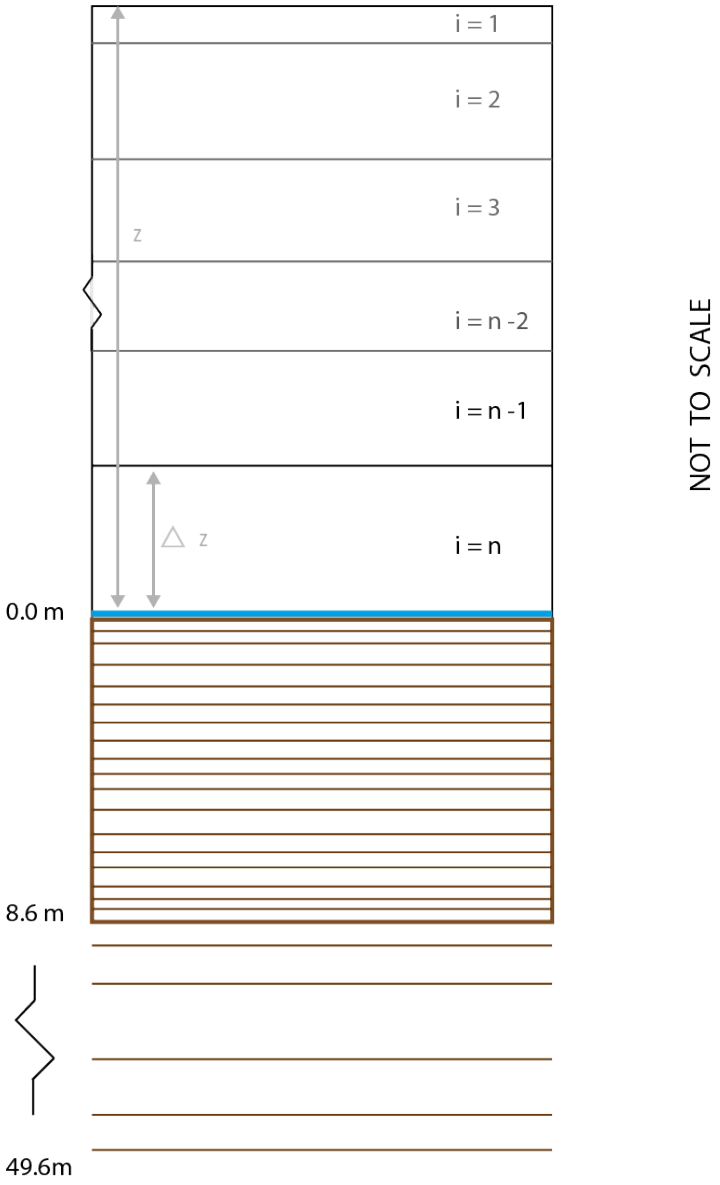

Figure 17: Snow and soil layers in CLM. The blue line denotes the snow:soil interface, with snow layers (labelled i = ...) shown above in black and soil layers shown below in brown. Soil layers within the box (to a depth of 8.6m) are used for representing biogeochemical processes, soil layers below this depth are only used for modelling thermodynamic processes.

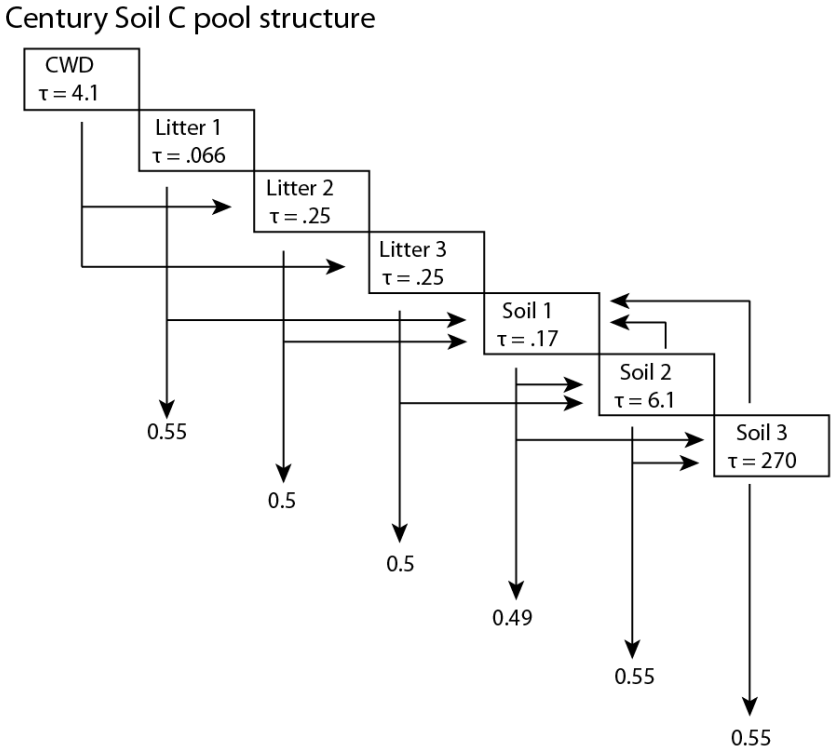

Figure 18: Pool structure of the Century decomposition scheme used in CLM. The default turnover time of each pool in years (τ) is given in each box, with the respired fraction given at the ends of the arrows. Figure taken from Lawrence et al. (2019).

where Q_{10} defines the temperature sensitivity of soil respiration, T_{soil_i} equals the temperature of soil layer i, and T_{ref} is a reference temperature with a default value of 25 °C. By default, CLM uses a global constant Q10 value of 1.5 (Foereid et al., 2014) for both frozen and unfrozen soils (Lawrence et al., 2018). This is lower than the value of Q10 used by many other earth system models (Meyer et al., 2018). Additionally, the use of a globally constant value does not take into account the inherent temperature sensitivity of Q10 itself (Lloyd and Taylor, 1994) nor spatiotemporal changes in observed Q10 as a result of soil moisture, texture or vegetation characteristics (Chen et al., 2020; Curiel Yuste et al., 2004; Meyer et al., 2018).

The scalar for the impact of moisture on decomposition takes the form described by Andrén and Paustian (1987):

$$r_W = \sum_{j=1}^{5} \left\{ \begin{array}{ll} 0 & \text{for } \Psi_i < \Psi_{\min} \\ \frac{\log(\Psi_{\min}/\Psi_i)}{\log(\Psi_{\min}/\Psi_{\max})} w_{soil,i} & \text{for } \Psi_{\min} \leq \Psi_i \leq \Psi_{\max} \\ 1 & \text{for } \Psi_i > \Psi_{\max} \end{array} \right\} \tag{3.9}$$

where Ψ_i is the soil water potential in soil layer i, and Ψ_{min} and Ψ_{max} are the upper and lower limits for soil water potential to impact the rate of soil decomposition, with default values of -2 MPa and -0.002 MPa respectively. When Ψ is greater than Ψ_{max}, the moisture content of the soil has no impact on the rate of carbon turnover. When Ψ is smaller than Ψ_{min}, the soil moisture is too low for decomposition to occur; this is noted to be a major influence on the respiration from frozen soils by Lawrence et al. (2018). Respiration of previously decomposed carbon may still occur when Ψ is less than Ψ_{min}, up until the point where labile carbon stocks are depleted.

3.4.3 Modifications to CLM

CLM5.0 simulations herein were run for a single grid cell with area 0.1° x 0.1°. However, in order to best represent snow cover properties over this small area, modifications were required to the 1D "point mode" version of CLM (PTCLM; Kluzek, 2013), similar to those outlined in Malle et al. (2021).

The proportion of a CLM grid cell that is snow-covered is calculated as per Swenson and Lawrence (2012). Prior to the start of the melt season, the snow-covered fraction (F_{sno}) at a given timestep

(n) is calculated as;

$$F_{sno}^{n+1} = 1 - ((1 - tanh(K_{accum} q_{sno} \Delta t))(1 - F_{sno}^{n})) \tag{3.10}$$

where K_{accum} is a constant and q_{sno} is the amount of snowfall falling between the two model timesteps n and $n + 1$. F_{sno} is therefore dependent only on the value of F_{sno} in the preceding timestep and the amount of snow that has fallen since. Without adjustment to this equation (undertaken through a change to value of K_{accum}), this resulted in too gradual a build up of snow cover, with full snow cover at TVC not being achieved until early March in the 2017-18 season despite observations of fully snow-covered ground much earlier in the season.

The constant K_{accum}, set to a default value of 0.1, describes the probability that a given sub-unit of the CLM grid cell will become snow covered after a snowfall event. In order to improve the simulated early season snow cover fraction, the value of this constant was iteratively increased (Fig. 19) until values of F_{sno} matched expected seasonal patterns. A K_{accum} value of 2.0 was chosen for all model simulations in Chapters 4 and 5.

During melt out, F_{sno} is influenced by the topography of the grid cell,

$$F_{sno} = 1 - \left(\frac{cos^{-1}(2R_{sno} - 1)}{\pi} \right)^{N_{melt}} \tag{3.11}$$

where R_{sno} is the ratio of the snow mass at the current timestep to the maximum accumulated snow mass for that season and N_{melt} is defined by the topographic variability within the grid cell in terms of the standard deviation of elevation (σ). The default standard deviation of elevation used by CLM is calculated from a 1 km DEM, arguably inappropriate for a point simulation with a grid cell approximately 11 km^2. Essery and Pomeroy (2004) observed a 140 m range in elevation at TVC, and this value was used to approximate a standard deviation of elevation of 35 m (Taylor, 2020), an order of magnitude lower than CLM's predicted value. Substituting this into CLM improved the melt-out rate somewhat, but the simulated snow cover fraction was still not very well matched to expectations (in part from Malle et al. (2021), who used a σ value of 25 m). A series of model runs where the standard deviation of elevation was iteratively reduced was undertaken in order to attempt to simulate an expected pattern of melt out (Fig. 20). Below a

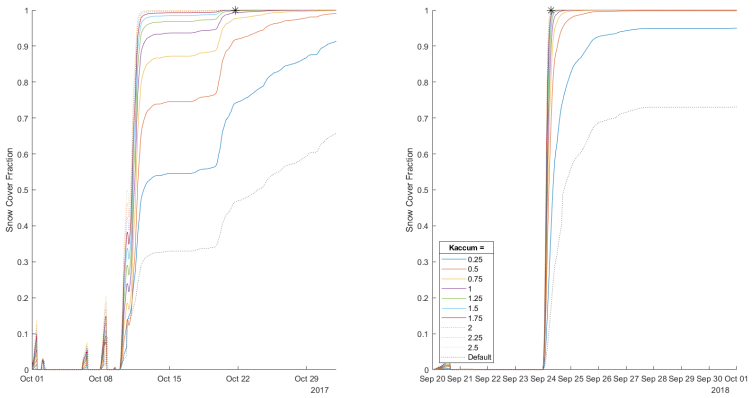

Figure 19: Impact of different values of K_{accum} on simulated snow cover fraction for winter 2017-18 & 2018-19. Black asterixes represent the date where complete snow cover was observed.

value of 10 m, changes to the standard deviation of elevation had no influence on the snow cover fraction. However, a value of 0.5 m was chosen to represent the standard deviation of elevation, as this is similar to the height of tussocks, a major feature controlling small-scale topographic variability at TVC.

3.4.4 Model Spin-up

Soil Temperature Equlibration

In order to determine the amount of model spin-up required for soil temperatures to equilibrate, iterative runs of PTCLM with an additional year of spin-up were undertaken from 1 January 2017 to 1 January 2013. This spin-up process was used for the modelling experiments in Chapter 4. For each model year, the forcing data was tower data from that same year, processed as described below in Section 3.4.6.

Soil temperatures throughout the soil column were compared; three depths are shown in Fig. 21. Internal system variability results in a difference of $\sim$ 1 °C between model runs, with a minimum of 2 years of spin-up required for K_{eff} adjusted runs to converge at a 10 cm soil depth. Deviation between different spin-up start times takes longer to level out deeper in the soil column, but as we only examine soil properties within the top 20 cm of the soil column, we feel this length of spin-up is sufficient. Changes to snow thermal conductivity were evident at all depths in the soil profile and have an impact on the thickness of the active layer with seasonal thawing seen to a depth of

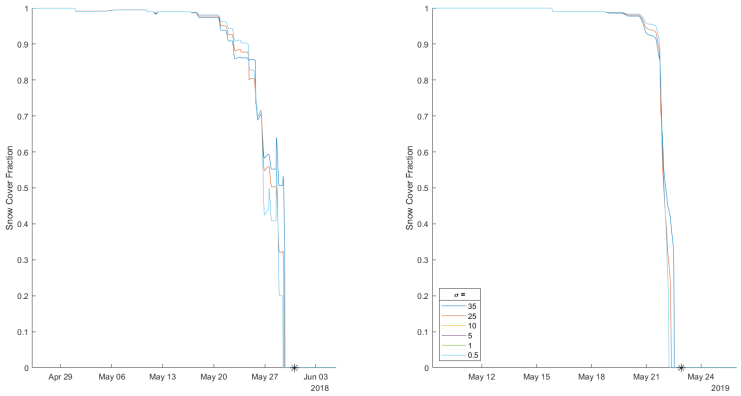

Figure 20: Snow Cover Fraction during meltout for different values of the standard deviation of elevation (σ). Black asterixes represent the date where a complete absence of snow cover was observed.

1.7m (Fig. 21b), in comparison to 1.35m for the unadjusted CLM runs and the 1m active-layer depth reported by Grünberg et al. (2020).

Carbon Pool Equilibration

This 5 year spinup process was not sufficent for carbon pools to equilibrate. For the study undertaken in Chapter 5, a longer spin up process was required in order for each of the carbon pools (described above in Section 3.4.2) to stabilise. Meteorological forcing data for the years 2013 - 2016 was looped to spin-up the model. As CLM was run using a leap year calendar, all leap years used the forcing for 2016, and centennial non-leap years used the February data for one of the other 3 years at random with the other months using the data for 2016.

Figure 22 shows the impact of the length of the spin up on the stablity of each of the soil carbon pools. Use of the alternative C:N decomposition scheme was also tested (not shown), but as this scheme did not allow new inputs of carbon, the size of each pool decreased considerably before the end of the spin-up period and this scheme was deemed inappropriate.

We considered the model spun-up once all 3 soil carbon pools in the decomposition scheme were in a steady state, with mean annual changes in the size of the pools less than 10 g C m^{-3} for the last 10 years of the simulation. We also examined the size and stability of the total ecosystem carbon and soil organic matter carbon (SOMC) pools, with the model considered spun-up once interannual changes in the sizes of each of these pools were less than 10 g C m^{-3} for the last 10

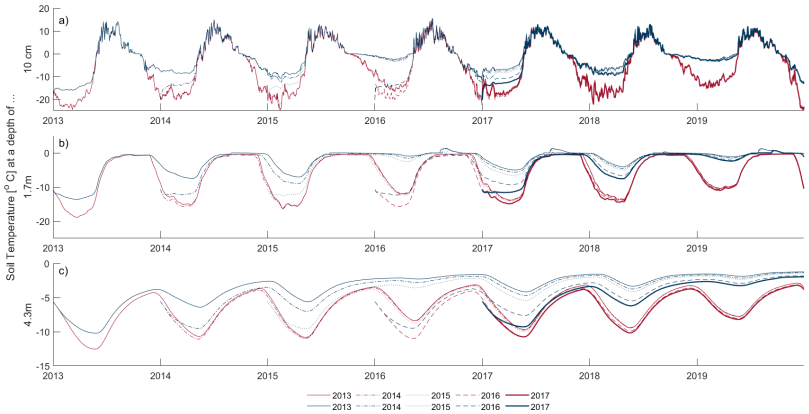

Figure 21: Soil temperatures at (a) 10 cm, (b) 1.7m and (c) 4.3m (3rd, 11th and 16th CLM soil layers) for varying lengths of model spin-up (line styles; all spin-ups from 1 January, year given in legend), for both baseline (α = 1; dark red) and K_{eff} adjusted (α = 0:3; navy blue) model conditions.

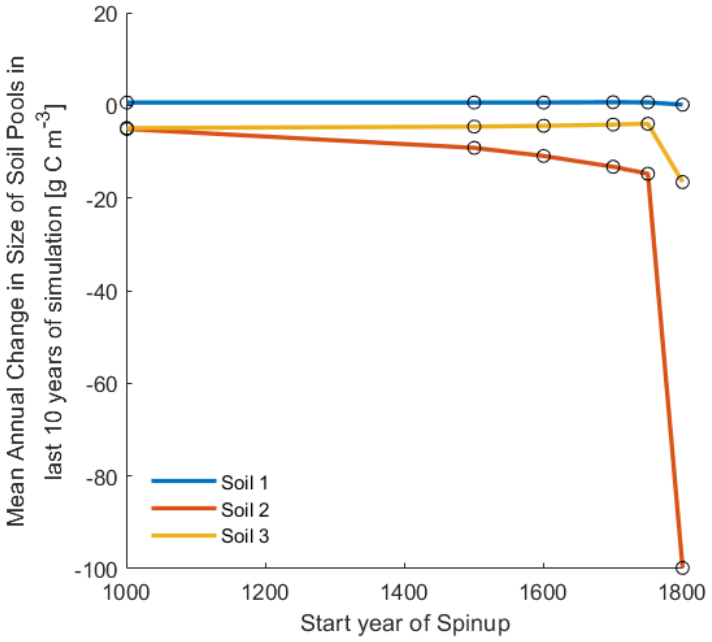

Figure 22: Impact of the length of spinup on the stability of each Soil Carbon pool, denoted in terms of the mean annual change in the size of each of the 3 Soil Carbon pools for the last 10 years for different spin-up start years.

years of the simulation and when the size of the soil carbon pools was within the range of observed values for the Mackenzie Delta region given in Figure 1 of Schuur et al. (2015). Ratios between NEE and NPP (Fig. 23) were also examined to test if known deficiencies in plant phenology impacted the stability of the carbon pools (Pers. Comm., Meyer, 2022). The rolling 4 year average of this ratio was greater than expected, but remained stable throughout a sufficiently long spin-up with the cyclicity of the forcing data appearing to have a greater impact on the values (Fig. 23). To achieve these conditions, we span the model up from the year 1500 for the study described in Chapter 5.

3.4.5 Limitations of CLM

Plant Phenology

Birch et al. (2021) details a number of issues with the phenology of plants in CLM5.0. The start of the growing season is delayed, with the onset of photosynthesis delayed due to the extrapolation of temperature based relationships governing leaf-out from the tropics to the Arctic-Boreal Zone (Birch et al., 2021). Furthermore, short vegetation (such as grasses) is presumed by CLM to be inactive if the snow depth is greater than 20 cm, and if less than 5% of leaves or stems are above the height of the snow the amount of exposed vegetation is set to zero (Lawrence et al., 2019). Observations of photosynthesis beneath shallow snow have been noted by Larsen et al. (2007); Starr and Oberbauer (2003); Tieszen (1974), among others. Heterogeneities in snow depth, particularly during snow melt, mean that despite a mean snow depth over the 20 cm threshold, there may be points in the grid cell where photosynthesis would still realistically occur.

Additionally, NEE in the autumn is too high as photosynthesis continues for too long, delaying the onset of plant senescence and the shift to net carbon release. Inaccuracies in the simulated productivity of plants in Arctic regions are also highlighted by Birch et al. (2021) and Wieder et al. (2019). Arctic grass, shrub and needleleaf evergreen tree plant functional types (PFTs) are too productive, and deciduous trees are not productive enough (although we do not observe or simulate deciduous trees at TVC).

Although solutions to improve the phenology and behaviour of Arctic plants in CLM have been proposed (Birch et al., 2021), computational limitations prevented their implementation in this study. Assessment of simulated fluxes is therefore limited to the snow-covered season. How-

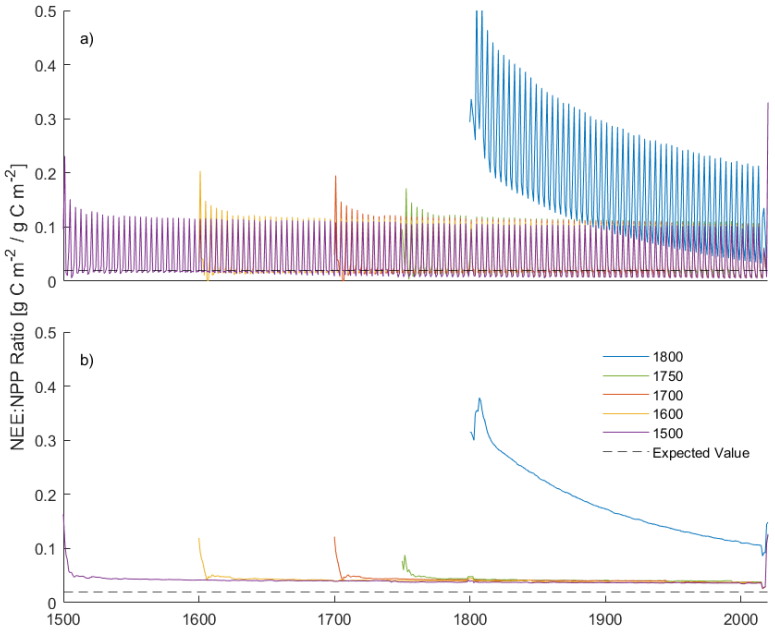

Figure 23: Ratio of Net Ecosystem Exchange to Net Primary Productivity for different starting years of model spin up. An additional run starting in the year 1000CE is not shown, as patterns are the same for all years earlier than 1700. a) shows yearly values, whereas b) shows a 4 year running mean to normalise for differences between the 4 looped years of forcing data.

ever, seasonal carry-over effects may still have some impacts on the results presented in Chapter 5.

Missing Processes

Like the majority of land surface or global climate models, CLM5.0 was not designed with the Arctic in mind. Numerous processes and features of relevance to simulations of Arctic regions are not currently included in CLM. These include, but are not limited to:

- Vapour Diffusion in Snowpacks

As aforementioned, CLM5.0 does not simulate the formation of depth hoar (van Kampenhout et al., 2017). This has implications for the thermal properties of the snow and the simulation of soil temperatures (Chapter 4).

- Moss

Mosses are a key component of tundra ecosystems, but no moss PFT is present in CLM. The presence of mosses has many influences on the below ground environment (Gornall et al., 2007), with impacts on soil temperature, moisture, active layer depth and biogeochemical cycling (Bueno et al., 2016; Park et al., 2018; Zha and Zhuang, 2021).

- Permafrost Subsidence

CLM5.0 does not consider the possibility of subsidence under warming permafrost. Changes in topography and water table height caused by subsidence may lead to changes in snow accumulation, local hydrology and carbon cycling (Schädel et al., 2018), as well as longer term landscape change (Grosse et al., 2016).

- Peat

Peat soils are common in tundra landscapes, storing vast amounts of carbon (Chaudhary et al., 2020), and yet not parameterised in CLM5.0. Other land surface or terrestrial biosphere models which allow for the simulation of peat soils, such as CLASSIC (Wu et al., 2016), JULES (Chadburn et al., 2022) and LPJ-GUESS (Chaudhary et al., 2020), allow better estimation of the carbon sink capacity of Arctic regions and also improved simulation of soil moisture dynamics.

3.4.6 Data Processing Protocol

Observations from the TVC tower (instrumented as described in Section 3.1) were used to force CLM as follows. Half hourly observations from the TVC tower were converted to hourly resolution using the MATLAB retime function. Data was then gap-filled as per Essery et al. (2016) prior to being reformatted and input into CLM. Gaps of 4 hours or less were filled using linear interpolation, with longer gaps being filled from ERA5 reanalysis (Hersbach et al., 2020). Of the variables required by CLM, only the radiation data required gap-filling. Comparison of observations and reanalysis data showed an offset of less than 60W m^{-2}, so bias correction of reanalysis data was not undertaken due the small size of this offset.

Precipitation data was also disaggregated from a daily amount to an hourly rate, using ERA5 reanalysis to calculate the proportion of daily precipitation falling each hour. Partitioning into rainfall and snowfall was also undertaken using ERA5 reanalysis, with timesteps listed as "mixed precipitation" being equally proportioned as rain and snow. This manually partitioned precipitation was compared to the linear ramp used by CLM, where all precipitation falling when air temperatures are below 0 °C is classed as snow, after which point an increasing proportion of

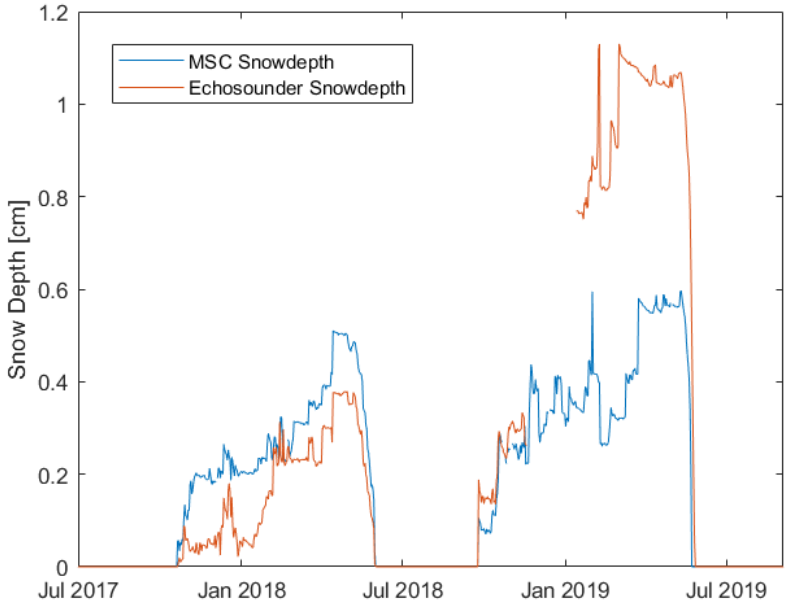

Figure 24: Snow Depth at the TVC Eddy Covariance (Echosounder) tower and Meteorological Service of Canada (MSC) towers for the winters of 2017-2018 and 2018-2019.

the precipitation is classed as rain until air temperatures are above 2 °C where all precipitation is classed as rain (Lawrence et al., 2019).

Due to the presence of a large snow drift in the 2019 at the TVC station (Pers. Comm., Walker, 2020), snow depth data from the Meteorological Service of Canada (MSC) station less than 100 m away was used instead. Gaps in this dataset were filled by converting the data to an hourly resolution using the MATLAB retime function, setting summer snow depths to zero and then using linear interpolation to fill missing values. Figure 24 compares the snow depth data from the TVC and MSC stations.

3.4.7 CLM Metholodology

Simulations of CLM are used for the experiments outlined in the next two chapters of this thesis. Briefly, Chapter 4 examines the parameterisation of snow thermal conductivity and the impact of simulated snow properties on soil temperatures. Chapter 5 then evaluates the impact of the preposed change in snow thermal conductivity on the simulation of net ecosystem exchange, with poor model performance driving a wider sensitivity study of the decomposition parameters outlined in Eq. 3.7 above.

Chapter 4

Impact of Measured and Simulated Tundra Snowpack Properties on Heat Transfer

4.1 Introduction

Seasonal snow is an effective insulator, with snow thermal properties influencing the soil microclimate (Lawrence and Slater, 2009; Wilson et al., 2020) and the distribution and state of permafrost (Biskaborn et al., 2019; Goncharova et al., 2019; Zhang, 2005). The temperature of the subnivean environment, particularly the extent to which it allows for the presence of small amounts of liquid water, acts as an important control on biogeochemical cycling, including soil respiration (Semenchuk et al., 2015; Sullivan et al., 2008; Williams et al., 2009). In addition, the soil temperature also impacts hydrology through controls on soil infiltration and runoff (Niu and Yang, 2006; Quinton and Marsh, 1999). Accounting for how well the thermal and hydrological conditions of subnivean soils (including the physical state of soil water content) are simulated is therefore critical for understanding how well current land models such as the Community Land Model (CLM; Lawrence et al., 2019) simulate winter carbon fluxes (e.g. Natali et al., 2019) and permafrost evolution (Koven et al., 2012).

The depth, [micro]structure, and stratigraphy of a snowpack determine its capacity to insulate the

underlying soil and are in turn influenced by the temperature of the ground surface. Tundra snowpacks typically consist of a basal depth hoar layer, formed as strong temperature gradients within the snowpack induce kinetic metamorphism, overlain by an upper wind slab layer, compacted and densified over the course of a snow season by strong Arctic winds (Sturm et al., 1995; Derksen et al., 2009, 2014; Rees et al., 2014, , amoung others). Between these two layers, an indurated hoar layer may also be formed (Sturm et al., 2008), where the lower part of the wind slab takes on some of the microstructural properties of depth hoar (e.g. faceted grains) while maintaining the density and hardness of a wind slab (Derksen et al., 2009).

The thermal influence of the snowpack on the underlying soil can be considered in terms of an effective snow depth ($S_{depth,eff}$), which describes the insulative properties of the snowpack by weighting the mean monthly snow depth by its relative position in the season at a given location across an entire winter (October – March) (Slater et al., 2017), emphasizing the timing of snow accumulation as more important than the end of season snow depth in determining wintertime soil temperatures (Lafrenière et al., 2013). Rapid snow accumulation and snowpack establishment early in the winter will insulate the ground thereby dampening soil temperature fluctuations, leading to a higher $S_{depth,eff}$ than steady accumulation throughout the entire winter, even if the total amount of precipitation is the same (Slater et al., 2017). The relationship between $S_{depth,eff}$ and the normalised temperature difference between air and soil (A_{norm}) can be used to understand heat transfer between the air and the soil and through the snowpack (Slater et al., 2017). The deviation of this relationship from the expected exponential form (Fig. 3 in Slater et al., 2017), termed the Snow Heat Transfer Metric (SHTM), can be calculated and used to evaluate simulated heat transfer processes in the soil and snowpack as was undertaken by Slater et al. (2017) for the land surface components of participating models in the CMIP5 model intercomparison project Taylor et al. (2012). The closer the value of the SHTM is to one, the smaller the disagreement between modelled and observed air and soil temperature differences. Being able to quantitatively assess snow heat transfer is of particular importance because model parameterisations of snow physical properties can lead to differences in soil temperature and therefore contribute to uncertainties in estimates of Arctic winter carbon fluxes and budgets, which are currently not well constrained (Fisher et al., 2014; Natali et al., 2019; Virkkala et al., 2021).

The effective thermal conductivity of the snowpack (K_{eff}; heat conducted through ice and in-

terstitial air) determines the rate of heat transfer to underlying soil (Domine et al., 2015; Jafarov et al., 2014). From here on, we refer to the effective thermal conductivity of the snowpack as snow thermal conductivity for brevity, after Jafarov et al. (2014). Snow has a low thermal conductivity, typically in the range 0.01 – 0.7 Wm^{-1} K^{-1} (Gouttevin et al., 2018). Typical K_{eff} values for tundra snowpacks are at the lower end of this range, for example Domine et al. (2016b) found a maximum value of 0.33 Wm^{-2} K^{-1}. Measurement of snow thermal conductivity is typically undertaken using a heated needle probe (Morin et al., 2010), although snow anisotropy causes 29% uncertainty in these estimates of K_{eff} (Domine et al., 2015), which is a notable limitation to this method (Riche and Schneebeli, 2013). Models typically parameterise K_{eff} as a function of the simulated snow density (Gouttevin et al., 2018), for which a number of different statistical relationships have been proposed (e.g. Sturm et al., 1997; Calonne et al., 2011).

This study characterises the variability of the thermal properties of tundra snow and resultant soil temperatures at Trail Valley Creek, Northwest Territories, Canada, over the 2017 - 18 and 2018 - 19 winters using in situ measurements. We then use these measurements to evaluate an ensemble of simulations from the Community Land Model (CLM5.0), particularly with regard to how thermal properties are simulated and the sensitivity of soil temperatures and SHTM to the properties of the snowpack.

4.2 Data and methods

4.2.1 Field methods

Comprehensive snow and soil data are used from four winter season intensive measurement periods (14 - 21 March 2018; 12 - 18 November 2018, 11 – 20 January 2019, and 18 – 27 March 2019). Additionally, meteorological data for the entirety of the study period (1 August 2017 – 31 August 2019; plus model spin-up), measured at the TVC eddy covariance tower (AWS; as detailed in Section 3.1) were also used.

Spatially distributed Snow MicroPenetrometer (SMP; Schneebeli and Johnson, 1998) profiles (n = 1050) were measured across the TVC sub-catchment. The SMP provides vertical profiles of force at 40 μm resolution (Proksch et al., 2015). Bespoke coefficients for tundra snowpacks were

calculated based on the methodology of King et al. (2020b) to derive high vertical resolution snow density profiles from the SMP force profiles (see 3.2.2 for detailed methodology).

During the March 2018 and March 2019 campaigns, thermal conductivity was also measured using a TP02 needle probe (Hukseflux, Delft, Netherlands) after Morin et al. (2010). Measurements of thermal conductivity of each snowpack layer, a total of 105 measurements from 37 different snowpits were made across these two campaigns. Almost 36,5000 GPS located snow depths (Toose et al., 2020; King et al., 2020b) were measured across the 4 campaigns using a Magnaprobe instrument (Sturm and Holmgren, 2018), allowing spatial distributions of snow depths across the catchment to be examined. Vertical profiles of snow density and stratigraphy from each snowpit (n = 115) were also used, as detailed in Section 3.2.1.

4.2.2 Snowpack simulations

Simulations of the Community Land Model v5.0 (CLM; Lawrence et al. (2019), introduced in Section 3.4.2) were run in 1D "point mode" (a 0.1° x 0.1° grid cell) CLM (PTCLM; Kluzek, 2013), centred at the location of the TVC station. Minor adjustments were made to the model in order to better emulate snow accumulation and melt at the point scale as described in Section 3.4.3. PTCLM simulations were run from August 2017 to August 2019, with model spin-up from January 2013. Spin-up of PTCLM was necessary in order to allow soil temperatures to equilibrate. Variation between model runs with the same parameterisation after more than 2 full years of spin-up is limited to $\sim$ 1 °C throughout the top 5 m of the soil column. The impact of spin-up on soil temperature is further discussed in Section 3.4.4. Simulations were forced with gap-filled AWS data from TVC, with the gapfilling process as described in Section 3.4.6.

Developments between CLM4.5 and CLM5.0, as outlined in van Kampenhout et al. (2017) improved the snow scheme in CLM. For brevity, explanation of relevant parts of CLM5.0 for both this and the subsequent chapter is contained within Section 3.4.2. Despite the simplicity of the snowpack scheme included in CLM, previous evaluation of snow heat transfer in CLM4.0 (Slater et al., 2017) suggests this modelling framework should perform well.

4.3 Results

4.3.1 Observed meteorological, soil moisture and thermal conditions

Mean annual air temperature for 2017 - 2019 was -7.4 °C, with minimum air temperatures of -33.9 °C (2018) and -36.9 °C (2019) reached in early January (Fig 25a). The cold period was twice as long as the growing season, with consistent subfreezing air temperatures from 10 October 2017 to 30 May 2018 (232 days) and from 23 September 2018 to 11 May 2019 (230 days).

Figure 25c shows snowpack initiation in 2018 was 26 days earlier than in the previous year, with snow-on dates of 25 September 2018 and 21 October 2017 respectively. A maximum snow depth of 51 cm (2017 - 18) and 59 cm (2018 - 19) was measured at the AWS on 14 April 2018 and 11 May 2019 respectively. Snow depth from spatially distributed magnaprobe measurement showed a greater difference between the two years than at the AWS, with mean March snow depths 11 cm higher in 2018 - 19 than 2017 - 18. Magnaprobe measurements also show a higher mean March snow depth than the AWS, with March 2018 snow depths more heavily skewed than snow depths in 2019 (Fig. 26). Snow-off date, as measured at the AWS snow depth sounder, was one week later in 2017 - 18 (30 May) than in the following year (23 May).

Soil freeze-up began with the onset of snowfall (Fig. 25b & d); 5 cm soil temperatures dropped to 0 °C on 13 October in 2017 and a month earlier on 15 September in 2018. Soil temperatures

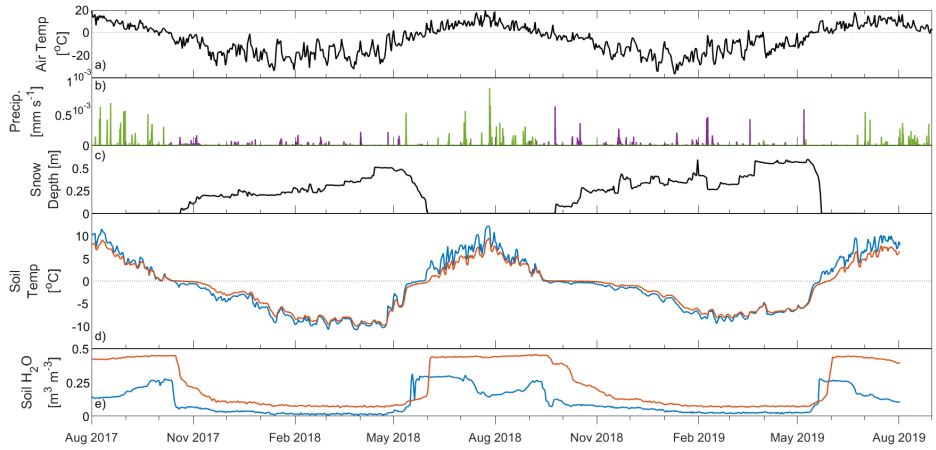

Figure 25: Daily averaged meteorological and soil conditions at Trail Valley Creek from 1 August 2017 to 31 August 2019: (a) 2m air temperature, (b) precipitation as snow (purple) and rain (green), (c) snow depth, (d) soil temperatures at depths of 5 cm (blue) and 20 cm (orange), and (e) volumetric soil water content at 5 cm (blue) and 20 cm (orange) depths.

remained around 0 °C as the soil froze and released latent heat. Soil saturation increased with depth causing a slower soil freeze-up at 20 cm than 5 cm depth in both years. A longer freeze-up in 2018 was evident from the more gradual liquid soil moisture decrease, particularly at depth (20 cm). Deeper soil (20 cm) stayed at 0 °C for longer than soil nearer the surface (5 cm), and generally remained warmer until the start of the thaw period. Minimum 2017 – 18 soil temperatures at both 5 cm (-10.9 °C) and 20 cm (-10.1 °C) depths in winter were colder than the following year (-9.5 °C and -8.2 °C), as the combined effect of earlier snowpack initiation and a deeper snow cover prevented colder soil temperatures being reached. Variations in soil temperature in response to diurnal and synoptic weather patterns of energy inputs from the atmosphere became increasingly muted with depth in the soil column once the snowpack was established. Anomalously warm mid-winter air temperatures that approached 0 °C (22 December 2017 and 9 February 2019) or exceeded 0 °C (18 and 31 March 2019, with a rain-on-snow event occurring on the latter of these dates) had only a muted influence on the soil temperature profile (Fig. 25d), with temperatures fairly stable until sharply increasing with thaw in early May. Soil temperatures at 5 cm increased above 0 °C for the first time on the final day of the snowmelt period in both years (Fig. 25d), with a five (2017 - 18) to seven (2018 - 19) day lag in the 20 cm soil temperatures.

4.3.2 Measured snow properties

Median density profiles from the SMP fall within the interquartile range of measured densities from volumetric sampling in snowpits (Table 5). Snowpacks in all three campaigns (Fig. 26b - d) had a very thin surface snow layer (composed of recent snowfall), with low near-surface snow densities (< 300 kg m^{-3}) rapidly increasing in the top 5 % of the snowpack. A higher density ($\sim$ 320 kg m^{-3}) wind slab layer was evident between 5 - 30% of normalised depth from the snow surface. The next $\sim$ 10% of the profile was a transitional section where density decreased by

	Snow Depth [cm]	
	March 2018	March 2019
AWS	35	36
Magnaprobe	33 ± 15.7 (n = 14,966)	44 ± 14.4 (n = 8541)
CLM	18	34

Table 4: End of March snow depth summary. Mean and standard deviation of spatially distributed measurements with a sample size greater than n = 1 are shown, otherwise the daily value for 31 March is shown.

about 100 kg m^{-3}. The lowest $\sim$ 60% of the profiles is dominated by a lower density ($\sim$ 230 kg m^{-3}) depth hoar layer, the density of which increases slightly towards the base of the snowpack. Differences between median layer densities exceed the $\sim$ 10% sampling error associated with the use of density cutters ((Proksch et al., 2016; Conger and McClung, 2009), and in all but one instance, there was no overlap in the interquartile ranges of different snow layers within a campaign (Fig. 27). Densities between 40 – 80% of normalised depth (low density depth hoar) are likely overestimated due to microstructural assumptions made by the algorithm of Proksch et al. (2015), which prevent the calculation of SMP densities below 200 kg m^{-3} (see Section 3.2.2).

The transitional section, or indurated hoar layer, with transitioning properties between wind slab

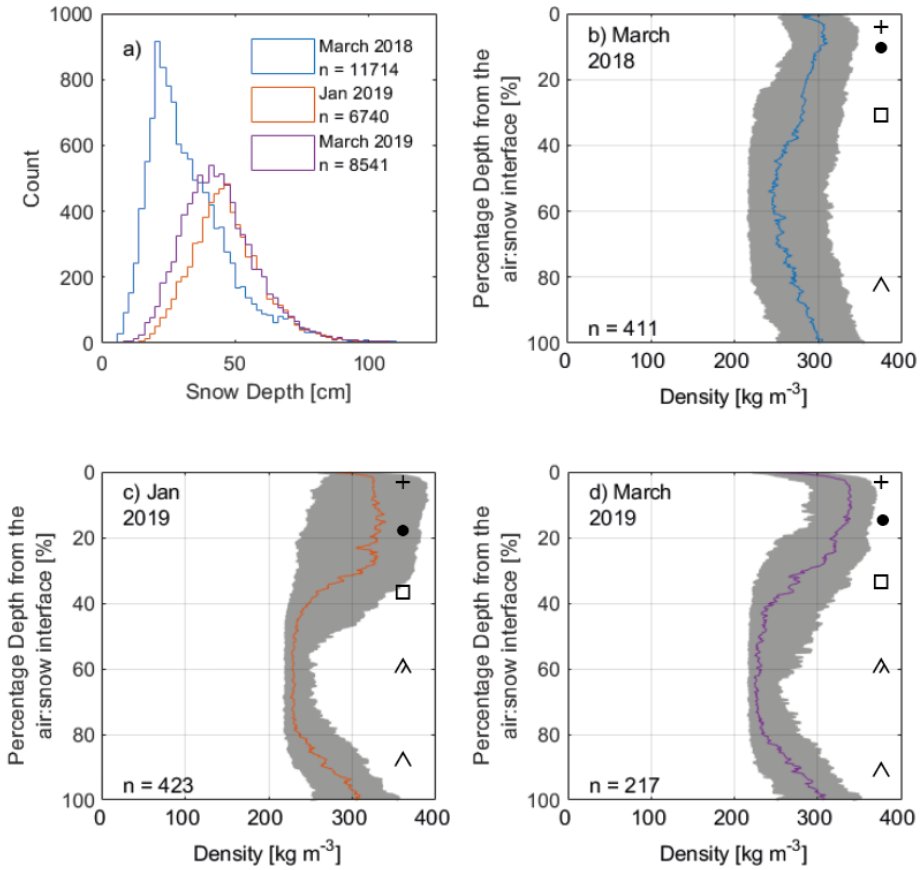

Figure 26: a) Frequency distributions of Magnaprobe depths for each sampling campaign where snow micropenetrometer (SMP) measurements are available. (b–d) Profiles of median SMP-derived densities (colour-coded for the respective campaigns (Fig. 26a); interquartile range shaded in grey). Symbols from Fierz et al. (2009) to denote approximate snow stratigraphy are superimposed.

and depth hoar, evident at between $\sim$ 30 – 40% depth, is often difficult to capture through traditional snowpit density profiles due to the 3 cm vertical resolution of density cutters and the layer being more defined by its crystal shape than density alone. The SMP enabled the detection of such features due to the increased vertical resolution and vastly reduced sampling times compared to traditional snow pits. Indurated hoar in SMP profiles was more pronounced in the 2019 campaigns; well-defined layers were not as clearly visible in the SMP measurements from March 2018 (Fig. 26b), despite different layer densities being statistically separate in the snowpit measurements, regardless of which year or when in the winter season the measurements were taken (Fig. 27). Ice lenses were present in March 2018, but not during the 2019 campaigns. Throughout the course of the 2018 - 19 winter, slight increases in the density of wind slab and depth hoar layers occurred as the snowpack developed. Late season snow densities in both 2018 and 2019 were similar, with the exception of surface snow. The density of this layer became more variable as each winter progressed due to the competing processes of wind compaction (increasing density) and temperature-gradient metamorphism (decreasing density). The timing of sampling relative to fresh snowfall events, noted during both March campaigns, also influenced measured surface snow densities.

SMP density profiles were used to parameterise profiles of thermal conductivity for the full depth of the snowpack. Patterns in parametrized thermal conductivity profiles (Fig. 28) resemble those in SMP densities from which they were derived (Fig. 26b-d). Surface snow thermal conductivities were low ($K_{eff-Sturm} \approx 0.1$ Wm^{-1} K^{-1}, $K_{effs-Calonne,Jordan,Fourteau} \approx 0.2$ Wm^{-1} K^{-1}), but sharply increased with depth for the upper 5 % of the snowpack (Fig. 28b & c). Below this, at normalised depths of $\sim$ 5 –30%, thermal conductivity reached maximum values ($K_{eff-Sturm} \approx 0.15$ Wm^{-1} K^{-1}, $K_{eff-Fourteau} \approx 0.25$ Wm^{-1} K^{-1}, $K_{eff-Calonne} \approx 0.3$ Wm^{-1} K^{-1}, $K_{eff-Jordan} \approx 0.35$ Wm^{-1} K^{-1}). Between $\sim$ 25 - 40% normalised depth, thermal conductivity declined before stabilising at minimum values ($K_{eff-Sturm} \approx 0.1$ Wm^{-1} K^{-1}, $K_{eff-Fourteau} \approx 0.15$ Wm^{-1} K^{-1}, $K_{effs-Calonne,Jordan} \approx 0.2$ Wm^{-1} K^{-1}) in the lower $\sim$ 60% of the snowpack. All 3 parameterisations showed similar variation in thermal conductivity with depth. Analysis of variance showed the mean K_{eff} from the Sturm et al. (1997) and Fourteau et al. (2021a) parameterisations to statistically significantly differ from those using the parameterisation of either Calonne et al. (2011) or Jordan (1991) and each other in all three months ($F_{March2018}$ = 3168, $F_{Jan2019}$ = 656,

		No. of Layers	Layer	Median	Interquartile range	
Density [kg m^{-3}]	Snowpit Obs.	3	Surface Snow	89	73	152
			Wind Slab	334	300	365
			Depth Hoar	249	228	270
	CLM	4	1	270	209	328
			2	328	285	346
			3	340	282	346
			4	309	291	326
Thermal Conductivity [W m^{-1} K^{-1}]	Snowpit Obs.	3	Surface Snow	-	-	-
			Wind Slab	0.20	0.15	0.28
			Depth Hoar	0.05	0.04	0.06
	CLM	4	1	0.25	0.17	0.35
			2	0.35	0.28	0.38
			3	0.37	0.27	0.38
			4	0.32	0.29	0.35

Table 5: Summary of modelled (CLM) and measured snow densities and thermal conductivities (from the manual density profiles and the needleprobe, respectively)

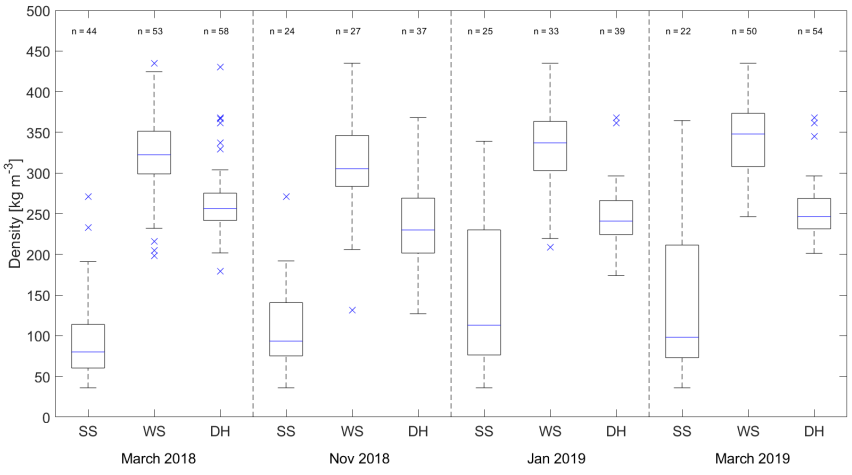

Figure 27: Distributions of measured layer densities (SS: surface snow, WS: wind slab, DH: depth hoar) from four sampling campaigns: box (interquartile range), blue line (median) and whiskers (dashed lines) extend from the end of each box to 1.5 times the interquartile range; blue crosses represent outliers beyond this range.

$F_{March2019}$ = 636). No significant difference was found between the Calonne et al. (2011) or Jordan (1991) parameterisations in either of the 2019 campaigns. All statistical tests in this Chapter gave a p-value less than 0.001, denoting significance at the 99.9% level.

Profiles of snowpack thermal conductivity were temporally consistent, with similar shape and values in January and March 2019. In March 2018, the amplitude of the thermal conductivity profiles was less pronounced than January and March 2019, particularly for the parameterisation of Sturm et al. (1997). We recognise that the thermal conductivity of a snowpack is dependent on more than just its density (Sturm et al., 2002), with other factors such as snow microstructure and temperature also having an influence (Calonne et al., 2011, i.e.) but these profiles still provide novel insights and a useful first-order approximation of snow heat transfer for model evaluation.

4.3.3 Modelled snowpack properties and comparison with observations

Simulated snow depths (Fig. 29a & d) were consistently lower than observations (from either Magnaprobe measurements (mean value) or the acoustic sounder depth on the 31 March at the AWS; Fig. 25b, Table 4). Timing of simulated snowpack accumulation leads to an effective snow depth in 2018 - 19 ($S_{depth,eff}CLM_{2018-19}$ = 66 cm) more than double that in 2017 - 18 ($S_{depth,eff}CLM_{2017-18}$ = 24 cm) with earlier snow onset allowing a greater degree of soil insulation. Simulated snow onset (11 October) and melt-out dates (25 May) were both approximately a week earlier than observed at the AWS in 2017 - 18; for the following year the length of this offset was reduced to just one day. Observations of effective snow depth ($S_{depth,eff}Obs_{2017-18}$ = 57 cm, $S_{depth,eff}Obs_{2018-19}$ = 101 cm) similarly reflect greater insulation of the soil surface in 2018 - 19 compared to 2017 - 18.

The physical properties of the simulated snow layers do not correspond to observations, with the number and thickness of snow layers only a function of overall snowpack depth. Figs. 29 b & e show three (or four) relatively homogenous layers, with a slight increase in density with depth. The highest mean (329 kg m^{-3}) and median (340 kg m^{-3}; Table 5) density are found in third snow layer (dark blue in Fig. 29).

This is in contrast to the three observed layers (surface snow, wind slab and depth hoar) consistently identified in the snowpit observations. Similar to other snow models (Domine et al., 2016b, 2019) the physical characteristics of the depth hoar layer at the base of the snowpack

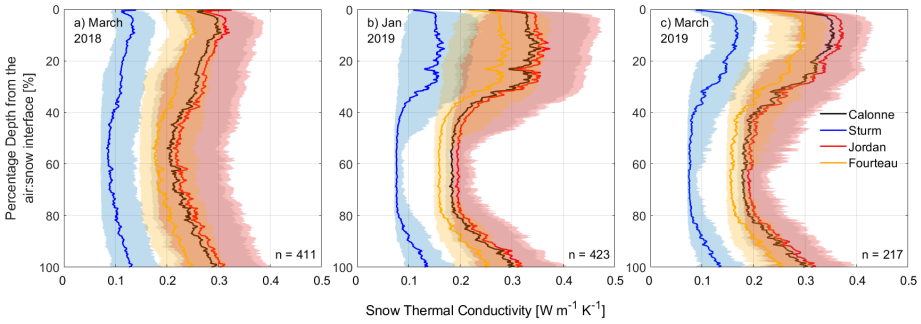

Figure 28: Median thermal conductivity profiles (lines) and interquartile range (shaded areas) approximated from SMP densities, using the parameterisations of Calonne et al. (2011) in black/grey, Sturm et al. (1997) in blue, Jordan (1991) in red and Fourteau et al. (2021a) in yellow.

(large faceted grains; low density) are not clearly distinct from an overlying wind slab layer (small rounded grains; high density). This is the result of the lack of representation of depth hoar layer development in CLM5.0 (van Kampenhout et al., 2017). These discrepancies between modelled and measured snow density and stratigraphy negatively impact the simulation of K_{eff}, as layer thermal conductivities were dependent on density of each layer (Eq. 2.4).

CLM5.0 overestimated the thermal conductivity of tundra snowpacks compared to in-situ measurements using needle probes or estimated from SMP profiles (Fig. 30a). Median simulated snow thermal conductivities (0.34 Wm^{-1} K^{-1}) were at least three times greater than either needle probe measurements (0.08 Wm^{-1} K^{-1}) or SMP-derived estimates using the Sturm parameterisation($x_{Keff-Sturm}$ = 0.11 Wm^{-1} K^{-1}), with the median thermal conductivity using the Calonne, Fourteau and Jordan approximations still lower ($x_{Keff-Calonne}$ = 0.25 Wm^{-1} K^{-1}, $x_{Keff-Fourteau}$ = 0.21 Wm^{-1} K^{-1}, $x_{Keff-Jordan}$ = 0.27 Wm^{-1} K^{-1}) than simulated thermal conductivities. SMP K_{eff} parameterisation from Sturm et al. (1997; derived from snow measurements in the Alaskan Arctic), are closer to values from needle probe measurements than SMP K_{eff} derived using Calonne et al. (2011) (Fig. 30a). The modelled thermal conductivity of simulated snow layers was relatively homogenous between layers in contrast to thermal conductivities derived from either the SMP (Fig. 28) or the needle probe measurements (Table 5). Analysis of variance only shows simulated snow layer thermal conductivities significantly differ from that of the surface layer (F = 39.74). Needle probe measurements of the depth hoar layer had low thermal conductivities (0.05 Wm^{-1} K^{-1}),

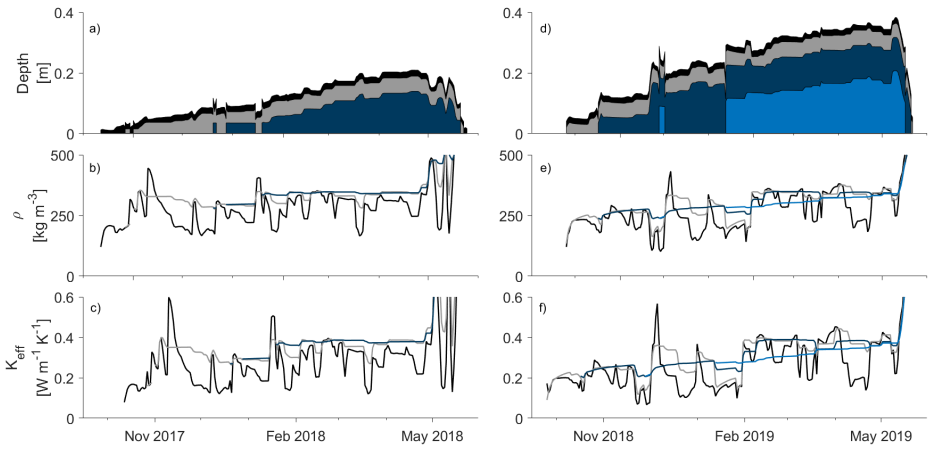

Figure 29: Simulated snow layers and their properties for winter 2017–2018: (a) simulated snow layer thicknesses, (b) snow layer densities and (c) snow layer thermal conductivities. (d–f) As before but for winter 2018–2019. Each colour represents a different computational snow layer.

with a slight increase in mean thermal conductivity for indurated hoar (0.09 Wm^{-1} K^{-1}) and a further increase for the mean wind slab thermal conductivity (0.20 Wm^{-1} K^{-1}). Distributions of simulated snow thermal conductivities were statistically significantly different from all measurement methods at the 0.01 level using a Kruskal-Wallis test. Differences between the distribution of needle probe measurements and SMP with the Sturm parameterisation were not statistically significant.

4.3.4 Improving simulated soil temperatures, snow thermal conductivity and snow heat transfer

Simulated soil temperatures were considerably colder than observations (RMSE = 5.0 °C, Bias = -2.2 °C), especially during the maximum annual duration of continuous simulated snow cover (15 Sept – 31 May; RMSE = 5.8 °C). Two approaches were taken to reduce simulated snow thermal conductivities, both of which resulted in warmer soil temperatures closer to observed values (Fig. 31a & b).

In order to see how results from the SMP (Fig 30a) manifested in simulations of soil temperature from CLM, we re-ran the model substituting the default parameterisation for snow thermal conductivity (Eq. 2.4; Jordan, 1991) for those of Sturm et al. (1997), Calonne et al. (2011) and Fourteau et al. (2021a) - Eqs 2.1, 2.2 and 2.3 respectively. The Sturm parameterisation resulted

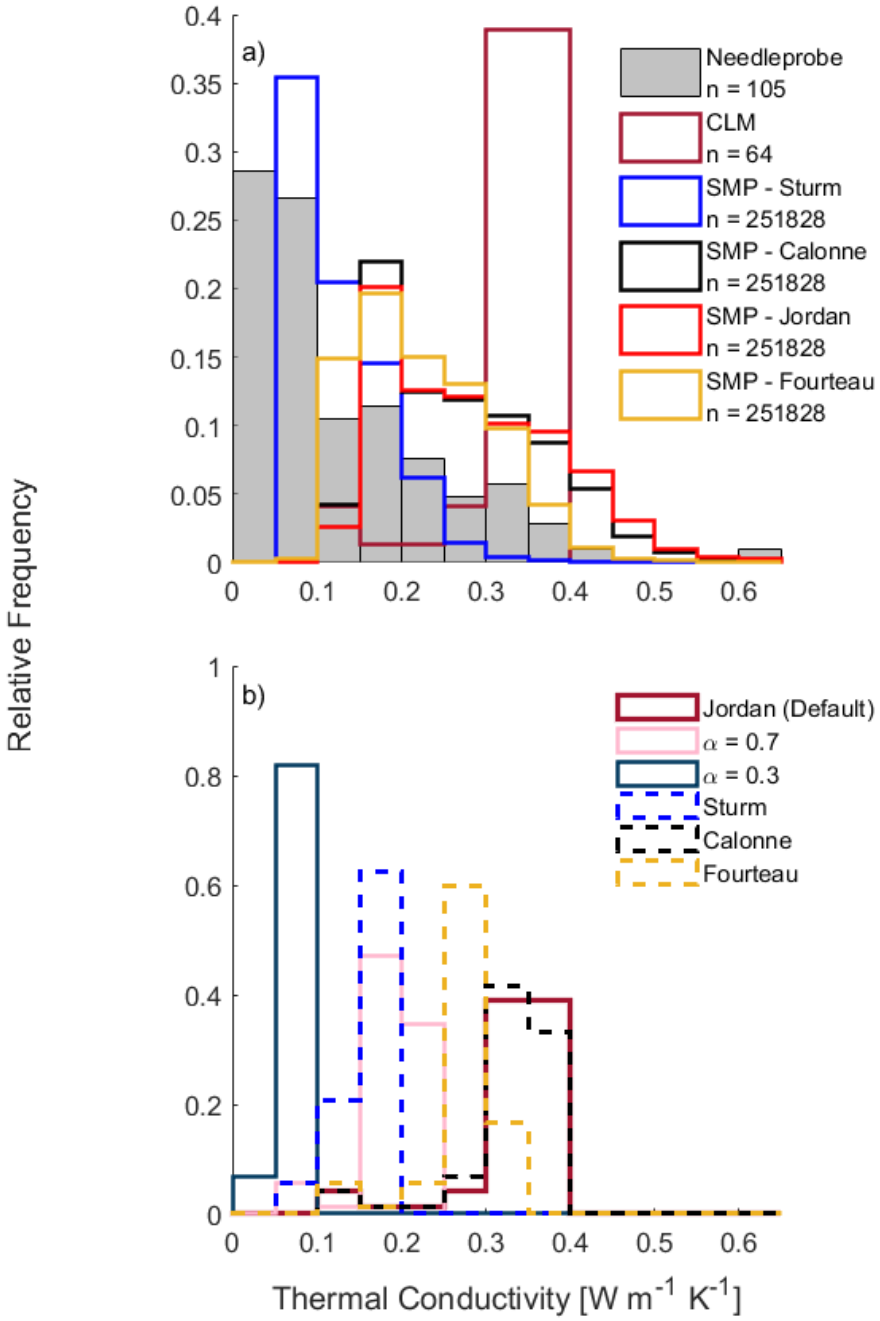

Figure 30: a) Histograms of measured and simulated thermal conductivity from March 2018 and 2019 sampling campaigns; dashed lines show the four different thermal conductivity parameterisations applied to the SMP densities. (b) Sensitivity testing of simulated thermal conductivities for the same time period using both the default CLM snow thermal conductivity parameterisation, application of the correction (solid lines) and alternative snow thermal conductivity parameterisations (Calonne et al. (2011); Fourteau et al. (2021a); Sturm et al. (1997) ; dashed lines). Note the different scales on the y axes.

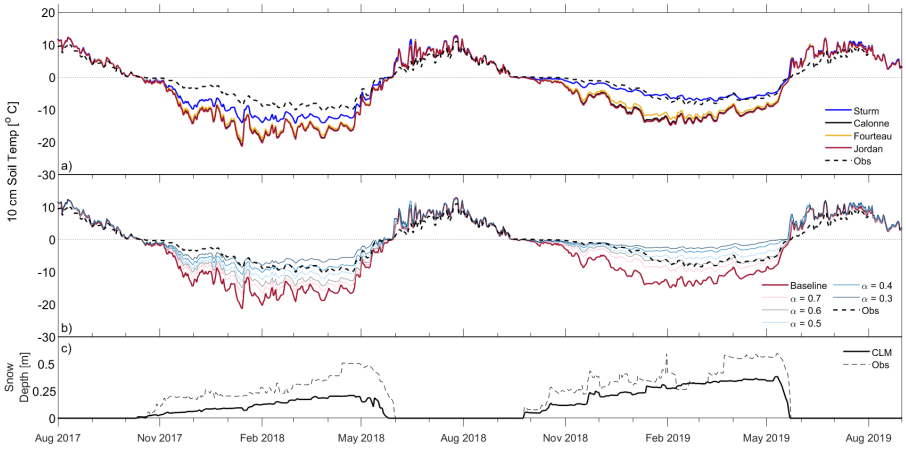

Figure 31: a) Simulated 10 cm soil temperature time series using the four different parameterisations of snow thermal conductivity compared to field measurements. (b) Time series of 10 cm soil temperatures when using different values of the correction factor compared to field measurements. (c) Observed and simulated snow depths for the same time period.

in lower simulated thermal conductivities (Fig. 30b) and closer temperatures to observations (Fig. 31b; RMSE = 2.5°C). Soil temperatures in 2017-18 were still too cold regardless of parameterisation used, likely due to model underestimation of snow depth (Fig 31c). As for the SMP, thermal conductivity values derived using the Calonne and Fourteau parameterisations are closer to the default Jordan (1991) parameterisation than those derived using the Sturm et al. (1997) parameterisation (Fig 30b). The impact of either of these parameterisations on simulated wintertime soil temperatures is limited (Fig 31a), particularly that of Calonne et al. (2011) which reduces the RMSE by only 0.2 °C. However, all 3 alternative parameterisations tested do show an improvement in simulated snow thermal conductivities (Fig 30b) and soil temperatures (Fig 31a), with an increase in the value of the SHTM in each case. We also tested the application of a multiplier (α) to the ice content term in Eq. 3.6:

$$\rho = \frac{(\alpha \times m_i) \times m_{lw}}{F_{sno} \times h_{sl}} \tag{4.1}$$

Although appearing to be a function of density, this multiplier is added separately from the calculation of layer snow densities, and only feeds into the calculation of snow thermal conductivity, and thus snow mass is conserved. Values of α were chosen which would reduce simulated densities to the range of observed values, with an α of 0.65 giving the K_{eff} for snow with a density

between the interquartile range of observed values for all snow types (73 – 365 kg m^{-}3). A set of sensitivity tests were then carried out where the value of α was iteratively changed from 0.75 to 0.25 in 0.05 increments. As the RMSE and the SHTM quantify changes over slightly different time periods (RMSE = entire winter, SHTM = Oct – March), different metrics may imply different adjustments give the best model performance. In 2018-19, a value of α between 0.65 and 0.6 resulted in the optimal model performance, with a SHTM value of 0.991 (or 0.979) and a RMSE of 1.5 °C (or 1.2 °C). However, a smaller value of α was required for best model performance in 2017-18, with an α of 0.4 giving the lowest RMSE of 1.6°C and highest SHTM of 0.986. Reducing simulated snow density in Eq. 4.1 ($0.3 \geq \alpha \geq 0.55$) below the lowest quartile of observed values was required to increase soil temperatures to the observed range, particularly for 2017 – 18 where wintertime minimum soil temperatures are up to 12.8 °C warmer relative to the baseline model run (Fig. 31b). Different α will better fit different years of the simulation, though using the same best-fit value of α for the entire model run can still give good model performance, with a maximum value for the SHTM of 0.987 for an α of 0.40.

Errors in the timing and depth of simulated snow cover (Fig. 31c) impact the magnitude of insulation it provides, and thus the best-fit value of α (Fig. 32). A multiple linear regression was undertaken to quantify the influence of snow depth and snow depth error on the value of the best fit correction factor, for the period from snow onset to the start of simulated snow melt (when the simulated snow cover fraction was equal to one). This showed errors in the simulated snow depth can be compensated by a greater adjustment to snow thermal conductivity (Fig 32b):

$$\alpha = 0.22 + 1.14S - 0.26E + 0.55SE \tag{4.2}$$

where S equals the simulated snow depth, and E equals the simulated snow depth error. Best fit correction values were strongly related to snow depth (R^2 = 0.77, RMSE = 0.066), with different values of α more appropriate for deep ($>$ 25 cm, $\alpha \approx 0.6$) and shallow ($<$ 15 cm, $\alpha \approx 0.3$) snow (Fig. 32a).

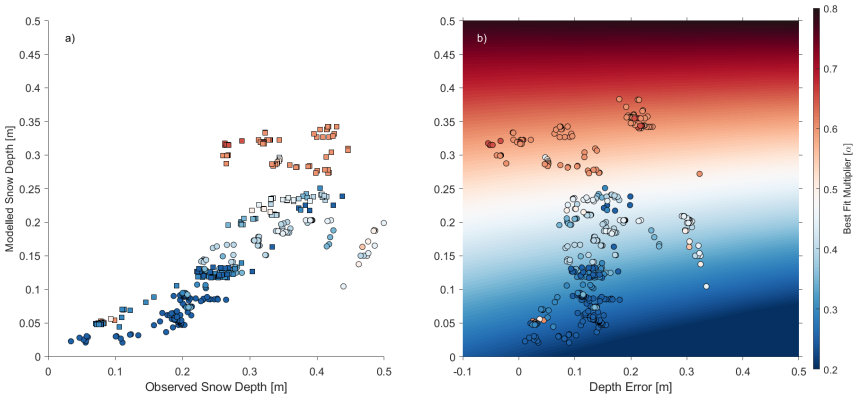

Figure 32: Influence of observed (x axis; a) and modelled (y axis; both) snow depth and snow depth error (x axis; b) on the best-fit correction (colour) at each time step for both the 2017–2018 (circles) and 2018–2019 (squares) snow seasons.

4.4 Discussion

4.4.1 Variability of snow thermal properties

SMP profiles, processed as detailed in Section 3.2.2, produced snow layer densities closely matched to density cutter measurements at TVC (Fig. 27) and consistent with measurements from other Arctic and sub-Arctic environments, e.g. ρ_{SS} = $\sim$ 100 kg m^{-3}, ρ_{WS} = 300 - 500 kg m^{-3}, ρ_{DH} = 150 - 250 kg m^{-3} in Barrere et al. (2017); Benson and Sturm (1993); Derksen et al. (2014); Domine and Shepson (2002); Domine et al. (2012, 2016a). SMP profiling has considerably increased the vertical resolution of density measurements and vastly reduced sampling times compared to traditional snowpits, enabling a far greater number of measurement profiles to be made across a wider distribution of snowpack conditions. Deriving profiles of thermal conductivity for the full depth of the snowpack, as facilitated by the SMP, is a novel approach, with most previous studies of snow thermal conductivity based on values sampled at a resolution of $\sim$ 5 - 10 cm (Domine et al., 2012, 2015, 2016b; Gouttevin et al., 2018; Morin et al., 2010).

Depth normalisation of SMP profiles (n $>$ 200 per measurement campaign) allowed comparison of snow properties with varying absolute depth. Snow depth distributions from all campaigns matched the shape and median values of tundra snow depths acquired across a $\sim$ 1500 km traverse as described in Derksen et al. (2009), which suggests transferability across wider Arctic tundra regions. Relative depth profiles of density at TVC remain consistent for all sampling campaigns, regardless of overall snowpack depth. Densities in the portion of the depth hoar layer located

between 40 - 80% depth were likely overestimated (although SMP estimates remain within the interquartile range of snowpit measurements) due to an assumption of heteroscedasticity made by the algorithm of Proksch et al. (2015), which may not apply for a material as anisotropic as depth hoar (Fig. 11). Additionally, pressure exerted on the ice matrix by the SMP may have caused wider collapse of the weak depth hoar structure during measurement (although SMP operators are easily able to profiles that are obviously affected by depth hoar collapse). As a result, the force required to penetrate the snow may be reduced (potentially below the detection limit of the SMP) in the gaps where the ice matrix has collapsed; required penetration force will conversely increase towards the base of the snowpack where the collapsed depth hoar has accumulated. This, plus an increased probability of SMP-vegetation interactions at the base of the snowpack, is likely the cause of density (and density-derived K_{eff}) increases in the lower $\sim$ 20% of all profiles. While exact impact of ice matrix collapse in depth hoar is not possible to quantify directly, this limitation is not without comparison in other direct, contact measurements of snow properties such as volumetric sampling of density (Conger and McClung, 2009; Proksch et al., 2016) and μ-CT (Zermatten et al., 2011).

The higher vertical resolution of SMP density profiles (1.25 mm, or 0.25% of snowpack depth) relative to traditional snowpit measurements (3 cm) allows snowpack features to be much more finely resolved (Calonne et al., 2020; King et al., 2020a; Proksch et al., 2015). Moving away from bulk sampling of layers with boundaries defined by abrupt binary transitions as identified by traditional stratigraphic techniques, to more continuous profiles enables features such as indurated hoar, typically a subtle transitional layer, to be captured and quantified (Pielmeier and Schneebeli, 2003; Proksch et al., 2016). Higher resolution measurements (μ-CT, SMP) of continuous profiles are increasingly implemented Proksch et al. (2016); Calonne et al. (2020); Wagner et al. (2021) but this conceptualisation of snow as a continuous profile rather than a series of discrete layers is not yet implemented in snowpack modelling, excepting the test case outlined by Simson et al. (2021).

4.4.2 Evaluation of snowpack and soil temperature simulations

Density profiles of Arctic snow from physical snow model simulations are inverted relative to observations, exhibiting low density snow in the upper part of the snowpack and high density

snow at the base, similar to what would be expected in alpine environments (Barrere et al., 2017; Domine et al., 2019). CLM is no exception, with the model producing three to four layers of uniformly high density snow, rather than a low density snow layer adjacent to the ground overlain by a higher density slab layer. Consequently, simulated density profiles are not representative of field measurements and the overall bulk density of the snowpack is overestimated. This is common of other snow models of similar physical complexity, e.g. ISBA-ES (Barrere et al., 2017), and higher complexity, e.g. SNOWPACK (Bartelt and Lehning, 2001) and Crocus (Vionnet et al., 2012), because they do not account for unique Arctic processes (Domine et al., 2016b, 2019), such as the snowpack vapour flux necessary to form depth hoar. As K_{eff} is simulated as a function of density, when models are unable to accurately describe the density profiles of Arctic snowpacks, this has a negative impact on how well K_{eff} can be simulated (Gouttevin et al., 2018). K_{eff} values from CLM are not only overestimated relative to field measurements, but also in comparison to simulations from more complex snow models in similar environments (Barrere et al., 2017; Domine et al., 2019). These problems with thermal conductivity simulations subsequently impact soil temperatures, with similar issues found for simulations of Arctic snowpacks using other models, i.e., Crocus, SNOWPACK, ISBA-ES (Barrere et al., 2017; Domine et al., 2016b, 2019; Royer et al., 2021b).

The impact of snow insulation on soil temperatures is dependent on both the depth and thermal conductivity of the snowpack (Gouttevin et al., 2012), as well as the timing of snow accumulation (Lafrenière et al., 2013). The start of the snow season is particularly important because erroneous modelled heat exchanges between air, snow and soil influence soil and snowpack properties and development, which are carried forward until the end of the snow season (Sandells et al., 2012). Temperature differences between soil and air induce a strong snowpack temperature gradient, leading to depth hoar formation and thus determining the structure of the snowpack and its capacity to insulate the soil (Domine et al., 2018).

4.4.3 Impact of approaches to correct snow thermal conductivity

Prescribing simulated snow thermal conductivity to a more physically representative value leads to an improvement in simulating soil temperatures in tundra environments, compared to both the findings herein and the permafrost model used in Yi et al. (2020). Cook et al. (2007) also found that

reducing simulated snow thermal conductivity to the lower end of observed values (0.1 Wm^{-3}) reduced soil temperature biases in an older version of CLM (CLM3.0). It has also been suggested that the simulation of wintertime soil temperatures at TVC may also be influenced by simulated soil properties and the impact of the snow cover on soil moisture content (Haagmans, 2021); bias is unlikely to be completely eliminated solely as a result of changes to snow thermal conductivity.

The impact of alternative parameterisations of snow thermal conductivity on simulated soil temperatures was tested, with a reduction in the RMSE and an improvement in the SHTM found for all 3 alternative parameterisations tested. Changing the parameterisation of snow thermal conductivity in CLM from that of Jordan (1991) to that of Sturm et al. (1997) gives the largest improvement to the simulation of both snow thermal conductivity values and underlying soil temperatures. Use of the Sturm et al. (1997) thermal conductivity parameterisation also improved soil temperature simulation in Crocus (Royer et al., 2021b), with a RMSE of 2.5 °C for soil temperatures from Crocus and CLM. The Sturm et al. (1997) parameterisation demonstrates transferability between tundra sites, having been derived from thermal conductivity measurements in the Alaskan Arctic and successfully applied to both CLM and SMP measurements at TVC. Although concern has been raised that the parameterisation of Sturm et al. (1997) may not be physically representative, we feel this provides the most feasible solution to improving soil temperature simulations in CLM given the sizeable improvement in RMSE and its use in more physically representative land surface models (Royer et al., 2021b).

Application of the correction factor α improves the simulation of soil temperatures, increasing the value of the SHTM by up to 0.3. The impact of differences between simulated and observed snow depth can be compensated by a greater adjustment to snow thermal conductivity (Figs. 31b & 32). This bias compensation between underestimates of snow depth and underestimates of snow thermal conductivity is also seen in other land surface models, e.g. JULES, LPJ-GUESS (Wang et al., 2016). However, as discrepancies between observed and simulated snow depth can vary considerably between years, this results in a best-fit correction factor value which also changes between years. These findings indicate that thermal conductivity correction factors are not the solution to soil temperature biases in models like CLM.

Differences between absolute and effective snow depths from both the model and the observational

record highlight the importance of the early season snowpack in regulating soil temperatures for the entire snow season. Simulations are sensitive to latent heat release during soil freeze-up, which maintains soil temperatures close to 0 °C for an extended period of time at the beginning of the winter (Yi et al., 2019). At this time, the soil thermal regime is also more sensitive to snow depth as snow depths are lower and have not yet reached a point where their insulative capacity has become saturated (Zhang, 2005; Lawrence and Slater, 2009; Slater et al., 2017), therefore a stronger correction is needed when snow cover is below $\sim$ 25 cm. Shallow snowpacks are likely to consist of a lower proportion of wind slab (Rutter et al., 2019) and thus their microstructural properties are less accurately represented by CLM, which does not simulate depth hoar (van Kampenhout et al., 2017), stipulating the need for a larger adjustment to α. We note that issues in simulating the initial accumulation of the snowpack are likely linked to uncertainties in the forcing data caused by measurement limitations surrounding the use of precipitation gauges in tundra environments (Smith, 2008; Watson et al., 2008; Pan et al., 2016).

Regardless of approach, these changes to the model are most applicable where snowpack structure is considerably influenced by depth hoar, as can be approximated by grid-cell plant functional type or climatology (Royer et al., 2021a; Sturm and Liston, 2021).

Ekici et al. (2015) suggests that representation of snow thermal conductivity in land surface models is less important for accurate simulation of soil temperatures than other processes not currently well represented in most land surface schemes, such as blowing snow and depth hoar formation. Further improvements in SHTM in future iterations of CLM will require a physically representative approach to snow density and thermal conductivity through explicit inclusion of vapour transport within the snowpack, currently under development in stand-alone snow microphysical models (Fourteau et al., 2021b; Jafari et al., 2020; Schürholt et al., 2021). However, this presents computational and mathematical challenges, as outlined in Jafari et al. (2020). The inclusion of physically representative parameterisations of snow properties in land surface models, such as that of Royer et al. (2021b) where the densities of lower snow layers are not allowed to exceed a maximum observation-based threshold, are more likely in the near future than the explicit representation of snowpack vapour transport. Meanwhile the substitution of the Sturm et al. (1997) thermal conductivity parameterisation provide a computationally efficient compromise, reducing

both the value of K_eff and the cold bias of simulated wintertime soil temperatures considerably (RMSE reduction of 3.3 °C).

Model underestimates of soil temperatures follow through into calculations of soil respiration, further contributing to uncertainties surrounding estimates of wintertime carbon flux (Natali et al., 2019) and suggesting that such modelled values are likely to be an underestimation of the true magnitude of these fluxes. Being able to accurately model fluxes outside of the growing season is important as these make a considerable contribution to the annual carbon budget (Natali et al., 2019; Schuur et al., 2021). A low soil temperature bias due to poorly simulated snow insulation also has consequences for predicting the evolution of permafrost (Barrere et al., 2017; Burke et al., 2020) and resultant carbon emissions when it degrades (Peng et al., 2016).

4.5 Conclusions

A new recalibration to derive profiles of tundra snow density and thermal conductivity from SMP profiles of penetration force is presented, with resulting densities and thermal conductivities then used to evaluate the performance of CLM5.0. SMP-derived density profiles show good agreement with measured snow layer densities at TVC. Comparison of measured snowpack properties from in situ SMP and needle probe techniques with simulations show the model tends to overestimate snow layer thermal conductivities by a up to factor of three, with implications for how well wintertime soil temperatures are simulated. Alternative relationships between snow density and snow thermal conductivity were considered, all of which improved the simulation of wintertime soil temperatures (RMSE reduction of 0.2 – 3.3 °C). Reducing simulated thermal conductivities through the use of a correction factor (α) also improves simulation of soil temperature (RMSE reduction of 3.7 °C for an α of 0.45). The optimal magnitude of this reduction is strongly linked to snow depth (with a greater reduction needed for shallower snowpacks). Different optimal correction factors for different snow seasons illustrate the limitations of this approach, but the results are still instructive as a diagnostic for model sensitivity to the treatment of snow thermal conductivity.

Further improvements to simulated snow properties will require more explicit representation of key processes not currently accounted for in CLM, chiefly the formation of depth hoar. A more

physically representative snowpack should also improve simulation of wintertime soil thermal conditions. Snowpack vapour kinetics are not currently included within global land surface models, which also have to consider a large variety of other processes and avenues for future development (Blyth et al., 2021; Fisher and Koven, 2020), although developments are being made to consider these in complex microscale snow physics models. Empirical scaling of snow thermal conductivity provides a computationally efficient interim solution with a similar impact on soil temperatures as the explicit representation of a large depth hoar fraction in point-scale simulations by Zhang et al. (1996), but the value of the required scaling factor changes with snow depth. Different parameterisations of snow thermal conductivity also improve simulation of soil temperatures, with that of Sturm et al. (1997) more appropriate for Arctic snowpacks (RMSE reduction of 3.3 °C) than that of Jordan (1991) which is used by default in CLM. Improving the accuracy with which Arctic wintertime soil temperatures can be simulated may help to reduce sizable uncertainties (Natali et al., 2019) surrounding current projections of wintertime carbon fluxes.

Chapter 5

Simulating net ecosystem exchange under seasonal snow cover at an Arctic tundra site

5.1 Introduction

Although considerably more attention has been paid to Arctic CO_2 fluxes during the growing season, winter (i.e. snow-covered non-growing season) CO_2 emissions are now understood to make a significant contribution to annual carbon budgets in Arctic environments (e.g. Campbell, 2019; Natali et al., 2019; Rafat et al., 2021). The cumulative effect of winter emissions may even offset plant uptake of CO_2 in the growing season, particularly as the climate warms (Belshe et al., 2013; Christiansen et al., 2012; Jeong et al., 2018), with the magnitude of non-growing season emissions likely to increase under climate change (Box et al., 2019; Commane et al., 2017; Watts et al., 2021). However, understanding of non-growing season CO_2 fluxes is limited (Lüers et al., 2014). CO_2 fluxes across the Arctic region quantified by either Terrestrial Biosphere Models (TBMs) or empirical estimates vary by a factor of three and a half (377 - 1301 Tg Carbon; Natali et al., 2019).

Uncertainties in process representation and parametrisation of TBM simulations of carbon fluxes limit our ability to assess and predict future changes (Braghiere et al., 2023; Treharne et al., 2022),

particularly in the non-growing season. The representation of biogeochemical cycles in TBMs is subject to a high degree of parametric uncertainty (Fisher et al., 2019), with non-growing season processes and mechanisms poorly represented (Larson et al., 2021). Model intercomparison studies show large differences between individual predictions, with uncertainty in many aspects of the Arctic carbon cycle greater than the absolute magnitude of carbon fluxes (Fisher et al., 2014). Variability in carbon flux estimates between models are particularly prevalent during the winter (Fisher et al., 2014) and fluxes in the early winter shoulder season are likely underestimated (Commane et al., 2017). Improving (or even just including) the representation and influence of snow, soil and biogeochemical non-growing season processes in TBMs will potentially improve our understanding of carbon dynamics and projections of Arctic climate change (Campbell and Laudon, 2019).

Mechanisms of non-growing season soil respiration are not well-studied, particularly the impact of environmental controls on heterotrophic respiration in subfreezing soils, leading to large uncertainties in their representation in models (Tao et al., 2021). Poor simulation of early winter respiration in many TBMs is possibly linked to underestimation of soil temperature (Tao et al., 2021). Error in simulated soil temperatures at the start of the non-growing season, when soil temperatures become disconnected from overlying air due to the insulation provided by nascent snowcover, continues to impact soils throughout the entire period when snow is on the ground. Such cold biases in wintertime soil temperature can be mitigated with a change in the parameterisation of snow thermal conductivity (Dutch et al., 2022; Royer et al., 2021b) because the stratigraphic and hence insulative properties of Arctic snowpacks are not well simulated (Barrere et al., 2017; Domine et al., 2019). Decreasing snow thermal conductivity, which increases near surface soil temperatures, has been found to increase simulated non-growing season Net Ecosystem Exchange (NEE), with winter emissions more than doubling in the Terrestrial Biosphere Model LPJ-GUESS after addition of a multi-layer snow scheme with temporally evolving snow properties (Pongracz et al., 2021). Additionally, the empirical formulae used by many TBMs to model relationships between soil temperature, moisture, and soil respiration are often derived from datasets which under-sample or do not include high-latitude regions (See citations in Bonan (2019) for examples). For example, the temperature sensitivity of soil respiration is typically described with the use of a single, globally averaged Q10 value, representing the proportional change in respiration

with a 10 °C rise in soil temperature (Lloyd and Taylor, 1994). However, Q10 is likely temperature dependant (Hamdi et al., 2013; Lloyd and Taylor, 1994; Kirschbaum, 1995) and may also be influenced by other environmental conditions such as soil moisture, texture and plant community composition (Chen et al., 2020; Curiel Yuste et al., 2004; Meyer et al., 2018). As a result, observed Q10 from studies of Arctic ecosystems are typically larger than globally averaged values, with the synthesis of Chen et al. (2020) finding a median Q10 for tundra ecosystems (5.4) approximately double that of their global median (2.3). However, differences between Arctic and global Q10 values are not reflected in Arctic climate simulations, with approximately half of the 11 models investigated by Huntzinger et al. (2020) using Q10 only half the size of observed values. Empirical relationships between soil moisture and respiration (often parameterised using Ψ) in many TBMs are derived from small scale studies which do not account for respiration from frozen soils (Andrén and Paustian, 1987; Orchard and Cook, 1983). Relationships between soil moisture and respiration are also likely to be influenced by other soil properties, such as bulk density, texture and carbon content, with different relationships observed for mineral and organic soils (Moyano et al., 2012). Interactions between temperature, moisture and respiration suggest that these properties should be considered together when working to improve our understanding of CO_2 fluxes.

As much of the Arctic tundra is snow-covered for up to 10 months of the year (Olsson et al., 2003), it is important to accurately simulate non-growing season carbon emissions under snow-covered conditions to better quantify annual carbon budgets. In our previous study (Dutch et al., 2022, the previous chapter of this thesis) examining the parameterisation of snow thermal conductivity in the Community Land Model version 5 (CLM5.0) at Trail Valley Creek (TVC), NWT, we found a cold soil temperature bias of 6 °C, and suggested this bias may impact the simulation of NEE during the snow-covered non-growing season. TVC makes an ideal type-site for much of the Arctic tundra, having been intensively studied and used to characterise the hydrology of tundra regions since the mid-1990s (Marsh et al., 2008; Pomeroy et al., 1993; Quinton and Marsh, 1999, e.g.). In this study, we assess whether the default parameterisation of CLM5.0 accurately simulates carbon fluxes (NEE) during the snow-covered non-growing season at Trail Valley Creek (TVC), NWT. We evaluate the impact on the simulation of NEE of the parameterisation of:

1. snow thermal conductivity (K_{eff}),
2. the relationship between soil moisture and soil decomposition (Ψ_{min}), and

3. the rate of change of soil respiration as a function of soil temperature (Q10).

The overall aim is to compare simulations of soil respiration and NEE to eddy covariance (EC) measurements for 3 snow-covered non-growing seasons and consider how to better parameterise the model in Arctic tundra environments on both sub-seasonal timescales and cumulatively throughout the snow-covered non-growing season.

5.2 Data and Methods

5.2.1 Field and Forcing Data

Model testing was undertaken at Trail Valley Creek (TVC; 68°45'N, 133°30'W); a boreal-tundra transition research watershed in the Inuvialuit Settlement Region, northeast of Inuvik, NWT, Canada. Mean annual air temperature at TVC was -7.9 °C for the period 1999 – 2018 (Grünberg et al., 2020), with typical end-of-season snow depths of $<$ 50 cm (King et al., 2018). A more thorough description of this site and forcing data used to drive CLM is given in Section 3.1.1 and Section 3.4.6.

5.2.2 Model Description

A description of soil processes in CLM relevant to this chapter is given in Section 3.4.2. Additionally, the parameterisation of soil freezing in CLM is given in Yang et al. (2018). For this chapter, cryoturbation, the mixing of soil material due to freeze thaw processes, was switched on with the maximum depth for cryoturbation set to to 1 m, in line with observations of active layer thickness at this site (Wilcox et al., 2019).

5.2.3 Experiment Setup

The sensitivity of simulated NEE was evaluated in comparison to measured NEE in response to changes in the model parameterisation of 1) snow thermal conductivity, 2) the relationship between soil moisture and soil decomposition (rW; Equation 3.9), and 3) the relationship between soil respiration and soil temperature (rT; Equation 3.8). Simulation sensitivity was evaluated over snow-cover dates simulated by CLM5.0 (9^{th} Oct 2016 – 23^{rd} May 2017; 12^{th} Oct 2017 – 30^{th} May 2018; 24^{th} September 2018 – 23^{rd} May 2019), which were always within a week of

observed snow cover onset and meltout (Dutch et al., 2022). We compared two options for the parameterisation of effective snow thermal conductivity (K_{eff}), that of Jordan (1991) used by default in CLM5.0, and that of Sturm et al. (1997) derived from Arctic snowpack measurements and shown to improve soil temperature simulation in both CLM5.0 (Dutch et al., 2022) and other land surface models (Royer et al., 2021b). We also adjusted the soil decomposition rate modifiers (r_T and r_W in Equation 1), similar to the approach of Tao et al. (2021), sampling a broad range of values for the parameters Ψ_{min} (for rW; Equation 3.9) and Q10 (for rT; Equation 3.8), as listed in Table 6. Values for Q10 sampled a wide range of measured Q10 from Arctic soils (based on Chen et al., 2020; Elberling, 2007; Elberling and Brandt, 2003; Grogan and Jonasson, 2005; Mikan et al., 2002; Schmidt et al., 2008), and values of Ψ_{min} were based on Tao et al. (2021) We note that the most negative ($<$ -200 MPa) of Ψ_{min} used by Tao et al. (2021) and herein are unlikely to be physically representative (Liang et al., 2022). In total, 32 model simulations were performed, perturbing K_{eff}, Q10 and Ψ_{min} simultaneously. We avoid the one-at-a-time approach typical of many parameter sensitivity analyses in order to examine the interaction between parameters (Gao et al., 2020) and evaluate their relative importance in improving wintertime carbon flux simulations.

5.3 Results

5.3.1 Measured NEE and soil temperatures

Measured NEE was broadly positive (with weekly NEE averages ranging from -0.1 to 1.1 g C m^{-2} day^{-1}) throughout the snow-covered non-growing season, suggesting that CO_2 was emitted from the ground at TVC throughout the winter (Figs. 33a & 34). Measured mean NEE was positive until mid-April, at which point measured NEE followed an increasingly negative trend, indicating potential photosynthetic uptake. Soil freeze-up began with the onset of snowfall in October, with weekly mean 10 cm soil temperatures reaching a minimum value of -10.2 °C in

Parameter to Adjust	Parameter Values			
Snow Thermal Conductivity	Jordan (1991) - *Default*		Sturm et al. (1997)	
Ψ_{min}	-2 MPa	-20 MPa	-200 MPa	-2000 MPa
Q10	1.5 - *Default*	2.5	5.0	7.5

Table 6: Parameters included in sensitivity analysis and the values sampled over.

early March. Soils began to warm as the snowpack melted, with observed weekly mean soil temperatures becoming positive in the second week of June (Fig. 33c). As considerably more NEE measurements were available for the snow-covered period of 2017 – 2018 than 2016 – 17 or 18 – 19 (Table 10), we primarily focused on 2017 – 2018 when presenting measurements or comparing measured and simulated fluxes. However, cumulative simulated fluxes were presented for all three winters.

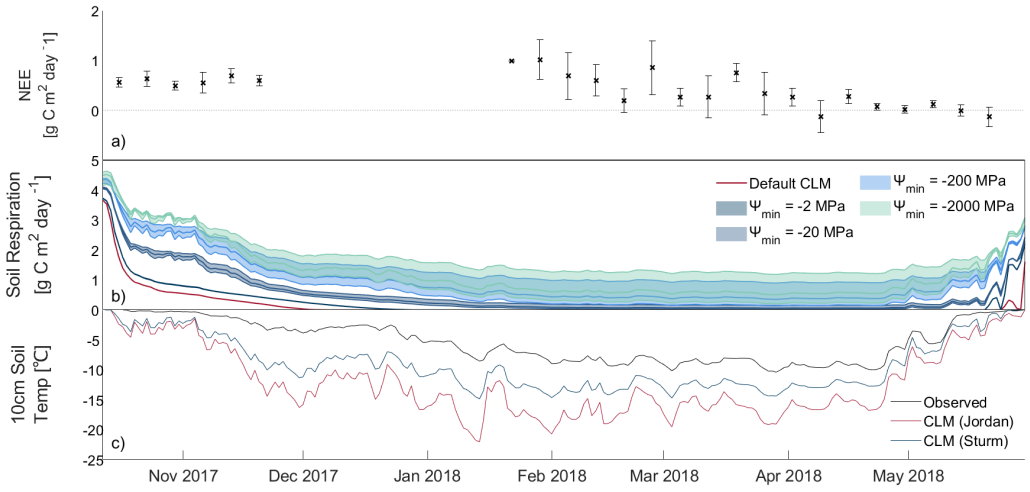

Figure 33: a) Mean (crosses) and uncertainty (as per Lasslop et al., 2008, ; error bars) of measured Net Ecosystem Exchange (NEE) at weekly intervals. b) Simulated soil respiration. The default simulation (red) uses the Jordan (1991) parameterisation of snow thermal conductivity, and blue tones represent simulations using the Sturm et al. (1997) parameterisation of snow thermal conductivity. Darker blue colours represent less negative values of Ψ_{min} and paler colours represent more negative values of Ψ_{min}. Shaded areas on b) represent the range of respiration fluxes for simulations using the Sturm et al. (1997) snow thermal conductivity and the same values of Ψ_{min}, but with different values of Q10 (1.5, 2.5, 5.0, 7.5). c) 10cm soil temperatures, both observed (purple) and simulated using both the default Jordan (1991; Red) and Sturm et al. (1997; blue) snow thermal conductivity parameterisations.

5.3.2 Simulated NEE

The default parameter configuration of CLM5.0 simulated negligible, near-zero NEE (all values below 0.01 g C m^{-2} d^{-1}) between late November and mid-May in all 3 winters. CLM5.0 does not simulate Gross Primary Productivity (GPP) during the entirety of the snow-covered season in all 3 winters. Autotrophic respiration is similarly negligible (all values below 0.01 g C m^{-2} d^{-1}) in all simulations of the snow-covered non-growing season, regardless of parameter choices. As heterotrophic respiration, other than soil biota, is also not simulated during periods of snow-cover,

simulated NEE and soil respiration can be considered equivalent for simulations of snow-covered non-growing seasons.

Sensitivity analysis of three parameters (Ψ_{min}, Q10 and snow thermal conductivity) resulted in considerable variability in the simulated soil respiration and NEE over all three snow-covered periods (Figs 33 & 34). Minimum total snow-covered non-growing season NEE was simulated for the default Ψ_{min} (-2 MPa) and the default Jordan (1991) snow thermal conductivity parameterisation. For all years, simulated fluxes were greatest for a Q10 of 1.5, Ψ_{min} of -2000 MPa, and the Sturm et al. (1997) snow thermal conductivity parameterisation. The minimum and maximum cumulative simulated NEE differed by 370 g C m^{-2} of magnitude between the different sets of parameter values (Fig. 35). This difference in cumulative simulated NEE was greater in years with earlier snow onset date, e.g. 2018-19, as this increased the duration of relatively warmer winter soils with higher respiration rates during freeze-up, in comparison to the total duration of colder soils throughout the non-growing season snow cover. In all 3 winters, simulations were most sensitive to chosen parameter values during the freeze up period, with the range of soil respiration fluxes approximately double that in midwinter (Fig. 33). Simulated NEE decreased gradually from snow-cover onset until December-January, and then remained at that level until increasing from late April onwards as soils warm and snow melts.

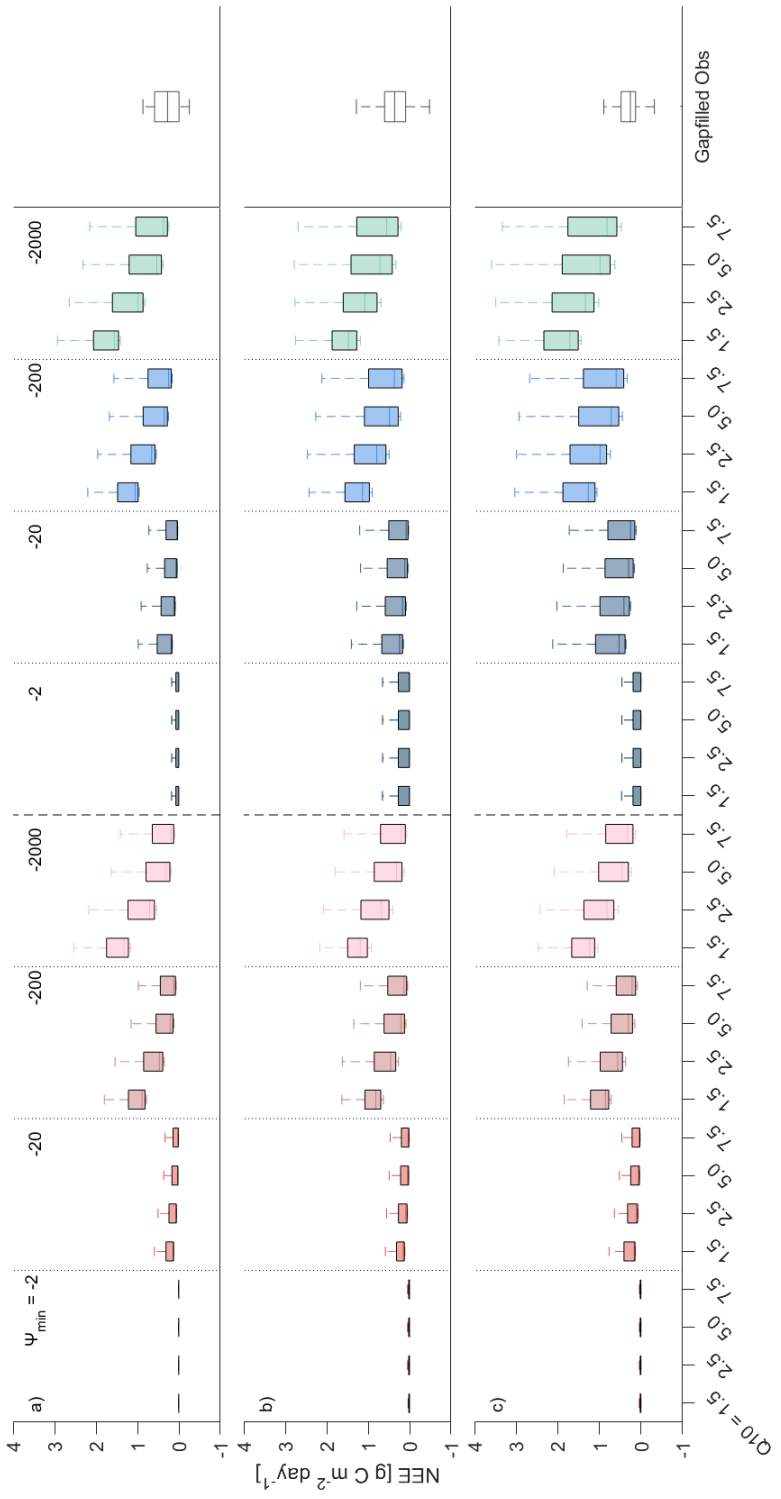

Figure 34: Wintertime Net Ecosystem Exchange (NEE) from each year of the study for each of the model runs and the eddy covariance tower observations. Red tones represent model runs using the Jordan (1991) parameterisation of snow thermal conductivity, and blue tones represent runs using that of Sturm et al. (1997). Darker colours (towards the left) represent less negative values of Ψ_{min} and paler colours (towards the right) represent more negative values of Ψ_{min}. Outliers are not shown.

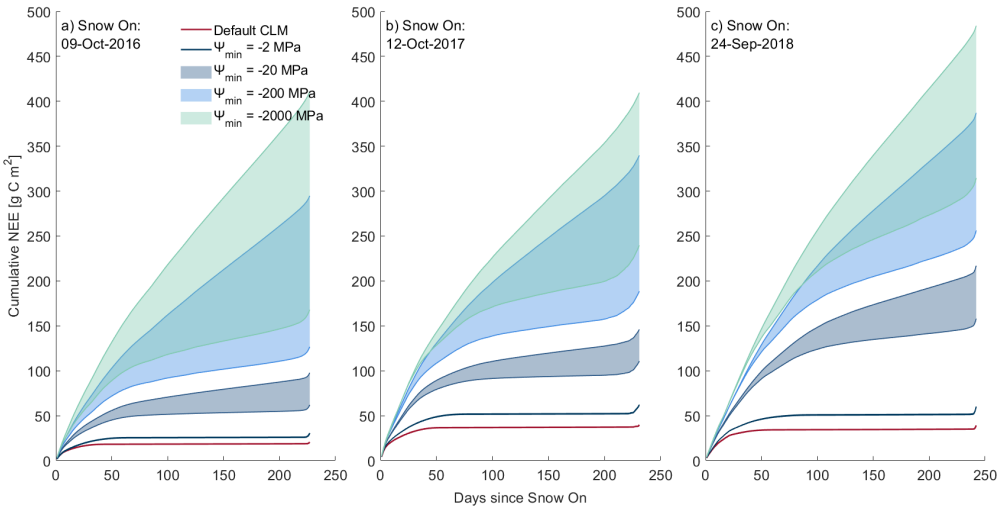

Figure 35: Cumulative Net Ecosystem Exchange (NEE) for the simulated snow cover duration in the seasons of a) 2016 – 17 (227 days), b) 2017 – 18 (231 days), and c) 2018 – 19 (242 days) from the ensemble of simulations. Blue tones represent simulations using the snow thermal conductivity parameterisation of Sturm et al. (1997), with darker colours for less negative values of Ψ_{min}. The shaded areas represent the range of Q10 values (1.5 – 7.5) for each value of Ψ_{min}. The dark red line represents the default CLM snow thermal conductivity parameterisation of Jordan (1991).

Changes from Jordan (1991) to Sturm et al. (1997) representations of snow thermal conductivity delayed, by approximately 2 months, the onset of moisture limitation for simulations with the default value of Ψ_{min}, enabling more positive simulation of NEE during freeze-up. The choice of snow thermal conductivity scheme significantly impacted simulations of mean winter soil respiration when considered throughout the total snow-covered non-growing season in all three years (student's t-test: t_{16-17} = -6.76, t_{17-18} = -8.01, t_{18-19} = -8.02, $p < 0.001$). Compared to the default Jordan (1991) parameterisation of snow thermal conductivity, the Sturm et al. (1997) parameterisation resulted in warmer near surface soil (Fig. 33c) and hence more positive NEE, provided soil respiration had not become moisture limited. Model sensitivity to Ψ_{min} was lower for the Jordan (1991) snow thermal conductivity parameterisation (Fig. 36a) than for Sturm et al. (1997) (Fig. 36b); differences between parameterisations were greatest with a more negative Ψ_{min} (Fig. 36c).

Simulated winter soil moisture potentials (Ψ_j; Eq. 3.7) had a typical value of approximately -15 MPa, lower than the default Ψ_{min} (-2 MPa), preventing soil decomposition and respiration for the majority of the winter. Analysis of variance showed significant differences between simulated mean snow season soil respiration (F_{16-17} = 19.45, F_{17-18} = 22.41, F_{18-19} = 23.80, $p < 0.001$)

and cumulative snow season NEE (F_{16-17} = 19.47, F_{17-18} = 22.45, F_{18-19} = 23.86, $p < 0.001$; Fig. 35) for Ψ_{min} of -2 and -2000 MPa, though differences between simulations with only one order of magnitude between their Ψ_{min} were not always deemed statistically significant (α = 0.001). Consequently, adjusting Ψ_{min} had the largest impact on simulated fluxes, with larger negative Ψ_{min} resulting in larger NEE.

Changes to Q10 had a smaller impact on simulated NEE than the parameterisation of K_{eff} or Ψ_{min}, with analysis of variance showing no significant difference between the mean snow season soil respiration for different Q10 (Table 6) in all 3 winters. Differences in simulated cumulative snow season fluxes were also not statistically significant. Additionally, simulation sensitivity to frozen Q10 values (Schmidt et al., 2008) were tested. An extreme frozen Q10 of 300, Schmidt et al. (2008), did not reduce the gap between simulated and measured NEE, with no appreciable difference between model runs where all other parameter choices were held constant.

Simulations with more negative Ψ_{min} ($<$ -200 MPa) and higher Q10 ($\geq$ 5) tended to have lower RMSE in comparison with to measured weekly mean NEE (Fig. 37). As changes to Ψ_{min} and Q10 had opposing impacts on the magnitude of simulated fluxes, different pairs of parameter values gave similar results. This counterbalancing effect strongly influences identification of an appropriate parameter space, e.g. simulations using a wide range of Ψ_{min} with lower Q10 more greatly overestimated measured NEE during freeze-up and thaw than model runs with higher Q10 values (Fig. 37). Overestimation of simulated NEE particularly impacted cumulative NEE during freeze-up in 2017 - 18 (Fig. 38), with a reduction in December to mid-March NEE compensat-

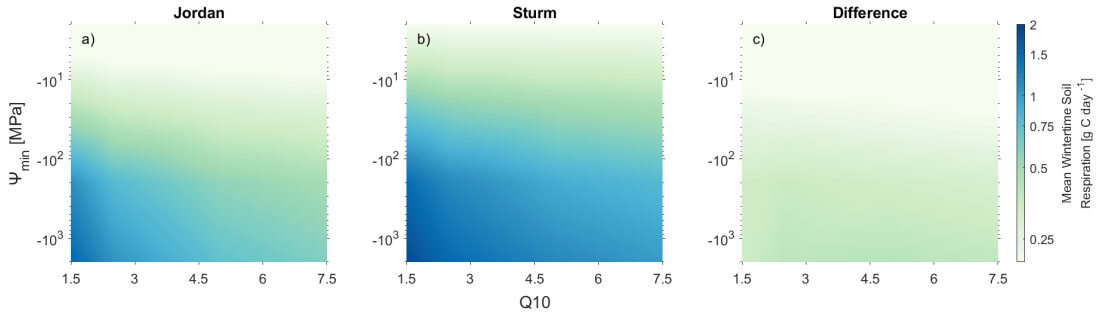

Figure 36: Contour plots showing the relative influence of the values of Ψ_{min} and Q10 on the simulation of mean soil respiration for all 3 snow-covered seasons for model runs using the snow thermal conductivity parameterisations of a) Jordan (1991) and b) Sturm et al. (1997). The difference between the two schemes is shown in c).

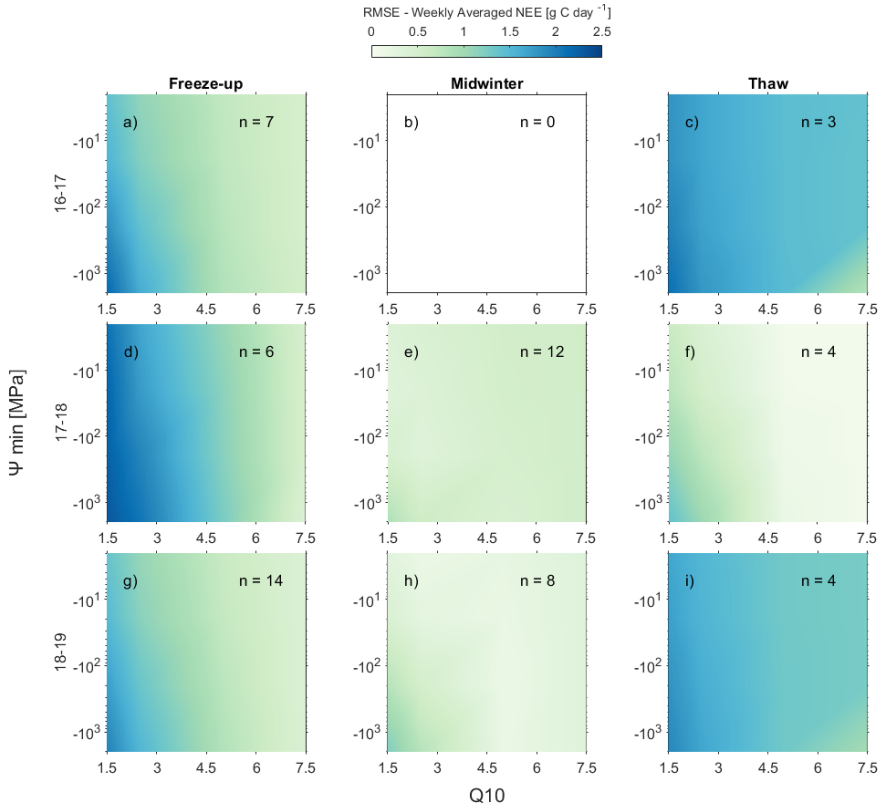

Figure 37: Evaluation of the impact of Ψ_{min} and Q10 parameterisations on simulated Net Ecosystem Exchange (NEE) during freeze-up (a,d,g), midwinter (b,e,h) and thaw (c,f,i) periods of each snow-covered season. n values denote the number of weekly averages included in each panel.

ing for freeze-up overestimations; using mid-range values of Ψ_{min} (-20 MPa) produced similar simulated and measured total cumulative non-growing season NEE.

5.4 Discussion

5.4.1 NEE & soil respiration variability throughout snow covered non-growing seasons

The default parameterisation of CLM5.0 prevented simulation of soil respiration for most of the snow-covered non-growing season, leading to negligible simulated NEE, contrary to broadly positive patterns of measured NEE. Application of the Sturm et al. (1997) snow thermal conductivity parameterisation reduced simulated soil temperature biases (Dutch et al., 2022; Royer et al., 2021b), which reduced the proportion of the snow-covered non-growing season for which simulated NEE was zero. Other TBMs have shown sensitivity of simulated NEE to snowpack rep-

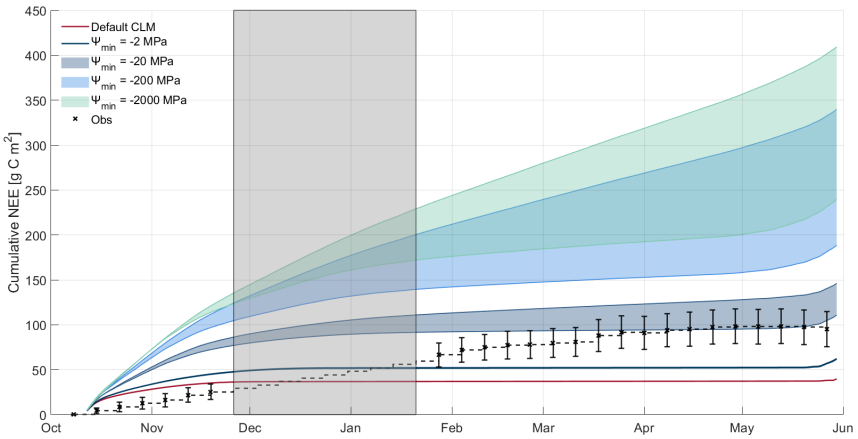

Figure 38: Cumulative Net Ecosystem Exchange (NEE) for winter 2017 – 18. The black crosses show cumulative weekly measured NEE, with the error bars representing measurement uncertainty as per Lasslop et al. (2008). The shaded grey box denotes the period where eddy covariance data is unavailable; the cumulative observed total at this time calculated using the mean value of the six weekly means post and prior to the period of data loss. The curves show the simulated cumulative NEE, with blue tones representing simulations using the snow thermal conductivity parameterisation of Sturm et al. (1997), and with darker colours for less negative values of Ψ_{min}. The shading of these curves represents the range of Q10 values (1.5 – 7.5) for each value of Ψ_{min}. The dark red line represents the default CLM snow thermal conductivity parameterisation of Jordan (1991).

resentations, with improvements to the representation of the snowpack (including a multi-layer snowpack with variable, as opposed to prescribed, snow thermal conductivity) in LPJ-GUESS improving the simulation of wintertime NEE (Pongracz et al., 2021).

Cumulative snow-covered non-growing season NEE is not only dependent on parameterisation of snow thermal conductivity, but also the timing of snow onset at the start of the winter. In 2018 – 19, when the snow-on date was 3 weeks earlier than the previous year, soils cooled more slowly due to thermal insulation against cold atmospheric air, leading to greater cumulative NEE. This was particularly evident for simulations using the Sturm thermal conductivity parameterisation, which better represents the early winter formation of low thermal conductivity basal snowpack depth hoar layers. Interannual variability in snow conditions are reflected in simulated fluxes, further substantiating the importance of improving simulations of Arctic snowpacks. Biases and uncertainties in simulated snow mass, (e.g. Kim et al., 2021; Mudryk et al., 2020), are likely to influence soil temperature (Dutch et al., 2022), heterotrophic respiration and CO_2 fluxes, particularly on regional scales (Tao et al., 2021). Improving the representation of snow and soil conditions, or

at least how these relate to respiration, at the start of the snow-covered non-growing season is also important as this is likely to be the most biologically active part of the season with comparatively high rates of soil respiration (Commane et al., 2017; Olsson et al., 2003).

Simulated NEE increased considerably after the start of snowmelt, regardless of parameter choices, but was less rapid for simulations with larger negative Ψ_{min}. Simulated NEE was most likely too positive at the end of the winter season due to delayed onset of simulated photosynthesis (Birch et al., 2021) and not well matched to trends in measured NEE, which decreased from late April through May. Simulated gross primary productivity was zero for the entirety of the snow-covered period, but the pattern of decreasing measured NEE during thaw suggested that photosynthesis could be occurring before snow had completely melted out, which has been observed at similar Arctic locations (Finderup Nielsen et al., 2019; Larsen et al., 2007; Starr and Oberbauer, 2003).

5.4.2 Parameterisation of soil moisture, temperature and respiration relationships

Of the three parameters investigated, Ψ_{min} had the largest impact on the simulated snow-covered non-growing season NEE. Without changes to Ψ_{min}, simulated soil moisture limited soil respiration, meaning simulated NEE was zero for the majority of the snow-covered non-growing season. Accurate simulation of a moisture threshold to soil respiration is important as moisture acts as a key control on soil respiration (Orchard and Cook, 1983), particularly in the shoulder season before snow onset (Liu et al., 2020) and in frozen soils (Öquist et al., 2009). Consequently, changes to soil moisture content have a strong influence on simulated soil respiration and wider carbon cycling (Chadburn et al., 2017). CLM5.0 represents limitation of respiration in frozen soils by an unavailability of liquid water (Lawrence et al., 2018), as shown by the strong dependence of simulated fluxes on Ψ_{min}. However, CLM5.0 has known deficiencies in simulating soil moisture in high-altitude and high-latitude environments (Deng et al., 2020, 2021; Schädel et al., 2018), overestimating soil moisture when soils are frozen (Deng et al., 2020) and with soil heating leading to increased soil dryness, as opposed to observed increases in soil wetness (Schädel et al., 2018). Soil moisture biases may even have been exacerbated by model development, with Deng et al. (2020) finding a greater difference between simulations and observations for CLM5.0 than CLM4.5.

Even in frozen soils, liquid water can be present within the soil matrix, enabling respiration at temperatures as low as -18 °C (Elberling and Brandt, 2003), whereas when Ψ_{min} exceeds Ψ simulated soil respiration ceases at warmer temperatures than -18 °C. Recent findings from Liang et al. (2022) suggest that mineral soils should be able to respire below a Ψ of -10 MPa, suggesting a Ψ_{min} below -10 MPa would be more physically representative than the current CLM5.0 default of -2 MPa. Tao et al. (2021) also highlighted the unsuitability of such a high Ψ_{min}: the default Ψ_{min} of -10 MPa in E3SM (a five times larger negative Ψ_{min} than the CLM5.0 default) prevented simulation of respiration when soil temperatures were sub-zero and failed to allow the accurate simulation of wintertime respiration in permafrost tundra environments. A more mechanistic approach, e.g. Yan et al. (2018), where respiration increases linearly from zero as soon as soil moisture is not zero (Chadburn et al., 2022) may produce more appropriate simulations of soil respiration in tundra environments than the commonly used thresholding approach of CLM5.0. The use of a Ψ_{min} threshold may still be appropriate if decomposition does not automatically drop to zero when the threshold is reached, for example, the rW scalar in JULES drops to 0.2, not zero, when Ψ is lower than Ψ_{min} (Burke et al., 2017), allowing for wintertime decomposition.

The impact of changing Q10 in CLM5.0 was lower than in other TBMs; smaller changes to Q10 had a larger influence on E3SM simulated fluxes at similar Arctic tundra sites (Tao et al., 2021). At most negative Ψ_{min} values, higher Q10 values were required to more accurately simulate soil respiration, similar to Tao et al. (2021) who found that a Q10 66% larger than the default of 1.5 led to improved simulations of wintertime soil respiration for sites in the Alaskan tundra. As observed Q10 changes with temperature, it may be more appropriate to generate Q10 at each timestep as a function of soil temperature, an approach already undertaken in other TBMs such as CLASSIC (Melton and Arora, 2016; Wu et al., 2016). By using both soil moisture and soil temperature to parameterise Q10, Kim et al. (2019) found an improvement to negative ecosystem respiration biases compared to the use of a Q10 of 1.5 in global CLM4 simulations. However, Byun et al. (2021) states that standard Q10 functions fail when describing the relationship between temperature and CO_2 production of frozen soils, and so the use of a Q10 function may not be the most appropriate way to model the relationship between soil respiration and temperature at sites such as TVC. Alternative parameterisations of rT (such as RothC; Jenkinson, 1990) may provide a more appropriate description of the relationship between temperature and soil respiration, as has been suggested

for other TBMs such as JULES (Burke et al., 2017). This may not lead to improved model performance; Tao et al. (2021) tested non-Q10 parameterisations of the soil temperature:respiration relationship in the CLM-based E3SM and found that a Q10 parameterisation gave the best result for 3 of their 4 Alaskan Arctic sites. Although limited observational data of soil respiration limits the assessment of suitability of Q10 functions (Kim et al., 2019), testing additional parameterisations (as opposed to just Q10) may give insight that could improve the simulation of NEE at Arctic tundra sites in CLM5.0.

5.4.3 Implications, Uncertainties & Modelling Approach

Across the Arctic, land surface models which attempt to describe the relationships between soil properties (such as temperature and moisture) and respiration tend to produce carbon flux estimates closer to observed flux values (Huntzinger et al., 2020). With the parameterisation of respiration and decomposition as functions of soil properties, we would therefore expect to see fluxes from CLM which are vaguely representative of real-world measurements, and yet simulated wintertime fluxes in the snow-covered season are typically zero for the default model configuration. Different factors control respiration in frozen and unfrozen soils (Sullivan et al., 2008), and thus the estimation of soil respiration in Arctic environments from parameters derived from mid-latitude studies does not adequately represent cold-region processes. Alternative values for a small selection of parameters (Table 6) have been tested, with some parameter combinations shown to decrease the mismatch with observations, although there are many other parameters that we have not tested, and we do not know what effect these would have on simulated fluxes. Without appropriate values for parameters such as Ψ_{min}, models will gradually drift back towards internal steady-state conditions (Huntzinger et al., 2020). However, individual parameter values in soil biogeochemical models are typically unable to be inferred from observed data (Marschmann et al., 2019), a problem exacerbated in polar regions by the challenging environmental conditions which in turn limit data collection. The integration of more processes (as is seen in a high-complexity model such as CLM5.0) further increases the likeliness of parametric uncertainties and the difficulty in deriving model parameter values from observed values (Luo et al., 2009).

Extrapolation of site-level parameterisations can bias regional flux estimates and over time lead to considerable variations in the magnitude of regional carbon stocks (Tang and Zhuang, 2008).

Spatially distributed measurements of wintertime carbon fluxes on a wider variety of spatial scales in order to verify flux tower estimates will assist in constraining modelled flux estimates and help us to back-calculate more appropriate parameter values. This is particularly important on seasonal timescales, as currently observational limitations prevent a whole season estimate of cumulative flux from being obtained (Fig. 38). Additionally, seasonal carryover effects have been shown to influence wintertime respiration in other land surface models, such as by controlling the availability of products for decomposition (Burke et al., 2017). Issues in simulating Net Primary Production raised by Birch et al. (2021) may therefore also contribute uncertainty towards simulated wintertime flux values.

Poor simulation of soil respiration in the snow-covered season under the default parameterisation of CLM has implications beyond the snow covered period. A lack of simulated emissions for a considerable proportion of the year leads to a misrepresentation of the annual carbon budget. The scale of unsimulated emissions, particularly when considered across the total areal extent of the Arctic tundra ($\sim$ 7.6 x 10^6 km^2; Bliss and Matveyeva, 1991), makes a considerable contribution to the global carbon budget – and thus its omission may have an impact on the simulation of future climate. Failure to appropriately quantify the wintertime release of CO_2 is also likely to affect future simulations of soil turnover and permafrost coverage.

5.5 Conclusions

The default parameterisation of CLM5.0 did not reproduce the broadly positive measured NEE during snow-covered non-growing seasons at an Arctic tundra site. Soil respiration was not simulated for the majority of the snow-covered non-growing season due to a moisture threshold limiting soil respiration in frozen soils, despite widely documented midwinter CO_2 emission at numerous sites across the Arctic tundra (Natali et al., 2019; Virkkala et al., 2021). Furthermore, the default parameterisation of CLM5.0 did not capture sub-seasonal patterns of measured NEE. Simulated NEE was too high towards the start of the snow-covered non-growing season, regardless of parameter values tested. Initial conditions at freeze-up are important in determining the magnitude of cumulative NEE for the entire snow-covered non-growing season, with changes to all parameters tested having the greatest impact at this time as the insulative capacity of the snow has not yet been reached.

Reducing soil temperature biases in CLM5.0 through a change to the parameterisation of snow thermal conductivity, from Jordan (1991) to Sturm et al. (1997), increased the magnitude of simulated NEE during the snow-covered period. However, without improvement to the soil moisture threshold term Ψ_{min}, other parameter changes had very little impact on simulated NEE. The default Ψ_{min} of –2 MPa was not appropriate for Arctic environments, with a five times larger negative Ψ_{min} producing snow-covered non-growing season NEE more similar to measured NEE. Not only did the default parameterisation of Ψ_{min} prevent wintertime respiration, poorly representing seasonal and annual carbon budgets and dynamics, it may also have longer term implications for the simulation of soil carbon turnover and the state of permafrost, limiting the reliability of longer term climate simulations. Larger positive Q10 had an opposite impact on simulations than larger negative Ψ_{min}, with larger Q10 depressing the magnitude of simulated NEE. Adjustments to both parameters in tandem provided the greatest improvement to simulated NEE, with larger negative Ψ_{min} and larger positive Q10 simulating greater NEE during the snow-covered non-growing season. Alternative approaches to the relationships between soil temperature, moisture and respiration may also provide a more appropriate solution in future iterations of CLM than changing the values of the parameters currently used - although this will require further investigation.

Chapter 6

Measurements of CO_2 Flux within Snowpacks at an Arctic Tundra site

6.1 Introduction

Many different methods are used to measure CO_2 fluxes in snow-covered environments, each with their own limitations (Table 3.3.5). Methodological limitations surrounding measurements of wintertime CO_2 fluxes limit our ability to evaluate model simulations, and thus hinder our ability to best parameterise models in order to predict future change (Section 5.4). Eddy covariance (EC) timeseries are typically used for such model evaluations, but these measurements are expensive and challenging to maintain. Such systems are not universally accessible or appropriate, even before considering the additional complexities of the Arctic winter, and are subject to a high degree of uncertainty, as detailed in Appendix A. Additionally, as EC towers take an aggregated measurement over footprints of hundreds of meters, this limits their ability to capture localised heterogenities in emission processes (Pirk et al., 2017).

The use of additional measurements alongside (theoretically) continuously operational EC towers can be used to help "ground-truth" these measurements, but still limitations persist. Snapshot profiles of gas concentrations using syringe samples do not account for potentially rapid temporal fluctuations in emissions. This makes it difficult to use these to capture process-driven changes, such as wind-pumping (Section 2.3.1). Static snapshot measurements also limit our ability to

estimate how consistent measured fluxes may be over time, and how the snowpack responds to change, such as diurnal temperature variations or during the movement of synoptic scale weather systems. Measurements accounting for both temporal and spatial variability tend to be costly and/or highly labour intensive (Bastviken et al., 2015), and to date we are unaware of any such measurement campaigns made at high temporal resolution (more than approximately weekly sampling) in Arctic shrub tundra - at least not outside of the growing season. Novel measurements and measurement approaches are required to distinguish local source and sink dynamics and reveal processes regulating CO_2 fluxes (Bastviken et al., 2022).

Capturing spatial variability in CO_2 flux at a high temporal resolution may tell us much more about what is being aggregated at the tower footprint scale. Such measurements will also provide insight into mechanisms unable to be inferred across large spatially heterogenous scales or from a single measurement, such as the influence of snowpacks on soil temperature (in turn affecting rates of microbial emission), the movement of CO_2 through the snowpack and what influence the atmosphere plays on gas concentrations inside the snowpack.

Low-cost gas sensors provide new opportunities for environmental observations (Eugster et al., 2020). Advances in sensor technologies now allow us to attempt to make timeseries point measurements of CO_2 concentrations, providing a cost and labour efficient alternative to more intensive measurements (Bastviken et al., 2015). Sensors originally developed for indoor air quality monitoring have been applied to environmental problems, providing the opportunity for low-cost measurement fo CO_2 fluxes from both soil and water to the atmosphere (Bastviken et al., 2015, 2020).

In this chapter, we describe a pilot study using the first iteration of a new design of low-cost sensors in order to measure CO_2 concentrations within the snowpack at TVC. Low-cost sensor measurements of CO_2 concentration and temperature are combined with measurements of snowpack properties to derive spatially distributed timeseries of CO_2 fluxes. This timeseries approach will help to elucidate mechanisms and drivers of CO_2 flux, in turn building process understanding that can later be applied to modelling studies. We aim to test if these sensors can be used to examine patterns and mechanisms of CO_2 flux across the TVC catchment and compare results from low-cost sensors to distributed point measurements of CO_2 concentration (and subsequently derived fluxes) and stable isotope ratios of CO_2.

6.2 Data and Methods

6.2.1 Fabrication of low-cost CO_2 sensors

Sensors were designed after Bastviken et al. (2015). Small changes were made due to the availability of components and in order to reduce power consumption. The design of the sensors is given in Section 3.3.4 and shown in Fig. 14. Briefly, commercially available Sensirion sensors measuring CO_2 concentration, temperature and relative humidity and a SD card reader were attached to an Arduino. This was connected to 6 D-Cell batteries and housed in an off-white plastic box. Holes were drilled in the lid of the box, backed with a waterproof gas-permeable membrane.

Sensors were calibrated as outlined in Appendix C, following Bastviken et al. (2015). Sensors were tested at the Havikpak Creek site (a black spruce site close to Inuvik - approximately 50km from TVC), in order to determine the impact of disturbing the snowpack to place the sensors and how best to orientate them (Appendix C.2). Based on these tests, lower sensors were placed with the membrane facing upwards, and upper sensors were placed with the membrance facing downwards. We aimed to place the upper sensor towards the bottom of the wind slab layer and the lower sensor at the base of the snowpack (Section 3.3.4), the feasibility of this varied depending on the presence of vegetation and the overall snowpack depth; lower sensors at RP02 were not at the very bottom of the snowpack due to the presence of a large shrub.

6.2.2 Deployment of low-cost CO_2 sensors

Two different deployments of the low-cost sensors were carried out. We term these the week long deployment (lasting from 21^{st} - 27^{th} March) and the long-term deployment (lasting from 28^{th} March until battery failure). The number and location of sensors for each deployment are summarised in Table 7.

The first deployment was designed to sample a stratified range of snow depths and land cover types, with sites chosen in part based on those previously sampled by Mavrovic et al. (in prep); site locations and naming convention are as per Fig. 8. Sensor locations were distributed across a range of snow depths, as these were associated with different vegetation types such as shrub or lichen dominated areas. Sensors were programmed to take one measurement every ten seconds, with fluxes calculated at the measurement resolution and then averaged to half hourly values.

Dates	Number of Sensors			Site Names	
	Top	Bottom	Total	Fluxes	Concentrations Only
21st - 27th March 2022	7	8	15	TS04, LC01,* POLY02, TR02, DS04, RP02	Mainmet †
28th March - 14th April 2022	5	10	15	TVC06, Trans1, Trans5	Mainmet, Trans4

* Lower sensor had to be placed with the membrane facing down (unlike sensors at the other sites) due to low snow depth, data discarded as difference in placement thought to affect gas concentrations † Instrument failure for top box, all concentrations read below 300ppm

Table 7: Summary of Sensor Deployments

Sites for the second deployment (28^{th} March onwards) were all within 100 m of the TVC EC tower for ease of collection after snowmelt and to capture the differences in snow cover conditions observed by the tower (Inset; Fig 39). Within this area, sites were chosen from previously visited locations, allowing timeseries measurements to be compared to gas profiles and isotopic measurement results. Higher snow depth sites were chosen in order to preserve the battery life of the boxes (insulation provided by deeper snow cover kept the batteries warmer, so less energy was wasted). The measurement resolution for each sensor was decreased from every 10 seconds to one measurement every minute in order to conserve battery life and aim to produce a longer timeseries, with the hope to potentially capture changes in soil conditions during snowmelt. For this second deployment, boxes remained untouched until being collected after snowmelt, with the length of the record obtained a function of the battery life.

Fluxes of CO_2 were calculated from the sensors as described in Section 3.3.2, except that mean snow density and temperature were calculated only for measurements between the heights of the boxes rather than for the entire snowpit profile. Instantaneous flux values were calculated at the same temporal resolution as the CO_2 concentration measurements, and then averaged to

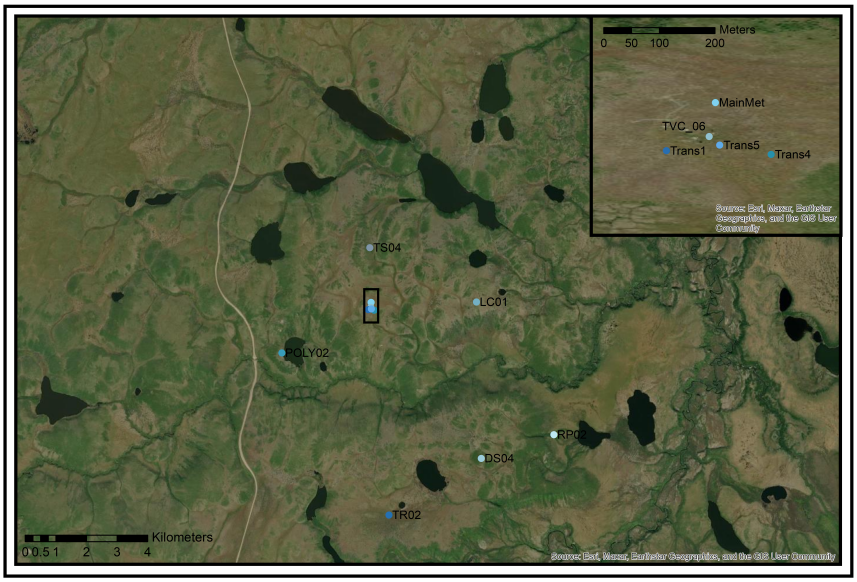

Figure 39: Low-Cost sensor locations. Site codes are matched to the land cover map in Figure 8 where applicable.

half hourly fluxes. This half hourly resolution was chosen to match EC tower measurements and to allow the measurements from both deployments to be compared at the same frequency.

A quality control protocol was then applied to the half hourly values. CO_2 concentrations below 300 ppm were removed, as this is considerably below atmospheric concentrations and thus thought to be erroneous. Fluxes for these same timestamps were then removed. Temperatures measured at each sensor were used as a check on the orientation of the sensors, as lower sensors would have a more stable temperature record than those nearer the top of the snowpack and more exposed to diurnal air temperature fluctuations. Data were also removed after step changes ($> \sim$ 200ppm) in the concentration values, as these were thought to be related to the battery power and not the ambient concentrations of CO_2.

6.2.3 Tower NEE/meteorological and soil measurements

Meteorological and eddy covariance measurements (Section 3.1.1) were used for comparison to point-scale flux measurements from both gas profiles and low-cost sensors. Meteorological data was also used to evaluate the effectiveness of snow insulation through comparison of 2 m air temperatures to box temperatures, and to examine patterns from the low-cost sensor timeseries.

6.2.4 Snow measurements

In order to calculate the snow properties required for the diffusive flux calculation and to characterise the snowpack, profiles of snow density and temperature were taken at each site. In most cases, this was done using the snowpit method outlined in Section 3.2.1. When snowpit profiles were not available, density profiles were then calculated from the nearest SMP measurement, as outlined in Section 3.2.2.

6.2.5 Gas Profiles & Isotopic Ratios

Gas samples were collected from each site at least once during the field campaign at TVC (Table 8). Concentration profiles using the LiCOR LI-850 were measured in the field (See Section 3.3.2), with duplicate samples taken at the majority of sites for isotopic analysis. CO_2 concentrations and stable carbon isotope ratios were measured using IRMS (Gasbench Infra Red Mass Spectrometry; Section 3.3.3). Processing and correction of raw δ13C values from the IRMS is detailed in Appendix B. Additional atmospheric samples were also taken at 3 different heights (0.5, 1.0 and 1.5 m) at the MainMet site in order to constrain the atmospheric ratio of C12:C13 and derive a mixing model, which was then used to approximate the relative abundances of atmospheric and soil-derived CO_2 in the profile samples.

The mixing model was created using the R package MixSIAR [1], which creates a Bayesian tracer mixing model to estimate the proportions of source contributions to a mixture. Bayesian frameworks allow prior error information to be specified, accounting for uncertainties in the end member measurements. This model framework allows more robust measurement of trends by allowing the user to label input data into different groups and random factors. Soil column δ13C values from Hicks Pries et al. (2015) were used as the soil end member in the mixing model. We assumed that when δ13C ratios are very negative, this was an indicator of soil respiration, and thus increasingly negative δ13C ratios could be used as a proxy for increasing soil microbial activity (or an increased proportion of soil-derived CO_2 within the sample).

[1] Available at https://github.com/brianstock/MixSIAR

Dates	Number of Sensors			Gas Profiles	
	Top	Bottom	Total	Li-Cor Samples	Isotope Ratios
MainMet	1*	1	2	22nd, 23rd, 24th, 26th, 27th	22nd (x2), 23rd (x2), 24th (x2 – and up to 1.5m atmospheric), 25th (x2), 26th (x2), 27th (x2)
	0	2	2		
TS04	1	1	2	23rd, 26th	26th (x2)
POLY02	1	1	2	23rd, 26th	26th (x2)
TR02	1	1	2	24th, 26th	-
DS04	1	1	2	25th, 26th	-
RP02	1	2	3	25th, 26th	26th (x2)
TVC06	2	2	4	22nd, 23rd, 24th, 25th, 26th, 27th	25th (x2)
Trans1	1	2	3	24th	24th (x2)
Trans4	0	2	2	24th	24th (x2)
Trans5	2	2	4	24th	24th (x2)

∗ Instrument Failure

Table 8: Summary of CO_2 flux measurements during the March 2022 TVC Field Campaign. Numbers in the gas profiles columns denote the date gas samples were collected.

6.3 Results

6.3.1 Meteorological conditions & snow properties

Meteorological conditions for the duration of both deployments (indicated with dashed vertical lines) are shown in Fig 40. Patterns of temperature change from both the upper sensors and the EC tower (Fig 40a & b) are broadly matched, although rising temperatures seen in the second deployment are more gradual in the sensor record than the peak seen in at the tower between the 6^{th} and 8^{th} April. Temperatures from the lower sensors do not correspond as well to air temperatures but are notably more variable than 10 cm soil temperatures (Fig. 40b & e). Bottom sensor temperatures show similarities to vertical probes integrating measurements from the top 12 cm of the soil; sensors at sites with deeper snow such as RP02 gave a more stable temperature record than these vertical temperature probes (not shown).

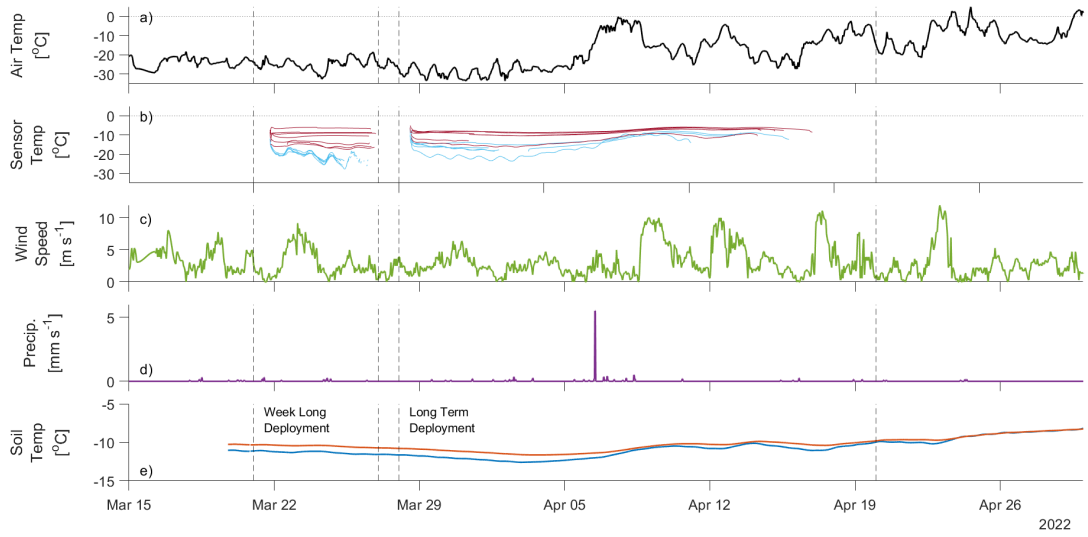

Figure 40: Meteorological and soil conditions at Trail Valley Creek from 15^{th} March to 30^{th} April 2022: (a) 2 m air temperature, (b) upper (cyan) and lower (maroon) sensor temperatures, (c) 10 m wind speed, (d) precipitation, (e) soil temperatures at depths of 10 cm (blue) and 20 cm (orange). The first two dashed vertical lines indicate the duration of the first deployment, and the second set of vertical dashed lines indicate the second deployment.

	Parameters for Flux Calculation					Site Characterisation	
Site	Distance between boxes [cm]	Mean Snow Density [kg m^{-3}]	Porosity	Tortuosity	Mean Temp [°C]	Total Snow Depth [cm]	PFT
TS04	130	316	0.66	0.51	-20	110	Tall Shrub
POLY02	14	206	0.77	0.63	-18	34	Polygon
TR02	85	306	0.67	0.52	-15	120	Trees (Shrub/Moss)
DS04	13	205	0.78	0.63	-22	40	Dwarf Shrub
RP02	101	366	0.60	0.46	-17	136	Riperian Shrub
TVC06	17	303	0.67	0.52	-13	81	-
Trans1	16	325	0.65	0.50	-12 *	59	-
Trans5	19	212	0.77	0.62	-12 *	77	-

∗ Not measured - Placeholder Value

Table 9: Measured snow properties at each of the low-cost sensor locations and how these link to calculated porosity & tortuosity for flux calculations

Variability in snow properties will influence calculated fluxes, as the density, depth and temperature of the snowpack are all included in the calculation of the fluxes (as seen in Eq. 3.2; values for each site are given in Table 9). Distances between boxes ranged from 13 cm to 1.3 m; mean densities ranged from 206 - 366 kg m^{-3}. Subsequent porosity and tortousity had a range of 0.2 (Table 9), with both quantities measured on a dimensionless scale between 0 and 1).

Typical stratigraphic profiles for Arctic snowpacks, with higher density wind-slab underlain by lower density depth hoar (Section 2.1.2), were seen at most sites. The layering of the snowpack and the relative position of the sensors is likely to have a greater impact on the calculated fluxes than in the case where snow properties were relatively homogeneous, such as at Trans5 where the SMP profile showed a near constant density of just over 200 kg m^{-3} (Fig. 41).

6.3.2 CO_2 Concentrations

Patterns in CO_2 concentrations are variable, both between sensor locations and over the durations of both deployments (Figs. 46 47). For some locations, differences in CO_2 concentration between upper and lower sensors are steady - in these instances fluxes are controlled by the properties of the overlying snow. Alternatively, for other locations relative differences between upper and lower sensors vary throughout the duration of the experiment. For example, at TS04, CO_2 concentrations

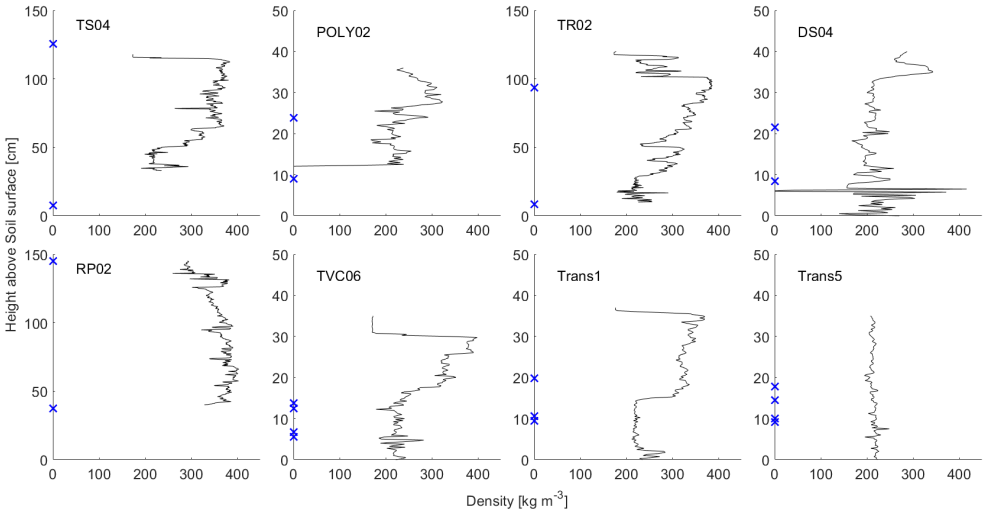

Figure 41: Profiles of snow density at each of the low cost sensor locations from the recalibrated SMP measurements. For sites with more than one SMP profile (TS04, TR02, DS04 & RP02), the mean profile is shown. Blue crosses on the y-axis show the heights of each sensor, normalised with respect to the length of the SMP profile.

gradually increase at both sensors, with a 10 - 20 ppm difference in the concentrations measured by each sensor at the start and end of the experiment - which may be indicative of increased emission of CO_2 from beneath the snowpack. Changes in ground emissions of CO_2 can also be observed at TR02, with an $\sim$ 100ppm difference between the highest and lowest CO_2 concentration measured by the lower sensor over the 6 days of the observational record.

The relative influence of the atmosphere changes over the duration of the experiment at some sites. From the 24^{th} March, CO_2 concentrations in the upper sensor at RP02 become more variable - potentially indicative of increased atmospheric influence, especially when considering the relative stability of subnivean concentrations measured in both lower sensors. At TVC06, there are multiple instances of synchronous decreases in the absolute magnitude of the CO_2 concentration measured by all 4 independent sensors (31^{st} March, 4^{th}, 6^{th} & 8^{th} April). Atmospheric dilution, followed by gradual recharge from soil CO_2 emissions is a possible cause of this pattern, with minima in CO_2 concentrations occurring shortly after peaks in wind speed (Fig. 40b).

6.3.3 Sources of CO_2

Our hypothesis was that CO_2 concentrations would be highest, and isotope ratios most negative, at the base of the snowpack - indicating that the measured CO_2 was from a soil respiration source. This was the most common case for the gas profile measurements, with 70% of LiCOR profiles having their maximum CO_2 concentration at the bottom of the profile.

Approximately 15% of LiCOR profiles had their highest CO_2 concentration in the 2nd or 3rd sample in the profile (within the upper $\sim$ 50% of the snowpack). Mavrovic et al. (in prep) found wind slab peaks in $\sim$ 10% of profiles from 2022, and from around 20% of sites in 2021. They suggest that this may be an indicator of snow microbial activity, with snow samples from TVC shipped to Université du Québec à Trois-Rivières for genetic analysis to test this hypothesis. Pockets of high CO_2 concentration might also be caused by circulation of air within the snowpack. Whatever process was driving the creation of wind slab peaks in CO_2 concentration was not noticeable in the isotopic ratios; the site with both isotope ratio measurements and a clear wind slab concentration peak ($\sim$ 900 ppm) did not show a different δ13C ratio in the wind slab layer than the other samples

Isotopic ratios of CO_2 were analysed to determine relative inputs of atmospheric and soil derived

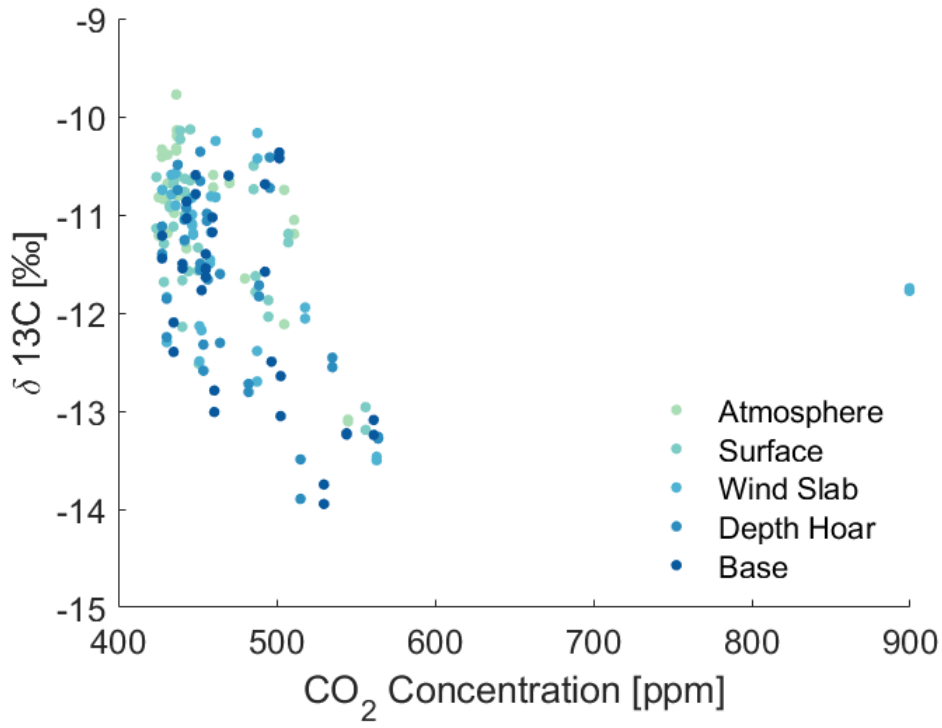

Figure 42: δ13C ratios and CO_2 concentrations from all snow profiles. Colours indicate where in the snow profile a sample was taken; atmospheric label includes samples measured at any height above the snowpack, surface samples are taken $\leq$ 5 cm below the air:snow interface. Uncertainity values for δ13C ratios are $<$ 0.5 ‰.

CO_2. 40% of profiles had their most negative δ13C values at the base of the snowpack, indicative of a greater amount of soil derived CO_2 closer to the soil surface. However, considerable variation in δ13C values for all layers was evident (Fig. 42). Samples with a higher CO_2 concentration typically had a more negative δ13C value, but this was not a statistically strong relationship (R^2 = 0.18).

Using the mean values at each of the sampling heights (i.e. atmosphere, surface, wind slab, depth hoar and the base of the snowpack), our mixing model shows a decrease in the provenance of atmospheric derived CO_2 with depth in the snowpack. All samples have a degree of atmospheric influence, but the magnitude of this is site-dependant. Sites with a lower snow depth typically had a greater proportion of atmospheric-derived CO_2, although this was not a strong statistical relationship (R^2 = 0.15). Snowpack structure may also influence the proportions of atmospheric and soil-derived CO_2 measured at any given site, acting as a direct control on the isotopic signature of CO_2. For example, averaged across all sampling heights, 15 % of CO_2 at TVC06 was soil

derived. This was the second highest proportion of soil derived CO_2 and this was also the site with a very dense ice crust in the upper portion of the snowpack, likely reducing the likelihood of wind pumping.

More testing is needed to check that the δ13C values from Alaska used in the mixing model (as given by Hicks Pries et al., 2015) are transferable to studies at TVC. We also used a Keeling curve approach to calculate soil end member δ13C values from the TVC IRMS measurements. This regression suggested emissions of CO_2 from the soil should have a CO_2 concentration of approximately 800 ppm and a δ13C value of -25.2‰. Use of either end member (from either Hicks Pries et al. (2015) or the Keeling curve) shows a small proportion of soil derived CO_2 and a larger proportion of atmospheric CO_2 in all samples. Values for surface soil δ13C ratios reported in Oelbermann et al. (2008) for the Western Canadian Arctic (-26.2 - -26.8‰) were also within the range of those used for the soil end member of our mixing model.

For sites where profiles of carbon isotope ratios were measured, we compared the relationship between temperature and δ13C values (Fig. 43), using the mean temperature from the low-cost sensor at the base of the snowpack. Sites with warmer mean temperatures have a more negative δ13C signature, supporting the hypothesis that conditions are more favourable for respiration, as this more isotopically negative CO_2 likely has a greater contribution from a respiratory source. However, it is important to note that isotopic fractionation in Arctic soils has itself been related to temperature (Oelbermann et al., 2008), and thus that measured differences in isotopic ratio could, at least in part, be caused by a difference in temperature.

6.3.4 CO_2 Fluxes

At most sites, higher CO_2 concentrations were usually found at the base of the snowpack, indicative of CO_2 release and a positive CO_2 flux to the atmosphere (Fig. 44); 72% of half hourly values from the weeklong deployment and 97% of half hourly values from the longer deployment gave positive fluxes. Negative fluxes, indicating higher CO_2 concentrations at the snow surface than at depth, were also found, but this was less common - accounting for less than 30% of fluxes from either deployment. Negative flux values were generally found at sites with a lower snow depth (less than approximately 20 cm; however not all sites with a < 20 cm distance gave negative flux values). Small distances between sensors magnify small relative distances in concentration; negative

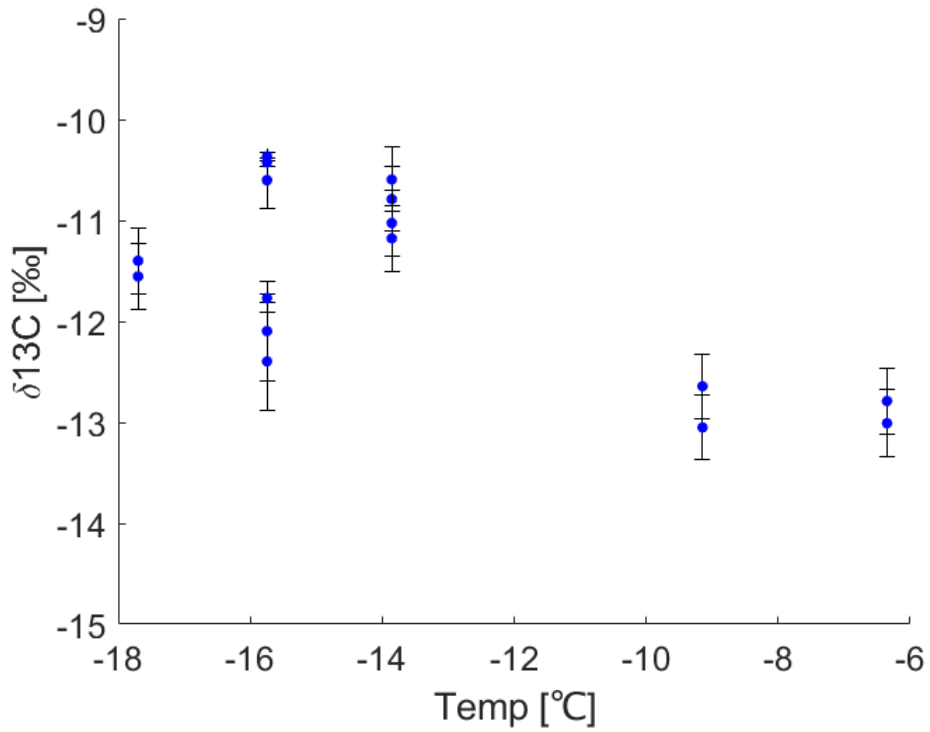

Figure 43: Mean temperatures from each low-cost sensor timeseries and δ13C ratios for the basal sample at each sensor location.

flux values could indicate that differences between sensors are within measurement error or that no measurable net flux has occurred rather than indicating the presence of a carbon sink.

Fluxes from both snow profile and low-cost sensor techniques are of a similar magnitude (Fig. 45). When aggregating data across all sites, both techniques give a median flux greater than zero, indicative of wintertime CO_2 release. However, analysis of variance suggests that fluxes derived using concentrations from the LiCOR are statistically significantly different at the 0.01 level; fluxes derived from the low-cost sensor method are more variable than those from the LiCOR profiles (although the difference in n value is considerable).

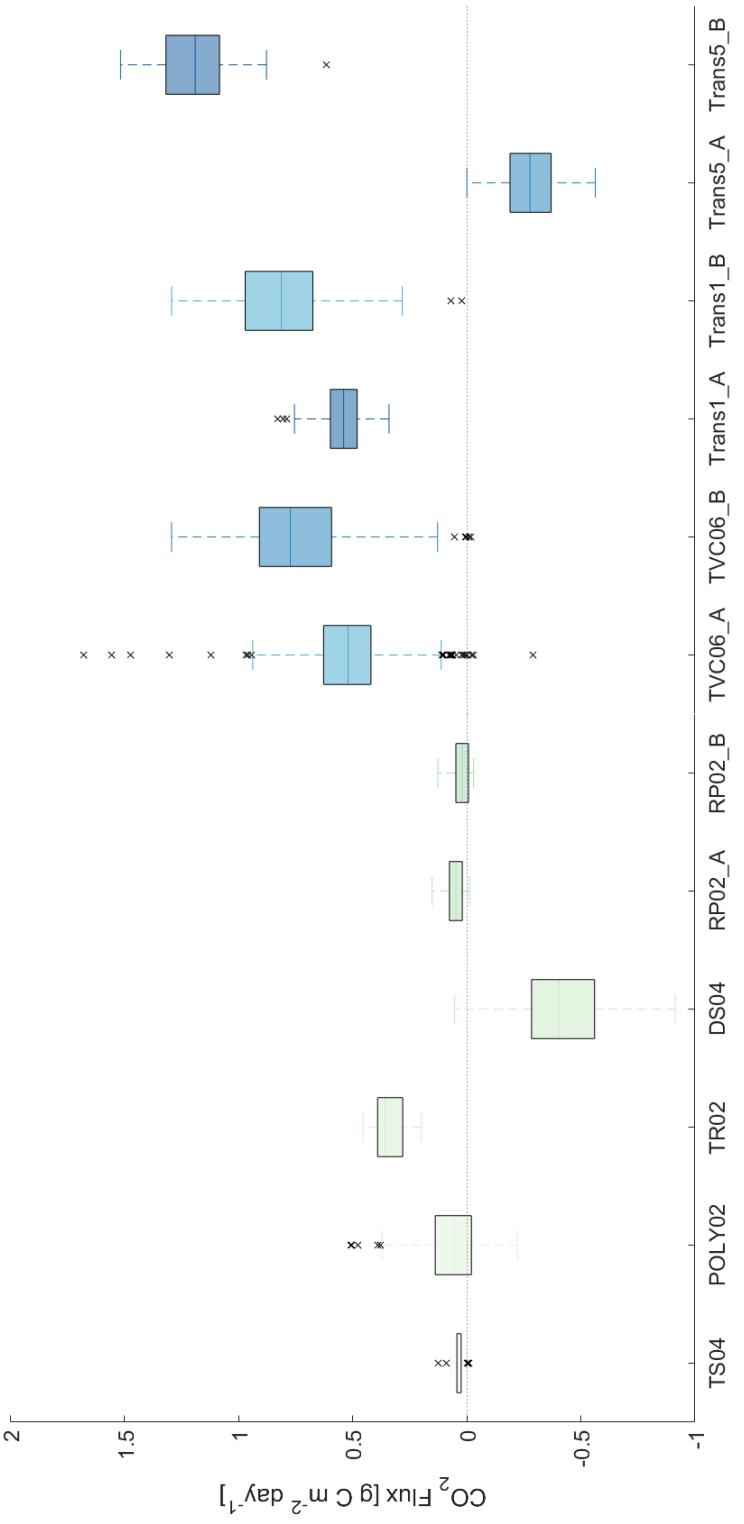

Figure 44: Fluxes from each pair of Low-Cost Sensors. The first 6 sensor pairs (green) are from the week long deployment, and the second six sensor pairs (blue) from the longer deployment. Sites with more than one sensor at the base of the snowpack are indicated by the suffix A or B.

In some instances, discrepancies present themselves between fluxes from the low-cost sensors and static LiCOR profiles. For example, the timeseries for DS04 shown in Fig. 46 shows higher concentrations of CO_2 measured by the upper sensor, but LiCOR measurements on multiple days show the bottom of snowpack having a higher CO_2 concentration.

6.3.5 Temporal Variability of CO_2 Fluxes

A key advantage of the low-cost sensors over the other, temporally discontinuous, methods discussed in this chapter is the high temporal resolution of the measurements, allowing us to capture changes in CO_2 concentration which are unable to be accounted for in point measurements. Fluxes are not static over time. Aggregated summaries such as Fig. 44 may hide changes in flux magnitude or direction in response to changes in meteorological conditions, which may be noteable over the variable length of the different sensor deployments.

Low, constant positive fluxes are seen at multiple sites through the Weeklong deployment (POLY02 & RP02; Fig. 46), and for the Trans1 site during the longer deployment (Fig. 47). At these sites, upper sensor CO_2 concentrations were consistently slightly lower than bottom sensor concentrations. Small changes in concentration in one sensor are reflected in the other; this is particularly clear for POLY02. Additionally, changes in one lower sensor are seen in the other (RP02 &

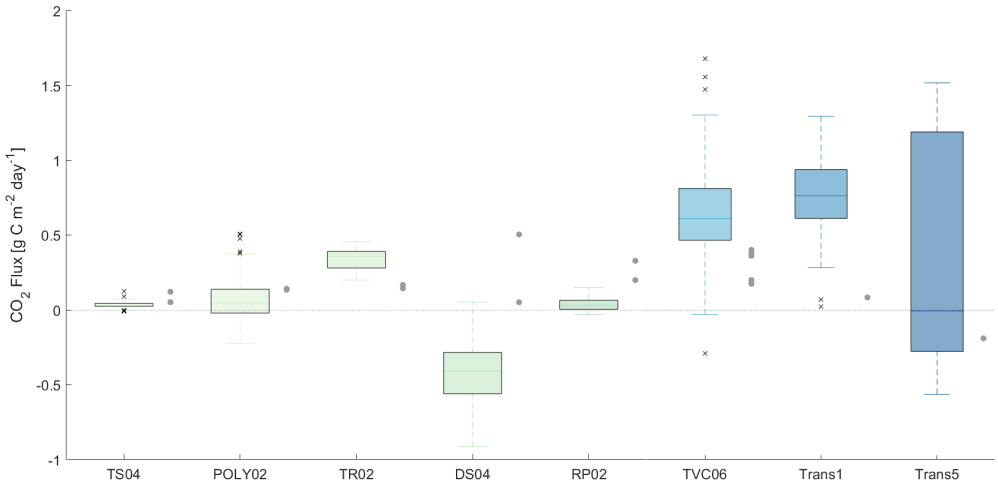

Figure 45: Comparison of fluxes measured using the LiCOR profiling technique and the low-cost sensors. Box plots show consolidated fluxes from both pairs of boxes at sites RP02, TVC06, Trans1 & Trans5. Sites shown in green are from the week long deployment, and sites shown in blue are from the longer deployment. Grey dots show fluxes from LiCOR profiles.

Trans1), despite being completely independent measurements, further substantiating patterns seen in both sensors.

Similarly temporally consistent CO_2 flux magnitudes are seen at TS04, although a sharp increase in the CO_2 concentration in both top and bottom sensors is seen on the evening of the 23^{rd}. We hypothesise that some local disturbance or activity (potentially cracking of the soil) may be releasing CO_2. Concentrations at both heights decrease in tandem after this event, suggesting that the source of CO_2 is not sustained.

At TR02, we see a build-up of CO_2 in the bottom box over the first day which is then flushed out, presumably by a wind event (with an increase in 10m wind speed seen in Fig 40b). Concentrations begin to rise again on the 24^{th}, indicating release of CO_2 from the underlying soil. CO_2 concentrations in the top box remain stable and close to 400ppm (the approximate atmospheric concentration) throughout the entire experiment, suggesting that this sensor is well-ventilated and CO_2 is prevented from building up in the upper part of the snowpack, in contrast to other sites such as TVC06.

Snow at TVC06 was the densest of all the sites (Table 9), with a thick ice lens present in the upper snow layer, likely preventing the release of subnivean CO_2 to the atmosphere. Air likely continued to circulate within the snow, leading to a high degree of variability in the calculated fluxes. Changes in all boxes are in phase with each other, with peaks and troughs in CO_2 concentrations for all 4 sensors measured simultaneously (Section 6.3.2), further substantiating such changes. These may be due to micrometerological factors (Fig. 40), with minima in concentration, and consequently lower CO_2 fluxes occuring shortly after peaks in wind speed. Concentrations measured on the evening of the 6^{th} decrease by at least 50 ppm for all of the sensors; this may be linked to a precipitation event earlier in the day (the only sizeable such event over the entire experiment), however similar drops in CO_2 concentration without accompanying precipitation were seen on three other occasions (31^{st} March, 4^{th} & 8^{th} April) so this may not be related. Measurements on half-hourly timescales from alpine sites have shown similar high temporal variability in CO_2 fluxes and subnivean CO_2 concentrations (Bowling et al., 2008; Seok et al., 2009).

Divergence in CO_2 fluxes is seen between the two pairs of sensors at Trans5, with one pair producing a positive and the second pair a negative flux. Although concentrations in the top box at

Trans5$_A$ were consistently higher than those in the lower box, this was never by more than about 20 ppm. Such a negative gradient is within instrumental error, with the size of the flux amplified by the short distance (19 cm) between the sensors. The negative flux record from Trans5$_A$ has the shortest duration of those from this deployment, accounting for less than 3% of measured fluxes. Similarly, negative fluxes were calculated for DS04, another site with a very short distance (13 cm) between the two sensors.

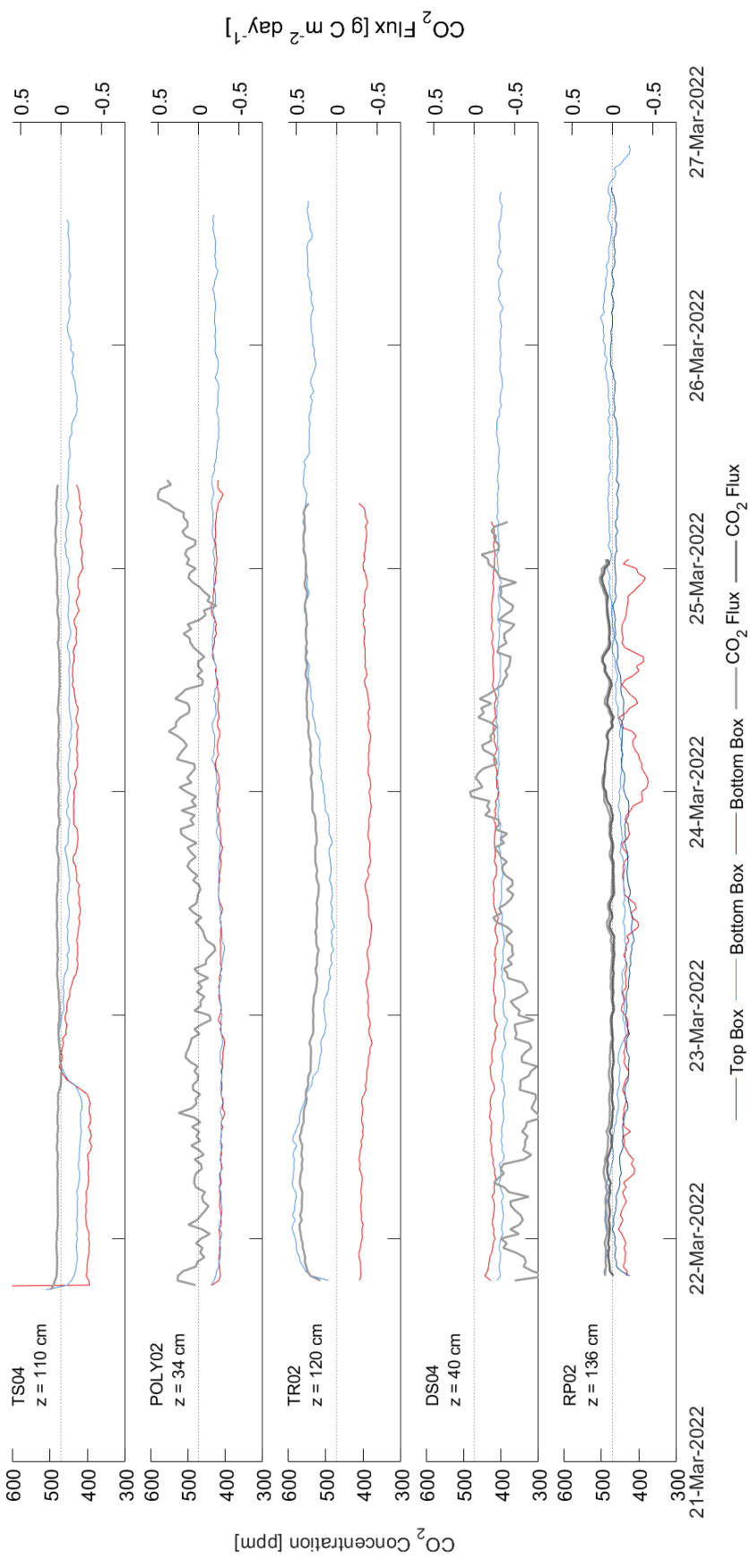

Figure 46: Timeseries of temperature and CO_2 concentration for each sensor and CO_2 flux for each sensor pair at all locations for the Weeklong deployment. The dashed black line indicts zero flux. Site names and snow depths are given in the top left corner of each plot. Two shades are used for RP02 as this site had two bottom boxes.

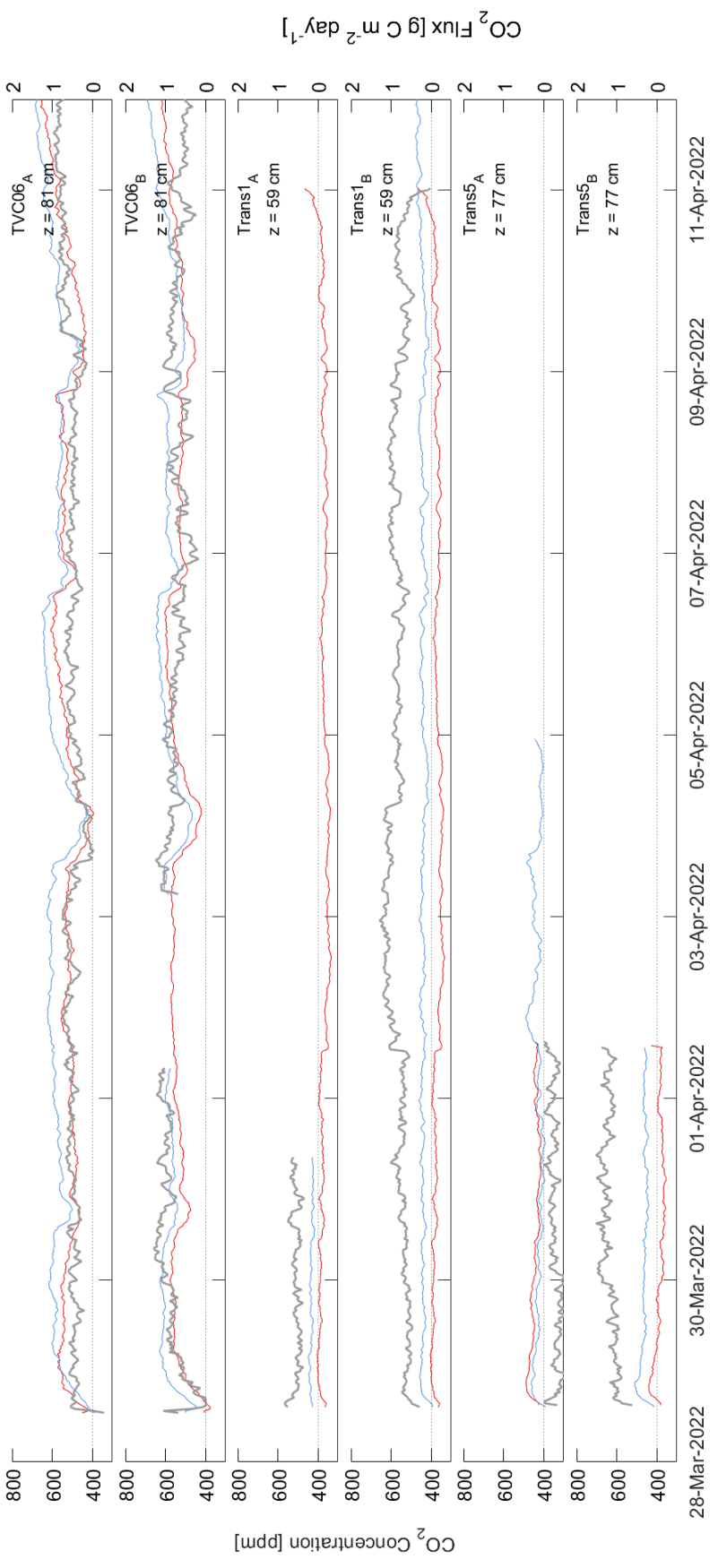

Figure 47: Timeseries of temperature and CO_2 concentration for each sensor and CO_2 flux for each sensor pair at all locations for the Long term deployment.The dashed black line indicts zero flux. Site names and snow depths are given in the top right corner of each plot. Note differences in the scales on both y-axes compared to the previous figure.

6.3.6 Relationships between CO_2 Fluxes & the Subnivean Environment

Concentrations of the CO_2 at the base of the snowpack showed a clear relationship with temperature, with higher CO_2 concentrations measured as temperatures increased (Fig. 48a). Concentrations measured by the lower sensors rapidly increase above a temperature of $\sim$ -10 °C. Higher CO_2 concentrations at the base of the snow pack may be indicative of higher CO_2 fluxes, caused by an increase in CO_2 production or soil respiration.

Although CO_2 fluxes generally increase as temperatures increase, this trend is not as clear as that for CO_2 concentrations. Similar patterns to those seen in Fig 48b were also found in the synthesis of winter flux observations by Natali et al. (2019). This relationship has the same exponential curve which is characteristic of Q10 relationships, possibly indicative of a physical mechanism enabling more respiration or greater CO_2 production as temperatures increase above this value. Uncertainties on these data look similar to those presented by Natali et al. (2019), and a considerable proportion of our data fits within the confidence interval of their analysis. As Natali et al. (2019) use the temperature of the soil and we use that measured at the lower sensor, this is not a true like-for-like comparison, with soil temperatures at our sites likely to be warmer than those provided by the sensors, which would give a better fit.

Many other factors affect the calculated fluxes rather than just basal CO_2 concentrations discussed in the previous paragraph and these other factors will depress the strength of this relationship. For example, a larger distance between two sensors with the same ppm difference in CO_2 concentration facilitated by a deeper snowpack will lead to to lower concentration gradient and subsequently a lower CO_2 flux.

As snowpacks act to insulate soils, and warmer soils allow for greater rates of soil respiration, it would be reasonable to suggest that sites with deeper snow would have higher (more positive) CO_2 fluxes. However, the relationship between snow depth and CO_2 flux across all low-cost sensor locations is unclear. High variability between fluxes measured at similar snow depths suggest the picture is more complex. Snow depths were measured during either profile sampling or at the time low-cost sensors were buried, and do not necessarily give any indication of preceding conditions; Chapter 4 discusses the importance of the timing of snowfall in setting subnivean conditions. Antecedent temperatures and snow cover conditions may be more important in governing CO_2

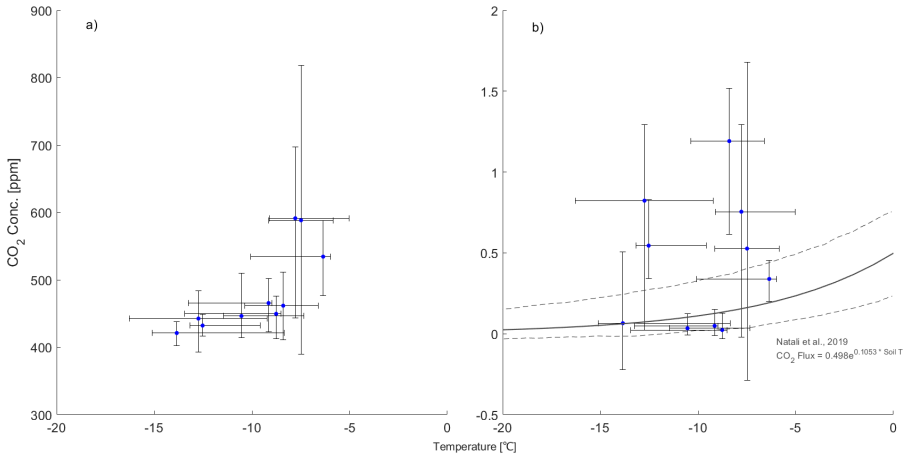

Figure 48: Mean temperature, a) CO_2 concentration and b) CO_2 flux for the entire duration of a deployment for each of sensors at the base of the snowpack. Negative mean values (n = 2) have been removed from this figure. Error bars show the range of half-hourly values. The fit of Natali et al. (2019) is shown on b, with the 95% confidence interval denoted using the dashed lines.

fluxes than instantaneous values. Timing of snow-cover onset is a key factor in determining the insulation, temperature (and potentially moisture content) of the soil for the entire snow-covered season, and thus acts a control on respiratory fluxes (Chapter 5).

6.3.7 Limitations & Uncertainties

Snow Measurement Uncertainities

Uncertainties in CO_2 concentrations, detailed separately for each method below, will impact calculated fluxes. Advective transport of CO_2 may occur on timescales shorter than the half-hourly averaging window used to present this data (Graham and Risk, 2018). Lateral transport of CO_2 through the snowpack is also likely, though this is unaccounted for using the diffusive gradient method (Graham and Risk, 2018) used to calculated fluxes from both low-cost sensors and LiCOR measurements.

Furthermore, uncertainties surrounding the measurement of snow properties will also impact fluxes. However, as the same methods are used to derive snow properties for all types of concentration measurement, sources of error in the snow properties can be presumed to have the same impact on all fluxes. Conger and McClung (2009); Proksch et al. (2016) give an 9% error estimate on the calculation on snow densities using the snowpit method, with Mavrovic et al (in prep) giving a 25% error estimate on the entirety of flux calculation method, although different instru-

mentation was used to calculate their CO_2 concentration values, so this figure may not give the exact uncertainty for the fluxes herein.

Snow heterogeneity will also impact flux calculations. The distance between CO_2 concentration measurements and the nearest SMP or snowpit may result in considerable variation in snow stratigraphy, known to impact the interpretation of SMP data (Section 3.2.2). Errors in density measurement on CO_2 fluxes are non-linear, but are less than 10% for the range of densities measured at our sites (Table 9 & Seok et al., 2009). The destructive nature of CO_2 sampling (particularly in the case of the low-cost sensor method) may also lead to differences in the snowpack properties post and prior to CO_2 measurement, resulting in uncertainity about the reflectiveness of the measurements. However, other established methods are similarly destructive (see Björkman et al., 2010a) and CO_2 concentrations quickly stabilised after boxes were buried. The use of a constant temperature value when temperatures were known to change over the course of the deployment may also have affect calculated fluxes. For the case of sites with no temperature measurement, the chosen value of -12 °C could be reconsidered or an average of temperatures from measured sites used.

CO_2 Measurement Uncertainities

Limitations surrounding the precision of IRMS measurements of CO_2 concentration, as discussed in Appendix B, prevented us from using IRMS concentrations to derive flux values. Additionally, sample contamination (leading to erroneous δ13C and CO_2 concentration) values may have occurred when transferring samples from syringes to exetainer vials. Notes of any suspected issues were made during this process, and if a sample did not match its replicate (as each syringe filled two exetainer vials) it was presumed to be an outlier and disregarded.

LiCOR measurements are rated to an accuracy of 1.5 % (Li-COR Biosciences), corresponding to approximately 5 - 10 ppm for the CO_2 concentrations seen at TVC. Similar contamination concerns as outlined above also apply for these samples - however without replicate measurements such outliers are more difficult to identify and thus no measurements were removed.

Differences in CO_2 concentration between low-cost sensors were commonly within the manufacturer specified accuracy of $\pm$ 30 ppm. Comparison of timeseries to co-located measurements usually helped to constrain appropriate CO_2 concentrations, although there were some exceptions

(DS04). Limitations surrounding the calibration of the low-cost sensors also impacts the reliability of the final results (Appendix C). The membrane of the sensor was also easily damaged, changes in gas exchange as a result of changes in the amount of exposed membrane may also have influenced our results.

6.4 Interim Conclusions & Future Method Development

Measurement of gas fluxes throughout the Arctic winter is difficult. This chapter presented a novel approach to this problem, which successfully measured spatially-distributed timeseries of subnivean CO_2 fluxes, albeit over a relatively short time period (less than one month). Development of the low-cost sensors continues in order to improve their robustness, accuracy and power demand. Alternative power solutions, such as integrating the use of a solar panel, will be more sustainable and improve the length of the battery life (and thus the duration of the measurements). Reducing the headspace of the sensors (and thus the amount of membrane required) may improve the precision of the results by reducing the likelihood of damage to the membrane and subsequent differences in gas transfer between boxes. Our understanding of wintertime processes has grown, but moreso has the need to further refine this approach in order to truly be able to grasp the mechanisms and variabilities of wintertime carbon fluxes - in turn enabling improvements in how these are modelled and what changes may occur alongside changes in climate.

Chapter 7

Summary & Outlook

7.1 Synopsis

In 2005, Callaghan et al., (p.109) wrote that "there is great uncertainty about the current CO_2 balance of the Arctic due to geographically inadequate measurements and inadequate representation of ecosystem dynamics in current models". The research questions set out in Section 1.2 aimed to untangle the influence of seasonal snow cover on Arctic carbon fluxes, and to reduce uncertainty in Earth System Model simulations. Model evaluation and developments outlined in Chapters 4 & 5 show routes to improve simulation of Arctic carbon flux, through examination first of snow thermal conductivity and then of the parameterisation of relationships between soil temperature, moisture and respiration. Chapter 6 then presented preliminary results from the use of new low-cost sensors to measure wintertime CO_2 fluxes, alongside co-located profiles of CO_2 concentrations and isotopic ratios.

The representation of seasonal snowpacks in Earth System Models is key for accurately representing the temperature and thermal regime of Arctic soils. Soil temperature is a key factor governing soil respiration, and yet as models fail to adequately represent a realistic stratigraphy of Arctic snowpacks, considerable biases in the simulation of wintertime soil temperatures can be expected. Changes to the snow thermal properties can change the simulated soil temperature, with Chapter 4 finding the default parameterisation of snow thermal conductivity in CLM5.0 gave soil temperatures that were up to 12 °C colder than observed. Three other parameterisations of snow thermal conductivity (Section 2.1.2) were tested alongside the application of a multiplier to the original pa-

rameterisation. All 4 parameterisations were applied to recalibrated SMP measurements to derive reasonable estimates for snow thermal conductivity. The parameterisation of Sturm et al. (1997) was found to provide the greatest improvement, reducing simulated 10 cm soil temperature biases to a third of their original value.

A sensitivity test examining the impact of parameter choices (including snow thermal conductivity) on simulated wintertime CO_2 emissions was then undertaken in Chapter 5. With the parameterisation of respiration and decomposition as functions of soil physical properties, we would expect to see fluxes from CLM5.0 which are representative of measurements, yet simulated fluxes in the snow-covered season are typically zero for the default model configuration. Different factors control respiration in frozen and unfrozen soils (Sullivan et al., 2008), and thus the estimation of soil respiration in Arctic environments from parameters derived from mid-latitude studies do not adequately represent cold-region processes. Changes to the parameterisation of snow thermal conductivity (Chapter 4) improve the simulation of soil temperatures and allow simulated soil respriation to continue for an additional two months relative to the default simulation - although there is still no respiration simulated for a large portion of the winter. Measurements of NEE from the TVC EC tower, however, confirm the possiblity of wintertime CO_2 release - although the examination of sub-seasonal trends is limited by poor data availability and high uncertainity. Adjustments to the relationship between soil moisture and decomposition are required in order to allow simulated soil respiration throughout the entirety of the winter, with adjustments to the value of Q10 also necessary to prevent overestimation of wintertime emissions. A more appropriate parameter space is outlined, however the choice of parameter values is hindered by observational limitations and varies on a sub-seasonal basis.

Poor simulation of soil respiration in the snow-covered season using the default parameterisation of CLM has implications beyond the snow covered period, with a lack of simulated emissions for around 6 months of the year leading to a misrepresentation of the annual carbon budget. Were this underestimation of snow-season emissions to occur more widely across the total areal extent of the Arctic tundra ($\sim$ 7.6 x 10^6 km ^{2}; Bliss and Matveyeva, 1991), this would account for a considerable missed contribution to the global carbon budget – and thus its omission may have an impact on the simulation of future climate. Failure to quantify the wintertime release of CO_2 appropriately may also affect future simulations of soil turnover and permafrost extent.

Uncertainties and limitations surrounding the interpretation of measured NEE from EC data during the Arctic winter led to the development of a new low-cost CO_2 sensors described and tested in Chapter 6. High temporal resolution measurement of subnivean CO_2 across spatially heterogenous landscapes allowed small scale processes and process variations unable to be captured by previously existing techniques to be explored. CO_2 release during the winter of 2022 (March and April) was captured, providing further evidence of the importance of CO_2 emissions from snow covered tundra. Further development of these sensors will allow greater interpretation of the processes driving wintertime carbon emissions, and could be used to to improve model parameterisation of subnivean CO_2 flux.

7.2 Future Directions

7.2.1 Reducing Spatial Biases

Results presented from TVC may be more broadly applicable across Arctic shrub tundra, but without comparison to additional sites this is unknown. Much of terrestrial Arctic research is spatially clustered, with a few key locations accounting for a disproportionate amount of publications (Metcalfe et al., 2018) and local evidence (Post et al., 2019). Including a greater number of sites, particularly in areas that are understudied, as outlined by Pallandt et al. (2021); Virkkala et al. (2017), is advisable and will improve the validity and applicability of these findings.

Future application of model parameterisations (Chapter 5) and evaluation at additional sites may narrow the appropriate parameter space, providing greater insight into spatial variability in CO_2 flux. A narrower range of parameter values could then be applied at the Pan-Arctic scale, to give upper and lower estimates of regional flux and get one step closer to closing the annual Arctic carbon budget. However, the choice of such sites is limited by the availability of model evaluation data. Arctic coverage of EC towers, particularly those that are operational during the winter months, is sparse (Pallandt et al., 2021), with the spatiotemporal resolution of available flux data often insufficient for robust model validation (Bastviken et al., 2022). Upscaling not only of model evaluations but also of measurement efforts is required to improve our understanding of Arctic wintertime CO_2 fluxes.

7.2.2 Continued Development of Low Cost Sensor Method

As mentioned in Section 6.4, many avenues present themselves for future development of low cost sensors and the methods used to evaluate these. Questions remain unanswered and the fidelity and reproduciblity of the data is low. Extending the spatial coverage of this study with higher precision sensors, more sites, and more gas samples would allow uncertainties to be better constrained.

Unfortunately, the EC tower at TVC was offline for a considerable proportion of the time the sensors were deployed. Although this further evidences the need for alternative methods, a repeat deployment where sensors and EC fluxes can be compared would add value to the study. Not only would this improve the confidence in absolute flux magnitudes, but using low cost sensor results to untangle spatial heterogenities in a manner similar to footprint models applied to EC data could provide valuable insight into fluxes across the entire footprint and beyond. Greater comparison with other approaches to wintertime flux measurement at this site would give an increased sample size and improve the detection of erroneous or negative measured fluxes - although temporal flucutations and differences between timeseries and snapshot measurements will need to be accounted for.

Extending the use of the isotopic mixing model in this study would provide more insight into the provenance of measured gas samples. Testing the sensitivity of calculated probable sources of CO_2 to end member values would allow the uncertainty in the calculated provenances to be constrained and greater discussed. This would also allow us to partition the sources of calculated CO2 fluxes by back-calculation of the likely isotopic ratios (and thus sources) of measured CO_2 concentrations from the low-cost sensors.

Improving power efficiencies and calibration protocols of the CO_2 sensors would provide longer and more accurate CO_2 timerseries. This would improve process understanding, and ideally facilitate the identification of spring thaw processes and the impact of snowmelt. Additionally, integration of a methane sensor into the low-cost sensor design, as outlined by Bastviken et al. (2020), would broaden our understanding wintertime carbon flux processes.

7.2.3 Non-CO_2 Greenhouse Gases

CO_2 is the most abundant, but far from the most powerful greenhouse gas. Microbial decomposition of soil organic matter can lead to the production of not just carbon dioxide but also methane and nitrous oxide (Jungkunst, 2010). Increased emissions of all three of these major greenhouse gases have been noted with increasing temperatures in Arctic shrub tundra (Voigt et al., 2017). Studies of non-CO_2 greenhouse gas emissions from Arctic environments lag behind those of CO_2 and are typically limited to the growing season; recently, Voigt et al. (2020) noted only half as many published studies on methane fluxes as for CO_2 and less than half again for nitrous oxide.

Northern ecosystems make a significant contributions to the global methane (CH_4) budget (IPCC, 2022) and emissions from permafrost are likely to play a key part in the Arctic carbon budget, with CH_4 having a global warming potential approximately 30 times that of CO_2 (IPCC, 2013). Net CH_4 release has been observed in all seasons in the Arctic tundra (Howard et al., 2020), but cold season emissions are thought to dominate the annual CH_4 budget (Zona et al., 2016). Howard et al. (2020) found that cold season emissions made up 82% of the annual budget of CH_4 in the first year of thier study. Process models considerably underestimate wintertime CH_4 release relative to observed values (Treat et al., 2018) and subsequently, confidence in projections of CH_4 release from permafrost thaw is low (IPCC, 2013). Considering non-growing season processes is crucial to accurately represent annual CH_4 budgets (Treat et al., 2018), and to understand how these will evolve as the climate changes.

Nitrous oxide (N_2O) is a greenhouse gas with a global warming potential approximately 300 times that of CO_2 (IPCC, 2013). N_2O emissions from permafrost ecosystems have traditionally been thought to be negligible and thus received little attention (Gil et al., 2022). Mechanisms behind N_2O production in these Arctic environments are poorly understood. A better understanding of N_2O production and release from Arctic soils is needed (Gil et al., 2022); as with CO_2 there is likely considerable spatial heterogenity in N_2O fluxes from Arctic and sub-Arctic environments (Voigt et al., 2020). N_2O release outside of the growing season may be of a similar magnitude to growing season emissions, with uncertainty in annual budgets again compounded by a lack of wintertime measurements (Voigt et al., 2020). Soil freeze-thaw cycles may promote N_2O emissions (Jungkunst, 2010), and snow cover may indirectly control N_2O fluxes. The inclusion of

wintertime estimates doubles the contribution to global N_2O emissions from permafrost regions (Voigt et al., 2020), but with only one published study of Arctic N_2O emissions outside of the growing season (Marushchak et al., 2011), more research is clearly needed in this area.

7.3 Concluding Remarks

The studies presented in this thesis represent a step towards improving our understanding of carbon fluxes in Arctic shrub tundra during the snow-covered season. We highlight the importance of the snow thermal properties in simulations of wintertime soil temperature, an important factor in controlling CO_2 emissions. Model sensitivity to the parameterisation of soil temperature and moisture relationships is also evaulated, with the use of default, mid-latitude parameterisations found to be inappropriate for Arctic shrub tundra environments. Field measurements, including those from novel low-cost CO_2 sensors, indicate subnivean emissions of CO_2 under a variety of land cover types not represented by default model configurations. Subnivean CO_2 concentrations and resultant fluxes are found to vary with temperature, further highlighting the importance of the insulative properties of the snowpack.

Improvements in our ability to evaluate models and prescribe more appropriate parameterisations for future simulations of wintertime NEE depend on improvement in the quality and quantity of wintertime CO_2 flux measurements. Comments made almost 20 years ago about the magnitude and causes of uncertainty in the Arctic carbon budget (Callaghan et al., 2005) still apply, and there is much more work to be done to close this gap and improve our understanding of winter time carbon fluxes in Arctic shrub tundra environments.

Appendix A

Processing of TVC Eddy Covariance Data

A.1 Data Processing Protocol

Fluxes used to evaluate simulations were derived from eddy covariance (EC) data collected at TVC. Fluctuations in CO_2 concentrations and water vapour densities, and vertical wind velocities and sonic temperatures were measured using an EC150 open-path infra-red gas analyser and CSAT3A sonic anemometer respectively (both Campbell Scientific, Logan, Utah) at a height of 4.08m. Sensor separation between the EC150 and CSAT was -3.2 cm northward separation and -2.4 cm eastward separation, with the CSAT orientated at 308° relative to true North. High frequency data was measured at a frequency of 10 Hz and recorded using a CR3000 datalogger (Campbell Scientific). Instruments were recalibrated twice annually; shortly before snow melt commenced and towards the end of the growing season (approximately late March and late August/September respectively).

Processing of eddy covariance data followed the procedure outlined in Helbig et al. (2017). Half hourly fluxes were calculated using EddyPro software (Version 6.0 +; Li-COR Biosciences, Lincoln, Nebraska). A double rotation was used for sonic anemometer tilt correction, then spikes in the high frequency timeseries were removed as per Vickers and Mahrt (1997), and sonic temperatures were corrected for humidity effects as per van Dijk et al. (2004). Block averaging was

used to create the half-hourly timeseries, and a covariance maximization procedure detected time lags. Corrections were then applied, as described in Section 2.1.1. A minimum friction velocity value 0.1 m s^{-1} was used for filtering data. This is reasonably conservative value, and due to the low-lying nature of the vegetation at TVC a smaller value could be used in the future, increasing data availability. After filtering, data was then gap-filled as outlined in Section A.3 below. For timeseries plots, mean daily values were calculated from the gap-filled half hourly fluxes and converted to g C m^{-2} day^{-1}. Fluxes were then converted to mean weekly values. Data in section 2 are shown in native measurement units (μmol CO_2 m^{-2} s^{-1}) as the unit conversation occurred at the end of the data processing protocol.

Uncertainties for the corrected half-hourly fluxes were derived as per Lasslop et al. (2008). This method accounts for random errors using the same autocorrelation principles used to gap-fill the dataset, with the standard deviation of residuals from the gap-filling algorithm used to determine the error.

A.2 Flux Corrections

The Webb-Pearman-Luening (WPL) correction is required to correct measurements of fluxes of trace gases in open-path gas analysers for changes in the density and temperature of air in the path of the analyser. WPL corrections are often of a similar magnitude to calculated fluxes, adding uncertainty to the derived fluxes. The impact of WPL corrections is magnified in Arctic environments, with WPL corrections orders of magnitude larger than calculated fluxes. In order to assess the contribution of this correction to the calculated flux values, we calculate the QWPL flag, as described by Jentzsch et al. (2021a). This flag is strongly influenced by very small flux values; QWPL values tend towards infinity as the measured flux approaches zero and small flux changes can lead to large changes in the QWPL flag. Jentzsch et al. (2021a) advise caution for QWPL values over 1. This occurs when the magnitude of the WPL correction is greater than the magnitude of the final, corrected flux. The proportion of this potentially lower quality data is presented in Table 10 & Fig. 49; however, we do not treat data with different quality flags differently when evaluating simulations.

Large values of WPL corrections, and subsequently QWPL flags, are likely to occur under stable

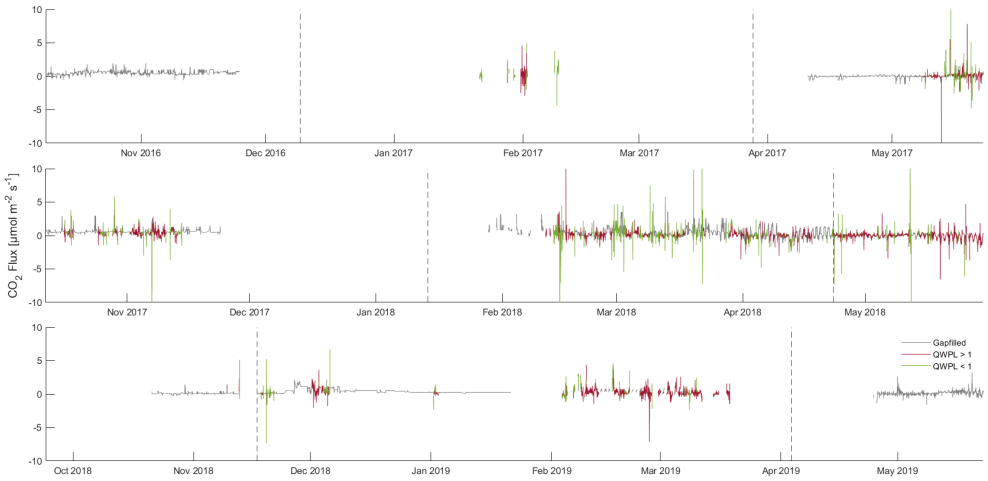

Figure 49: Quality and availability of reference Eddy Covariance Data for all 3 winters. Dashed vertical lines represent freeze-up, midwinter and thaw periods, as used for model evaluation (Fig. 37). Note that the units used in this figure differ from those in Chapter 5.

atmospheric conditions, accompanied by large fluxes of sensible heat. Additionally, multiple terms in the WPL correction equation are temperature dependant, with values up to 15% larger derived for temperatures of approximately -30°C than at 0°C (Jentzsch et al., 2021b). Spectral corrections, after Moncrieff et al. (1997, 2004), were also applied to the calculated CO2 flux values prior to gap-filling.

A.3 Gap-filling

Data were gap-filled as per Reichstein et al. (2005). The covariation of flux magnitudes with meteorological conditions were used to assign values to missing datapoints, as outlined in Figure A1 of Reichstein et al. (2005). Gap-filled data were assigned one of three quality flags, depending on availability of meteorological observations and measured fluxes under similar meteorological conditions (defined as observed air temperature within $\pm$ 2.5 °C, vapour pressure deficit within $\pm$ 5.0 hPa and radiation within $\pm$ 50Wm^2 of observed values when flux data was available). Data were unable to be gap-filled when no NEE values were available within a window of 140 days either side of the data point, or when no radiation, air temperature or vapour pressure deficit data were available. Such conditions were common when power outages occurred.

Table 10 shows that the proportion of available data is low, particularly in 2018-19, with a high

($> 30\%$) amount of gap-filling needed for model evaluation. However, of data that are available, at least a third and usually closer to half of available data has a QWPL flag indicative of highest quality (QWPL < 1).

A.4 Limitations

Measurements of CO2 concentrations between December and February were highly intermittent. Data loss due to power issues was common; many challenges are presented in maintaining a constant power supply at a remote Arctic field site during periods of 24-hour darkness and extreme cold. Icing of the instrument (where the optical path of sensors becomes obstructed by rime or precipitation), temperatures below the specification of the instrument, and stable atmospheric conditions impact data coverage and further contribute to data uncertainty. Atmospheric stability also leads to changes in the footprint of the EC tower (Burba and Anderson, 2005), increasing uncertainty about the area being measured and thus the magnitude per m^2 of the derived fluxes. Additionally, Pirk et al. (2017) suggest that fluxes derived from the eddy covariance method during snowmelt may be subject to sizable biases due to increased surface heterogeneity, e.g. patchy snow cover, and subsequent variable surface roughness lengths in the tower footprint.

To compare the impact of post-processing and data quality flagging procedures on calculated fluxes, data were grouped by the magnitude of the WPL correction (green or red in Figs 49 & 50) and if it was derived by the gap-filling process (grey in Figs 49 & 50). Fluxes within these different groups were of similar magnitudes, with no group having a significantly different mean value in all 3 years (analysis of variance gives F_{16-17} = 2.32, F_{17-18} = 0.69 and F_{18-19} = 1.71,

	% QWPL $\mid < 1 \mid$	% QWPL $\mid > 1 \mid$	% Gapfilled	% Available
2016 - 17	6.3 (52.9)	5.6 (47.1)	24.0	*35.9*
2017 - 18	17.8 (43.2)	23.4 (56.8)	24.6	*65.7*
2018 - 19	5.5 (36.1)	9.7 (63.9)	41.8	*56.7*

Table 10: Summary of the quality and availability of eddy covariance data for all 3 winters. The proportion of measured values (i.e. available and non-gapfilled data) for either quality flag is given in brackets.

none of which are significant at the 0.01 level), suggesting that the inclusion of data with a QWPL flag > 1 does not unduly influence the analysis.

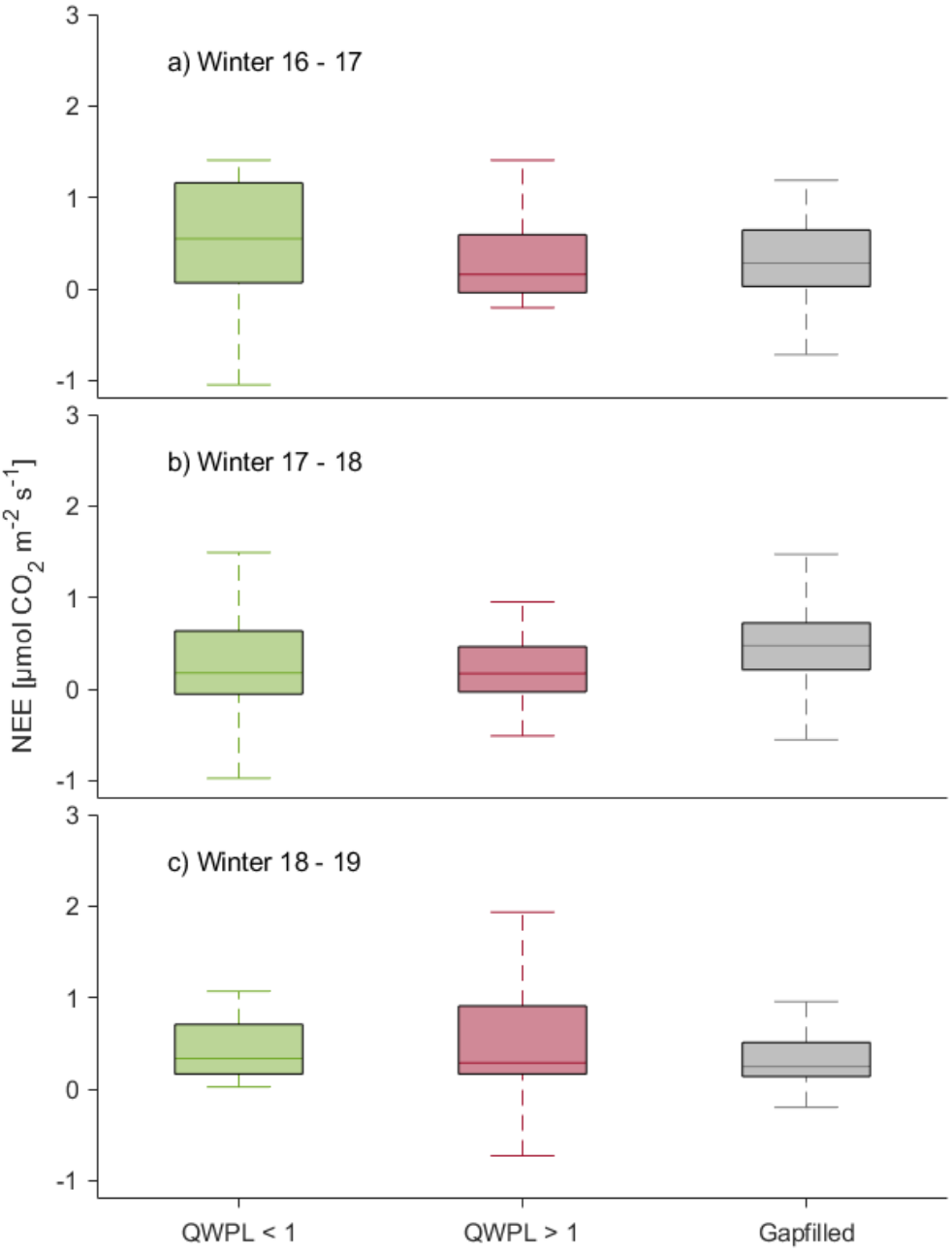

Figure 50: Magnitude of the reference measured NEE with eddy covariance data for all 3 winters for each of the different quality flags; high (red) and low (green) values of the QWPL flag and fluxes produced by the gap-filling algorithm (grey). Note that the units used in this figure differ from those in Chapter 5.

Appendix B

Processing of IRMS Data

B.1 Preparation of Gas Standards

Approximately 2 grams of two different in-house laboratory carbonate standards ('Plessen' and 'Pol2') were reacted with 105% phosphoric acid to liberate CO_2 using a manual vacuum line at the Godwin Laboratory at Cambridge University. Each sample was evacuated for at least an hour, to a pressure less than $3x10^3$ mbar, and then reacted with excess acid until the reaction was completed (with no more visible bubbles having formed from the acid for at least ten minutes). The acid was maintained at 70 °C during the reaction via a circulating water bath surrounding the reaction vessel. A liquid nitrogen trap acted to immediately freeze the gas released during this reaction. The CO_2 was then dried by it passing across a slush trap (held at - 90 °C) and back into a liquid nitrogen trap three times. The CO_2 was collected into bespoke 1.2 L vacuum flasks (manufactured with an additional septum port). This septum port was added to allow mixing of other gases via syringe to create in-house standard gas mixtures with a similar matrix to atmospheric samples - for which we used commercially available 'zero air' (19.9 – 21.9% O_2, balance N_2, 3 ppm CO_2; BOC Ltd., Woking, UK), which could then be subsequently transferred to exetainer vials. 3 L Tedlar bags (Adtech Polymer Engineering Ltd, Stroud, UK; typically used for atmospheric gas sampling) were rinsed three times from the cylinder of 'zero air',and then filled to approximately three quarters full. A 60 mL Luer lock syringe with a 23 gauge needle was triple 'rinsed' from the first Tedlar bag. The syringe was then filled at a rate of 0.5 mL s^{-1}, in order to avoid fractionation and maintain the same matrix from aliquot to aliquot. This syringe was then injected into to one

of the glass vacuum flasks. This process was repeated until the syringe was no longer drawn by vacuum force on insertion through the vacuum flask septum (i.e., until the inside of the flask was at atmospheric pressure).

In order to dilute the CO_2 to an appropriate concentration, a smaller syringe was used to remove 6 mL of gas from the flask, e.g. Plessen or Pol2 in N_2/O_2 matrix, and inject it into a second pre-filled Tedlar bag containing the same 'zero air' mixture. After gas from the flask was added to the bag, the same volume of gas was removed and added to a flushed 12 mL exetainer vial with butyl rubber septum (Labco Ltd.; see below for flushing procedure), and run on the IRMS to check signal intensity. This process was repeated until the intensity of the gas in the exetainer vials as measured on the IRMS was in an appropriate range compared to the expected sample intensity. This second Tedlar bag was then used to fill multiple pre-flushed exetainer vials to be run as matrix matched standards alongside samples. Transfer to pre-flushed exetainers was as per Yu and Lee (2020) (Method A; Figure 1 therein). A 25 gauge needle was used to vent the samples, and the equilbration time prior to removing both needles was reduced to 3 seconds.

Exetainer vials were flushed with helium prior to standard gas injection using a bespoke 'flush-box' autosampler (Sercon Ltd., Crewe, UK). Flushing was performed at $\sim$ 150 mL/min for 480 seconds. This process is similar to the automated Gasbench II flushing procedure, with a two-hole needle allowing gas to escape passively during flushing, resulting in vials which were slightly overpressurised. When analysed on the IRMS, vials have no perceptible background intensity at CO_2 peak positions and less than 10 mV in the 'air' peak position after flushing. Flushed vials were prepared in large batches and tested at 1, 5, 14 and 28 days to ensure the septum maintained a seal; no change in background was detected at any of these times.

Gas mixtures containing 310, 640, and 1022 ppm of CO_2 (all $\pm$ 10 ppm; termed the 300, 600 and 1000 ppm standards respectively) in the same 'zero air' mixture as above were purchased for use as concentration standards (BOC Ltd.). Cylinders of these gases were connected to the flushbox and injected into 12 mL exetainer vials as described above. Flush timing was tested by selecting several vials at random from a large batch, and running these on the IRMS to check that signal intensity and raw isotope ratios were consistent.

The δ13C composition of these concentration standards and the gas mixtures with Plessen and

Gas Standard	Number of Replicates	δ13C [‰VPDB] Mean	σ
Plessen	15	2.4	0.2
Pol2	10	-6.9	0.1
300 ppm	8	-38.5	0.3
600 ppm	8	-38.7	0.2
1000 ppm	8	-37.5	0.1

Table 11: Carbon isotope compositions of CO_2 in the in-house standard gases used in this work as normalization standards for atmospheric CO_2 samples. σ denotes one standard deviation of the mean value.

Pol2 were determined by calibration against in-house and international standards, and is given in Table 11. The calibration measurement sequence included ten replicate measurements of an in-house carbonate standard (Plessen), used to correct for linearity and drift, and normalized to VPDB (Vienna Pee Dee Belemnite standard) using the average of four NBS 18 and NBS 19 measurements from the same run, following Kim et al. (2015). Pol2 was used as a secondary standard to check for internal consistency and assess normalization. Over the course of all runs, the average δ13C value of Pol2 was -6.9 ‰VPDB (n = 45, σ = 0.4 ‰). The 1000 ppm gas standard was selected for use in the normalization as this standard had the highest precision, but due to the extremely negative value of the concentration standards, choosing a different standard for the normalisation process would not change the final sample values.

B.2 Measurement Protocol

IRMS measurements were performed by 'blanking' gases other than CO_2 using timed helium dilution, with dilution set to 100% in the Conflo IV after Levitt (2014). The dilution was timed to stop two and a half seconds before the CO_2 peaks in order to minimize fractionation. The IRMS method was otherwise identical to standard continuous flow-IRMS methods used for measurement of solid carbonate samples (e.g. Spötl and Vennemann, 2003). Samples were run as-is, without processing to separate CO_2 from major and other trace atmospheric gases.

B.3 Correction of Raw Mass Spectrometer Data and Derivation of Isotopic Ratios

The IRMS was operated using Isodat Gas Ratio MS software (version 3.0.94.12). For each sample, 3 reference peaks were measured prior to the sample peaks. Eight sample peaks of gradually decreasing magnitude were then measured, corresponding to sample injections into the source of the mass spec. For each injection, isodat calculates raw ratios of 13C:12C, and the area and amplitude of the mass 44 peak. Sample averages were calculated as the mean of the values for sample peaks 2 - 7, in order to avoid the inclusion of measurements impacted by memory effects from the previous sample. When fewer than 7 sample peaks were measured, all but the first peak were included.

B.3.1 Stretching Correction

Standard gases were measured as above and interspersed around and amoungst samples to facilitate data corrections. Peak averages for Plessen, Pol2, and known concentration standards were used to derive a stretching correction which was then applied to all of the samples (Table 12). This correction took the form of a linear regression $y = mx+c$, where m is the slope of the relationship between the measured peak averaged raw δ13C values and known δ13C values for the 1000ppm and Ples2 standards, and c is the intercept of this line. Uncertainties for the $\delta 13C$ ratios were calculated as the standard deviation of the corrected $\delta 13C$ values for all the Ples2 standards in a run, as shown in Table 13.

	Stretching Correction	
	m	c
Run 152	1.03	-1.26
Run 155	1.02	-1.20
Run 157	1.03	-1.43
Run 158	1.02	-1.18
Run 172	1.04	-1.41
Run 173	1.04	-1.43
Run 174	1.04	-1.30
Run 175	1.03	-2.12

Table 12: Stretching Corrections for the $\delta 13C$ ratios of CO_2 for the IRMS samples. m is a multiplier and c is a constant in ‰

	$\delta 13C$ Uncertainty
Run 152	0.32
Run 155	0.18
Run 157	0.49
Run 158	0.04
Run 172	0.13
Run 173	0.28
Run 174	0.33
Run 175	0.45

Table 13: Uncertainty values for the $\delta 13C$ ratios of CO_2 for the IRMS samples. All values are given in $‰$.

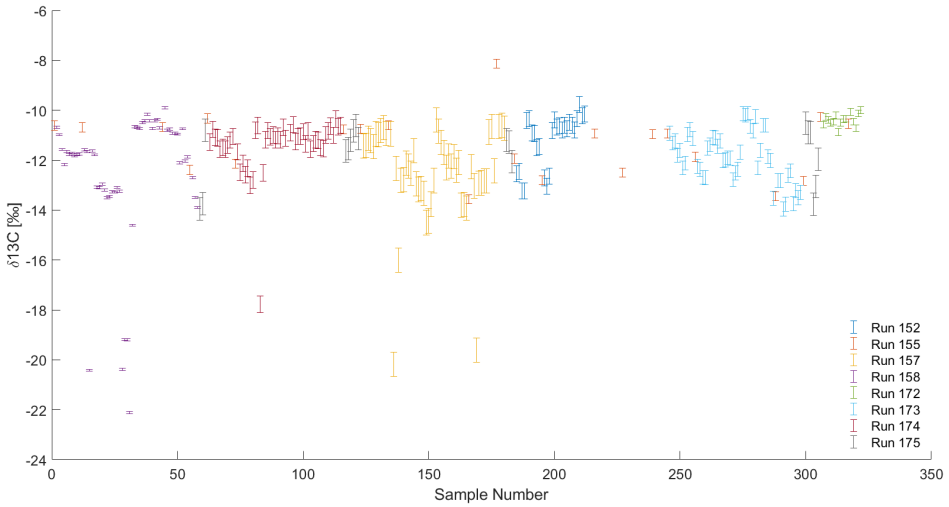

Figure 51: δ13C ratios and uncertainities colour-coded by run for all IRMS samples

B.3.2 Additional Corrections

Typically, samples analysed using IRMS also undergo linearity and drift corrections. However, in this instance, neither linearity nor drift corrections improved the precision of the results.

For the linearity correction, this is likely due to the large range of signal intensity between samples, and the subsequent changes in the relationship (parameterised as a linear regression) between raw isotope ratio and signal intensity over that large range. As this was the first time the IRMS in the NICEST lab was used to measure CO_2 in air samples, some teething problems can be expected. To improve this method in the future, samples could be divided into groups with smaller concentration ranges with additional standards more closely spanning the concentration ranges of each group (Pers. Comm., Modestou, 2023). However, as concentrations of each gas sample are unknown unless co-located with LiCOR profiles (Section 3.3.2), this may not always be feasible. To perform this extra step, additional sacrifical samples would be required in order to pre-determine IRMS signal intensity and subsequently optimise the running order as needed.

Further corrections are also usually implemented to correct for instrumental drift over the measurement period. This correction essentially acts to normalise any changes in raw isotope ratios with time, as a full 88 sample run takes approximately 24 hours, and thus the system may be subject to changes in humidity or temperature due to diurnal temperature changes in the room where it is situated. A lack of improvement from the drift correction suggests that the IRMS was stable enough during each of the runs that any instrument drift had a neglible impact on the measurements. For standard carbonate analysis with this equipment, this correction is typically an order of magnitude lower than measurement precision, and thus can be ignored (Pers. Comm., Modestou, 2023).

B.4 Concentrations from Mass Spectrometry

CO_2 concentrations of the samples were derived using the averages of the amplitudes of the mass 44 peaks (as for the isotopic ratios) for 3 known concentration standards. The linear relationship between amplitude and known concentration was then used to derive a concentration calibration of the form $y = mx + c$ for each run (Table 14).

Concentration uncertainties were intially derived using the 2nd order polynomial relationship be-

	CO_2 Concentration	
	m	c
Run 152	2.26	-5.90
Run 155	2.34	-13.4
Run 157	2.36	-15.8
Run 158	2.32	-5.14
Run 172	2.16	-0.09
Run 173	2.15	8.78
Run 174	2.18	16.3
Run 175	2.21	13.1

Table 14: Derivation of CO_2 concentrations from the IRMS. m is the concentration multiplier and c is a constant in parts per million.

tween the known concentrations and the standard deviation of the amplitude averages. However, for two of the runs, this gave negative uncertainty values. This can occur if the regression does not fully represent the relationship between signal intensity and concentration. As errors in the peak amplitudes and errors in the concentrations of the known concentrations standards are uncorrelated, we performed error propagation by quadrature to recalculate the uncertainties. To do this, we take the differential of the linear regression equation used to calculate the concentrations with respect to the concentration term:

$$\delta x = \sqrt{(\frac{1}{m}\delta y + \frac{-1}{m}\delta c + (\frac{y-c}{m^2}\delta m)^2} \tag{B.1}$$

and evaluated using the concentration of each sample to calculate its uncertainty value. Although errors we no longer negative, there were still many cases where this quantification of error gave an unfeasibly small error, given the known limitations of the method.

Precision in the measurement of the CO_2 concentrations is mostly likely variable between runs because internal conditions in the measurement system may have changed. Helium dilution via the Conflo V masks the dominant gases (nitrogen and oxygen) which elute from the Gasbench II GC column first; dilution prevents the majority of these gases from entering the mass spectrometer source. If the pressure inside the system changes, the timing of these dilutions may change. Even nearly imperceptible changes in the amounts of these gases entering the source can impact measurement. Additionally, whether singularly or through recombination in the source of the mass spectrometer, some gases may produce additional molecules with the same atomic mass as CO_2

which will then cause isobaric interference with the CO_2 peaks. This phenomenon is known as a matrix effect. Changes in the procedure between runs may amplify or cause variation in the magnitude of matrix effects. As the CO_2 concentration standards only contain nitrogen, oxygen and CO_2, the relationship between peak intensity and ppm concentration of CO_2 may not be exactly the same for standards and samples, in particular, the relationship for samples may not be as linear as that derived from the standards.

Appendix C

Testing and Calibration of Low-Cost Sensors

C.1 Calibration of Low-Cost Sensors

For the two field calibrations, the low-cost sensors were placed in a Perspex box, sealed using Tuck Tape. Sensors were set up to record CO_2 concentrations approximately every 10 seconds. The lid of the box had two inlets with three-way valves, one of these was connected to a cylinder of standard gas (either 399 ppm or zero-air; LindeCanada, Edmonton, Alberta) and the other inlet connected to a Los Gatos Ultraportable Greenhouse Gas Analyser (LGA; Los Gatos Research, San Jose, California) analyser. The box was flooded with standard gas until the measured CO_2 concentration from the LGA stabilised. Sensors were then left in the box for about an hour. The process was then repeated for the other standard gas.

For the first calibration, the mean measured concentrations for both standard gases were used. A two point calibration, of the form $y = mx + c$ was derived for each sensor, where y is equal to the recalibrated concentration for each sensor, x is equal to the measured concentration from the LGA, m is a multiplier and c is the concentration from each sensor when the measured LGA concentration is zero. Figure 52 shows the application of these recalibrations (termed Cal 1) to each of the 15 sensors over the time period for which they were derived. However, issues with air circulation within the box and measuring very low concentrations on the LGA when flooding

the box with the zero-air standard reduced the quality of this calibration. The use of this two-point linear calibration (Cal 1) lead to very high variability in CO_2 concentrations during the box deployments, and occasionally gave physically impossible negative concentrations.

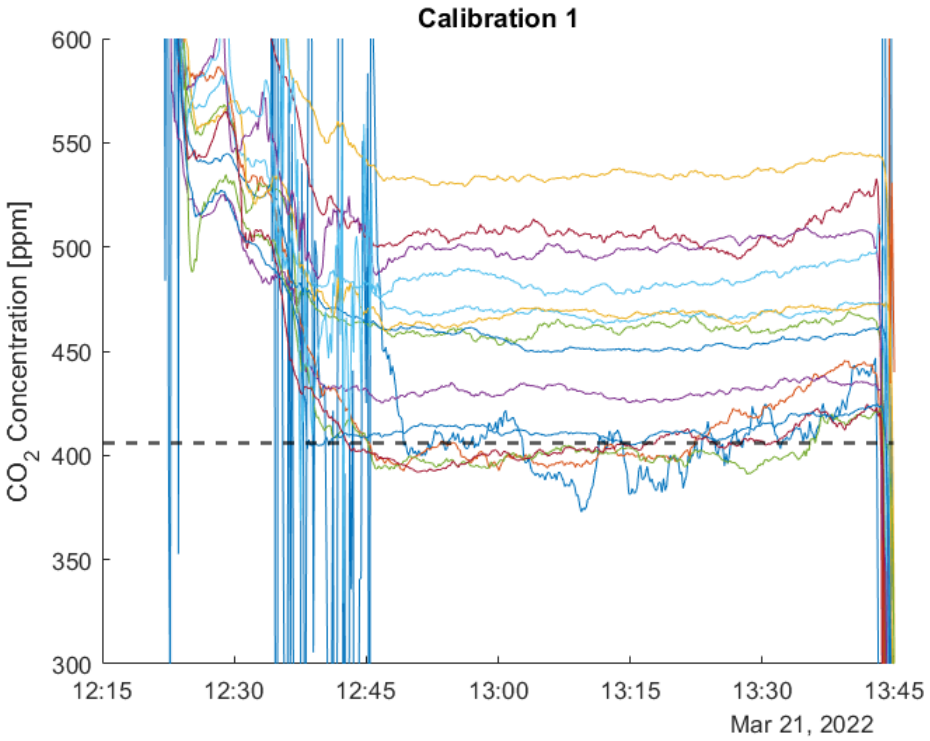

Figure 52: Calibration 1. Each of the 15 coloured lines represents an individual sensor, with the black dashed line showing the mean measured concentration from the Los Gatos Analyser.

A second calibration was therefore derived using only the 399 ppm standard, and calculating the offset between the mean measured LGA and sensor concentrations for each sensor. This calibration showed improved performance, with all but one of the sensors giving reasonable values (Fig 53). This one sensor was later excluded from the analysis.

Although multiple calibration efforts were undertaken in order to attempt to reduce the impact of calibration error, uncertainties still persisted. Pockets of higher and lower concentrations of CO_2 may have been present within the container where the calibration took place as there was no fan or pump to aid air circulation. Additionally, we cannot verify that the container used for the calibration was definitely gas-tight. High ambient concentrations of CO_2 in the tent where this calibration was undertaken may have fed into the box, leading to a drift in concentration (although this was not marked enough to be visible on the Los Gatos instrument).

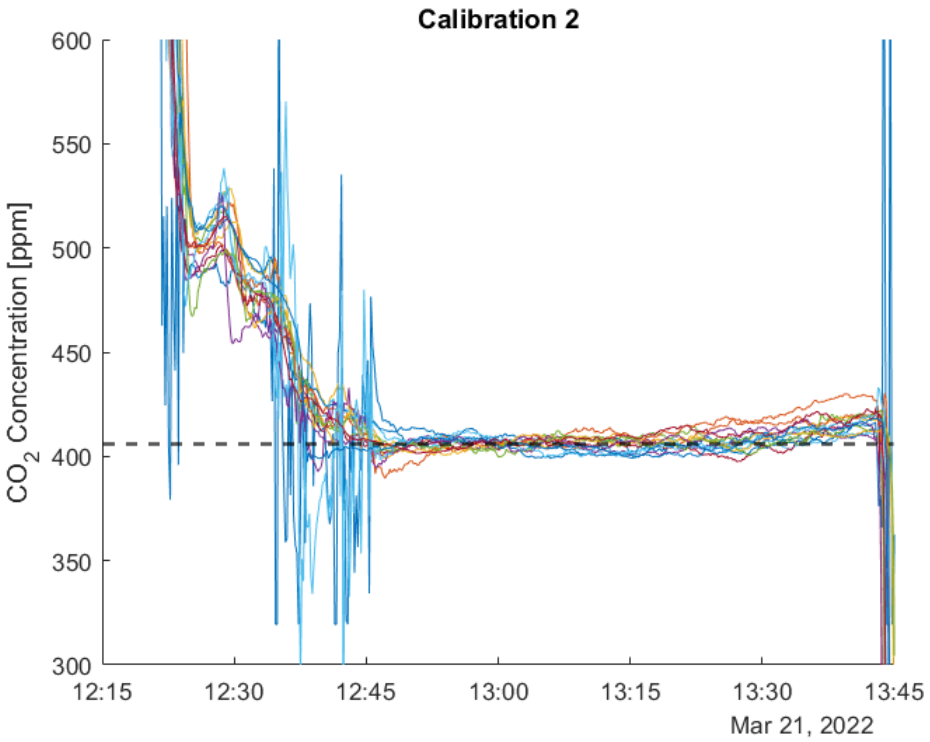

Figure 53: Calibration 2. Each of the 15 coloured lines represents an individual sensor, with the black dashed line showing the mean measured concentration from the Los Gatos Analyser.

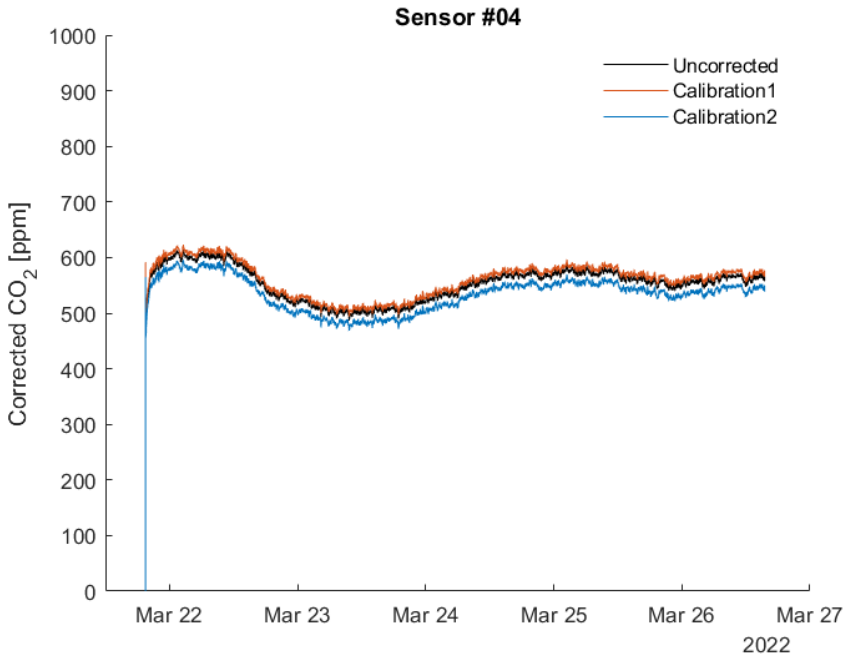

Figure 54: Example recalibration of low-cost sensor timeseries - showing the lower sensor from TR02. Calibration 2 (shown in blue) gives the final CO_2 concentrations used to calculate fluxes.

C.2 Predeployment Testing of Low-Cost Sensors

For the first test, we buried one sensor overnight to test how long it took the sensors to adjust to ambient temperature, humidity and CO_2 conditions. Temperatures took longer to equilibriate than humidity or CO_2 concentration, but all 3 factors had stabilised after 12 hours.

Two pairs of sensors were buried at the base of a $\sim$ 70 cm snowpack, one with the membranes facing upwards and the other with the membrane facing downwards. Concentrations from both sensor pairs appeared to be anti-correlated. For the lower sensor with the downward facing membrane, we suspect CO_2 became trapped in the box due to restricted airflow between the membrane and the ground surface. Based on this test, we decided to deploy the lower sensor with the membrane facing up. We also decided that the upper sensor should be deployed with the membrane facing down (i.e. towards the lower sensor) to better capture transport between the boxes and reduce the likeliness of erroneously measuring atmospheric influences.

References

Aanderud, Z. T., Jones, S. E., Schoolmaster, D. R., Fierer, N., and Lennon, J. T.: Sensitivity of soil respiration and microbial communities to altered snowfall, Soil Biology and Biochemistry, 57, 217–227, https://doi.org/10.1016/j.soilbio.2012.07.022, 2013.

Adams, E. E. and Brown, R. L.: Metamorphism of Dry Snow as a result of Temperature Gradient and Vapor Density Differences, Annals of Glaciology, 4, https://doi.org/10.3189/S0260305500005140, 1983.

Albert, M. R. and Shultz, E. F.: Snow and Firn properties and air–snow transport processes at Summit, Greenland, 2002.

Ancin-Murguzur, F. and Hausner, V.: Research gaps and trends in the Arctic tundra: a topic-modelling approach, One Ecosystem, 5, https://doi.org/10.3897/oneeco.5.e57117, 2020.

Anderson, E.: A point energy and mass balance model of a snow cover, Tech. rep., National Oceanic and Atmospheric Administration, Silver Spring, Maryland, URL https://repository.library.noaa.gov/view/noaa/6392, 1976.

Anderson, T. R., Hawkins, E., and Jones, P. D.: CO, the greenhouse effect and global warming: from the pioneering work of Arrhenius and Callendar to today's Earth System Models, Endeavour, 40, https://doi.org/10.1016/j.endeavour.2016.07.002, 2016.

Andrén, O. and Paustian, K.: Barley Straw Decomposition in the Field: A Comparison of Models, Ecology, https://doi.org/10.2307/1939203, 1987.

Arndt, K. A., Lipson, D. A., Hashemi, J., Oechel, W. C., and Zona, D.: Snow melt stimulates ecosystem respiration in Arctic ecosystems, Glob Chang Biol, https://doi.org/10.1111/gcb.15193, 2020.

Azizi-Rad, M., Guggenberger, G., Ma, Y., and Sierra, C. A.: Sensitivity of soil respiration rate with respect to temperature, moisture and oxygen under freezing and thawing, Soil Biology and Biochemistry, 165, https://doi.org/10.1016/j.soilbio.2021.108488, 2022.

Baker, I.: Microstructural characterization of snow, firn and ice, Philos Trans A Math Phys Eng Sci, 377, 20180 162, https://doi.org/10.1098/rsta.2018.0162, 2019.

Barrere, M., Domine, F., Decharme, B., Morin, S., Vionnet, V., and Lafaysse, M.: Evaluating the performance of coupled snow–soil models in SURFEXv8 to simulate the permafrost thermal regime at a high Arctic site, Geoscientific Model Development, 10, 3461–3479, https://doi.org/10.5194/gmd-10-3461-2017, 2017.

Bartels-Rausch, T., Jacobi, H. W., Kahan, T. F., Thomas, J. L., Thomson, E. S., Abbatt, J. P. D., Ammann, M., Blackford, J. R., Bluhm, H., Boxe, C., Domine, F., Frey, M. M., Gladich, I., Guzmán, M. I., Heger, D., Huthwelker, T., Klán, P., Kuhs, W. F., Kuo, M. H., Maus, S., Moussa, S. G., McNeill, V. F., Newberg, J. T., Pettersson, J. B. C., Roeselová, M., and Sodeau, J. R.: Relationship between snow microstructure and physical and chemical processes, Atmospheric Chemistry and Physics Discussions, 12, 30 409–30 541, https://doi.org/10.5194/acpd-12-30409-2012, 2012.

Bartelt, P. and Lehning, M.: A physical SNOWPACK model for the Swiss avalanche warning Part I: numerical model, Cold Regions Science and Technology, 35, 123–145, https://doi.org/10.1016/S0165-232X(02)00074-5, 2001.

Bastviken, D., Sundgren, I., Natchimuthu, S., Reyier, H., and Gålfalk, M.: Technical Note: Cost-efficient approaches to measure carbon dioxide (CO2) fluxes and concentrations in terrestrial and aquatic environments using mini loggers, Biogeosciences, 12, https://doi.org/10.5194/bg-12-3849-2015, 2015.

Bastviken, D., Nygren, J., Schenk, J., Parellada Massana, R., and Duc, N. T.: Technical note: Facilitating the use of low-cost methane (CH4) sensors in flux chambers – calibration, data processing, and an open source make-it-yourself logger, Biogeosciences Discussions, https://doi.org/10.5194/bg-2019-499, 2020.

Bastviken, D., Wilk, J., Duc, N. T., Gålfalk, M., Karlson, M., Neset, T.-S., Opach, T., Enrich-Prast,

A., and Sundgren, I.: Critical method needs in measuring greenhouse gas fluxes, Environmental Research Letters, 17, https://doi.org/10.1088/1748-9326/ac8fa9, 2022.

Belshe, E. F., Schuur, E. A., and Bolker, B. M.: Tundra ecosystems observed to be CO2 sources due to differential amplification of the carbon cycle, Ecol Lett, 16, 1307–15, https://doi.org/10.1111/ele.12164, 2013.

Benson, C. S. and Sturm, M.: Structure and wind transport of seasonal snow on the Arctic slope of Alaska, Annals of Glaciology, 18, 261–267, https://doi.org/10.3189/s0260305500011629, 1993.

Birch, L., Schwalm, C. R., Natali, S., Lombardozzi, D., Keppel-Aleks, G., Watts, J., Lin, X., Zona, D., Oechel, W., Sachs, T., Black, T. A., and Rogers, B. M.: Addressing biases in Arctic–boreal carbon cycling in the Community Land Model Version 5, Geoscientific Model Development, 14, 3361–3382, https://doi.org/10.5194/gmd-14-3361-2021, 2021.

Biskaborn, B. K., Smith, S. L., Noetzli, J., Matthes, H., Vieira, G., Streletskiy, D. A., Schoeneich, P., Romanovsky, V. E., Lewkowicz, A. G., Abramov, A., Allard, M., Boike, J., Cable, W. L., Christiansen, H. H., Delaloye, R., Diekmann, B., Drozdov, D., Etzelmuller, B., Grosse, G., Guglielmin, M., Ingeman-Nielsen, T., Isaksen, K., Ishikawa, M., Johansson, M., Johannsson, H., Joo, A., Kaverin, D., Kholodov, A., Konstantinov, P., Kroger, T., Lambiel, C., Lanckman, J. P., Luo, D., Malkova, G., Meiklejohn, I., Moskalenko, N., Oliva, M., Phillips, M., Ramos, M., Sannel, A. B. K., Sergeev, D., Seybold, C., Skryabin, P., Vasiliev, A., Wu, Q., Yoshikawa, K., Zheleznyak, M., and Lantuit, H.: Permafrost is warming at a global scale, Nat Commun, 10, 264, https://doi.org/10.1038/s41467-018-08240-4, 2019.

Bjorkman, A. D., Myers-Smith, I. H., Elmendorf, S. C., Normand, S., Ruger, N., Beck, P. S. A., Blach-Overgaard, A., Blok, D., Cornelissen, J. H. C., Forbes, B. C., Georges, D., Goetz, S. J., Guay, K. C., Henry, G. H. R., HilleRisLambers, J., Hollister, R. D., Karger, D. N., Kattge, J., Manning, P., Prevey, J. S., Rixen, C., Schaepman-Strub, G., Thomas, H. J. D., Vellend, M., Wilmking, M., Wipf, S., Carbognani, M., Hermanutz, L., Levesque, E., Molau, U., Petraglia, A., Soudzilovskaia, N. A., Spasojevic, M. J., Tomaselli, M., Vowles, T., Alatalo, J. M., Alexander, H. D., Anadon-Rosell, A., Angers-Blondin, S., Beest, M. T., Berner, L., Bjork, R. G., Buchwal, A., Buras, A., Christie, K., Cooper, E. J., Dullinger, S., Elberling, B., Eskelinen, A., Frei,

E. R., Grau, O., Grogan, P., Hallinger, M., Harper, K. A., Heijmans, M., Hudson, J., Hulber, K., Iturrate-Garcia, M., Iversen, C. M., Jaroszynska, F., Johnstone, J. F., Jorgensen, R. H., Kaarlejarvi, E., Klady, R., Kuleza, S., Kulonen, A., Lamarque, L. J., Lantz, T., Little, C. J., Speed, J. D. M., Michelsen, A., Milbau, A., Nabe-Nielsen, J., Nielsen, S. S., Ninot, J. M., Oberbauer, S. F., Olofsson, J., Onipchenko, V. G., Rumpf, S. B., Semenchuk, P., Shetti, R., Collier, L. S., Street, L. E., Suding, K. N., Tape, K. D., Trant, A., Treier, U. A., Tremblay, J. P., Tremblay, M., Venn, S., Weijers, S., Zamin, T., Boulanger-Lapointe, N., Gould, W. A., Hik, D. S., Hofgaard, A., Jonsdottir, I. S., Jorgenson, J., Klein, J., Magnusson, B., Tweedie, C., Wookey, P. A., Bahn, M., Blonder, B., van Bodegom, P. M., Bond-Lamberty, B., Campetella, G., Cerabolini, B. E. L., Chapin, F. S., Cornwell, W. K., Craine, J., Dainese, M., de Vries, F. T., Diaz, S., Enquist, B. J., Green, W., Milla, R., Niinemets, U., Onoda, Y., Ordonez, J. C., Ozinga, W. A., Penuelas, J., Poorter, H., Poschlod, P., Reich, P. B., Sandel, B., Schamp, B., Sheremetev, S., and Weiher, E.: Plant functional trait change across a warming tundra biome, Nature, 562, 57–62, https://doi.org/10.1038/s41586-018-0563-7, 2018.

Björk, R. G., Björkman, M. P., Andersson, M. X., and Klemedtsson, L.: Temporal variation in soil microbial communities in Alpine tundra, Soil Biology and Biochemistry, 40, 266–268, https://doi.org/10.1016/j.soilbio.2007.07.017, 2008.

Björkman, M. P., Morgner, E., Björk, R. G., Cooper, E. J., Elberling, B., and Klemedtsson, L.: A comparison of annual and seasonal carbon dioxide effluxes between sub-Arctic Sweden and High-Arctic Svalbard, Polar Research, 29, 75–84, https://doi.org/10.1111/j.1751-8369.2010.00150.x, 2010a.

Björkman, M. P., Morgner, E., Cooper, E. J., Elberling, B., Klemedtsson, L., and Björk, R. G.: Winter carbon dioxide effluxes from Arctic ecosystems: An overview and comparison of methodologies, Global Biogeochemical Cycles, 24, n/a–n/a, https://doi.org/10.1029/2009gb003667, 2010b.

Blanc-Betes, E., Welker, J. M., Sturchio, N. C., Chanton, J. P., and Gonzalez-Meler, M. A.: Winter precipitation and snow accumulation drive the methane sink or source strength of Arctic tussock tundra, Glob Chang Biol, 22, 2818–33, https://doi.org/10.1111/gcb.13242, 2016.

Bliss, L. C. and Matveyeva, N. V.: Circumpolar Arctic vegetation, in: Arctic Ecosystems in a

Changing Climate: An Ecophysiological Perspective, edited by Chapin, F. S. I., Jefferies, R. L., Reynolds, J. F., Shaver, G. R., Svoboda, J., and Chu, E. W., pp. 59–89, San Diego: Elsevier Science & Technology, San Diego, 1991.

Bliss, L. C., Courtin, G. M., Pattie, D. L., Riewe, R. R., Whitfield, D. W. A., and Widden, P.: Arctic Tundra Ecosystems, 1973.

Blyth, E. M., Arora, V. K., Clark, D. B., Dadson, S. J., De Kauwe, M. G., Lawrence, D. M., Melton, J. R., Pongratz, J., Turton, R. H., Yoshimura, K., and Yuan, H.: Advances in Land Surface Modelling, Current Climate Change Reports, 7, 45–71, https://doi.org/10.1007/s40641-021-00171-5, 2021.

Boike, J., Cable, W. L., Bornemann, N., and Lange, S.: Trail Valley Creek, NWT, Canada Soil Moisture and Temperature 2016 - 2019, Tech. rep., PANGAEA, 2020.

Bokhorst, S., Pedersen, S. H., Brucker, L., Anisimov, O., Bjerke, J. W., Brown, R. D., Ehrich, D., Essery, R. L., Heilig, A., Ingvander, S., Johansson, C., Johansson, M., Jonsdottir, I. S., Inga, N., Luojus, K., Macelloni, G., Mariash, H., McLennan, D., Rosqvist, G. N., Sato, A., Savela, H., Schneebeli, M., Sokolov, A., Sokratov, S. A., Terzago, S., Vikhamar-Schuler, D., Williamson, S., Qiu, Y., and Callaghan, T. V.: Changing Arctic snow cover: A review of recent developments and assessment of future needs for observations, modelling, and impacts, Ambio, 45, 516–37, https://doi.org/10.1007/s13280-016-0770-0, 2016.

Bonan, G.: Climate Change and Terrestrial Ecosystem Modelling, Cambridge University Press, Cambridge, UK, type: Book, 2019.

Bonan, G. B. and Doney, S. C.: Climate, ecosystems, and planetary futures: The challenge to predict life in Earth system models, Science, 359, https://doi.org/10.1126/science.aam8328, 2018.

Bonan, G. B., Levis, S., Kergoat, L., and Oleson, K. W.: Landscapes as patches of plant functional types: An integrating concept for climate and ecosystem models, Global Biogeochemical Cycles, 16, 5–1–5–23, https://doi.org/10.1029/2000gb001360, 2002.

Bonan, G. B., Lombardozzi, D. L., Wieder, W. R., Oleson, K. W., Lawrence, D. M., Hoffman, F. M., and Collier, N.: Model Structure and Climate Data Uncertainty in Historical Simulations

of the Terrestrial Carbon Cycle (1850–2014), Global Biogeochem Cycles, 33, https://doi.org/10.1029/2018GB006141, 2019.

Bowling, D. R., Massman, W. J., Schaeffer, S. M., Burns, S. P., Monson, R. K., and Williams, M. W.: Biological and physical influences on the carbon isotope content of CO2 in a subalpine forest snowpack, Niwot Ridge, Colorado, Biogeochemistry, 95, https://doi.org/10.1007/s10533-008-9233-4, 2008.

Box, J. E., Colgan, W. T., Christensen, T. R., Schmidt, N. M., Lund, M., Parmentier, F.-J. W., Brown, R., Bhatt, U. S., Euskirchen, E. S., Romanovsky, V. E., Walsh, J. E., Overland, J. E., Wang, M., Corell, R. W., Meier, W. N., Wouters, B., Mernild, S., Mård, J., Pawlak, J., and Olsen, M. S.: Key indicators of Arctic climate change: 1971–2017, Environmental Research Letters, 14, https://doi.org/10.1088/1748-9326/aafc1b, 2019.

Braghiere, R. K., Fisher, J. B., Miner, K. R., Miller, C. E., Worden, J. R., Schimel, D. S., and Frankenberg, C.: Tipping point in North American Arctic-Boreal carbon sink persists in new generation Earth system models despite reduced uncertainty, Environmental Research Letters, 18, https://doi.org/10.1088/1748-9326/acb226, 2023.

Brown, R. D. and Mote, P. W.: The Response of Northern Hemisphere Snow Cover to a Changing Climate, Journal of Climate, 22, https://doi.org/10.1175/2008jcli2665.1, 2009.

Buckeridge, K. M., Banerjee, S., Siciliano, S. D., and Grogan, P.: The seasonal pattern of soil microbial community structure in mesic low arctic tundra, Soil Biology and Biochemistry, 65, 338–347, https://doi.org/10.1016/j.soilbio.2013.06.012, 2013.

Bueno, C. G., Williamson, S. N., Barrio, I. C., Helgadottir, A., and Hi, K. D.: Moss Mediates the Influence of Shrub Species on Soil Properties and Processes in Alpine Tundra, PLoS One, 11, https://doi.org/10.1371/journal.pone.0164143, 2016.

Burba, G.: Eddy Covariance Method for Scientific, Regulatory, and Commercial Applications, type: Book, 2022.

Burba, G. and Anderson, D.: A Brief Practical Guide to Eddy Covariance Flux Measurements: Principles and Workflow Examples for Scientific and Industrial Applications, Li-COR Biosciences, Licoln, Nebraska, 2005.

Burke, E. J., Chadburn, S. E., and Ekici, A.: A vertical representation of soil carbon in the JULES land surface scheme (vn4.3_permafrost) with a focus on permafrost regions, Geoscientific Model Development, 10, 959–975, https://doi.org/10.5194/gmd-10-959-2017, 2017.

Burke, E. J., Zhang, Y., and Krinner, G.: Evaluating permafrost physics in the Coupled Model Intercomparison Project 6 (CMIP6) models and their sensitivity to climate change, The Cryosphere, 14, 3155–3174, https://doi.org/10.5194/tc-14-3155-2020, 2020.

Byun, E., Rezanezhad, F., Fairbairn, L., Slowinski, S., Basiliko, N., Price, J. S., Quinton, W. L., Roy-Leveillee, P., Webster, K., and Van Cappellen, P.: Temperature, moisture and freeze-thaw controls on CO2 production in soil incubations from northern peatlands, Sci Rep, 11, 23 219, https://doi.org/10.1038/s41598-021-02606-3, 2021.

Callaghan, T. V., Björn, L. O., Chernov, Y., Chapin, T., Christensen, T. R., Huntley, B., Ims, R., Jolly, D., Jonasson, S., Matveyeva, N., Panikov, N., Oechel, W., Shaver, G., Elster, J., Henttonen, H., Johansson, M., Jónsdóttir, I. S., Laine, K., Schaphoff, S., Sitch, S., Taulavuori, K., Taulavuori, E., and Zöckler, C.: Arctic Tundra and Polar Desert Ecosystems, in: ACIA Scientific Report, 2005.

Callaghan, T. V., Johansson, M., Brown, R. D., Groisman, P. Y., Labba, N., Radionov, V., Barry, R. G., Bulygina, O. N., Essery, R. L. H., Frolov, D. M., Golubev, V. N., Grenfell, T. C., Petrushina, M. N., Razuvaev, V. N., Robinson, D. A., Romanov, P., Shindell, D., Shmakin, A. B., Sokratov, S. A., Warren, S., and Yang, D.: The Changing Face of Arctic Snow Cover: A Synthesis of Observed and Projected Changes, Ambio, 40, 17–31, https://doi.org/10.1007/s13280-011-0212-y, 2012.

Calonne, N., Flin, F., Morin, S., Lesaffre, B., du Roscoat, S. R., and Geindreau, C.: Numerical and experimental investigations of the effective thermal conductivity of snow, Geophysical Research Letters, 38, https://doi.org/10.1029/2011gl049234, 2011.

Calonne, N., Richter, B., Löwe, H., Cetti, C., ter Schure, J., Van Herwijnen, A., Fierz, C., Jaggi, M., and Schneebeli, M.: The RHOSSA campaign: multi-resolution monitoring of the seasonal evolution of the structure and mechanical stability of an alpine snowpack, The Cryosphere, 14, 1829–1848, https://doi.org/10.5194/tc-14-1829-2020, 2020.

Campbell, J. L.: Arctic Loses Carbon as Winters Wane, Nature Climate Change, 9, 806–807, https://doi.org/10.1038/s41558-019-0606-6, 2019.

Campbell, J. L. and Laudon, H.: Carbon response to changing winter conditions in northern regions: current understanding and emerging research needs, Environmental Reviews, 27, 545–566, https://doi.org/10.1139/er-2018-0097, 2019.

Campbell, J. L., Mitchell, M. J., Groffman, P. M., Christenson, L. M., and Hardy, J. P.: Winter in northeastern North America: a critical period for ecological processes, 2005.

Carbone, A., Chiaia, B., Frigo, B., and Turk, C.: Snow metamorphism: a fractal approach, 2010.

Chadburn, S. E., Krinner, G., Porada, P., Bartsch, A., Beer, C., Belelli Marchesini, L., Boike, J., Ekici, A., Elberling, B., Friborg, T., Hugelius, G., Johansson, M., Kuhry, P., Kutzbach, L., Langer, M., Lund, M., Parmentier, F.-J. W., Peng, S., Van Huissteden, K., Wang, T., Westermann, S., Zhu, D., and Burke, E. J.: Carbon stocks and fluxes in the high latitudes: using site-level data to evaluate Earth system models, Biogeosciences, 14, 5143–5169, https://doi.org/10.5194/bg-14-5143-2017, 2017.

Chadburn, S. E., Burke, E. J., Gallego-Sala, A. V., Smith, N. D., Bret-Harte, M. S., Charman, D. J., Drewer, J., Edgar, C. W., Euskirchen, E. S., Fortuniak, K., Gao, Y., Nakhavali, M., Pawlak, W., Schuur, E. A. G., and Westermann, S.: A new approach to simulate peat accumulation, degradation and stability in a global land surface scheme (JULES vn5.8_accumulate_soil) for northern and temperate peatlands, Geoscientific Model Development, 15, 1633–1657, https://doi.org/10.5194/gmd-15-1633-2022, 2022.

Chaudhary, N., Westermann, S., Lamba, S., Shurpali, N., Sannel, A. B. K., Schurgers, G., Miller, P. A., and Smith, B.: Modelling past and future peatland carbon dynamics across the pan-Arctic, Glob Chang Biol, 26, 4119–4133, https://doi.org/10.1111/gcb.15099, 2020.

Chen, S., Wang, J., Zhang, T., and Hu, Z.: Climatic, soil, and vegetation controls of the temperature sensitivity (Q10) of soil respiration across terrestrial biomes, Global Ecology and Conservation, 22, https://doi.org/10.1016/j.gecco.2020.e00955, 2020.

Christiansen, C. T., Schmidt, N. M., and Michelsen, A.: High Arctic Dry Heath CO2 Exchange

During the Early Cold Season, Ecosystems, 15, 1083–1092, https://doi.org/10.1007/s10021-012-9569-4, 2012.

Clarke, G. K. C. and Waddington, E. D.: A three-dimensional theory of wind pumping, Journal of Glaciology, 37, https://doi.org/10.3189/s0022143000042830, 1991.

Clien, J. S. and Schimel, J. P.: Microbial Activity of Tundra and Taiga Soils at Subzero Temperatures, 1995.

Colbeck, S. C.: Snow Particle Morphology in the Seasonal Snow Cover, Bulletin of the American Meteorological Society, 64, 1983.

Colbeck, S. C.: The Layered Charecter of Snow Covers, 1991.

Colbeck, S. C.: Model of wind pumping for layered snow, 1997.

Commane, R., Lindaas, J., Benmergui, J., Luus, K. A., Chang, R. Y., Daube, B. C., Euskirchen, E. S., Henderson, J. M., Karion, A., Miller, J. B., Miller, S. M., Parazoo, N. C., Randerson, J. T., Sweeney, C., Tans, P., Thoning, K., Veraverbeke, S., Miller, C. E., and Wofsy, S. C.: Carbon dioxide sources from Alaska driven by increasing early winter respiration from Arctic tundra, Proc Natl Acad Sci U S A, 114, 5361–5366, https://doi.org/10.1073/pnas.1618567114, 2017.

Conger, S. M. and McClung, D. M.: Comparison of density cutters for snow profile observations, Journal of Glaciology, 55, 163–169, 2009.

Cook, B. I., Bonan, G. B., Levis, S., and Epstein, H. E.: The thermoinsulation effect of snow cover within a climate model, Climate Dynamics, 31, 107–124, https://doi.org/10.1007/s00382-007-0341-y, 2007.

Curiel Yuste, J., Janssens, I. A., Carrara, A., and Ceulemans, R.: Annual Q10 of soil respiration reflects plant phenological patterns as well as temperature sensitivity, Global Change Biology, 10, 161–169, https://doi.org/10.1111/j.1529-8817.2003.00727.x, 2004.

Danabasoglu, G., Lamarque, J.-F., Bacmeister, J., Bailey, D. A., DuVivier, A. K., Edwards, J., Emmons, L. K., Fasullo, J., Garcia, R., Gettelman, A., Hannay, C., Holland, M. M., Large, W. G., Lauritzen, P. H., Lawrence, D. M., Lenaerts, J. T. M., Lindsay, K., Lipscomb, W. H., Mills, M. J., Neale, R., Oleson, K. W., Otto-Bliesner, B., Phillips, A. S., Sacks, W., Tilmes, S.,

Kampenhout, L., Vertenstein, M., Bertini, A., Dennis, J., Deser, C., Fischer, C., Fox-Kemper, B., Kay, J. E., Kinnison, D., Kushner, P. J., Larson, V. E., Long, M. C., Mickelson, S., Moore, J. K., Nienhouse, E., Polvani, L., Rasch, P. J., and Strand, W. G.: The Community Earth System Model Version 2 (CESM2), Journal of Advances in Modeling Earth Systems, 12, https://doi.org/10.1029/2019ms001916, 2020.

Deng, M., Meng, X., Lyv, Y., Zhao, L., Li, Z., Jing, H., and Hu, Z.: Comparison of Soil Water and Heat Transfer Modeling Over the Tibetan Plateau Using Two Community Land Surface Model (CLM) Versions, Journal of Advances in Modeling Earth Systems, https://doi.org/10.1029/2020MS002189, 2020.

Deng, M., Meng, X., Lu, Y., Li, Z., Zhao, L., Hu, Z., Chen, H., Shang, L., Wang, S., and Li, Q.: Impact and Sensitivity Analysis of Soil Water and Heat Transfer Parameterizations in Community Land Surface Model on the Tibetan Plateau, Journal of Advances in Modeling Earth Systems, 13, https://doi.org/10.1029/2021ms002670, 2021.

Depledge, D. and Kennedy-Pipe, C.: The changing world of the Arctic, Geography, 103, https://doi.org/10.1080/00167487.2018.12094052, 2020.

Derksen, C., Sturm, M., Holmgren, J., Liston, G. E., Huntington, H., Silis, A., and Solie, D.: Northwest Territories and Nunavut Snow Characteristics from a Subarctic Traverse: Implications for Passive Microwave Remote Sensing, Journal of Hydrometeorology, 10, 448–463, https://doi.org/10.1175/2008jhm1074.1, 2009.

Derksen, C., Lemmetyinen, J., Toose, P., Silis, A., Pulliainen, J., and Sturm, M.: Physical properties of Arctic versus subarctic snow: Implications for high latitude passive microwave snow water equivalent retrievals, Journal of Geophysical Research: Atmospheres, 119, 7254–7270, https://doi.org/10.1002/2013jd021264, 2014.

Dodds, K.: Global Arctic, Journal of Borderlands Studies, 33, https://doi.org/10.1080/08865655.2017.1332488, 2017.

Domine, F. and Shepson, P.: Air-Snow Interactions and Atmospheric Chemistry, Science, 297, 1506–1510, 2002.

Domine, F., Gallet, J.-C., Bock, J., and Morin, S.: Structure, specific surface area and thermal conductivity of the snowpack around Barrow, Alaska, Journal of Geophysical Research: Atmospheres, 117, https://doi.org/10.1029/2011jd016647, 2012.

Domine, F., Barrere, M., Sarrazin, D., Morin, S., and Arnaud, L.: Automatic monitoring of the effective thermal conductivity of snow in a low-Arctic shrub tundra, The Cryosphere, 9, 1265–1276, https://doi.org/10.5194/tc-9-1265-2015, 2015.

Domine, F., Barrere, M., and Morin, S.: The growth of shrubs on high Arctic tundra at Bylot Island: impact on snow physical properties and permafrost thermal regime, Biogeosciences, 13, 6471–6486, https://doi.org/10.5194/bg-13-6471-2016, 2016a.

Domine, F., Barrere, M., and Sarrazin, D.: Seasonal evolution of the effective thermal conductivity of the snow and the soil in high Arctic herb tundra at Bylot Island, Canada, The Cryosphere, 10, 2573–2588, https://doi.org/10.5194/tc-10-2573-2016, 2016b.

Domine, F., Belke-Brea, M., Sarrazin, D., Arnaud, L., Barrere, M., and Poirier, M.: Soil moisture, wind speed and depth hoar formation in the Arctic snowpack, Journal of Glaciology, 64, 990–1002, https://doi.org/10.1017/jog.2018.89, 2018.

Domine, F., Picard, G., Morin, S., Barrere, M., Madore, J.-B., and Langlois, A.: Major Issues in Simulating Some Arctic Snowpack Properties Using Current Detailed Snow Physics Models: Consequences for the Thermal Regime and Water Budget of Permafrost, Journal of Advances in Modeling Earth Systems, 11, 34–44, https://doi.org/10.1029/2018ms001445, 2019.

Dutch, V. R., Rutter, N., Wake, L., Sandells, M., Derksen, C., Walker, B., Hould Gosselin, G., Sonnentag, O., Essery, R., Kelly, R., Marsh, P., King, J., and Boike, J.: Impact of measured and simulated tundra snowpack properties on heat transfer, The Cryosphere, 16, https://doi.org/10.5194/tc-16-4201-2022, 2022.

Eerkes-Medrano, L. and Huntington, H. P.: Untold Stories: Indigenous Knowledge Beyond the Changing Arctic Cryosphere, Frontiers in Climate, 3, https://doi.org/10.3389/fclim.2021.675805, 2021.

Ekici, A., Chadburn, S., Chaudhary, N., Hajdu, L. H., Marmy, A., Peng, S., Boike, J., Burke, E., Friend, A. D., Hauck, C., Krinner, G., Langer, M., Miller, P. A., and Beer, C.: Site-level model

intercomparison of high latitude and high altitude soil thermal dynamics in tundra and barren landscapes, The Cryosphere, 9, 1343–1361, https://doi.org/10.5194/tc-9-1343-2015, 2015.

Elberling, B.: Annual soil CO2 effluxes in the High Arctic: The role of snow thickness and vegetation type, Soil Biology and Biochemistry, 39, 646–654, https://doi.org/10.1016/j.soilbio.2006.09.017, 2007.

Elberling, B. and Brandt, K. K.: Uncoupling of microbial CO2 production and release in frozen soil and its implications for field studies of arctic C cycling, 2003.

Essery, R. and Pomeroy, J.: Vegetation and Topographic Control of Wind-Blown Snow Distributions in Distributed and Aggregated Simulations for an Arctic Tundra Basin, Journal of Hydrometeorology, 5, 735–744, 2004.

Essery, R., Kontu, A., Lemmetyinen, J., Dumont, M., and Ménard, C. B.: A 7-year dataset for driving and evaluating snow models at an Arctic site (Sodankylä, Finland), Geoscientific Instrumentation, Methods and Data Systems, 5, 219–227, https://doi.org/10.5194/gi-5-219-2016, 2016.

Eugster, W., Laundre, J., Eugster, J., and Kling, G. W.: Long-term reliability of the Figaro TGS 2600 solid-state methane sensor under low-Arctic conditions at Toolik Lake, Alaska, Atmospheric Measurement Techniques, 13, https://doi.org/10.5194/amt-13-2681-2020, 2020.

Euskirchen, E. S., Bruhwiler, L. M., Commane, R., Parmentier, F.-J. W., Schädel, C., Schuur, E. A. G., and Watts, J.: Current knowledge and uncertainties associated with the Arctic greenhouse gas budget, in: Balancing Greenhouse Gas Budgets, pp. 159–201, https://doi.org/10.1016/b978-0-12-814952-2.00007-1, type: Book Section, 2022.

Eyring, V., Bony, S., Meehl, G. A., Senior, C. A., Stevens, B., Stouffer, R. J., and Taylor, K. E.: Overview of the Coupled Model Intercomparison Project Phase 6 (CMIP6) experimental design and organization, Geoscientific Model Development, 9, https://doi.org/10.5194/gmd-9-1937-2016, 2016.

Fahnestock, J. T., Jones, M. H., Brooks, P. D., Walker, D. A., and Welker, J. M.: Winter and early spring CO2 efflux from tundra communities of northern Alaska, Journal of Geophysical Research: Atmospheres, 103, 29 023–29 027, https://doi.org/10.1029/98jd00805, 1998.

Fierz, C., Armstrong, R. L., Durand, Y., Etchevers, P., Greene, E., McClung, D. M., Nishimura, K., Satyawali, P. K., and Sokratov, S. A.: The International Classification for Seasonal Snow on the ground, URL https://unesdoc.unesco.org/ark:/48223/pf0000, 2009.

Finderup Nielsen, T., Ravn, N. R., and Michelsen, A.: Increased CO2 efflux due to long-term experimental summer warming and litter input in subarctic tundra – CO2 fluxes at snowmelt, in growing season, fall and winter, Plant and Soil, 444, 365–382, https://doi.org/10.1007/s11104-019-04282-9, 2019.

Fisher, J. B., Sikka, M., Oechel, W. C., Huntzinger, D. N., Melton, J. R., Koven, C. D., Ahlström, A., Arain, M. A., Baker, I., Chen, J. M., Ciais, P., Davidson, C., Dietze, M., El-Masri, B., Hayes, D., Huntingford, C., Jain, A. K., Levy, P. E., Lomas, M. R., Poulter, B., Price, D., Sahoo, A. K., Schaefer, K., Tian, H., Tomelleri, E., Verbeeck, H., Viovy, N., Wania, R., Zeng, N., and Miller, C. E.: Carbon cycle uncertainty in the Alaskan Arctic, Biogeosciences, 11, 4271–4288, https://doi.org/10.5194/bg-11-4271-2014, 2014.

Fisher, R. A. and Koven, C. D.: Perspectives on the Future of Land Surface Models and the Challenges of Representing Complex Terrestrial Systems, Journal of Advances in Modeling Earth Systems, 12, https://doi.org/10.1029/2018ms001453, 2020.

Fisher, R. A., Wieder, W. R., Sanderson, B. M., Koven, C. D., Oleson, K. W., Xu, C., Fisher, J. B., Shi, M., Walker, A. P., and Lawrence, D. M.: Parametric Controls on Vegetation Responses to Biogeochemical Forcing in the CLM5, Journal of Advances in Modeling Earth Systems, 11, 2879–2895, https://doi.org/10.1029/2019ms001609, 2019.

Foereid, B., Ward, D. S., Mahowald, N., Paterson, E., and Lehmann, J.: The sensitivity of carbon turnover in the Community Land Model to modified assumptions about soil processes, Earth System Dynamics, 5, 211–221, https://doi.org/10.5194/esd-5-211-2014, 2014.

Fourteau, K., Domine, F., and Hagenmuller, P.: Impact of water vapor diffusion and latent heat on the effective thermal conductivity of snow, The Cryosphere, 15, 2739–2755, https://doi.org/10.5194/tc-15-2739-2021, 2021a.

Fourteau, K., Domine, F., and Hagenmuller, P.: Macroscopic water vapor diffusion is not enhanced in snow, The Cryosphere, 15, 389–406, https://doi.org/10.5194/tc-15-389-2021, 2021b.

Friedlingstein, P. and Solomon, S.: Contributions of past and present human generations to committed warming caused by carbon dioxide, Proc Natl Acad Sci U S A, 102, https://doi.org/10.1073/pnas.0504755102, 2005.

Fukuzawa, T. and Akitaya, E.: Depth-hoar crystal growth in the surface layer under high temperature gradien, Annals of Glaciology, pp. 39–45, 1993.

Gallet, J. C., Domine, F., Zender, C. S., and Picard, G.: Measurement of the specific surface area of snow using infrared reflectance in an integrating sphere at 1310 and 1550 nm, 2009.

Gao, X., Avramov, A., Saikawa, E., and Schlosser, C. A.: Emulation of Community Land Model Version 5 (CLM5) to Quantify Sensitivity of Soil Moisture to Uncertain Parameters, Tech. rep., 2020.

Gil, J., Marushchak, M. E., Rütting, T., Baggs, E. M., Pérez, T., Novakovskiy, A., Trubnikova, T., Kaverin, D., Martikainen, P. J., and Biasi, C.: Sources of nitrous oxide and the fate of mineral nitrogen in subarctic permafrost peat soils, Biogeosciences, 19, https://doi.org/10.5194/bg-19-2683-2022, 2022.

Goncharova, O. Y., Matyshak, G. V., Epstein, H. E., Sefilian, A. R., and Bobrik, A. A.: Influence of snow cover on soil temperatures: Meso- and micro-scale topographic effects (a case study from the northern West Siberia discontinuous permafrost zone), Catena, 183, https://doi.org/10.1016/j.catena.2019.104224, 2019.

Gornall, J. L., Jonsdottir, I. S., Woodin, S. J., and Van der Wal, R.: Arctic mosses govern below-ground environment and ecosystem processes, Oecologia, 153, https://doi.org/10.1007/s00442-007-0785-0, 2007.

Gouttevin, I., Menegoz, M., Dominé, F., Krinner, G., Koven, C., Ciais, P., Tarnocai, C., and Boike, J.: How the insulating properties of snow affect soil carbon distribution in the continental pan-Arctic area, Journal of Geophysical Research: Biogeosciences, 117, n/a–n/a, https://doi.org/10.1029/2011jg001916, 2012.

Gouttevin, I., Langer, M., Löwe, H., Boike, J., Proksch, M., and Schneebeli, M.: Observation and modelling of snow at a polygonal tundra permafrost site: spatial variability and thermal implications, The Cryosphere, 12, 3693–3717, https://doi.org/10.5194/tc-12-3693-2018, 2018.

Graham, L. and Risk, D.: Explaining CO2 fluctuations observed in snowpacks, Biogeosciences, 15, 847–859, https://doi.org/10.5194/bg-15-847-2018, 2018.

Gray, D. M. and Male, D. H.: Handbook of Snow: Principles, Processes, Management & Use, Blackburn Press, Caldwell, New Jersey, 1981.

Grogan, P. and Jonasson, S.: Temperature and substrate controls on intra-annual variation in ecosystem respiration in two subarctic vegetation types, Global Change Biology, 11, 465–475, https://doi.org/10.1111/j.1365-2486.2005.00912.x, 2005.

Grosse, G., Goetz, S., McGuire, A. D., Romanovsky, V. E., and Schuur, E. A. G.: Changing permafrost in a warming world and feedbacks to the Earth system, Environmental Research Letters, 11, https://doi.org/10.1088/1748-9326/11/4/040201, 2016.

Grünberg, I., Wilcox, E. J., Zwieback, S., Marsh, P., and Boike, J.: Linking tundra vegetation, snow, soil temperature, and permafrost, Biogeosciences, 17, 4261–4279, https://doi.org/10.5194/bg-17-4261-2020, 2020.

Haagmans, V.: Modelling the significance of snow-vegetation interactions for active layer dynamics in an Arctic permafrost region subjected to tundra shrubification, Master's thesis, ETH Zurich, Zurich, 2021.

Haei, M., Rousk, J., Ilstedt, U., Öquist, M., Bååth, E., and Laudon, H.: Effects of soil frost on growth, composition and respiration of the soil microbial decomposer community, Soil Biology and Biochemistry, 43, 2069–2077, https://doi.org/10.1016/j.soilbio.2011.06.005, 2011.

Hall, D. K., Chang, A. T. C., and Foster, J. L.: Detection of the Depth-Hoar layer in the snow-pack of the Arctic Coastal Plain of Alaska, USA, using satellite data, 1986.

Hamdi, S., Moyano, F., Sall, S., Bernoux, M., and Chevallier, T.: Synthesis analysis of the temperature sensitivity of soil respiration from laboratory studies in relation to incubation methods and soil conditions, Soil Biology and Biochemistry, 58, 115–126, https://doi.org/10.1016/j.soilbio.2012.11.012, 2013.

Hayashi, M.: The Cold Vadose Zone: Hydrological and Ecological Significance of Frozen-Soil Processes, Vadose Zone Journal, 12, https://doi.org/10.2136/vzj2013.03.0064, 2013.

Hayes, D. J., McGuire, A. D., Kicklighter, D. W., Gurney, K. R., Burnside, T. J., and Melillo, J. M.: Is the northern high-latitude land-based CO2 sink weakening?, Global Biogeochemical Cycles, 25, https://doi.org/10.1029/2010gb003813, 2011.

Helbig, M., Chasmer, L. E., Kljun, N., Quinton, W. L., Treat, C. C., and Sonnentag, O.: The positive net radiative greenhouse gas forcing of increasing methane emissions from a thawing boreal forest-wetland landscape, Glob Chang Biol, 23, https://doi.org/10.1111/gcb.13520, 2017.

Helmig, D., Apel, E., Blake, D., Ganzeveld, L., Lefer, B. L., Meinardi, S., and Swanson, A. L.: Release and uptake of volatile inorganic and organic gases through the snowpack at Niwot Ridge, Colorado, Biogeochemistry, 95, 167–183, https://doi.org/10.1007/s10533-009-9326-8, 2009.

Henry, H. A. L.: Soil freeze–thaw cycle experiments: Trends, methodological weaknesses and suggested improvements, Soil Biology and Biochemistry, 39, 977–986, https://doi.org/10.1016/j.soilbio.2006.11.017, 2007.

Hersbach, H., Bell, B., Berrisford, P., Hirahara, S., Horányi, A., Muñoz-Sabater, J., Nicolas, J., Peubey, C., Radu, R., Schepers, D., Simmons, A., Soci, C., Abdalla, S., Abellan, X., Balsamo, G., Bechtold, P., Biavati, G., Bidlot, J., Bonavita, M., Chiara, G., Dahlgren, P., Dee, D., Diamantakis, M., Dragani, R., Flemming, J., Forbes, R., Fuentes, M., Geer, A., Haimberger, L., Healy, S., Hogan, R. J., Hólm, E., Janisková, M., Keeley, S., Laloyaux, P., Lopez, P., Lupu, C., Radnoti, G., Rosnay, P., Rozum, I., Vamborg, F., Villaume, S., and Thépaut, J.-N.: The ERA5 global reanalysis, Quarterly Journal of the Royal Meteorological Society, 146, 1999–2049, https://doi.org/10.1002/qj.3803, 2020.

Hicks Pries, C. E., Schuur, E. A. G., Natali, S. M., and Crummer, K. G.: Old soil carbon losses increase with ecosystem respiration in experimentally thawed tundra, Nature Climate Change, 6, https://doi.org/10.1038/nclimate2830, 2015.

Hinzman, L. D., Bettez, N. D., Bolton, W. R., Chapin, F. S., Dyurgerov, M. B., Fastie, C. L., Griffith, B., Hollister, R. D., Hope, A., Huntington, H. P., Jensen, A. M., Jia, G. J., Jorgenson, T., Kane, D. L., Klein, D. R., Kofinas, G., Lynch, A. H., Lloyd, A. H., McGuire, A. D., Nelson, F. E., Oechel, W. C., Osterkamp, T. E., Racine, C. H., Romanovsky, V. E., Stone, R. S., Stow, D. A., Sturm, M., Tweedie, C. E., Vourlitis, G. L., Walker, M. D., Walker, D. A., Webber,

P. J., Welker, J. M., Winker, K. S., and Yoshikawa, K.: Evidence and Implications of Recent Climate Change in Northern Alaska and Other Arctic Regions, Climatic Change, 72, 251–298, https://doi.org/10.1007/s10584-005-5352-2, 2005.

Hobbie, J., Shaver, G., Høye, T. T., and Bowden, J.: Arctic Tundra, in: Arctic Ecology, pp. 103–132, https://doi.org/10.1002/9781118846582.ch5, type: Book Section, 2021.

Howard, D., Agnan, Y., Helmig, D., Yang, Y., and Obrist, D.: Environmental controls on ecosystem-scale cold-season methane and carbon dioxide fluxes in an Arctic tundra ecosystem, Biogeosciences, 17, 4025–4042, https://doi.org/10.5194/bg-17-4025-2020, 2020.

Hugelius, G., Tarnocai, C., Broll, G., Canadell, J. G., Kuhry, P., and Swanson, D. K.: The Northern Circumpolar Soil Carbon Database: spatially distributed datasets of soil coverage and soil carbon storage in the northern permafrost regions, Earth System Science Data, 5, 3–13, https://doi.org/10.5194/essd-5-3-2013, 2013.

Hugelius, G., Strauss, J., Zubrzycki, S., Harden, J. W., Schuur, E. A. G., Ping, C. L., Schirrmeister, L., Grosse, G., Michaelson, G. J., Koven, C. D., O'Donnell, J. A., Elberling, B., Mishra, U., Camill, P., Yu, Z., Palmtag, J., and Kuhry, P.: Estimated stocks of circumpolar permafrost carbon with quantified uncertainty ranges and identified data gaps, Biogeosciences, 11, https://doi.org/10.5194/bg-11-6573-2014, 2014.

Huntzinger, D. N., Schaefer, K., Schwalm, C., Fisher, J. B., Hayes, D., Stofferahn, E., Carey, J., Michalak, A. M., Wei, Y., Jain, A. K., Kolus, H., Mao, J., Poulter, B., Shi, X., Tang, J., and Tian, H.: Evaluation of simulated soil carbon dynamics in Arctic-Boreal ecosystems, Environmental Research Letters, 15, https://doi.org/10.1088/1748-9326/ab6784, 2020.

IPCC: Climate Change 2013: The Physical Science Basis WORKING GROUP I CONTRIBUTION TO THE FIFTH ASSESSMENT REPORT OF THE INTERGOVERNMENTAL PANEL ON CLIMATE CHANGE, Report, 2013.

IPCC: AR6 Climate Change 2021: The Physical Science Basis, Tech. rep., 2021.

IPCC: Summary for Policymakers, in: Special Report on the Ocean and Cryosphere in a Changing Climate, pp. 3–35, Cambridge University Press, Cambridge, UK, https://doi.org/https://doi.org/10.1017/9781009157964.001, section: Spm Type: Book Section, 2021.

IPCC: Polar Regions, in: The Ocean and Cryosphere in a Changing Climate, edited by Meredith, M. and Sommerkorn, M., pp. 203–320, https://doi.org/10.1017/9781009157964.005, section: Chapter 3 Type: Book Section, 2022.

Jafari, M., Gouttevin, I., Couttet, M., Wever, N., Michel, A., Sharma, V., Rossmann, L., Maass, N., Nicolaus, M., and Lehning, M.: The Impact of Diffusive Water Vapor Transport on Snow Profiles in Deep and Shallow Snow Covers and on Sea Ice, Frontiers in Earth Science, 8, https://doi.org/10.3389/feart.2020.00249, 2020.

Jafarov, E. E., Nicolsky, D. J., Romanovsky, V. E., Walsh, J. E., Panda, S. K., and Serreze, M. C.: The effect of snow: How to better model ground surface temperatures, Cold Regions Science and Technology, 102, https://doi.org/10.1016/j.coldregions.2014.02.007, 2014.

Jenkinson, D. S.: The turnover of organic carbon and nitrogen in soil, Philos Trans R Soc Lond B Biol Sci, 329, 1990.

Jentzsch, K., Boike, J., and Foken, T.: Importance of the WPL correction for the measurement of small CO2 fluxes, Atmospheric Measurement Techniques Discussions, https://doi.org/10.5194/amt-2021-249, 2021a.

Jentzsch, K., Schulz, A., Pirk, N., Foken, T., Crewell, S., and Boike, J.: High Levels of CO2 Exchange During Synoptic-Scale Events Introduce Large Uncertainty Into the Arctic Carbon Budget, Geophysical Research Letters, 48, https://doi.org/10.1029/2020gl092256, 2021b.

Jeong, S.-J., Bloom, A. A., Schimel, D., Sweeney, C., Parazoo, N. C., Medvigy, D., Schaepman-Strub, G., Zheng, C., Schwalm, C. R., Huntzinger, D. N., Michalak, A. M., and Miller, C. E.: Accelerating rates of Arctic carbon cycling revealed by long-term atmospheric CO2 measurements, Science Advances, 4, 2018.

Jones, H. G.: The ecology of snow-covered systems: a brief overview of nutrient cycling and life in the cold, Hydrological Processes, 13, 2135–2147, 1999.

Jones, H. G., Pomeroy, J., Davies, T. D., Tranter, M., and Marsh, P.: CO2 in Arctic snow cover: landscape form, in-pack gas concentration gradients, and the implications for the estimation of gaseous fluxes, Hydrological Processes, 13, 2977–2989, 1999.

Jordan, R.: A One-Dimensional Temperature Model for a Snow Cover - Technical Documentation for SNTHERM.89, URL https://hdl.handle.net/11681/11677, 1991.

Jorgenson, M. T., Romanovsky, V., Harden, J., Shur, Y., O'Donnell, J., Schuur, E. A. G., Kanevskiy, M., and Marchenko, S.: Resilience and vulnerability of permafrost to climate change, Canadian Journal of Forest Research, 40, https://doi.org/10.1139/x10-060, 2010.

Jungkunst, H. F.: Arctic thaw, Nature Geoscience, 3, https://doi.org/10.1038/ngeo851, 2010.

Kaplan, J. O. and New, M.: Arctic climate change with a 2 C global warming: Timing, climate patterns and vegetation change, Climatic Change, 79, https://doi.org/10.1007/s10584-006-9113-7, 2006.

Kelley, J. J., Weaver, D. F., and Smith, B. P.: The Variation of Carbon Dioxide Under the Snow in the Arctic, Ecology, 49, 358–361, 1968.

Kielland, K., Olson, K., Ruess, R. W., and Boone, R. D.: Contribution of winter processes to soil nitrogen flux in taiga forest ecosystems, Biogeochemistry, 81, 349–360, https://doi.org/10.1007/s10533-006-9045-3, 2006.

Kim, D., Lee, M.-I., and Seo, E.: Improvement of Soil Respiration Parameterization in a Dynamic Global Vegetation Model and Its Impact on the Simulation of Terrestrial Carbon Fluxes, Journal of Climate, 32, 127–143, https://doi.org/10.1175/JCLI-D-18-0018.1, 2019.

Kim, R. S., Kumar, S., Vuyovich, C., Houser, P., Lundquist, J., Mudryk, L., Durand, M., Barros, A., Kim, E., Forman, B. A., Gutmann, E., Wrzesien, M., Garnuad, C., Sandells, M., Marshall, H.-P., Cristea, N., Pflug, J. M., Johnston, J., Cao, Y., Mocko, D., and Wang, S.: Snow Ensemble Uncertainty Project (SEUP): quantification of snow water equivalent uncertainty across North America via ensemble land surface modeling, The Cryosphere, 15, 771–791, https://doi.org/10.5194/tc-15-771-2021, 2021.

Kim, S.-T., Coplen, T. B., and Horita, J.: Normalization of stable isotope data for carbonate minerals: Implementation of IUPAC guidelines, Geochimica et Cosmochimica Acta, 158, https://doi.org/10.1016/j.gca.2015.02.011, 2015.

King, J., Derksen, C., Toose, P., Langlois, A., Larsen, C., Lemmetyinen, J., Marsh, P., Montpetit, B., Roy, A., Rutter, N., and Sturm, M.: The influence of snow microstructure on dual-frequency

radar measurements in a tundra environment, Remote Sensing of Environment, 215, 242–254, https://doi.org/10.1016/j.rse.2018.05.028, 2018.

King, J., Howell, S., Brady, M., Toose, P., Derksen, C., Haas, C., and Beckers, J.: Local-scale variability of snow density on Arctic sea ice, The Cryosphere Discussions, https://doi.org/10.5194/tc-2019-305, 2020a.

King, J., Toose, P., Silis, A., and Derksen, C.: TVC Snow 2018-2019 tundra snow depth probe measurements (Version 1), Tech. rep., 2020b.

Kirschbaum, M. U. F.: The Temperature Dependance of Soil Organic Matter Decomposition, and the Effect of Global Warming on Soil Organic C Storage, Soil Biology and Biochemistry, 27, 753–760, 1995.

Kluzek, E.: CESM research tools: CLM4.5 in CESM1.2.0 user's guide documentation, URL https://www.cesm.ucar.edu/models/cesm1.2/clm/models/lnd/clm/doc/UsersGuide/x13167.html, 2013.

Knowles, J. F., Blanken, P. D., and Williams, M. W.: Wet meadow ecosystems contribute the majority of overwinter soil respiration from snow-scoured alpine tundra, Journal of Geophysical Research: Biogeosciences, 121, 1118–1130, https://doi.org/10.1002/2015jg003081, 2016.

Koven, C., Riley, W. J., and Stern, A.: Analysis of Permafrost Thermal Dynamics and Response to Climate Change in the CMIP5 Earth System Models, Journal of Climate, 26, 1877–1900, https://doi.org/10.1175/JCLI-D-12-00228.1, 2012.

Koven, C. D., Riley, W. J., Subin, Z. M., Tang, J. Y., Torn, M. S., Collins, W. D., Bonan, G. B., Lawrence, D. M., and Swenson, S. C.: The effect of vertically resolved soil biogeochemistry and alternate soil C and N models on C dynamics of CLM4, Biogeosciences, 10, 7109–7131, https://doi.org/10.5194/bg-10-7109-2013, 2013.

Lafleur, P. M. and Humphreys, E. R.: Spring warming and carbon dioxide exchange over low Arctic tundra in central Canada, Global Change Biology, 14, 740–756, https://doi.org/10.1111/j.1365-2486.2007.01529.x, 2008.

Lafrenière, M. J., Laurin, E., and Lamoureux, S. F.: The Impact of Snow Accumulation on the

Active Layer Thermal Regime in High Arctic Soils, Vadose Zone Journal, 12, https://doi.org/10.2136/vzj2012.0058, 2013.

Larsen, K. S., Ibrom, A., Jonasson, S., Michelsen, A., and Beier, C.: Significance of cold-season respiration and photosynthesis in a subarctic heath ecosystem in Northern Sweden, Global Change Biology, 13, 1498–1508, https://doi.org/10.1111/j.1365-2486.2007.01370.x, 2007.

Larson, E. J. L., Schiferl, L. D., Commane, R., Munger, J. W., Trugman, A. T., Ise, T., Euskirchen, E. S., Wofsy, S., and Moorcroft, P. M.: The changing carbon balance of tundra ecosystems: results from a vertically-resolved peatland biosphere model, Environmental Research Letters, 17, https://doi.org/10.1088/1748-9326/ac4070, 2021.

Lasslop, G., Reichstein, M., Kattge, J., and Papale, D.: Influences of observation errors in eddy flux data on inverse model parameter estimation, 2008.

Lawrence, D. M. and Slater, A. G.: The contribution of snow condition trends to future ground climate, Climate Dynamics, 34, 969–981, https://doi.org/10.1007/s00382-009-0537-4, 2009.

Lawrence, D. M., Koven, C. D., Swenson, S. C., Riley, W. J., and Slater, A. G.: Permafrost thaw and resulting soil moisture changes regulate projected high-latitude CO2 and CH4 emissions, Environmental Research Letters, 10, https://doi.org/10.1088/1748-9326/10/9/094011, 2015.

Lawrence, D. M., Fisher, R. A., Koven, C., Oleson, K., Swenson, S., Vertenstein, M., Andre, B., Bonan, G., Ghimire, B., van Kampenhout, L., Kennedy, D., Kluzek, E., Knox, R., Lawrence, P., Li, F., Li, H., Lombardozzi, D., Lu, Y., Perket, J., Riley, W. J., Sacks, W. J., Shi, M., Wieder, W. R., Xu, C., Ali, A. A., Badger, A. M., Bisht, G., Broxton, P. D., Brunke, M. A., Buzan, J., Clark, M., Craig, T., Dahlin, K., Drewniak, B., Emmons, L., Fisher, J. B., Flanner, M., Gentine, P., Lenaerts, J., Levis, S., Leung, L. R., Lipscomb, W. H., Pelletier, J. D., Ricciuto, D. M., Sanderson, B. M., Shuman, J., Slater, A., Subin, Z. M., Tang, J., Tawfik, A., Thomas, Q., Tilmes, S., Vitt, F., and Zeng, X.: Technical Description of version 5.0 of the Community Land Model (CLM), Report, National Centre for Atmospheric Research, URL https://www.cesm.ucar.edu/models/cesm2/land/CLM50_Tech_Note.pdf, 2018.

Lawrence, D. M., Fisher, R. A., Koven, C. D., Oleson, K. W., Swenson, S. C., Bonan, G., Collier, N., Ghimire, B., Kampenhout, L., Kennedy, D., Kluzek, E., Lawrence, P. J., Li, F., Li, H.,

Lombardozzi, D., Riley, W. J., Sacks, W. J., Shi, M., Vertenstein, M., Wieder, W. R., Xu, C., Ali, A. A., Badger, A. M., Bisht, G., Broeke, M., Brunke, M. A., Burns, S. P., Buzan, J., Clark, M., Craig, A., Dahlin, K., Drewniak, B., Fisher, J. B., Flanner, M., Fox, A. M., Gentine, P., Hoffman, F., Keppel-Aleks, G., Knox, R., Kumar, S., Lenaerts, J., Leung, L. R., Lipscomb, W. H., Lu, Y., Pandey, A., Pelletier, J. D., Perket, J., Randerson, J. T., Ricciuto, D. M., Sanderson, B. M., Slater, A., Subin, Z. M., Tang, J., Thomas, R. Q., Val Martin, M., and Zeng, X.: The Community Land Model Version 5: Description of New Features, Benchmarking, and Impact of Forcing Uncertainty, Journal of Advances in Modeling Earth Systems, 11, 4245–4287, https://doi.org/10.1029/2018ms001583, 2019.

Leppänen, L., Kontu, A., Vehviläinen, J., Lemmetyinen, J., and Pulliainen, J.: Comparison of traditional and optical grain-size field measurements with SNOWPACK simulations in a taiga snowpack, Journal of Glaciology, 61, 151–162, https://doi.org/10.3189/2015JoG14J026, 2017.

Levitt, N. P.: Sample matrix effects on measured carbon and oxygen isotope ratios during continuous-flow isotope-ratio mass spectrometry, Rapid Commun Mass Spectrom, 28, https://doi.org/10.1002/rcm.7019, 2014.

Li-COR Biosciences, .: Support: LI-830 and LI-850 Gas Analysers, URL https://www.licor.com/env/support/LI-850/topics/specifications.html, issue: 06.03.2023 Pages: Specs for LiCOR sensors Type: Web Page Volume: 2023.

Liang, J., Chen, K., Siqintana, Huo, T., Zhang, Y., Jing, J., and Feng, W.: Towards improved modeling of SOC decomposition: soil water potential beyond the wilting point, Glob Chang Biol, 28, https://doi.org/10.1111/gcb.16127, 2022.

Liu, Z., Kimball, J. S., Parazoo, N. C., Ballantyne, A. P., Wang, W. J., Madani, N., Pan, C. G., Watts, J. D., Reichle, R. H., Sonnentag, O., Marsh, P., Hurkuck, M., Helbig, M., Quinton, W. L., Zona, D., Ueyama, M., Kobayashi, H., and Euskirchen, E. S.: Increased high-latitude photosynthetic carbon gain offset by respiration carbon loss during an anomalous warm winter to spring transition, Glob Chang Biol, 26, 682–696, https://doi.org/10.1111/gcb.14863, 2020.

Liu, Z., Kimball, J. S., Ballantyne, A. P., Parazoo, N. C., Wang, W. J., Bastos, A., Madani, N., Natali, S. M., Watts, J. D., Rogers, B. M., Ciais, P., Yu, K., Virkkala, A.-M., Chevallier, F.,

Peters, W., Patra, P. K., and Chandra, N.: Respiratory loss during late-growing season determines the net carbon dioxide sink in northern permafrost regions, Nature Communications, 13, https://doi.org/10.1038/s41467-022-33293-x, 2022.

Lloyd, J. and Taylor, J. A.: On the temperature dependence of soil respiration, Functional Ecology, 8, 315–323, 1994.

Lundberg, A., Gustafsson, D., Stumpp, C., Kløve, B., and Feiccabrino, J.: Spatiotemporal Variations in Snow and Soil Frost—A Review of Measurement Techniques, Hydrology, 3, https://doi.org/10.3390/hydrology3030028, 2016.

Luo, Y., Weng, E., Wu, X., Gao, C., Zhou, X., and Zhang, L.: Parameter Identifiability, Constraint, and Equifinality in Data Assimilation with Ecosystem Models, Ecological Applications, 19, 571–574, 2009.

Lupascu, M., Welker, J. M., Xu, X., and Czimczik, C. I.: Rates and radiocarbon content of summer ecosystem respiration in response to long-term deeper snow in the High Arctic of NW Greenland, Journal of Geophysical Research: Biogeosciences, 119, 1180–1194, https://doi.org/10.1002/2013jg002494, 2014.

Lupascu, M., Czimczik, C. I., Welker, M. C., Ziolkowski, L. A., Cooper, E. J., and Welker, J. M.: Winter Ecosystem Respiration and Sources of CO2 From the High Arctic Tundra of Svalbard: Response to a Deeper Snow Experiment, Journal of Geophysical Research: Biogeosciences, 123, https://doi.org/10.1029/2018jg004396, 2018.

Lutz, E. R.: Spatial and Temporal Analysis of Snowpack Strength and Stablity and Environmental Determinants on an Inclined, Forest Opening, Thesis, URL https://scholarworks.montana.edu/xmlui/handle/1/1765, 2009.

Löwe, H. and van Herwijnen, A.: A Poisson shot noise model for micro-penetration of snow, Cold Regions Science and Technology, 70, 62–70, https://doi.org/10.1016/j.coldregions.2011.09.001, 2012.

Lüers, J., Westermann, S., Piel, K., and Boike, J.: Annual CO2 budget and seasonal CO2 exchange signals at a high Arctic permafrost site on Spitsbergen, Svalbard archipelago, Biogeosciences, 11, 6307–6322, https://doi.org/10.5194/bg-11-6307-2014, 2014.

Magnusson, R. I., Hamm, A., Karsanaev, S. V., Limpens, J., Kleijn, D., Frampton, A., Maximov, T. C., and Heijmans, M.: Extremely wet summer events enhance permafrost thaw for multiple years in Siberian tundra, Nat Commun, 13, https://doi.org/10.1038/s41467-022-29248-x, 2022.

Malle, J., Rutter, N., Webster, C., Mazzotti, G., Wake, L., and Jonas, T.: Effect of Forest Canopy Structure on Wintertime Land Surface Albedo: Evaluating CLM5 Simulations With InSitu Measurements, Journal of Geophysical Research: Atmospheres, https://doi.org/10.1029/2020JD034118, 2021.

Marchand, N., Royer, A., Krinner, G., Roy, A., Langlois, A., and Vargel, C.: Snow-Covered Soil Temperature Retrieval in Canadian Arctic Permafrost Areas, Using a Land Surface Scheme Informed with Satellite Remote Sensing Data, Remote Sensing, 10, https://doi.org/10.3390/rs10111703, 2018.

Marschmann, G. L., Pagel, H., Kügler, P., and Streck, T.: Equifinality, sloppiness, and emergent structures of mechanistic soil biogeochemical models, Environmental Modelling & Software, 122, https://doi.org/10.1016/j.envsoft.2019.104518, 2019.

Marsh, P. and Pomeroy, J. W.: Spatial and temporal variations in snowmelt runoff chemistry, Northwest Territories, Canada, Water Resources Research, 35, 1559–1567, https://doi.org/10.1029/1998wr900109, 1999.

Marsh, P., Pomeroy, J., Pohl, S., Quinton, W., Onclin, C., Russell, M., Neumann, N., Pietroniro, A., Davison, B., and McCartney, S.: Snowmelt Processes and Runoff at the Arctic Treeline: Ten Years of MAGS Research, in: Cold Region Atmospheric and Hydrologic Studies. The Mackenzie GEWEX Experience, edited by Woo, M.-k., vol. 2, pp. 97–123, Springer Berlin, Heidelberg, https://doi.org/10.1007/978-3-540-75136-6_6, section: Chapter 6 Type: Book Section, 2008.

Marushchak, M. E., Pitkämäki, A., Koponen, H., Biasi, C., Seppälä, M., and Martikainen, P. J.: Hot spots for nitrous oxide emissions found in different types of permafrost peatlands, Global Change Biology, 17, https://doi.org/10.1111/j.1365-2486.2011.02442.x, 2011.

McGuire, A. D., Lawrence, D. M., Koven, C., Clein, J. S., Burke, E., Chen, G., Jafarov, E., MacDougall, A. H., Marchenko, S., Nicolsky, D., Peng, S., Rinke, A., Ciais, P., Gouttevin, I., Hayes, D. J., Ji, D., Krinner, G., Moore, J. C., Romanovsky, V., Schadel, C., Schaefer, K.,

Schuur, E. A. G., and Zhuang, Q.: Dependence of the evolution of carbon dynamics in the northern permafrost region on the trajectory of climate change, Proc Natl Acad Sci U S A, 115, 3882–3887, https://doi.org/10.1073/pnas.1719903115, 2018.

McMahon, S. K., Wallenstein, M. D., and Schimel, J. P.: Microbial growth in Arctic tundra soil at -2 degrees C, Environ Microbiol Rep, 1, 162–6, https://doi.org/10.1111/j.1758-2229.2009.00025.x, 2009.

Mekonnen, Z. A., Riley, W. J., Berner, L. T., Bouskill, N. J., Torn, M. S., Iwahana, G., Breen, A. L., Myers-Smith, I. H., García Criado, M., Liu, Y., Euskirchen, E. S., Goetz, S. J., Mack, M. C., and Grant, R. F.: Arctic tundra shrubification: a review of mechanisms and impacts on ecosystem carbon balance, Environmental Research Letters, 16, https://doi.org/10.1088/1748-9326/abf28b, 2021.

Meltofte, H., Barry, T., Berteaux, D., Bültmann, H., Christiansen, J. S., Cook, J. A., Dahlberg, A., Daniëls, F. J. A., Ehrich, D., Fjeldså, J., Fririksson, F., Ganter, B., Gaston, A. J., Gillespie, L. J., Grenoble, L., Hoberg, E. P., Hodkinson, I. D., Huntington, H. P., Ims, R. A., Josefson, A. B., Kutz, S. J., Kuzmin, S. L., Laidre, K. L., Lassuy, D. R., Lewis, P. N., Lovejoy, C., Michel, C., Mokievsky, V., Mustonen, T., Payer, D. C., Poulin, M., Reid, D. G., Reist, J. D., Tessler, D. F., and Wrona, F. J.: Arctic Biodiveristy Assessment, Report, Conservation of Arctic Flora and Fauna (CAFF), Arctic Council, 2013.

Melton, J. R. and Arora, V.: Competition between plant functional types in the Canadian Terrestrial Ecosystem Model (CTEM) v. 2.0, Geoscientific Model Development, 9, 323–361, https://doi.org/10.5194/gmd-9-323-2016, 2016.

Metcalfe, D. B., Hermans, T. D. G., Ahlstrand, J., Becker, M., Berggren, M., Bjork, R. G., Bjorkman, M. P., Blok, D., Chaudhary, N., Chisholm, C., Classen, A. T., Hasselquist, N. J., Jonsson, M., Kristensen, J. A., Kumordzi, B. B., Lee, H., Mayor, J. R., Prevey, J., Pantazatou, K., Rousk, J., Sponseller, R. A., Sundqvist, M. K., Tang, J., Uddling, J., Wallin, G., Zhang, W., Ahlstrom, A., Tenenbaum, D. E., and Abdi, A. M.: Patchy field sampling biases understanding of climate change impacts across the Arctic, Nat Ecol Evol, 2, https://doi.org/10.1038/s41559-018-0612-5, 2018.

Meyer, N., Welp, G., and Amelung, W.: The Temperature Sensitivity (Q10) of Soil Respiration: Controlling Factors and Spatial Prediction at Regional Scale Based on Environmental Soil Classes, Global Biogeochemical Cycles, 32, 306–323, https://doi.org/10.1002/2017gb005644, 2018.

Mikan, C., Schimel, J. P., and Doyle, A. P.: Temperature controls of microbial respiration in arctic tundra soils above and below freezing, Soil Biology and Biochemistry, 34, 1785–1795, 2002.

Miner, K. R., Turetsky, M. R., Malina, E., Bartsch, A., Tamminen, J., McGuire, A. D., Fix, A., Sweeney, C., Elder, C. D., and Miller, C. E.: Permafrost carbon emissions in a changing Arctic, Nature Reviews Earth & Environment, 3, 55–67, https://doi.org/10.1038/s43017-021-00230-3, 2022.

Moncrieff, J., Massheder, J., de Bruin, H., Elbers, J., Friborg, T., Heusinkveld, B., Kabat, P., Scott, S., Soegaard, H., and Verhoef, A.: A system to measure surface fluxes of momentum, sensible heat, water vapour and carbon dioxide, Journal of Hydrology, 188-189, 1997.

Moncrieff, J., Clement, R., Finnigan, J., and Meyers, T.: Averaging, detrending, and filtering of eddy covariance time series, in: Handbook of Micrometerology, edited by Lee, X., Massman, W., and B, L., vol. 29, pp. 7–31, section: 1 Type: Book Section, 2004.

Morgner, E., Elberling, B., Strebel, D., and Cooper, E. J.: The importance of winter in annual ecosystem respiration in the High Arctic: effects of snow depth in two vegetation types, Polar Research, 29, 58–74, https://doi.org/10.1111/j.1751-8369.2010.00151.x, 2016.

Morin, S., Domine, F., Arnaud, L., and Picard, G.: In-situ monitoring of the time evolution of the effective thermal conductivity of snow, Cold Regions Science and Technology, 64, 73–80, https://doi.org/10.1016/j.coldregions.2010.02.008, 2010.

Moyano, F. E., Vasilyeva, N., Bouckaert, L., Cook, F., Craine, J., Curiel Yuste, J., Don, A., Epron, D., Formanek, P., Franzluebbers, A., Ilstedt, U., Kätterer, T., Orchard, V., Reichstein, M., Rey, A., Ruamps, L., Subke, J. A., Thomsen, I. K., and Chenu, C.: The moisture response of soil heterotrophic respiration: interaction with soil properties, Biogeosciences, 9, 1173–1182, https://doi.org/10.5194/bg-9-1173-2012, 2012.

Mudryk, L., Santolaria-Otín, M., Krinner, G., Ménégoz, M., Derksen, C., Brutel-Vuilmet, C., Brady, M., and Essery, R.: Historical Northern Hemisphere snow cover trends and projected changes in the CMIP-6 multi-model ensemble, The Cryosphere Discussions, https://doi.org/10.5194/tc-2019-320, 2020.

Mudryk, L. R., Derksen, C., Howell, S., Laliberté, F., Thackeray, C., Sospedra-Alfonso, R., Vionnet, V., Kushner, P. J., and Brown, R.: Canadian snow and sea ice: historical trends and projections, The Cryosphere, 12, 1157–1176, https://doi.org/10.5194/tc-12-1157-2018, 2018.

Musselman, R. C., Massman, W. J., Frank, J. M., and Korfmacher, J. L.: The Temporal Dynamics of Carbon Dioxide under Snow in a High Elevation Rocky Mountain Subalpine Forest and Meadow, Arctic, Antarctic, and Alpine Research, 37, 527–538, https://doi.org/10.1657/1523-0430(2005)037[0527:Ttdocd]2.0.Co;2, 2005.

Myers-Smith, I. H., Kerby, J. T., Phoenix, G. K., Bjerke, J. W., Epstein, H. E., Assmann, J. J., John, C., Andreu-Hayles, L., Angers-Blondin, S., Beck, P. S. A., Berner, L. T., Bhatt, U. S., Bjorkman, A. D., Blok, D., Bryn, A., Christiansen, C. T., Cornelissen, J. H. C., Cunliffe, A. M., Elmendorf, S. C., Forbes, B. C., Goetz, S. J., Hollister, R. D., de Jong, R., Loranty, M. M., Macias-Fauria, M., Maseyk, K., Normand, S., Olofsson, J., Parker, T. C., Parmentier, F.-J. W., Post, E., Schaepman-Strub, G., Stordal, F., Sullivan, P. F., Thomas, H. J. D., Tømmervik, H., Treharne, R., Tweedie, C. E., Walker, D. A., Wilmking, M., and Wipf, S.: Complexity revealed in the greening of the Arctic, Nature Climate Change, 10, 106–117, https://doi.org/10.1038/s41558-019-0688-1, 2020.

Nadelhoffer, K. and Geiser, L. H.: Tundra, Chapter 5, in: Assessment of Nitrogen deposition effects and empirical critical loads of Nitrogen for ecoregions of the United States, edited by Pardo, L. H., Robin-Abbott, M. J., and Driscoll, C. T., pp. 37–47, Department of Agriculture, Forest Service, Newtown Square, Pennsylvania, section: 5 Type: Book Section, 2011.

Natali, S. M., Watts, J. D., Rogers, B. M., Potter, S., Ludwig, S. M., Selbmann, A.-K., Sullivan, P. F., Abbott, B. W., Arndt, K. A., Birch, L., Björkman, M. P., Bloom, A. A., Celis, G., Christensen, T. R., Christiansen, C. T., Commane, R., Cooper, E. J., Crill, P., Czimczik, C., Davydov, S., Du, J., Egan, J. E., Elberling, B., Euskirchen, E. S., Friborg, T., Genet, H., Göckede, M., Goodrich, J. P., Grogan, P., Helbig, M., Jafarov, E. E., Jastrow, J. D., Kalhori, A. A. M., Kim,

Y., Kimball, J. S., Kutzbach, L., Lara, M. J., Larsen, K. S., Lee, B.-Y., Liu, Z., Loranty, M. M., Lund, M., Lupascu, M., Madani, N., Malhotra, A., Matamala, R., McFarland, J., McGuire, A. D., Michelsen, A., Minions, C., Oechel, W. C., Olefeldt, D., Parmentier, F.-J. W., Pirk, N., Poulter, B., Quinton, W., Rezanezhad, F., Risk, D., Sachs, T., Schaefer, K., Schmidt, N. M., Schuur, E. A. G., Semenchuk, P. R., Shaver, G., Sonnentag, O., Starr, G., Treat, C. C., Waldrop, M. P., Wang, Y., Welker, J., Wille, C., Xu, X., Zhang, Z., Zhuang, Q., and Zona, D.: Large loss of CO2 in winter observed across the northern permafrost region, Nature Climate Change, 9, 852–857, https://doi.org/10.1038/s41558-019-0592-8, 2019.

Niu, G.-Y. and Yang, Z.-L.: Effects of Frozen Soil on Snowmelt Runoff and Soil Water Storage at a Continental Scale, Journal of Hydrometeorology, 7, 937–952, 2006.

Nobrega, S. and Grogan, P.: Deeper Snow Enhances Winter Respiration from Both Plant-associated and Bulk Soil Carbon Pools in Birch Hummock Tundra, Ecosystems, 10, 419–431, https://doi.org/10.1007/s10021-007-9033-z, 2007.

Oelbermann, M., English, M., and Schiff, S. L.: Evaluating carbon dynamics and microbial activity in arctic soils under warmer temperatures, Canadian Journal of Soil Science, 88, 31–44, https://doi.org/10.4141/cjss07060, 2008.

Ohkubo, S., Iwata, Y., and Hirota, T.: Influence of snow-cover and soil-frost variations on continuously monitored CO 2 flux from agricultural land, Agricultural and Forest Meteorology, 165, 25–34, https://doi.org/10.1016/j.agrformet.2012.06.012, 2012.

Olsen, A., Anderson, L. G., and Heinze, C.: Arctic Carbon Cycle: Patterns, Impacts and Possible Changes, in: The New Arctic, pp. 95–115, 2015.

Olsson, P. Q., Sturm, M., Racine, C. H., Romanovsky, V., and Liston, G. E.: Five Stages of the Alaskan Arctic Cold Season with Ecosystem Implications, Arctic, Antarctic, and Alpine Research, 35, 74–81, https://doi.org/10.1657/1523-0430(2003)035[0074:Fsotaa]2.0.Co;2, 2003.

Orchard, V. A. and Cook, F. J.: Relationship Between Soil Respriation and Soil Moisture, Soil Biology and Biochemistry, 15, 447–453, 1983.

Overland, J. E., Wang, M., Walsh, J. E., and Stroeve, J. C.: Future Arctic climate changes: Adaptation and mitigation time scales, Earth's Future, 2, https://doi.org/10.1002/2013ef000162, 2014.

Pallandt, M., Kumar, J., Mauritz, M., Schuur, E., Virkkala, A.-M., Celis, G., Hoffman, F., and Göckede, M.: Representativeness assessment of the pan-Arctic eddy-covariance site network, and optimized future enhancements, Biogeosciences Discussions, https://doi.org/10.5194/bg-2021-133, 2021.

Pan, X., Yang, D., Li, Y., Barr, A., Helgason, W., Hayashi, M., Marsh, P., Pomeroy, J., and Janowicz, R. J.: Bias corrections of precipitation measurements across experimental sites in different ecoclimatic regions of western Canada, The Cryosphere, 10, 2347–2360, https://doi.org/10.5194/tc-10-2347-2016, 2016.

Panikov, N. S., Flanagan, P. W., Oechel, W. C., Mastepanov, M. A., and Christensen, T. R.: Microbial activity in soils frozen to below 39°C, Soil Biology and Biochemistry, 38, 785–794, https://doi.org/10.1016/j.soilbio.2005.07.004, 2006.

Park, H., Launiainen, S., Konstantinov, P. Y., Iijima, Y., and Fedorov, A. N.: Modeling the Effect of Moss Cover on Soil Temperature and Carbon Fluxes at a Tundra Site in Northeastern Siberia, Journal of Geophysical Research: Biogeosciences, https://doi.org/10.1029/2018JG004491, 2018.

Parton, W. J., Stewart, J. W. B., and Cole, C. V.: Dynamics of C, N, P and S in Grassland Soils: A Model, Biogeochemistry, 5, URL https://www.jstor.org/stable/1468632, 1988.

Peng, S., Ciais, P., Krinner, G., Wang, T., Gouttevin, I., McGuire, A. D., Lawrence, D., Burke, E., Chen, X., Decharme, B., Koven, C., MacDougall, A., Rinke, A., Saito, K., Zhang, W., Alkama, R., Bohn, T. J., Delire, C., Hajima, T., Ji, D., Lettenmaier, D. P., Miller, P. A., Moore, J. C., Smith, B., and Sueyoshi, T.: Simulated high-latitude soil thermal dynamics during the past 4 decades, The Cryosphere, 10, 179–192, https://doi.org/10.5194/tc-10-179-2016, 2016.

Pielmeier, C. and Schneebeli, M.: Developments in the Stratigraphy of Snow, Surveys in Geophysics, 24, 389–416, 2003.

Pirk, N., Tamstorf, M. P., Lund, M., Mastepanov, M., Pedersen, S. H., Mylius, M. R., Parmentier, F.-J. W., Christiansen, H. H., and Christensen, T. R.: Snowpack fluxes of methane and carbon dioxide from high Arctic tundra, Journal of Geophysical Research: Biogeosciences, 121, 2886–2900, https://doi.org/10.1002/2016jg003486, 2016.

Pirk, N., Sievers, J., Mertes, J., Parmentier, F.-J. W., Mastepanov, M., and Christensen, T. R.: Spatial variability of CO2 uptake in polygonal tundra: assessing low-frequency disturbances in eddy covariance flux estimates, Biogeosciences, 14, 3157–3169, https://doi.org/10.5194/bg-14-3157-2017, 2017.

Pomeroy, J., Marsh, P., and Lesack, L.: Relocation of Major Ions in Snow along the Tundra-Taiga Ecotone, Nordic Hydrology, 24, 151–168, 1993.

Pomeroy, J. W. and Brun, E.: Physical Properties of Snow, in: Snow Ecology: An Interdisciplinary Examination of Snow-Covered Ecosystems, edited by Jones, H. G., Pomeroy, J. W., Walker, D. A., and Hoham, R. W., Cambridge Univeristy Press, Cambridge, type: Book Section, 2001.

Pongracz, A., Wårlind, D., Miller, P. A., and Parmentier, F.-J. W.: Model simulations of arctic biogeochemistry and permafrost extent are highly sensitive to the implemented snow scheme in LPJ-GUESS, Biogeosciences, 18, 5767–5787, https://doi.org/10.5194/bg-18-5767-2021, 2021.

Post, E., Alley, R. B., Christensen, T. R., Macias-Fauria, M., Forbes, B. C., Gooseff, M. N., Iler, A., Kerby, J. T., Laidre, K. L., Mann, M. E., Olofsson, J., Stroeve, J. C., Ulmer, F., Virginia, R. A., and Wang, M.: The polar regions in a 2 °C warmer world, Science Advances, 5, https://doi.org/10.1126/sciadv.aaw9883, 2019.

Previdi, M., Smith, K. L., and Polvani, L. M.: Arctic amplification of climate change: a review of underlying mechanisms, Environmental Research Letters, 16, https://doi.org/10.1088/1748-9326/ac1c29, 2021.

Proksch, M., Löwe, H., and Schneebeli, M.: Density, specific surface area, and correlation length of snow measured by high-resolution penetrometry, Journal of Geophysical Research: Earth Surface, 120, 346–362, https://doi.org/10.1002/2014jf003266, 2015.

Proksch, M., Rutter, N., Fierz, C., and Schneebeli, M.: Intercomparison of snow density measurements: bias, precision, and vertical resolution, The Cryosphere, 10, 371–384, https://doi.org/10.5194/tc-10-371-2016, 2016.

Pruitt, W. O. J.: Why and How to Study a Snowcover, Canadian Field-Naturalist, 119, 118–128, 2005.

Quinton, W. L. and Marsh, P.: The Influence of Mineral Earth Hummocks on Subsurface Drainage in the Continuous Permafrost Zone, Permafrost and Periglacial Processes, 9, 213–228, 1998.

Quinton, W. L. and Marsh, P.: A Conceptual Framework for Runoff Generation in a Permafrost Environment, Hydrological Processes, 13, 2563–2581, 1999.

Rafat, A., Rezanezhad, F., Quinton, W. L., Humphreys, E. R., Webster, K., and Van Cappellen, P.: Non-growing season carbon emissions in a northern peatland are projected to increase under global warming, Communications Earth & Environment, 2, https://doi.org/10.1038/s43247-021-00184-w, 2021.

Rafat, A., Byun, E., Rezanezhad, F., Quinton, W. L., Humphreys, E. R., Webster, K., and Van Cappellen, P.: The definition of the non-growing season matters: a case study of net ecosystem carbon exchange from a Canadian peatland, Environmental Research Communications, 4, https://doi.org/10.1088/2515-7620/ac53c2, 2022.

Rains, F. A., Stoy, P. C., Welch, C. M., Montagne, C., and McGlynn, B. L.: A Comparison of Methods Reveals that Enhanced Diffusion Helps Explain Cold-Season Soil CO2 Efflux in a Lodgepole Pine Ecosystem, Cold Regions Science and Technology, 121, 16–24, https://doi.org/10.1016/j.coldregions.2015.10.003, 2016.

Rantanen, M., Karpechko, A. Y., Lipponen, A., Nordling, K., Hyvärinen, O., Ruosteenoja, K., Vihma, T., and Laaksonen, A.: The Arctic has warmed nearly four times faster than the globe since 1979, Communications Earth & Environment, 3, https://doi.org/10.1038/s43247-022-00498-3, 2022.

Raynolds, M. K., Walker, D. A., Balser, A., Bay, C., Campbell, M., Cherosov, M. M., Daniëls, F. J. A., Eidesen, P. B., Ermokhina, K. A., Frost, G. V., Jedrzejek, B., Jorgenson, M. T., Kennedy, B. E., Kholod, S. S., Lavrinenko, I. A., Lavrinenko, O. V., Magnússon, B., Matveyeva, N. V., Metúsalemsson, S., Nilsen, L., Olthof, I., Pospelov, I. N., Pospelova, E. B., Pouliot, D., Razzhivin, V., Schaepman-Strub, G., Šibík, J., Telyatnikov, M. Y., and Troeva, E.: A raster version of the Circumpolar Arctic Vegetation Map (CAVM), Remote Sensing of Environment, 232, https://doi.org/10.1016/j.rse.2019.111297, 2019.

Rees, A., English, M., Derksen, C., Toose, P., and Silis, A.: Observations of late winter Canadian

tundra snow cover properties, Hydrological Processes, 28, 3962–3977, https://doi.org/10.1002/hyp.9931, 2014.

Reichstein, M., Falge, E., Baldocchi, D., Papale, D., Aubinet, M., Berbigier, P., Bernhofer, C., Buchmann, N., Gilmanov, T., Granier, A., Grunwald, T., Havrankova, K., Ilvesniemi, H., Janous, D., Knohl, A., Laurila, T., Lohila, A., Loustau, D., Matteucci, G., Meyers, T., Miglietta, F., Ourcival, J.-M., Pumpanen, J., Rambal, S., Rotenberg, E., Sanz, M., Tenhunen, J., Seufert, G., Vaccari, F., Vesala, T., Yakir, D., and Valentini, R.: On the separation of net ecosystem exchange into assimilation and ecosystem respiration: review and improved algorithm, Global Change Biology, 11, 1424–1439, https://doi.org/10.1111/j.1365-2486.2005.001002.x, 2005.

Riche, F. and Schneebeli, M.: Thermal conductivity of snow measured by three independent methods and anisotropy considerations, The Cryosphere, 7, 217–227, https://doi.org/10.5194/tc-7-217-2013, 2013.

Rixen, C., Freppaz, M., Stoeckli, V., Huovinen, C., Huovinen, K., and Wipf, S.: Altered Snow Density and Chemistry Change Soil Nitrogen Mineralization and Plant Growth, Arctic, Antarctic, and Alpine Research, 40, 568–575, https://doi.org/10.1657/1523-0430(07-044)[rixen]2.0.Co;2, 2008.

Royer, A., Domine, F., Roy, A., Langlois, A., Marchand, N., and Davesne, G.: New northern snowpack classification linked to vegetation cover on a latitudinal mega-transect across northeastern Canada, Écoscience, pp. 1–18, https://doi.org/10.1080/11956860.2021.1898775, 2021a.

Royer, A., Picard, G., Vargel, C., Langlois, A., Gouttevin, I., and Dumont, M.: Improved Simulation of Arctic Circumpolar Land Area Snow Properties and Soil Temperatures, Frontiers in Earth Science, 9, https://doi.org/10.3389/feart.2021.685140, 2021b.

Rutter, N., Sandells, M. J., Derksen, C., King, J., Toose, P., Wake, L., Watts, T., Essery, R., Roy, A., Royer, A., Marsh, P., Larsen, C., and Sturm, M.: Effect of snow microstructure variability on Ku-band radar snow water equivalent retrievals, The Cryosphere, https://doi.org/10.5194/tc-2019-167, 2019.

Sandells, M. J., Flerchinger, G. N., Gurney, R. J., and Marks, D.: Simulation of snow and soil water

content as a basis for satellite retrievals, Hydrology Research, 43, 720–735, https://doi.org/10.2166/nh.2012.028, 2012.

Schadt, C. W., Martin, A. P., Lipson, D. A., and Schmidt, S. K.: Seasonal Dynamics of Previously Unknown Fungal Lineages in Tundra Soils, Science, 301, 1359–1361, 2003.

Schimel, J. P., Bilbrough, C., and Welker, J. M.: Increased snow depth affects microbial activity and nitrogen mineralization in two Arctic tundra communities, Soil Biology and Biochemistry, 36, 217–227, https://doi.org/10.1016/j.soilbio.2003.09.008, 2004.

Schimel, J. P., Fahnestock, J., Michaelson, G., Mikan, C., Ping, C.-L., Romanovsky, V. E., and Welker, J.: Cold-season Production of CO2 in Arctic Soils: Can Laboratory and Field Estimates Be Reconciled through a Simple Modeling Approach?, Arctic, Antarctic, and Alpine Research, 38, 249–256, https://doi.org/10.1657/1523-0430(2006)38[249:Cpocia]2.0.Co;2, 2006.

Schmidt, S. K., Wilson, K. L., Monson, R. K., and Lipson, D. A.: Exponential growth of "snow molds" at sub-zero temperatures: an explanation for high beneath-snow respiration rates and Q 10 values, Biogeochemistry, 95, 13–21, https://doi.org/10.1007/s10533-008-9247-y, 2008.

Schneebeli, M. and Johnson, J. B.: A constant-speed penetrometer for high-resolution snow stratigraphy, Annals of Glaciology, 26, 107–111, 1998.

Schuur, E. A., Vogel, J. G., Crummer, K. G., Lee, H., Sickman, J. O., and Osterkamp, T. E.: The effect of permafrost thaw on old carbon release and net carbon exchange from tundra, Nature, 459, 556–9, https://doi.org/10.1038/nature08031, 2009.

Schuur, E. A., McGuire, A. D., Schadel, C., Grosse, G., Harden, J. W., Hayes, D. J., Hugelius, G., Koven, C. D., Kuhry, P., Lawrence, D. M., Natali, S. M., Olefeldt, D., Romanovsky, V. E., Schaefer, K., Turetsky, M. R., Treat, C. C., and Vonk, J. E.: Climate change and the permafrost carbon feedback, Nature, 520, 171–9, https://doi.org/10.1038/nature14338, 2015.

Schuur, E. A. G., Bracho, R., Celis, G., Belshe, E. F., Ebert, C., Ledman, J., Mauritz, M., Pegoraro, E. F., Plaza, C., Rodenhizer, H., Romanovsky, V., Schädel, C., Schirokauer, D., Taylor, M., Vogel, J. G., and Webb, E. E.: Tundra Underlain By Thawing Permafrost Persistently Emits Carbon to the Atmosphere Over 15 Years of Measurements, Journal of Geophysical Research: Biogeosciences, 126, https://doi.org/10.1029/2020jg006044, 2021.

Schädel, C., Koven, C. D., Lawrence, D. M., Celis, G., Garnello, A. J., Hutchings, J., Mauritz, M., Natali, S. M., Pegoraro, E., Rodenhizer, H., Salmon, V. G., Taylor, M. A., Webb, E. E., Wieder, W. R., and Schuur, E. A. G.: Divergent patterns of experimental and model-derived permafrost ecosystem carbon dynamics in response to Arctic warming, Environmental Research Letters, 13, https://doi.org/10.1088/1748-9326/aae0ff, 2018.

Schürholt, K., Kowalski, J., and Löwe, H.: Elements of future snowpack modeling - part 1: A physical instability arising from the non-linear coupling of transport and phase changes, The Cryosphere Discussions, https://doi.org/10.5194/tc-2021-72, 2021.

Semenchuk, P. R., Elberling, B., Amtorp, C., Winkler, J., Rumpf, S., Michelsen, A., and Cooper, E. J.: Deeper snow alters soil nutrient availability and leaf nutrient status in high Arctic tundra, Biogeochemistry, 124, 81–94, https://doi.org/10.1007/s10533-015-0082-7, 2015.

Seok, B., Helmig, D., Williams, M. W., Liptzin, D., Chowanski, K., and Hueber, J.: An automated system for continuous measurements of trace gas fluxes through snow: an evaluation of the gas diffusion method at a subalpine forest site, Niwot Ridge, Colorado, Biogeochemistry, 95, 95–113, https://doi.org/10.1007/s10533-009-9302-3, 2009.

Serreze, M. C., Walsh, J. E., Chapin, F. S., r., Osterkamp, T. E., Dyurgerov, M., Romanovsky, V., Oechel, W. C., Morison, J., Zhang, T., and Barry, R. G.: OBSERVATIONAL EVIDENCE OF RECENT CHANGE IN THE NORTHERN HIGH-LATITUDE ENVIRONMENT, Climatic Change, 46, 2000.

Sharp, Z. D.: Principles of Stable Isotope Geochemistry, 2 edn., 2017.

Simson, A., Löwe, H., and Kowalski, J.: Elements of future snowpack modeling - part 2: A modular and extendable Eulerian–Lagrangian numerical scheme for coupled transport, phase changes and settling processes, The Cryosphere Discussions, https://doi.org/10.5194/tc-2021-73, 2021.

Skrzypek, G., Allison, C. E., Böhlke, J. K., Bontempo, L., Brewer, P., Camin, F., Carter, J. F., Chartrand, M. M. G., Coplen, T. B., Gröning, M., Hélie, J.-F., Esquivel-Hernández, G., Kraft, R. A., Magdas, D. A., Mann, J. L., Meija, J., Meijer, H. A. J., Moossen, H., Ogrinc, N., Perini, M., Possolo, A., Rogers, K. M., Schimmelmann, A., Shemesh, A., Soto, D. X., Thomas, F., Wiel-

gosz, R., Winchester, M. R., Yan, Z., and Dunn, P. J. H.: Minimum requirements for publishing hydrogen, carbon, nitrogen, oxygen and sulfur stable-isotope delta results (IUPAC Technical Report), Pure and Applied Chemistry, 0, https://doi.org/10.1515/pac-2021-1108, 2022.

Slater, A. G. and Lawrence, D. M.: Diagnosing Present and Future Permafrost from Climate Models, Journal of Climate, 26, https://doi.org/10.1175/JCLI-D-12-00341.1, 2013.

Slater, A. G., Lawrence, D. M., and Koven, C. D.: Process-level model evaluation: a snow and heat transfer metric, The Cryosphere, 11, 989–996, https://doi.org/10.5194/tc-11-989-2017, 2017.

Smith, C. D.: Correcting the Wind Bias in Snowfall Measurements Made with a Geonor T-200B Precipitation Gauge and Alter Wind Shield, Bulletin of the Canadian and Oceanographic Meteorological Society, 36, 162–167, 2008.

Sommerfeld, R. A. and Lachapelle, E.: The Classification of Snow Metamorphism, Journal of Glaciology, 9, 3–17, 1970.

Spötl, C. and Vennemann, T. W.: Continuous-flow isotope ratio mass spectrometric analysis of carbonate minerals, Rapid Commun Mass Spectrom, 17, https://doi.org/10.1002/rcm.1010, 2003.

Starr, G. and Oberbauer, S. F.: Photosynthesis of arctic evergreens under snow: implications for tundra ecosystem carbon balance, Ecology, 84, 1415–1420, 2003.

Sturm, M. and Holmgren, B.: An Automatic Snow Depth Probe for Field Validation Campaigns, Water Resources Research, 54, 9695–9701, https://doi.org/10.1029/2018WR023559, 2018.

Sturm, M. and Liston, G. E.: Revisiting the Global Seasonal Snow Classification: An Updated Dataset for Earth System Applications, Journal of Hydrometeorology, https://doi.org/10.1175/jhm-d-21-0070.1, 2021.

Sturm, M. and Massom, R. A.: Snow in the sea ice system: friend or foe?, in: Sea Ice, edited by Thomas, D. N., pp. 65–109, Wiley Blackwell, Chichester, UK, 3 edn., section: 3 Type: Book Section, 2017.

Sturm, M., Holmgren, J., and Liston, G. E.: A Seasonal Snow Cover Classification for Local to Global Applications, Journal of Climate, 8, 1261–1283, 1995.

Sturm, M., Holmgren, J., Konig, M., and Morris, K.: The thermal conductivity of seasonal snow, Journal of Glaciology, 43, 26–41, 1997.

Sturm, M., Perovich, D. K., and Holmgren, J.: Thermal conductivity and heat transfer through the snow on the ice of the Beaufort Sea, Journal of Geophysical Research, 107, https://doi.org/10.1029/2000jc000409, 2002.

Sturm, M., Derksen, C., Liston, G., Silis, A., Solie, D., Holmgren, J., and Huntington, H.: A reconnaissance snow survey across northwest territories and Nunavut, Canada, April 2007, Tech. rep., Cold Regions Research and Engineering laboratory, Hanover, New Hampshire, 2008.

Sullivan, P. F., Welker, J. M., Arens, S. J. T., and Sveinbjörnsson, B.: Continuous estimates of CO2 efflux from arctic and boreal soils during the snow-covered season in Alaska, Journal of Geophysical Research: Biogeosciences, 113, https://doi.org/10.1029/2008jg000715, 2008.

Swenson, S. C. and Lawrence, D. M.: A new fractional snow-covered area parameterization for the Community Land Model and its effect on the surface energy balance, Journal of Geophysical Research: Atmospheres, 117, n/a–n/a, https://doi.org/10.1029/2012jd018178, 2012.

SWIPA: Snow Water Ice and Permafrost in the Arctic (SWIPA), Report, Arctic Monitioring and Assessment Program, 2017.

Tang, J. and Zhuang, Q.: Equifinality in parameterization of process-based biogeochemistry models: A significant uncertainty source to the estimation of regional carbon dynamics, Journal of Geophysical Research: Biogeosciences, 113, https://doi.org/10.1029/2008jg000757, 2008.

Tao, J., Zhu, Q., Riley, W. J., and Neumann, R. B.: Improved ELMv1-ECA simulations of zero-curtain periods and cold-season CH4 and CO2 emissions at Alaskan Arctic tundra sites, The Cryosphere, 15, 5281–5307, https://doi.org/10.5194/tc-15-5281-2021, 2021.

Tape, K. E. N., Sturm, M., and Racine, C.: The evidence for shrub expansion in Northern Alaska and the Pan-Arctic, Global Change Biology, 12, https://doi.org/10.1111/j.1365-2486.2006.01128.x, 2006.

Taylor, K. E., Stouffer, R. J., and Meehl, G. A.: An Overview of CMIP5 and the Experiment Design, Bulletin of the American Meteorological Society, 93, 485–498, https://doi.org/10.1175/bams-d-11-00094.1, 2012.

Thackeray, C. W., Derksen, C., Fletcher, C. G., and Hall, A.: Snow and Climate: Feedbacks, Drivers, and Indices of Change, Current Climate Change Reports, 5, 322–333, https://doi.org/10.1007/s40641-019-00143-w, 2019.

Tieszen, L. L.: Photosynthetic Competence of the Subnivean Vegetation of an Arctic Tundra, Arctic and Alpine Research, 6, 253–256, https://doi.org/10.1080/00040851.1974.12003780, 1974.

Tong, D., Li, Z., Xiao, H., Nie, X., Liu, C., and Zhou, M.: How do soil microbes exert impact on soil respiration and its temperature sensitivity?, Environ Microbiol, 23, 3048–3058, https://doi.org/10.1111/1462-2920.15520, 2021.

Toose, P., King, J., Silis, A., and Derksen, C.: TVC Snow 2017-2018 tundra snow depth probe measurements (Version 1), Tech. rep., 2020.

Treat, C. C., Bloom, A. A., and Marushchak, M. E.: Nongrowing season methane emissions-a significant component of annual emissions across northern ecosystems, Glob Chang Biol, 24, 3331–3343, https://doi.org/10.1111/gcb.14137, 2018.

Treharne, R., Rogers, B. M., Gasser, T., MacDonald, E., and Natali, S.: Identifying Barriers to Estimating Carbon Release From Interacting Feedbacks in a Warming Arctic, Frontiers in Climate, 3, https://doi.org/10.3389/fclim.2021.716464, 2022.

Tu, K. and Dawson, T.: Partitioning Ecosystem Respriration using Stable Carbon Isotope Analysis of CO2, pp. 125–152, 2005.

University of Lapland, .: The Arctic Region, URL https://www.arcticcentre.org/EN/arcticregion, issue: 18.01.2023 Type: Web Page Volume: 2023.

van Bochove, E., Thériault, G., Rochette, P., Jones, H. G., and Pomeroy, J. W.: Thick ice layers in snow and frozen soil affecting gas emissions from agricultural soils during winter, Journal of Geophysical Research: Atmospheres, 106, 23 061–23 071, https://doi.org/10.1029/2000jd000044, 2001.

van Dijk, A., Moene, A., and de Bruin, H.: The principles of surface flux physics: Theory, practice and description of the ECPACK library, Report, Wageningen University, 2004.

van Kampenhout, L., Lenaerts, J. T. M., Lipscomb, W. H., Sacks, W. J., Lawrence, D. M., Slater, A. G., and van den Broeke, M. R.: Improving the Representation of Polar Snow and Firn in the Community Earth System Model, Journal of Advances in Modeling Earth Systems, 9, 2583–2600, https://doi.org/10.1002/2017ms000988, 2017.

Vickers, D. and Mahrt, L.: Quality Control and Flux Sampling Problems for Tower and Aircraft Data, Journal of Atmospheric and Oceanic Technology, 14, 1997.

Vionnet, V., Brun, E., Morin, S., Boone, A., Faroux, S., Le Moigne, P., Martin, E., and Willemet, J. M.: The detailed snowpack scheme Crocus and its implementation in SURFEX v7.2, Geoscientific Model Development, 5, 773–791, https://doi.org/10.5194/gmd-5-773-2012, 2012.

Virkkala, A.-M., Virtanen, T., Lehtonen, A., Rinne, J., and Luoto, M.: The current state of CO2 flux chamber studies in the Arctic tundra, Progress in Physical Geography: Earth and Environment, 42, 162–184, https://doi.org/10.1177/0309133317745784, 2017.

Virkkala, A. M., Aalto, J., Rogers, B. M., Tagesson, T., Treat, C. C., Natali, S. M., Watts, J. D., Potter, S., Lehtonen, A., Mauritz, M., Schuur, E. A. G., Kochendorfer, J., Zona, D., Oechel, W., Kobayashi, H., Humphreys, E., Goeckede, M., Iwata, H., Lafleur, P. M., Euskirchen, E. S., Bokhorst, S., Marushchak, M., Martikainen, P. J., Elberling, B., Voigt, C., Biasi, C., Sonnentag, O., Parmentier, F. W., Ueyama, M., Celis, G., St Louis, V. L., Emmerton, C. A., Peichl, M., Chi, J., Jarveoja, J., Nilsson, M. B., Oberbauer, S. F., Torn, M. S., Park, S. J., Dolman, H., Mammarella, I., Chae, N., Poyatos, R., Lopez-Blanco, E., Christensen, T. R., Kwon, M. J., Sachs, T., Holl, D., and Luoto, M.: Statistical upscaling of ecosystem CO2 fluxes across the terrestrial tundra and boreal domain: Regional patterns and uncertainties, Glob Chang Biol, https://doi.org/10.1111/gcb.15659, 2021.

Voigt, C., Lamprecht, R. E., Marushchak, M. E., Lind, S. E., Novakovskiy, A., Aurela, M., Martikainen, P. J., and Biasi, C.: Warming of subarctic tundra increases emissions of all three important greenhouse gases - carbon dioxide, methane, and nitrous oxide, Glob Chang Biol, 23, 3121–3138, https://doi.org/10.1111/gcb.13563, 2017.

Voigt, C., Marushchak, M. E., Abbott, B. W., Biasi, C., Elberling, B., Siciliano, S. D., Sonnentag, O., Stewart, K. J., Yang, Y., and Martikainen, P. J.: Nitrous oxide emissions from permafrost-

affected soils, Nature Reviews Earth & Environment, 1, https://doi.org/10.1038/s43017-020-0063-9, 2020.

Wagner, D. N., Shupe, M. D., Persson, O. G., Uttal, T., Frey, M. M., Kirchgaessner, A., Schneebeli, M., Jaggi, M., Macfarlane, A. R., Itkin, P., Arndt, S., Hendricks, S., Krampe, D., Ricker, R., Regnery, J., Kolabutin, N., Shimanshuck, E., Oggier, M., Raphael, I., and Lehning, M.: Snowfall and snow accumulation processes during the MOSAiC winter and spring season, The Cryosphere Discussions, https://doi.org/10.5194/tc-2021-126, 2021.

Walker, D. A.: Hierarchical subdivision of Arctic tundra based on vegetation response to climate, parent material and topography, Glob Chang Biol, 6, 2002.

Walker, D. A., Gould, W. A., Maier, H. A., and Raynolds, M. K.: The Circumpolar Arctic Vegetation Map: AVHRR-derived base maps, environmental controls, and integrated mapping procedures, International Journal of Remote Sensing, 23, https://doi.org/10.1080/01431160110113854, 2002.

Walker, D. A., Raynolds, M. K., Daniëls, F. J. A., Einarsson, E., Elvebakk, A., Gould, W. A., Katenin, A. E., Kholod, S. S., Markon, C. J., Melnikov, E. S., Moskalenko, N. G., Talbot, S. S., Yurtsev, B. A., and The other members of the, C. T.: The Circumpolar Arctic vegetation map, Journal of Vegetation Science, 16, https://doi.org/10.1111/j.1654-1103.2005.tb02365.x, 2005.

Wang, T., Ottlé, C., Boone, A., Ciais, P., Brun, E., Morin, S., Krinner, G., Piao, S., and Peng, S.: Evaluation of an improved intermediate complexity snow scheme in the ORCHIDEE land surface model, Journal of Geophysical Research: Atmospheres, 118, 6064–6079, https://doi.org/10.1002/jgrd.50395, 2013.

Wang, W., Rinke, A., Moore, J. C., Ji, D., Cui, X., Peng, S., Lawrence, D. M., McGuire, A. D., Burke, E. J., Chen, X., Decharme, B., Koven, C., MacDougall, A., Saito, K., Zhang, W., Alkama, R., Bohn, T. J., Ciais, P., Delire, C., Gouttevin, I., Hajima, T., Krinner, G., Lettenmaier, D. P., Miller, P. A., Smith, B., Sueyoshi, T., and Sherstiukov, A. B.: Evaluation of air–soil temperature relationships simulated by land surface models during winter across the permafrost region, The Cryosphere, 10, 1721–1737, https://doi.org/10.5194/tc-10-1721-2016, 2016.

Watson, S., Smith, C. D., Lassi, M., and Misfeldt, J.: An Evaluation of the Effectiveness of the

Double Alter Wind Shield for Increasing the Catch Efficiency of the Geonor T-200B Precipitation Gauge, Bulletin of the Canadian and Oceanographic Meteorological Society, 36, 168–175, 2008.

Watts, J., Natali, S. M., Minions, C., Risk, D., Arndt, K. A., Zona, D., Euskirchen, E. S., Rocha, A. V., Sonnentag, O., Helbig, M., Kalhori, A., Oechel, W. C., Ikawa, H., Ueyama, M., Suzuki, R., Kobayashi, H., Celis, G., Schuur, E. A. G., Humphreys, E. R., Kim, Y., Lee, B.-Y., Goetz, S. J., Madani, N., Schiferl, L., Commane, R., Kimball, J. S., Liu, Z., Torn, M. S., Potter, S., Wang, J. A., Jorgenson, T., Xiao, J., Li, X., and Edgar, C.: Soil respiration strongly offsets carbon uptake in Alaska and Northwest Canada, Environmental Research Letters, https://doi.org/10.1088/1748-9326/ac1222, 2021.

Welker, J. M., Fahnestock, J. T., and Jones, M. H.: Annual CO2 flux in dry and moist arctic tundra: field responses to increases in summer temperatures and winter snow depth, 2000.

Wieder, W. R., Lawrence, D. M., Fisher, R. A., Bonan, G. B., Cheng, S. J., Goodale, C. L., Grandy, A. S., Koven, C. D., Lombardozzi, D. L., Oleson, K. W., and Thomas, R. Q.: Beyond Static Benchmarking: Using Experimental Manipulations to Evaluate Land Model Assumptions, Global Biogeochem Cycles, 33, https://doi.org/10.1029/2018GB006141, 2019.

Wilcox, E. J., Keim, D., de Jong, T., Walker, B., Sonnentag, O., Sniderhan, A. E., Mann, P., and Marsh, P.: Tundra shrub expansion may amplify permafrost thaw by advancing snowmelt timing, Arctic Science, 5, 202–217, https://doi.org/10.1139/as-2018-0028, 2019.

Wilkman, E., Zona, D., Arndt, K., Gioli, B., Nakamoto, K., Lipson, D. A., and Oechel, W. C.: Ecosystem scale implication of soil CO2 concentration dynamics during soil freezing in Alaskan Arctic tundra ecosystems, Journal of Geophysical Research: Biogeosciences, https://doi.org/10.1029/2020jg005724, 2021.

Williams, M. W., Helmig, D., and Blanken, P.: White on green: under-snow microbial processes and trace gas fluxes through snow, Niwot Ridge, Colorado Front Range, Biogeochemistry, 95, 1–12, https://doi.org/10.1007/s10533-009-9330-z, 2009.

Wilson, G., Green, M., Brown, J., Campbell, J., Groffman, P., Durán, J., and Morse, J.: Snowpack

affects soil microclimate throughout the year, Climatic Change, 163, 705–722, https://doi.org/10.1007/s10584-020-02943-8, 2020.

Wookey, P. A.: Experimental approaches to predicting the future of tundra plant communities, Plant Ecology & Diversity, 1, 299–307, https://doi.org/10.1080/17550870802338354, 2008.

Wu, Y., Verseghy, D. L., and Melton, J. R.: Integrating peatlands into the coupled Canadian Land Surface Scheme (CLASS) v3.6 and the Canadian Terrestrial Ecosystem Model (CTEM) v2.0, Geoscientific Model Development, 9, 2639–2663, https://doi.org/10.5194/gmd-9-2639-2016, 2016.

Yan, Z., Bond-Lamberty, B., Todd-Brown, K. E., Bailey, V. L., Li, S., Liu, C., and Liu, C.: A moisture function of soil heterotrophic respiration that incorporates microscale processes, Nat Commun, 9, 2562, https://doi.org/10.1038/s41467-018-04971-6, 2018.

Yang, K., Wang, C., and Li, S.: Improved Simulation of Frozen-Thawing Process in Land Surface Model (CLM4.5), Journal of Geophysical Research: Atmospheres, 123, https://doi.org/10.1029/2017jd028260, 2018.

Yi, Y., Kimball, J. S., Chen, R. H., Moghaddam, M., and Miller, C. E.: Sensitivity of active-layer freezing process to snow cover in Arctic Alaska, The Cryosphere, 13, 197–218, https://doi.org/10.5194/tc-13-197-2019, 2019.

Yi, Y., Kimball, J. S., Watts, J. D., Natali, S. M., Zona, D., Liu, J., Ueyama, M., Kobayashi, H., Oechel, W., and Miller, C. E.: Investigating the sensitivity of soil respiration to recent snow cover changes in Alaska using a satellite-based permafrost carbon model, Biogeosciences, 17, 5861–5882, https://doi.org/10.5194/bg-2020-182, 2020.

Yosida, Z., Oura, R., Kuroiwa, D., Ruzioka, T., Kojima, K., Aoki, S.-i., and Kinosita, S.: Physical Studies on Deposited Snow. I. ; Thermal Properties, Contributions from the Institute of Low Temperature Science, 7, 1955.

Yu, E.-J. and Lee, K.-S.: Improved method for simultaneous determination of the carbon isotopic composition and concentration of atmospheric CO2 using CF-IRMS, International Journal of Mass Spectrometry, 452, https://doi.org/10.1016/j.ijms.2020.116327, 2020.

Zermatten, E., Haussener, S., Schneebeli, M., and Steinfeld, A.: Tomography-based determination of permeability and Dupuit–Forchheimer coefficient of characteristic snow samples, Journal of Glaciology, 57, https://doi.org/10.3189/002214311798043799, 2011.

Zha, J. and Zhuang, Q.: Quantifying the role of moss in terrestrial ecosystem carbon dynamics in northern high latitudes, Biogeosciences, 18, 6245–6269, https://doi.org/10.5194/bg-18-6245-2021, 2021.

Zhang, T.: Influence of the seasonal snow cover on the ground thermal regime: An overview, Reviews of Geophysics, 43, https://doi.org/10.1029/2004rg000157, 2005.

Zhang, T., Osterkamp, T. E., and Stamnes, K.: Influence of the depth hoar layer of the seasonal snow cover on the ground thermal regime, Water Resour Res, 32, 2075–2086, https://doi.org/Doi10.1029/96wr00996, 1996.

Zhang, W., Jansson, P.-E., Schurgers, G., Hollesen, J., Lund, M., Abermann, J., and Elberling, B.: Process-Oriented Modeling of a High Arctic Tundra Ecosystem: Long-Term Carbon Budget and Ecosystem Responses to Interannual Variations of Climate, Journal of Geophysical Research: Biogeosciences, 123, 1178–1196, https://doi.org/10.1002/2017jg003956, 2018a.

Zhang, W., Jansson, P.-E., Sigsgaard, C., McConnell, A., Jammet, M. M., Westergaard-Nielsen, A., Lund, M., Friborg, T., Michelsen, A., and Elberling, B.: Model-data fusion to assess year-round CO2 fluxes for an arctic heath ecosystem in West Greenland (69°N), Agricultural and Forest Meteorology, 272-273, 176–186, https://doi.org/10.1016/j.agrformet.2019.02.021, 2019.

Zhang, Y., Sherstiukov, A. B., Qian, B., Kokelj, S. V., and Lantz, T. C.: Impacts of snow on soil temperature observed across the circumpolar north, Environmental Research Letters, 13, https://doi.org/10.1088/1748-9326/aab1e7, 2018b.

Zinger, L., Shahnavaz, B., Baptist, F., Geremia, R. A., and Choler, P.: Microbial diversity in alpine tundra soils correlates with snow cover dynamics, ISME J, 3, 850–9, https://doi.org/10.1038/ismej.2009.20, 2009.

Zona, D., Gioli, B., Commane, R., Lindaas, J., Wofsy, S. C., Miller, C. E., Dinardo, S. J., Dengel, S., Sweeney, C., Karion, A., Chang, R. Y., Henderson, J. M., Murphy, P. C., Goodrich, J. P., Moreaux, V., Liljedahl, A., Watts, J. D., Kimball, J. S., Lipson, D. A., and Oechel, W. C.: Cold

season emissions dominate the Arctic tundra methane budget, Proc Natl Acad Sci U S A, 113, 40–5, https://doi.org/10.1073/pnas.1516017113, 2016.

Öquist, M. G., Sparrman, T., Klemedtsson, L., Drotz, S. H., Grip, H., Schleucher, J., and Nilsson, M.: Water availability controls microbial temperature responses in frozen soil CO2 production, Global Change Biology, 15, 2715–2722, https://doi.org/10.1111/j.1365-2486.2009.01898.x, 2009.